Fluorescence Based Detection of Environmental and Biological Threats by Functionalized Aqua-Stable Metal-Organic Frameworks

A Dissertation Submitted to the

Indian Institute of Technology Guwahati

as Partial Fulfillment for the Degree of

DOCTOR of PHILOSOPHY

in

CHEMISTRY

by

Soutick Nandi

DEPARTMENT OF CHEMISTRY

INDIAN INSTITUTE OF TECHNOLOGY GUWAHATI

GUWAHATI, INDIA

June 2020

Fluorescence Based Detection of Environmental and Biological Threats by Functionalized Aqua-Stable Metal-Organic Frameworks

A Dissertation Submitted to the

Indian Institute of Technology Guwahati

as Partial Fulfillment for the Degree of

DOCTOR of PHILOSOPHY

in

CHEMISTRY

by

Soutick Nandi

Roll No. 156122053

DEPARTMENT OF CHEMISTRY

INDIAN INSTITUTE OF TECHNOLOGY GUWAHATI

GUWAHATI, INDIA

June 2020

DECLARATION:

I hereby declare that the submitted thesis entitled "**Fluorescence Based Detection of Environmental and Biological Threats by Functionalized Aqua-Stable Metal-Organic Frameworks**" is the output of research work carried out by me in the Department of Chemistry, Indian Institute of Technology Guwahati, under the supervision of Dr. Shyam P. Biswas. This work has not been submitted by me to any other institution or university. The result included in this thesis obtained from collaborative work has been acknowledged. Such materials as obtained from other sources have been also acknowledged in the thesis.

On following the scientific tradition all information provided in this thesis are correct according to the best of my knowledge.

IIT Guwahati **Soutick Nandi**

June 2020 Candidate

Dr. Shyam P. Biswas
Associate Professor
Department of Chemistry
Indian Institute of Technology Guwahati
Guwahati – 781039, India
Tel: +91 – 361 – 258 3309
Email: sbiswas@iitg.ac.in

CERTIFICATE

This is to certify that the work presented in the thesis entitled "**Fluorescence Based Detection of Environmental and Biological Threats by Functionalized Aqua-Stable Metal-Organic Frameworks**" by Mr. Soutick Nandi, was carried out by the candidate at the Department of Chemistry, Indian Institute of Technology Guwahati, under my supervision and has not been submitted elsewhere for a degree.

IIT Guwahati
June 2020

Dr. Shyam P. Biswas
Thesis supervisor
Department of Chemistry
Indian Institute of Technology Guwahati
Guwahati – 781039, Assam, India

ACKNOWLEDGEMENT

I would like to express my heartfelt and sincere gratitude to all who gave me the opportunity to complete the dissertation successfully. First and foremost, I wish to express my sincere thanks to my supervisor, Dr. Shyam P. Biswas, who introduced me to an interesting world of Metal-Organic Frameworks (MOFs). His motivation, encouragement, inspiration and persistent guidance helped me to explore the scientific work assembled in this thesis.

Besides my supervisor, I wish to avail this opportunity to express my deep gratefulness and indebtedness to the Head, Prof. Gopal Das, Department of Chemistry, Indian Institute of Technology Guwahati. I would also like to extend my gratitude to the doctoral committee members: Prof. Gopal Das, Prof. A. S. Achalkumar and Dr. Animesh Das for their suggestions and valuable guidance during the work. I would also like to thank all faculty members and staff members of the Department of Chemistry.

I wish to express my profound gratitude to our collaborators: Prof. Norbert Stock, Dr. Helge Reinsch, Prof. Vishal Trivedi for their invaluable contribution to my research work.

I am highly grateful to the Department of Chemistry and Central Instrument Facility (CIF) of IIT Guwahati for providing me the various sophisticated instruments for characterization of compounds. I am also thankful to the entire technical officers and the operators in the Chemistry Department and CIF, who helped me a lot to collect the data.

I ardently thank my lab seniors namely Dr. Amlan Buragohain, Dr. Rana Dalapati, Dr. Mostakim SK and Dr. Kaustuv Banerjee for their skillful, invaluable help and support during the course of this work. I would also like to thank all my lab colleagues namely Aniruddha Das, Chiranjib Gogoi, Masud Alam and Subhrajyoti Ghosh for their timely help, support and keeping a constant joyful atmosphere in laboratory. I also like to thank Ena Sharma, Ankita Mandal and Shubasis Roy, who helped me in my research work during their project works.

I extend my sincere thanks to all my friends who helped me a lot throughout my research work. I want to thank Debojit, Nrmalya, Tanmay, Sayantan, Souvick and Milan for their unasked help during my research work.

I owe my obligations to all the teachers and professors from my school, college and university who gave me the direction and insightful information to march forward in this field.

I am highly grateful to the Ministry of Human and Research Development (MHRD), Govt. of India for providing me the fellowship.

Finally, my Ph. D. endeavor could not have been completed without the endless love, support and blessings from my family. I would like to express my deepest gratitude to my parents Dilip Nandi and Bhanumoti Nandi for their unconditional love and sacrifices they have made for the sake of my upbringing. I am also grateful to my beloved sister Sharmisttha, her husband Rajaram and their son Kuntal for their affection and deep concern for my career.

My greatest regards to the Almighty for bestowing upon me the courage to face the complexities of life and complete this dissertation successfully.

Still many names are missing whose contribution and help are worth mentioning.

Soutick Nandi

Dedicated to My Loving Family

TABLE OF CONTENTS

Thesis Title:	**Fluorescence Based Detection of Environmental and Biological Threats by Functionalized Aqua-Stable Metal-Organic Frameworks**
Name of the Candidate:	Mr. Soutick Nandi
Roll No.:	156122053
Thesis Supervisor:	Dr. Shyam P. Biswas
Department:	Chemistry
Institute:	Indian Institute of Technology Guwahati, Assam, India

Thesis Overview:

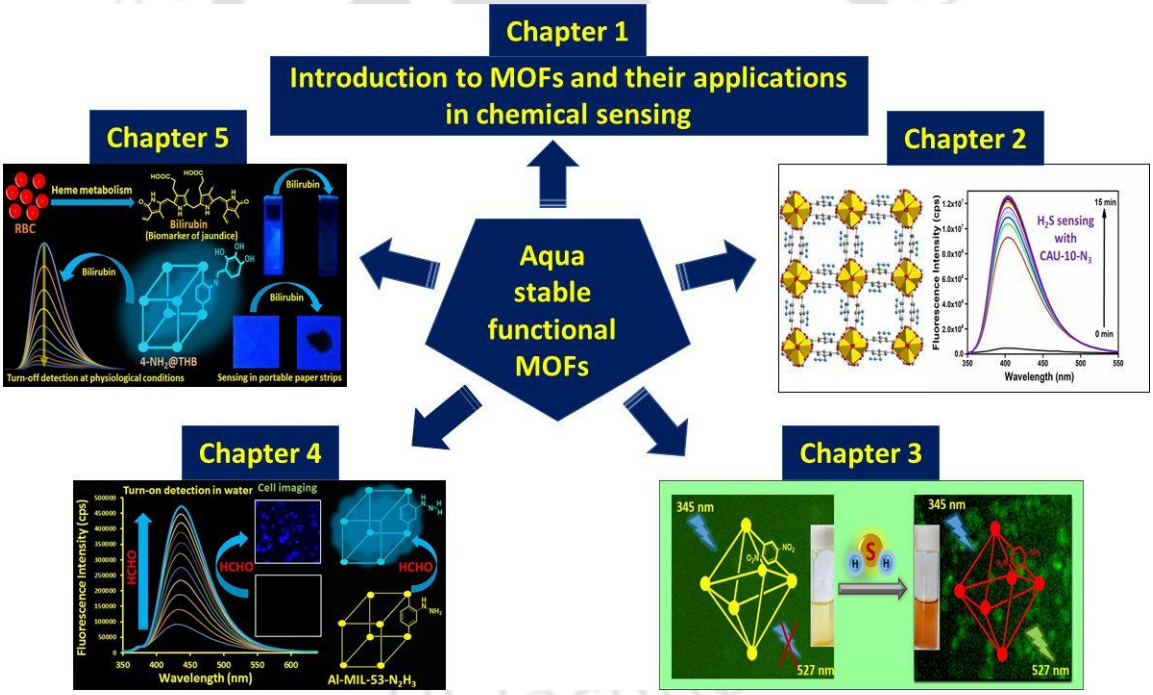

Chapter 1: Introduction to metal-organic frameworks and their applications in chemical sensing

This chapter presents a brief description of design, synthesis and applications of aqua stable metal-organic frameworks for chemical sensing. MOFs possess highly crystalline framework with predictable structures, tunable and functionalizable pores, which make MOFs as eligible materials for gas adsorption, gas separation, catalysis, drug delivery, chemical sensing etc. Fluorometric detection of environmental and biological threats by MOFs become a hot topic in recent days. Stability of MOFs under moisture/aqueous conditions is a crucial factor, particularly for those functional MOFs which are employed for real time detection purpose. Apart from hydrolytic stability, robustness of the material under biological conditions is also an important factor for developing MOFs for the detection of biologically relevant molecules. The hydrolytic stability of a MOF material largely depends on the coordination geometry, extent of orbital overlap, high connectivity of metal cluster and steric factors. The high connectivity of metal cluster in the framework provides high thermal and chemical stability to the MOF. Use of hydrophobic ligands during the synthesis is a simple and single-step procedure for the synthesis of hydrophobic and water-stable MOFs. On the other hand, straight forward synthesis, predictable structures, great stability, collaborative functionality and predictable host-guest interaction make the MOFs a potential candidate for fluorogenic detection purpose. For sensing purpose, the frameworks were judiciously functionalized by particular functionality with the specially functionalized ligand or by post-synthetic modification. The specific functionalities act as recognition sites for the targeted analytes.

Chapter 2: Rapid and highly sensitive detection of extracellular and intracellular H_2S by an azide-functionalized Al(III)-based metal-organic framework

This chapter describes the synthesis, comprehensive characterization and fluorometric detection of H_2S by an Al(III)-based, azide-functionalized MOF material called CAU-10-N_3 (**1′**). The framework structure of **1** is presented in Figure 1. As revealed from the figure, the framework of CAU-10-N_3 is formed by the interconnection of cis-corner sharing [AlO_6] octahedra with the azide-functionalized isophthalate ligands. Specific arrangement of the inorganic building units and ligand molecules results in formation of square-shaped one-dimensional channels in the framework.

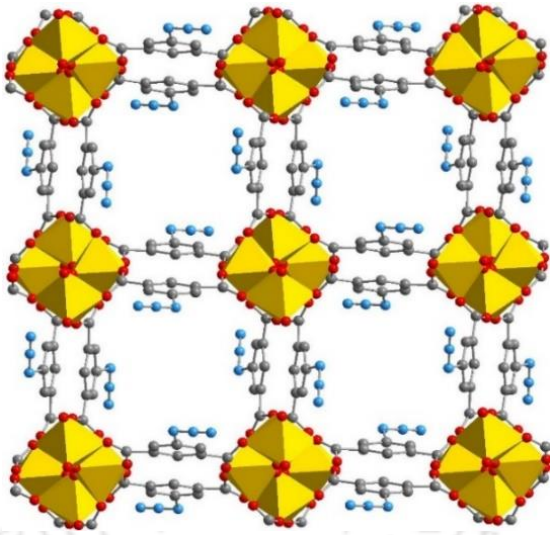

Figure 1. Framework structure of CAU-10-N3 (1) in ball-and-stick representation. Color codes: Coordination environment of Al, yellow polyhedra; C, grey; N, blue; O, red. Guest molecules have been removed from the structural diagram for clarity.

The activated material has been demonstrated to detect extracellular H_2S (in 10 mM HEPES having pH of 7.4) with rapidness, selectivity and high sensitivity. The compound is capable of sensing H_2S even in the presence of other interfering biological molecules and anions commonly found in biological systems. The limit of detection of the material (2.65 μM) for H_2S is lower than for the existing MOF-type fluorescent probes for H_2S. The MOF compound shows very short response time and considerably high fold-increase (~26 fold) in fluorescence emission intensity when treated with H_2S in HEPES buffer (Figure 2). Interestingly, the probe is capable of detecting H_2S inside the macrophage cells (Figure 3). H_2S-mediated reduction of azide groups into auxo-chromic amine group is the main reason behind the rapid emission enhancement of the material. The conversion of azide functionality to amine group was confirmed by several analytical techniques such as FT-IR spectroscopy, mass spectrometry and ^1H NMR spectroscopy. Furthermore, the excellent detection performance (in terms of short response time and extraordinary fold-increment in fluorescence intensity) in pure aqueous medium makes CAU-10-N_3 a potential candidate for the regulation of H_2S concentration in environmental (aqueous) samples.

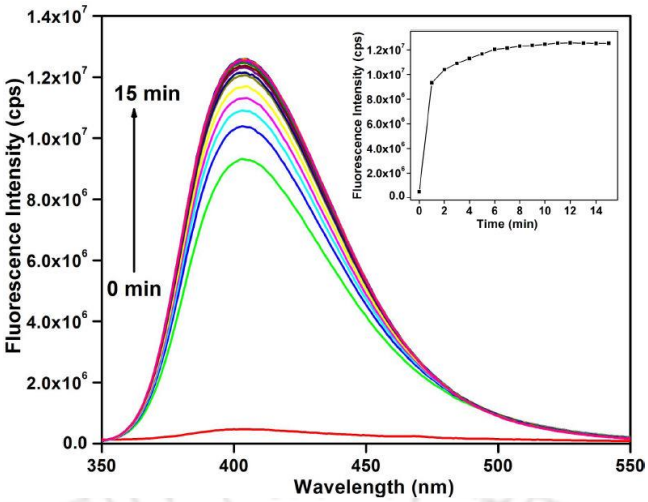

Figure 2. Fluorescence enhancement behavior of **1′** in HEPES buffer (10 mM, pH = 7.4) upon gradual addition of Na_2S at a systematic time gap (1 min) up to 15 min. Inset: plot of fluorescence intensity versus time (λ_{ex} = 330 nm and λ_{em} = 405 nm).

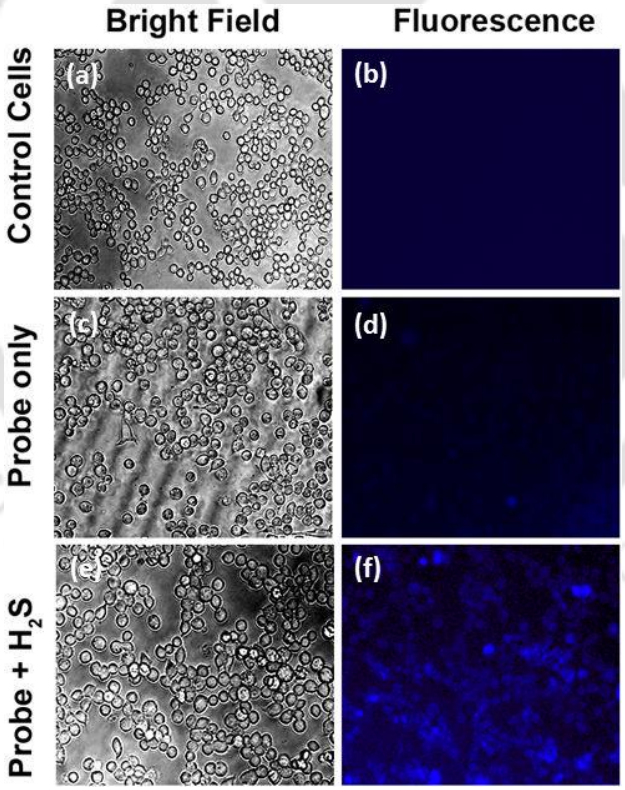

Figure 3. Ability of **1'** to detect H_2S in macrophage J774A.1 cells. Bright-field images of untreated cells (a), cells treated with 5 μM probe (c), and cells treated with 5 μM probe and 10 μM Na_2S (e). (b, d, f) are the fluorescence microscopy images of (a, c, e), respectively. Bright fluorescence was observed for H_2S-treated cells (f) only.

Chapter 3: A dinitro-functionalized metal-organic framework featuring visual and fluorogenic sensing of H_2S in living cells, human blood plasma and environmental samples

This chapter presents a new dinitro-functionalized Zr(IV) MOF (MOF = metal-organic framework) having UiO-66 (UiO = University of Oslo) framework topology called UiO-66-$(NO_2)_2$ (**2**), which shows fluorescence turn-on behavior towards H_2S in simulated biological medium (HEPES buffer, pH = 7.4) (Scheme 1). By employing solvothermal conditions, **2** was successfully synthesized by reacting $ZrCl_4$, H_2BDC-$(NO_2)_2$ [H_2BDC-$(NO_2)_2$ = 2,5-dinitro-1,4-benzenedicarboxylic acid] ligand and benzoic acid with a molar ratio of 1:1:10 in DMF (DMF = *N*,*N*-dimethylformamide) at 130 °C for 24 h. The material was characterized by infrared spectroscopy, X-ray powder diffraction (XRPD) and thermogravimetric (TG) analyses. The compound not only displays highly sensitive fluorometric sensing of H_2S but also exhibits visually detectable colorimetric change towards H_2S under day light. Moreover, **2′** showed great selectivity towards H_2S over several other biologically intrusive species (Figure 4). The limit of detection (LOD) of the compound is 14.14 μM which lies in the range of H_2S concentration found in biological systems. Fluorescence microscopy studies in J774A.1 cells revealed the efficacy of the probe for imaging H_2S in living cells. Moreover, this material can detect H_2S in human blood plasma (HBP) and monitor sulfide concentration in real water samples. The reduction of nitro functional groups towards amine functionality in the framework is the reason behind the drastic emission enhancement in presence of H_2S. The possible detection mechanism was characterized with the help of mass spectrometry and ^1H NMR spectroscopy.

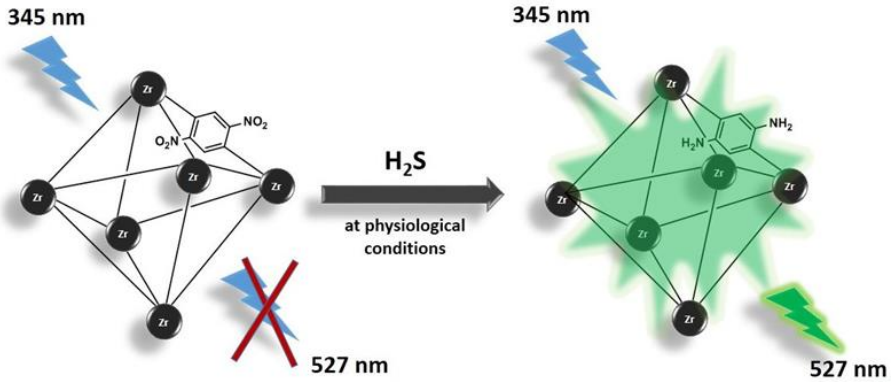

Scheme 1. Fluorescence increment behaviour of activated UiO-66-$(NO_2)_2$ MOF (**2'**) due to reduction of nitro groups into amines by H_2S at physiological conditions.

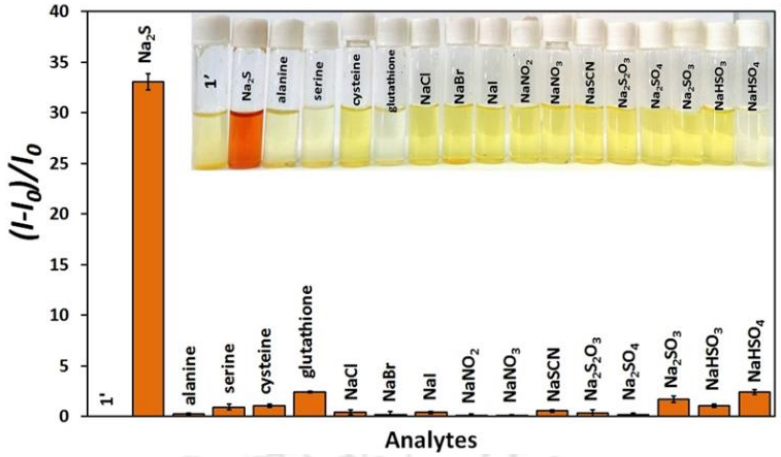

Figure 4. Comparative fluorescence response of the HEPES suspension of **2'** towards different analytes (10 equiv. of BDC-$(NO_2)_2$) after 40 min of the addition of analytes. Inset shows the corresponding visual change in color upon addition of each analyte. The error bars show the standard deviations of three measurements.

Chapter 4: A metal-organic framework showing selective and sensitive detection of exogenous and endogenous formaldehyde

This chapter reports a new hydrazine functionalized Al(III) metal-organic framework (MOF) having MIL-53 (MIL = Material of Institute Lavoisier) framework topology for the sensitive and selective detection of formaldehyde (FA). The phase-purity of the thermally activated and as-synthesized forms of the material was examined by XRPD experiments, FT-IR spectroscopy and TG analysis. The desolvated material (**3′**) showed great potential for the selective sensing of FA over other potentially competitive aldehydes in both aqueous and 10 mM HEPES buffer (pH = 7.4) media (Figure 5). The fluorescence "turn-on" behavior of the reaction-based probe can be ascribed to the inhibition of photo-induced electron transfer (PET) process (from hydrazine group to phenyl ring) due to the formation of hydrazone moiety. The anticipated mechanism has been confirmed by mass analyses as well as by the specially designed inhibition experiments.

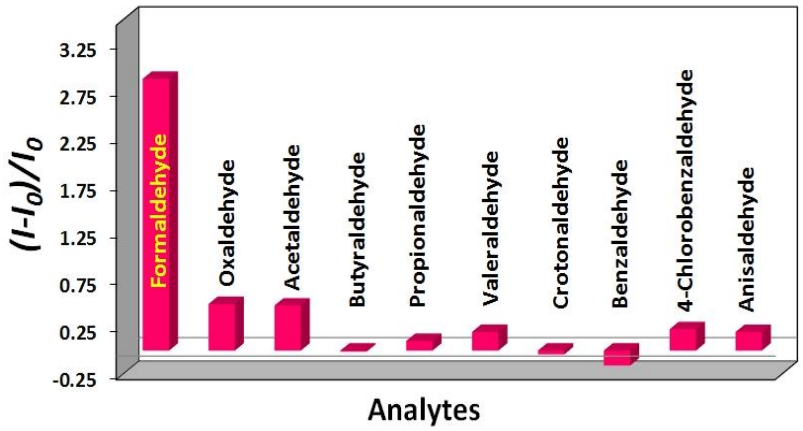

Figure 5. Relative fluorescence turn-on signal of **3′** towards the addition of different aldehydes (20 mM, 500 µL) in HEPES buffer.

The detection limit towards FA for the probe in HEPES buffer is 8.37 µM (0.25 ppm), which lies below the intracellular concentration of FA (100-400 µM). A very short response time (1 min) has been displayed by **3′** for FA sensing. Moreover, a remarkable enhancement in the emission intensity (7 fold and 4 fold in aqueous and HEPES buffer medium, respectively) of **3′** was observed after 1 min of FA addition (Figure 6). Furthermore, the ability of the probe to detect FA in the vapor phase was also demonstrated (Figure 7). Interestingly, the material is also capable to detect endogenous FA in cancer cells. All the above discussed features clearly reveal that the present material has a huge potential for selective recognition of FA in both real water and biological samples.

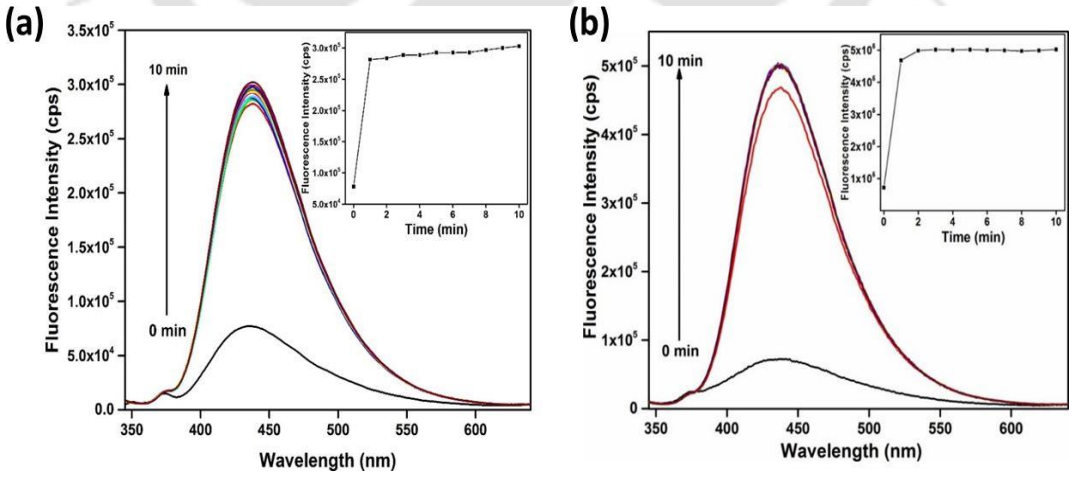

Figure 6. Increment in emission intensity of **3′** after the introduction of 20 mM formaldehyde (500 µL) from 1 min to 10 min in (a) HEPES buffer and (b) aqueous medium. Inset plot shows the enhancement in emission intensity as a function of time (monitored at 436 nm).

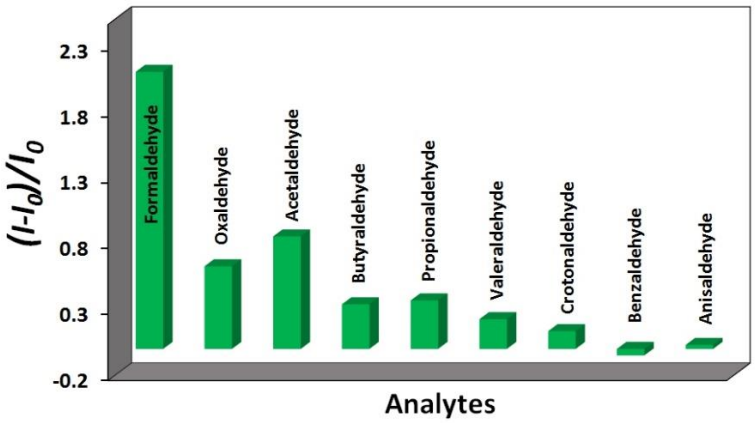

Figure 7. Relative fluorescence turn-on signal of **3′** coated film on quartz slide (after 20 min) towards the addition of different aldehydes (100 μL).

Chapter 5: A recyclable post-synthetically modified Al(III) based metal-organic framework for fast and selective fluorogenic recognition of bilirubin in human biofluids

This chapter presents the synthesis, characterization and through detection investigation of bilirubin by an imine bond incorporated MIL-53 metal-organic framework, which was synthesized by the aldimine condensation reaction between MIL-53-NH_2 and 2,3,4-trihydroxy benzaldehyde (Scheme 2). FT-IR spectroscopy, mass spectrometry and NMR spectroscopy clearly revealed the successful formation of an imine bond after the condensation reaction. Moreover, X-ray powder diffraction experiments revealed that the material retained its structural integrity even after the condensation reaction.

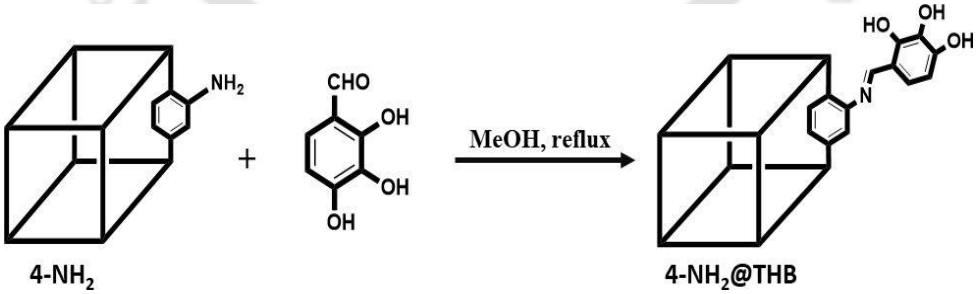

Scheme 2. Reaction scheme for the synthesis of **4-NH_2@THB**.

The post-synthetically modified material was successfully employed for the selective and sensitive recognition of bilirubin (a key biomarker for jaundice) in HEPES buffer medium. The strong blue fluorescence of the HEPES buffer suspension of the probe was completely quenched by bilirubin solution due to static

quenching process, which can be clearly visualized by naked eye. Moreover, the detection limit (1.26 pM) of the probe towards bilirubin is quite lower than the normal concentration level of bilirubin in human blood plasma (25 μmol/L to 50 μmol/L). Furthermore, other bio-molecules and common biologically relevant metal ions had no interference during the fluorescence quenching of the probe by bilirubin (Figure 8). The details mechanistic investigation was also performed to find out the actual mechanism behind the quenching of emission intensity of the material in presence of bilirubin. The detection efficacy of bilirubin by the material was further examined in human blood serum and urine samples. Hence, this material can be applied as a clinical diagnostic tool for the identification of jaundice.

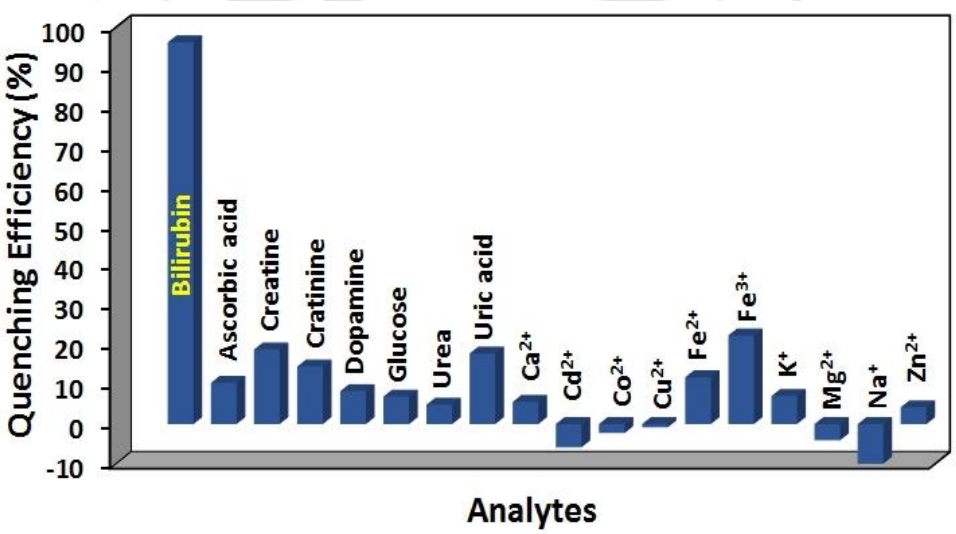

Figure 8. Fluorescence quenching effect of **4-NH_2@THB** towards the introduction of different intrusive analytes (1 mM, 200 μL) in HEPES buffer.

Conclusions

The thesis work mainly focuses on the design and synthesis of aqua stable MOFs and their potential applications in fluorescence-based detection of environmental and biological threats under physiological conditions. The fluorogenic sensing of environmental and biological hazards by MOFs is still in the stage of infancy. There is a huge challenge and opportunity for the development of new MOF probes and evaluation of their sensing performances in terms of LOD, fold increment, response time, etc. Hence, it is believed that our study will stimulate the research interests in the field of MOF-related sensors for chemical sensing.

CHAPTER 1

Introduction to metal-organic frameworks and their applications in chemical sensing

Metal-organic frameworks (MOFs) are a new class of hybrid crystalline materials self-assembled from organic polytopic ligands and metal ions/clusters. Various combinations of organic ligands and metal ions/clusters lead to formation of huge number of MOFs having interesting properties and various applications (gas storage/separation, heterogeneous catalysis, chemical sensing, proton conduction, drug delivery, etc.). This chapter mainly presents the design and applications of MOFs for chemical sensing. The incorporated functional groups act as recognition sites for specific analytes. How fine tuning of MOF by inclusion of specific functionality in the ligand moiety is useful for the detection of targeted analyte is briefly described here.

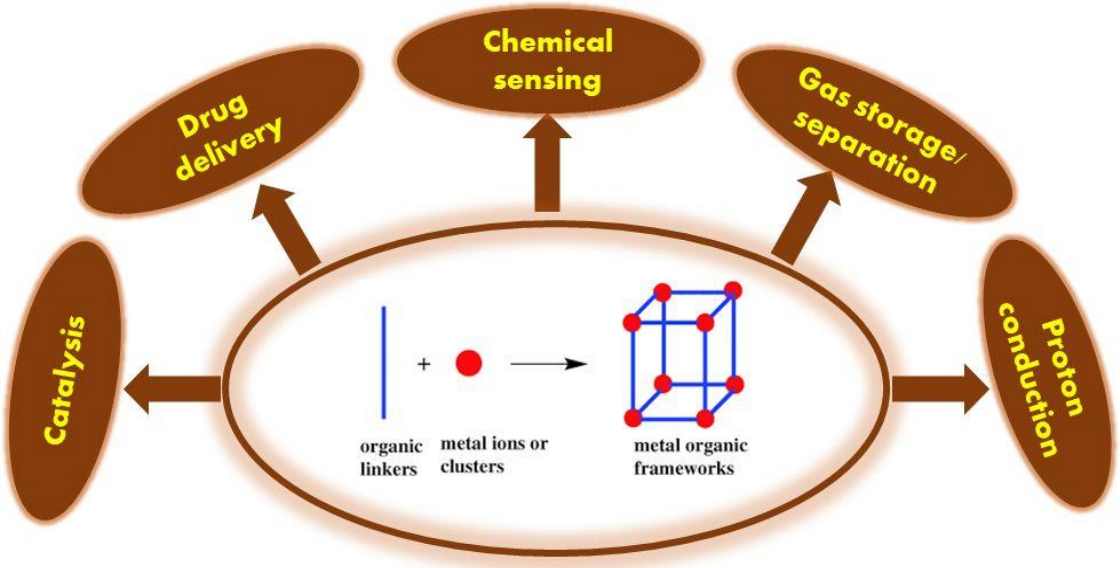

1.1 Introduction

Over past few decades, with rapid growth of urban population and industrial development, the environmental pollution has become a serious threatening problem for living beings.[1] Several kinds of environmental contaminants such as heavy metal ions, oxo-anions, toxic organic compounds, poisonous volatile compounds etc. are associated with public health risk factors.[2] Now-a-days, standard techniques (i.e. several types of chromatography,[3, 4] electrochemical detection,[5-7] flow injection analysis[8] etc.) for chemical threat detection are not suitable because of their expensive and bulky instrumentation, high power consumption, slow response, complicated methodology and destruction of cell lysates.[9] Hence, modern sensing methods for real time monitoring of toxic compounds with short response time, great selectivity, high sensitivity and suitability for in-vivo application are highly desirable.

Generally, sensor materials contain two units, one is sensing unit and another is transduction unit which actually transform the sensing response into detectable signal. Hence, the working principle of a sensor material is based on the change in electrical, optical, photophysical or mechanical properties of the parent sensing compound while interacting with the targeted analyte.[10, 11] An ideal sensor compound should exhibit some characteristic features such as fast response time, great selectivity and sensitivity towards analyte, reusability, long term stability and low-cost detection process.[12] Hence, design and development of ideal sensor compounds are challenging tasks. Till now, a lot of sensors including nanocarbon materials (carbon nanotube and graphene),[13, 14] metal oxides,[15] organic small molecules,[16] quantum dots[17] and polymers[18, 19] have been employed for targeted detection purpose. The development of ideal sensing materials with excellent sensing performance greatly enhances the field related to sensor materials.

Metal–organic frameworks (MOFs) are generally regarded as porous coordination polymers (PCPs) with open framework structures containing potential voids.[20] Actually, MOFs are a class of porous materials comprised of metal ions or metal ion clusters linked via organic ligand molecules to form extended, crystalline and porous frameworks.[21] The chemical and physical properties of MOFs can be finely tuned by altering the metal ions and organic ligands as well as by changing synthetic conditions such as employed solvent, temperature and concentration of various modulating agents.[22] The tunable pores and high porosity of MOFs enable their applications in gas storage and separation,[23] drug

delivery,[24, 25] chemical separation,[26, 27] proton conduction,[28] chemical and physical sensing,[29-32] optoelectronics,[33] catalysis,[34, 35] and bio-imaging.[36, 37]

The tunable chemical functionalization, reversible adsorption, high catalytic activity and diverse structures of MOFs make them ideal candidates as chemical sensors.[38] The chemical, physical or structural changes in a MOF upon adsorption or interaction with guest molecules have been employed in recent years for the detection of various target components including toxic species, solvents, pesticides, antibiotics, explosives, volatile organic compounds and biological markers.[39-42] Furthermore, not only targeted components but also pH,[43] humidity[44] and temperature[45] can also be sensed by MOFs. The sensory activity of MOFs is directly related to the signal transduction mechanism. This host–guest interaction is mainly responsible for producing observable signal in MOFs. A huge number of research articles have been published in the last decade related with MOF materials. Among them, only few papers focused on the fluorescence sensing applications of MOF materials (Figure 1.1).

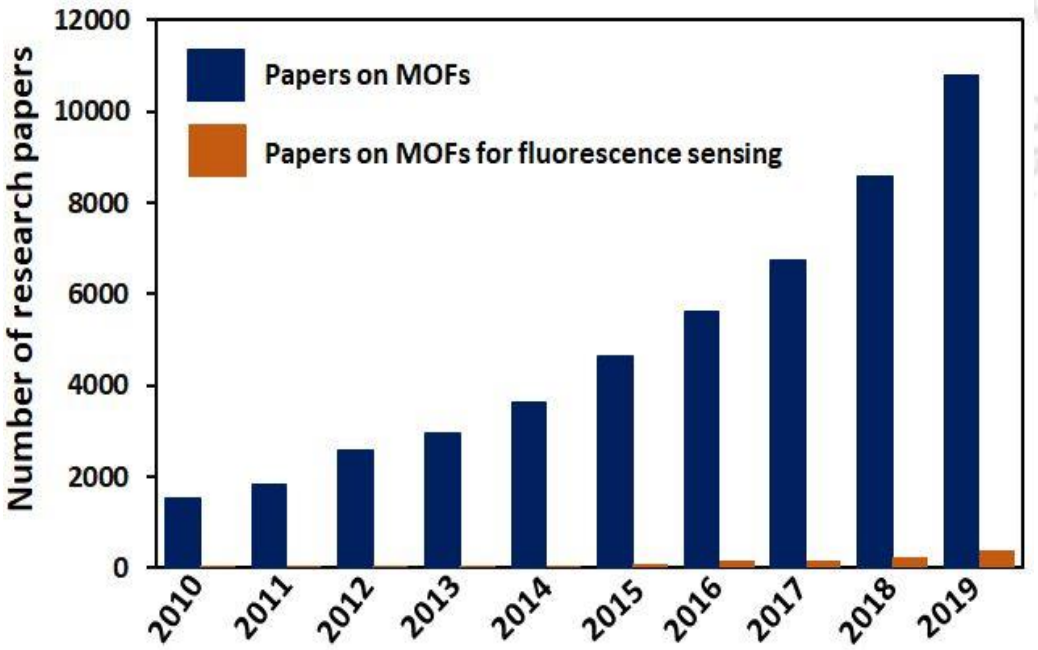

Figure 1.1 Number of research papers per year from 2010-2019 on the topics of "metal-organic framework" and "metal-organic framework for fluorescence sensing". The numbers were determined based on a Scifinder search in May 2020 spanning from 2010 to 2019 using keywords: metal-organic framework and water stable metal-organic framework for fluorescence sensing.

1.2 Background and development of MOFs

From the time of Alfred Werner (1893), investigation of coordination compounds started. In the meantime, several types of coordination compounds were discovered such as Werner complexes, Hofmann clathrates and Prussian blue.[46-48] Some interesting properties such as molecular inclusion and magnetism were studied with these complexes. But, before 1989, no systematic investigation was observed for the construction of metal-organic solid materials. In 1756, Axel Frederik Cronstedt first discovered the natural zeolites, namely stilbite and since then, research on this class of porous materials has increased rapidly. Discovery of functional microporous materials began in 1990 when Robson and co-workers prepared some porous coordination polymers which displayed ion exchange properties.[49 50] The synthesis of the 3D porous framework was further extended by Prof. O. M. Yaghi.[51] In 1999 , Prof. Yaghi reported the hydrothermal synthesis route to prepare a crystalline, metal-organic, open framework system having extended channel called MOF-5 which was compared to zeolite and activated carbon.[52] MOF-5, which has a **pcu**-topology, was synthesized from zinc acetate and benzene-1,4-dicarboxylic acid.

Though Prof. Yaghi first introduced the term "MOF" for metal-organic porous materials having node-spaced connectivity but several research groups used different terminologies such as coordination polymers, coordination networks, organic analogues of zeolites, etc. To terminate the unnecessary confusion, the International Union of Pure and Applied Chemistry (IUPAC) task group in 2012 has revealed a provisional definition of MOF as: 'Metal-Organic Framework, abbreviated to MOF, is a Coordination Polymer (or alternatively Coordination Network) with an open framework containing potential voids.[53] After Yaghi, Férey et al., Kitagawa et al., Stock et al. and several other scientists started working on MOFs. They reported a huge number of MOF materials and applied in several fields.

Over last two decades, MOFs have become one of the hottest topics in material science. Due to inherent porosity, MOFs were previously applied for gas storage and separation. But, recently, the door of various applications has been opened up for MOFs due to variability in the structure, adjustable pore size and easy functionalization.[54] Recently, MOFs have been found to be very much useful for fluorescence sensing of various kinds of analytes. For sensing of environmental contaminants and biomolecules, most of the sensing studies are accomplished in aqueous medium. Hence, for the detection of toxic species and biomolecules by MOF materials, they should be biocompatible and

hydrolytically stable. Over last 25 years, a huge number of MOFs have been prepared and applied in several fields. Based on metal ions and ligands used for synthesis, MOFs are broadly classified in the below mentioned category:

(i) M^{4+}-Carboxylate based MOFs (M = Ti, Zr, Hf and Ce)

(ii) M^{3+}-Carboxylate based MOFs (M = Al, Cr, Ga, Fe, Sc, V, Ga and In)

(iii) M^{2+}-Azolate based MOFs (M = Zn, Co)

This study is mainly based on Zr^{4+} and Al^{3+}-based carboxylate MOFs because they are highly aqua stable and biocompatible.

1.2.1 Zr^{4+}–Carboxylate based MOFs

In the year 2008, the first example of a Zr-based MOF called UiO-66 was reported by Lillerud et al.[55] The framework is constructed by linear dicarboxylate ligands (terephthalic acid) and $[Zr_6(\mu_3\text{-}O)_4((\mu_3\text{-}OH)_4(COO)_{12}]$ clusters. Six vertices of the octahedra are occupied by Zr^{4+} and eight triangular faces are alternatively capped by four μ_3-OH and four μ_3-O. This connectivity gives rise to the generation of a three-dimensional (3D) cubic framework, which has tetrahedral as well as octahedral cages (Figure 1.2). Eight tetrahedral cages are located at the corner of every central octahedral cage. BET surface area of UiO-66 was close to 1200 $m^2\ g^{-1}$. At the same time, two isoreticular structures such as UiO-67 and UiO-68 were also synthesized by simple elongation of ligand. It is worth to mention that UiO-66, UiO-67 and UiO-68 were obtained as polycrystalline powders. Hence, to characterize the structure, complicated Rietveld refinement of synchrotron PXRD data was needed. In the year 2011, Schaate et al. first obtained and examined the single crystals of UiO-68-NH_2, which was prepared by following modulated synthetic strategy.[56] This study dramatically enhanced the development of Zr-MOFs because single crystalline samples allow precise structure determination by single-crystal X-ray diffraction. After that, over few years, a large number of Zr-MOFs were synthesized and their applications were extensively explored. Zr-MOFs based on tetratopic ligand was obtained having similar clusters with $[Zr_6O_4(OH)_4]$ core but different connection numbers. For example, an 8-connected cluster was observed in PCN-222.[57] Later on, similar 8-connected Zr-clusters with square planar, tetrahedral or linear carboxylate linkers were discovered.[58-60] Interestingly, PCN-222 and its analogous compounds can survive in conc. HCl. Furthermore, the unsaturated Zr-cluster opens a platform for versatile applications.[61, 62] Afterward, 6-connected and 10-

connected Zr-clusters were also found.[63-65] Though most of the Zr-MOFs are found to have $[Zr_6O_4(OH)_4]$ core but MOFs with other Zr-clusters were also found. For example, MIL-140 series are composed by polymeric double chains of edge sharing ZrO_7 polyhedra connected through linear ligands.[66] Recently, few Zr-MOFs have been explored with $[Zr_{12}(\mu_3\text{-}O)_8(\mu_3\text{-}OH)_8(\mu_2\text{-}OH)_6(COO)_{18}]$ clusters.[67] Actually, in these frameworks, two Zr_6 clusters are linked by face to face by six μ_2-OH groups. Last of all, with different types of ligands having different symmetry and length, various kinds of new Zr-MOFs can be expected in future. Some representative stable Zr-MOFs discussed herein are listed in Table 1.1.

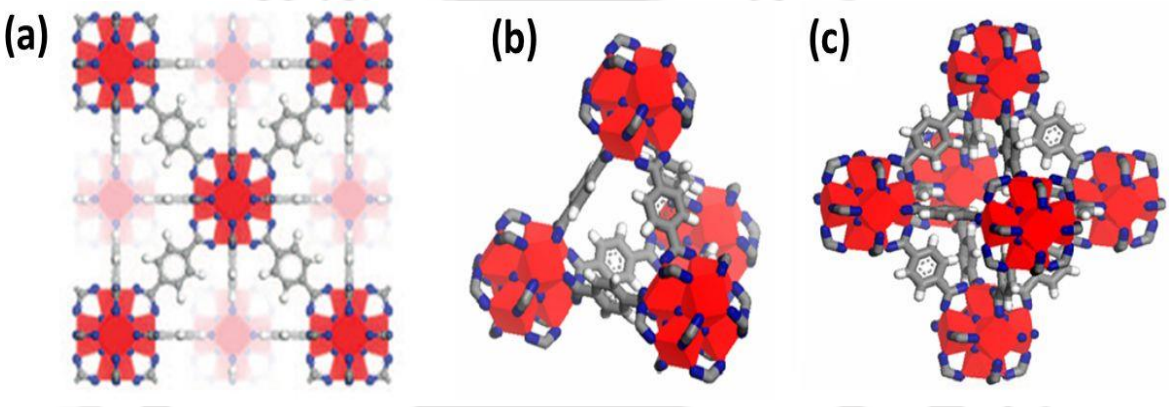

Figure 1.2 (a) Unit cell of UiO-66 MOF, (b) tetrahedral and (c) octahedral cages of UiO-66 MOF. Color codes: Coordination environment of Zr, red polyhedra; C, grey; O, blue; H, white. Reproduced with permission from ref. 55. Copyright 2008, American Chemical Society.

Table 1.1 Summary of some Zr(IV) based MOFs.

MOFs	Cluster/Cores	Linkers[a]	Surface Area (m^2/g)	Ref.
UiO-66	$[Zr_6(\mu_3\text{-}O)_4(\mu_3\text{-}OH)_4(COO)_{12}]$	BDC	1187	55
UiO-67	$[Zr_6(\mu_3\text{-}O)_4(\mu_3\text{-}OH)_4(COO)_{12}]$	BPDC	3000	55
UiO-68	$[Zr_6(\mu_3\text{-}O)_4(\mu_3\text{-}OH)_4(COO)_{12}]$	TPDC	4170	55
PCN-222	$[Zr_6(\mu_3\text{-}O)_4(\mu_3\text{-}OH)_4(OH)_4(H_2O)_4(COO)_8]$	TCPP	2223	57
PCN-223	$[Zr_6(\mu_3\text{-}O)_4(\mu_3\text{-}OH)_4(COO)_{12}]$	TCPP	1600	68

MOFs	Cluster/Cores	Linkers[a]	Surface Area (m^2/g)	Ref.
PCN-224	$[Zr_6(\mu_3\text{-}O)_4(\mu_3\text{-}OH)_4(OH)_6(H_2O)_6(COO)_6]$	TCPP	2600	65
PCN-225	$[Zr_6(\mu_3\text{-}O)_4(\mu_3\text{-}OH)_4(OH)_4(H_2O)_4(COO)_8]$	TCPP	1902	69
MOF-801	$[Zr_6(\mu_3\text{-}O)_4(\mu_3\text{-}OH)_4(COO)_{12}]$	FUM	990	64
MOF-808	$[Zr_6(\mu_3\text{-}O)_4(\mu_3\text{-}OH)_4(OH)_6(H_2O)_6(COO)_6]$	BTC	2060	64
MOF-812	$[Zr_6(\mu_3\text{-}O)_4(\mu_3\text{-}OH)_4(COO)_{12}]$	MTB	2335	64
MOF-841	$[Zr_6(\mu_3\text{-}O)_4(\mu_3\text{-}OH)_4(OH)_4(H_2O)_4(COO)_8]$	MTB	1390	64
NU-1000	$[Zr_6(\mu_3\text{-}O)_4(\mu_3\text{-}OH)_4(OH)_4(H_2O)_4(COO)_8]$	TBAPy	2320	58
MIL-140A	$[ZrO(COO)_2]_n$	BDC	415	66
MIL-140B	$[ZrO(COO)_2]_n$	2,6-NDC	460	66
MIL-140C	$[ZrO(COO)_2]_n$	BPDC	670	66
MIL-140D	$[ZrO(COO)_2]_n$	Cl_2ABDC	701	66
DUT-52	$[Zr_6(\mu_3\text{-}O)_4(\mu_3\text{-}OH)_4(COO)_{12}]$	2,6-NDC	1399	63
DUT-84	$[Zr_6(\mu_3\text{-}O)_4(\mu_3\text{-}OH)_4(OH)_6(H_2O)_6(COO)_6]$	2,6-NDC	637	63
Zr_{12}-TPDC	$[Zr_{12}(\mu_3\text{-}O)_8(\mu_3\text{-}OH)_8(\mu_2\text{-}OH)_6(COO)_{18}]$	TPDC	1967	67

[a] Linkers are abbreviated as: BDC = terephthalate, BPDC = biphenyl-4,4′-dicarboxylate, TPDC = [1,1′:4′,1″-terphenyl]-4,4″-dicarboxylate, TCPP = meso-tetrakis(4-carboxylatephenyl) porphyrin,, FUM = fumarate, BTC = benzene-1,3,5-tricarboxylate, MTB = 4,4′,4″,4‴-methanetetrayltetrabenzoate, TBAPy = 1,3,6,8-tetrakis(p-benzoate)pyrene, 2,6-NDC = naphthalene-2,6-dicarboxylate, Cl_2ABDC = dichloro-4,4-azobenzenedicarboxylate.

1.2.2 Al^{3+}–Carboxylate based MOFs

Férey et al. reported Al-MOF with [Al(OH)(BDC)] formula which is popularly known as MIL-53(Al) (MIL= Materials of Institute Lavoisier).[70] MIL-53(Al) contains infinite linear zigzag chains of $AlO_4(OH)_2$ octahedra. The 1D rhombic channels are obtained by linking the parallel chains and BDC ligands. An interesting breathing

phenomenon was visualized in MIL-53(Al) MOF, in which the framework adapted its structure with respect to adsorbed guest molecules. The "np" (narrow pore) and "lp" (large pore) forms could be observed by reversible removal and incorporation of guest molecules, respectively (Figure 1.3). Furthermore, several MOFs based on the MIL-53(Al)-type structure were explored by using functionalized or extended linkers, such as DUT-4 and DUT-5 (DUT stands for Dresden University of Technology).[71] Another MIL-53 isomer is MIL-68(Al) which has more rigid network.[72] Further elongation of linker in MIL-68(Al) led to CYCU-3 (CYCU stands for Chung-Yuan Christian University).[73]

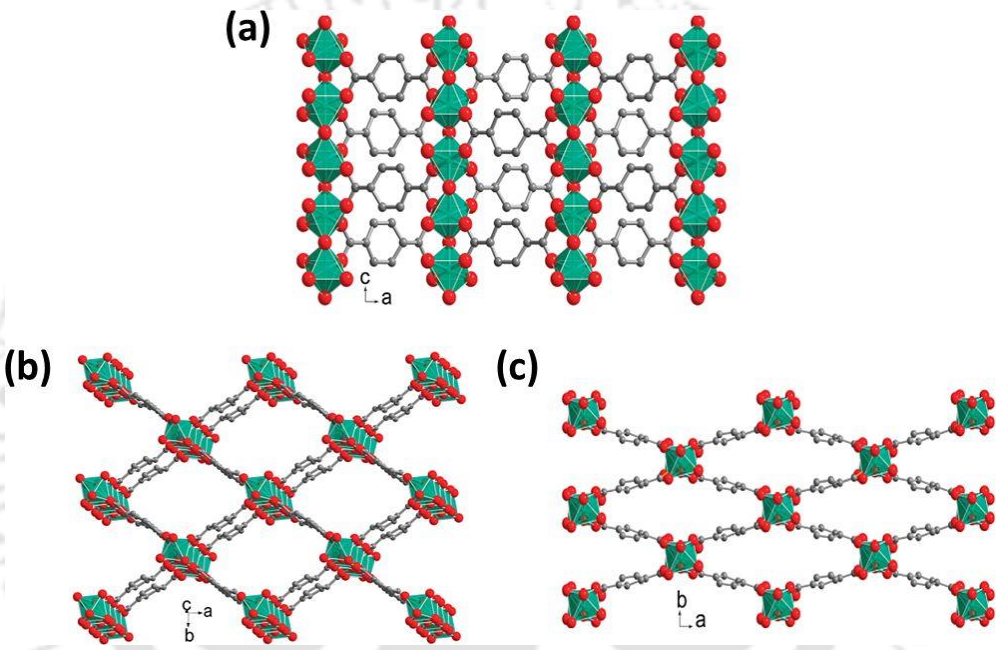

Figure 1.3 Ball-and-stick representations of the 3D framework structure of Al-MIL-53: (a) Infinite chains of corner-sharing octahedral $[AlO_4(OH)_2]$ units interconnected by the BDC linkers, (b) The large pore (LP) and (c) narrow pore (NP) forms of the framework viewed along the crystallographic c-axis. For clarity, hydrogen atoms and guest molecules have been omitted from all structural plots. color codes: Coordination environment of Al, green polyhedra; C, gray; O, red. Reproduced with permission from ref. 74. Copyright 2011, American Chemical Society.

Tritopic carboxylate ligand BTTB and $[Al(OH)(COO)_2]_n$ chains led to the formation super stable 467-MOF.[75] Beside tritopic ligand, Al-MOFs based on $[Al(OH)(COO)_2]_n$ chains and tetratopic caboxylic ligands were also explored such as MIL-121, MIL-118 and MIL-120.[76, 77 78] NOTT-300 (NOTT stands for University of Not-tingham) is another Al-MOF which is comprised of $[Al(OH)(COO)_2]_n$ chains bridged by

four-connected BPTA linker.[79] Moreover, the MOF with combination of $[Al(OH)(COO)_2]_n$ chains and porphyrin linker (TCPP) was also reported and named as Al-PMOF.[80] In spite of the large structure of the ligand, the Al-PMOF can withstand in aqueous medium with pH values from 5 to 8. The first example of an Al-MOF having the $[Al_3(\mu_3\text{-}O)(COO)_6]$ cluster is MIL-96.[81] MIL-96 contains two types of isolated clusters: one is $[Al_3(\mu_3\text{-}O)(COO)_6]$ cluster and another is infinite chains with $AlO_4(OH)_2$ units. These two building units are connected by the ligand (BTC) to form three types of cages. The combination of $[Al_3(\mu_3\text{-}O)(COO)_6]$ clusters and tricarboxylate linkers led to formation of MIL-100(Al).[82] This structure is built up from super-tetrahedral blocks based on $[Al_3(\mu_3\text{-}O)(COO)_6]$ SBUs and BTC linkers. In addition, an extended form of MIL-100 called PCN-333(Al) was reported, which is built from $[Al_3(\mu_3\text{-}O)(COO)_6]$ SBUs and TATB linkers having D_{3h} symmetry.[83] PCN-333(Al) showed good stability in aqueous medium with pH range from 3 to 9. Further extension of the tricarboxylate ligand led to the formation of PCN-888 having two hierarchal mesoporous cages.[84] The combination of linear linker ($BDC\text{-}NH_2$) molecule and $[Al_3(\mu_3\text{-}O)(COO)_6]$ gave rise to MIL-101-NH_2 (Al).[85] This structure exhibited great thermal and chemical stability. Another MOF called Al-soc-MOF was found with the combination of $[Al_3(\mu_3\text{-}O)(COO)_6]$ clusters and tetratopic TCPT ligands. This MOF is well-known for high uptake of carbon dioxide and deliverable uptake for oxygen.[86]

Stock et al. reported another Al-MOF called CAU-10 (CAU = Christian-Albrechts-University) with the combination $[Al(OH)(COO)_2]$ cluster and V-shaped linker molecule 1,3-benzene dicarboxylic acid.[87] The inorganic building unit of CAU-10-framework is basically a chain of *cis*-connected, corner-sharing AlO_6 polyhedra. Four of the oxygen atoms come from four different carboxylate groups, while two bridging OH^- ions remain in *cis*-position to each other to form octahedral coordination environment around the Al-center. By virtue of this connectivity mode, helices are formed. This helical inorganic building unit is unique since most often linear chains of *trans*-connected $M(III)O_6$-polyhedra are observed in MOFs with one-dimensional inorganic units such as MIL-53. Specific arrangement of the inorganic building units and ligand molecules results in formation of square-shaped one-dimensional channels in CAU-10-MOF (Figure 1.4). In CAU-1 MOF, the 12-connected octanuclear wheels $[Al_8(OH)_4(OCH_3)_8(COO)_{12}]$ are linked by BDC linkers with four linkers in the plane of the wheel which leads to the formation of distorted octahedral and tetrahedral cages.[88] On the other side, in CAU-3 MOF, strongly distorted tetrahedral and octahedral cavities are observed, which is built

from 12-connected $Al_{12}(OCH_3)_{24}$ dodecanuclear wheels and BDC linkers.[89] Till now, extensive research efforts have been dedicated for the design and synthesis of Al-MOFs with unique topology and further applications in different fields. Some representative stable Al-MOFs discussed herein are listed in Table 1.2.

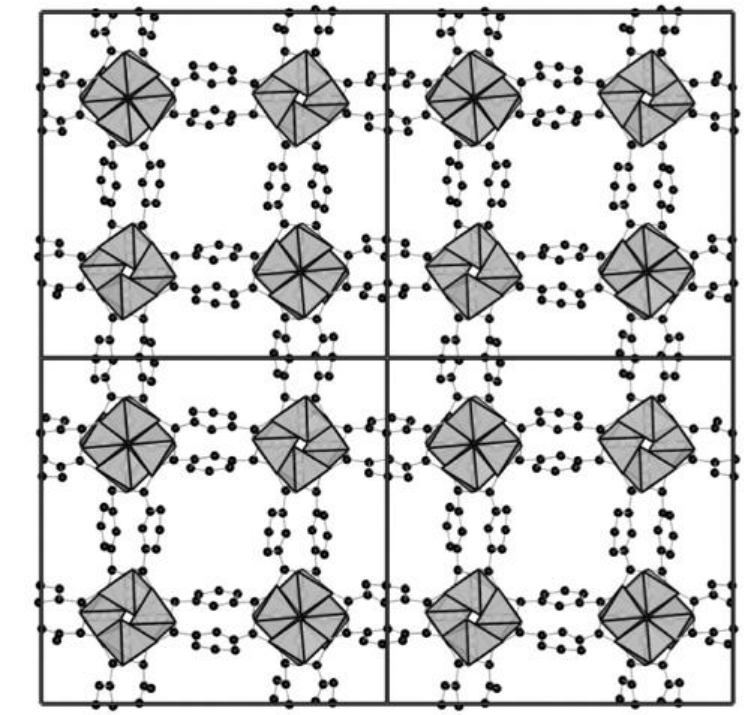

Figure 1.4 2×2 Supercell of the framework of CAU-10 showing 4-fold connectivity of the helices and square-shaped channels. Reproduced with permission from ref. 87. Copyright 2013, American Chemical Society.

Table 1.2 Summary of some Al(III) based MOFs.

MOFs	Cluster/Cores	Linkers[a]	Surface Area (m^2/g)	Ref.
MIL-53(Al)	$[Al(OH)(COO)_2]_n$	BDC	1181	70
DUT-5	$[Al(OH)(COO)_2]_n$	BPDC	1613	71
467-MOF	$[Al(OH)(COO)_2]_n$	BTTB	725	75
MIL-118	$[Al(OH)(COO)_2(COOH)_2]_n$	BTEC	-	77
MIL-120	$[Al(OH)(COO)_2]_n$	BTEC	308	78
MIL-121	$[Al(OH)(COO)_2]_n$	BTEC	162	76
NOTT-300	$[Al(OH)(COO)_2]_n$	BPTA	1370	79
Al-PMOF	$[Al(OH)(COO)_2]_n$	TCPP	1400	80

MOFs	Cluster/Cores	Linkers[a]	Surface Area (m^2/g)	Ref.
MIL-96(Al)	$[Al_3(\mu_3\text{-}O)(COO)_6]$ $[Al(OH)(COO)_2]_n$	BTC	-	81
MIL100(Al)	$[Al_3(\mu_3\text{-}O)(COO)_6]$	BTC	2151	82
PCN-333(Al)	$[Al_3(\mu_3\text{-}O)(COO)_6]$	TATB	4000	83
MIL-101(Al)	$[Al_3(\mu_3\text{-}O)(COO)_6]$	BDC-NH_2	2100	85
Al-soc-MOF	$[Al_3(\mu_3\text{-}O)(COO)_6]$	TCPT	5585	86
CAU-10	$[Al(OH)(COO)_2]_n$	1,3-BDC	635	87
CAU-1	$[Al_8(OH)_4(OCH_3)_8(COO)_{12}]$	BDC-NH_2	1700	88
CAU-3-BDC	$[Al_{12}(OCH_3)_{24}(COO)_{12}]$	BDC	1550	89
CAU-3-BDC-NH_2	$[Al_{12}(OCH_3)_{24}(COO)_{12}]$	BDC-NH_2	1250	89
CAU-3-NDC	$[Al_{12}(OCH_3)_{24}(COO)_{12}]$	2,6-NDC	2320	89

[a] Linkers are abbreviated as: BDC = terephthalate, BPDC = biphenyl-4,4′-dicarboxylate, BTTB = 4,4′,4″-[benzene-1,3,5-triyl-tris(oxy)]tribenzoate, BTEC = 1,2,4,5-benzenetetracar-boxylate, BPTA = biphenyl-3,3′,5,5′-tetracarboxylate, TCPP = meso-tetrakis(4-carboxylatephenyl) porphyrin, BTC = benzene-1,3,5-tricarboxylate, TATB = 4,4′,4″-s-triazine-2,4,6-triyl-tribenzoate,, BDC-NH_2 = 2-aminoterephthalate, TCPT = 3,3″,5,5″-tetrakis(4-carboxyphenyl)-p-terphenyl, 1,3-BDC = isophthalate, 2,6-NDC = naphthalene-2,6-dicarboxylate.

1.3 Basic design strategies of MOFs

As suggested by the name, there are mainly two components present in the backbones of MOFs, one is the metal center and another one is organic ligand. During construction of the framework, metal nodes serve as connecting points, whereas the organic ligands act as bridging molecules (or net forming molecules).[90] The metal ions and organic ligands utilized in the synthesis of a MOF are also called as "primary building units."

The selection of metal nodes for the synthesis of a MOF lies in very wide range which may include transition-metal ions, alkali metal ions, alkaline-earth metal ions and also rare-earth metal ions.[91] Furthermore, some other characteristics of metal ions should be considered such as oxidation state, coordination number (e.g., 2–7) and coordination geometry. Metal-coordination geometry (e.g., Y- or T-shaped, square-planar, tetrahedral,

cubic, square-pyramidal or octahedral) is also an important part for the construction and prediction of framework structure of MOFs (Figure 1.5).

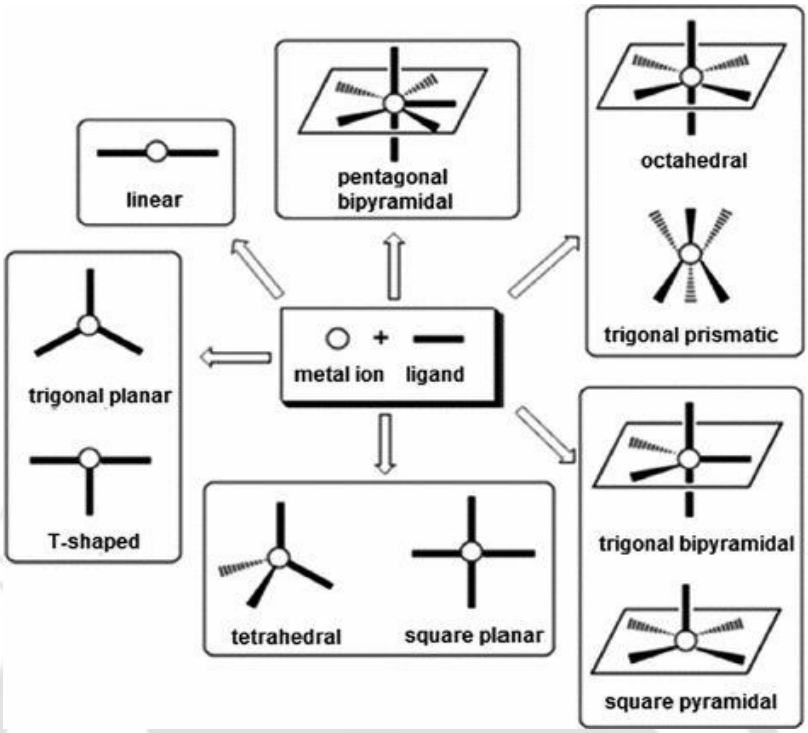

Figure 1.5 Coordination geometries of metal ions. Reproduced with permission from ref. 92. Copyright 2009, Elsevier.

The choice of an organic linker depends on the number of Lewis-basic sites present in ligands and relative angularity of the binding sites. There are various types of ligands including neutral, anionic and cationic organic ligands (Figure 1.6).[93] Ligands should possess some common characters for MOF formation such as: they should be rigid so that after removing the guest molecules in the pores, the ligands can still maintain the open pore structure. For that reason, organic ligands containing rigid phenyl rings are widely used, while flexible long chain molecules such as alkanes are not employed commonly. Moreover, the ligands should be multi-dentate so that they are able to connect between metal centers to form extended networks. Neutral organic ligands such as 4,4'-bipyridyl and anionic organic ligands like benzene-1,4-dicarboxylic acid (H_2BDC) are widely used to build a variety of MOF structures. As carboxylates have the ability to aggregate metal into M-O-C clusters and result in more stable structures than others, they are widely used in MOF construction. Cationic ligands are not generally employed due to their low affinity towards metal ions.[94] During the formation of the spacer-node-spacer unit, the spacer linearity breaks. Hence, coordination geometry, size of linkers and angularity of the

ligands and metal clusters are essential components to describe the crystal structure of the MOFs.

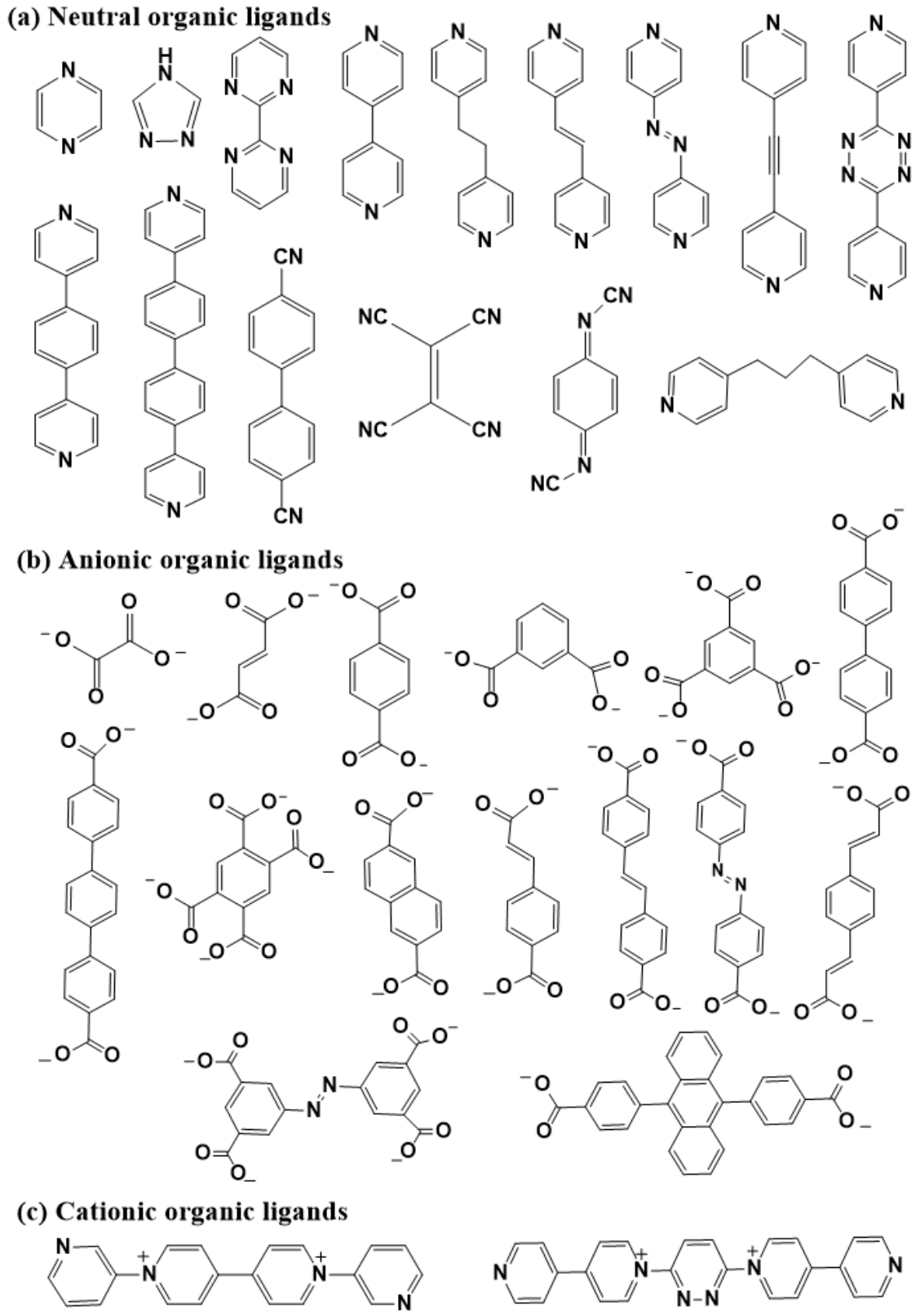

Figure 1.6 Examples of some neutral, anionic and cationic ligands employed for the synthesis of MOFs.

The concept of a secondary building unit (SBU) was considered as an organizing concept for the classification of MOF structures. The SBU concept is very much essential to design, identify and describe the geometry of MOF materials.[95] SBUs are basically constructed from metal containing clusters which are formed by the aggregation of metal ions and multi-dentate linkers to form well-defined and highly symmetric coordination geometries (Figure 1.7).[96] The SBUs serve as rigid vertices which are connected through organic ligand molecules to form robust frameworks with high structural stability and permanent porosity. Relative spatial arrangements and modification of the SBU can bring interesting properties in MOFs for its application in a particular field. Interestingly, the chemical structural flexibility of MOFs can also lead to dramatic changes in local coordination environment, which varies the luminescent properties and make them suitable for sensing applications.[97]

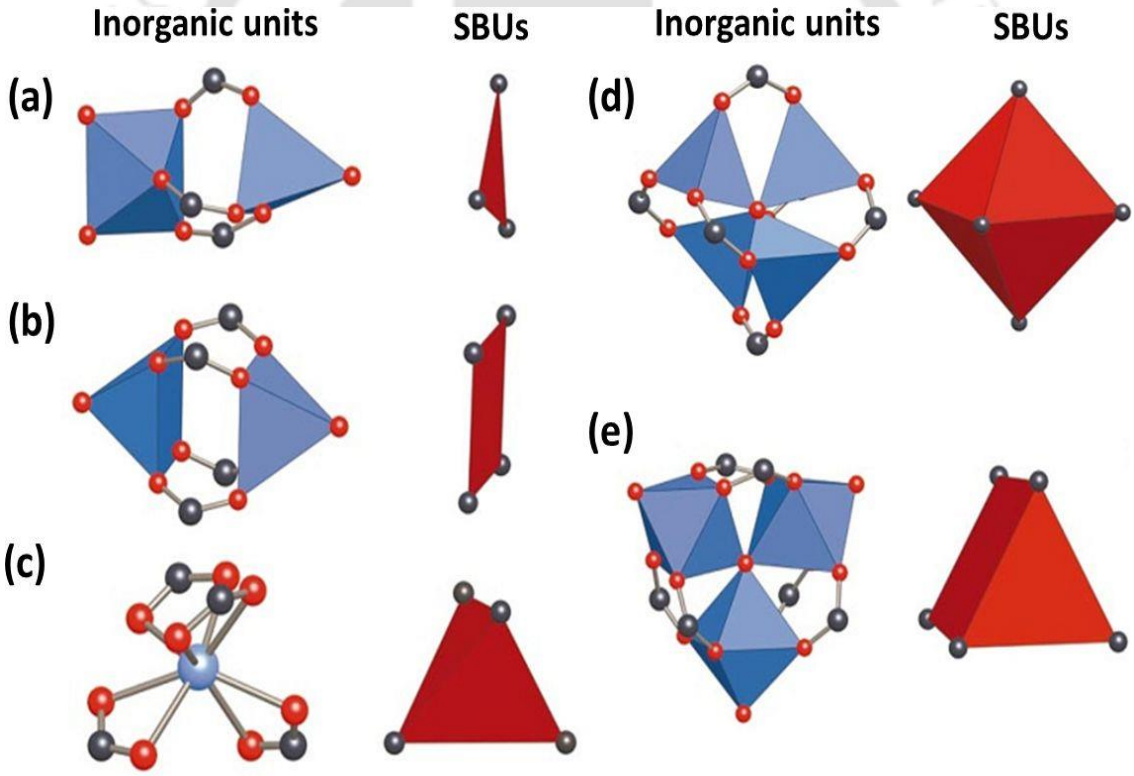

Figure 1.7 Examples of SBUs: (a) triangular, (b) square planar, (c) tetrahedral, (d) octahedral and (e) trigonal prismatic. Color codes: O, red; C, black. In inorganic units, metal-oxygen polyhedra are blue and the polygon or polyhedron defined by carboxylate carbon atoms (SBUs) are red. Reproduced with permission from ref. 98. Copyright 2003, Nature publishing group.

Several types of interactions exist during the formation of MOFs. Formation of coordination bonds between metal centers and ligands is the most common interaction. In addition, hydrogen bonds and other interactions like metal-metal bonds and π-π interactions are also found in the structures. Coordination bond is the strongest interaction among all of the interactions in MOFs. Structures with more coordination bonds show great stability. On the other hand, structures with more hydrogen bonds or other weak interactions suffer from structural stability.[99]

The last component present in framework of MOFs may be the guest molecules or template molecules, which can be removed later to leave open pore in MOF structures. As nature does not tend to form big void structures, MOFs are usually filled with guest molecules during synthesis. So, it is possible to add template molecules with specific sizes to modulate the pore size of MOFs. For example, organic amines can help to arrange the metal centers and ligands at appropriate distance during synthesis of MOF structures.[100]

1.4 Synthesis protocols of MOFs

Synthetic methods utilized for the preparation of MOFs have been developed in several stages. Traditional method is basically based on slow evaporation of the solvents or their diffusion over time to form large single crystals of very small quantity over weeks to months. Later, solvothermal method was applied to reduce the reaction time and get product with good yield. Since products are considered to be thermodynamically or kinetically controlled, several factors such as solubility of the organic linker and metal salt, solvent polarity, pH, ionic strength of the medium, temperature or pressure can play key roles to determine the nature of the products. Ligands need to be deprotonated before coordination with the metal ions. For deprotonation of the organic linker molecules, generally amide co-solvents (such as alkyl formamides and pyrrolidinones) are used, which undergo thermal decomposition on heating. To increase the crystallinity, modulated synthesis of several MOFs has been employed by utilizing common mono carboxylic acids (e.g., acetic acid, formic acid, trifluoroacetic acid and benzoic acid) and HCl. It is assumed that modulators play two important roles during the synthesis: (i) facilitate the formation of metal clusters and the growth of crystals and (ii) slow down the crystal growth rate by competing with organic ligand molecules for the coordination sites at the metal centers. Current research work is mainly focused on the development of industrial applications of MOFs as functional devices. In this context, different methods are adopted in modern days, which are discussed below.

1.4.1 Diffusion method

Diffusion method is a traditional method to form crystalline materials. Generally, two types of diffusion methods have been followed. In one method, layering is done by immiscible solvents: one is the precipitant solvent and the other one dissolves the product. They are divided by a layer of solvent. The precipitant solvent is regarded as 'anti-solvent' as the reactant is insoluble in it and the liquid in which the dissolution of reactant takes place is regarded as 'solvent'. At the interface, crystal growth occurs due to the gradual diffusion of the precipitant solvent into the separate layer. In another method, generally gradual diffusion of reactant occurs through dividing barrier. Sometimes, gels are applied as crystallization and diffusion media to reduce the diffusion rate and prevent the precipitation. The obtained single crystalline compound is characterized by X-ray diffraction technique.[101, 102]

1.4.2 Hydro/solvothermal synthesis

Originally, this method was first employed during synthesis of zeolites. It has also been set for the synthesis of MOFs.[103] Generally, stainless steel autoclaves or sealed Pyrex tubes are used at high temperature and pressure containing mixture of linker, metal salt and solvent (Figure 1.8).[104] In hydrothermal synthesis, only water is employed as the solvent. On the other hand, solvothermal synthesis includes various solvents other than water that are heated above the boiling point of the solvent under autogenous pressure. The superheated solvents reduce the viscosity and enhance the diffusion of chemical species. Furthermore, at higher temperature, the dielectric constant decreases which help to solubilize the chemical species in the solvent.[105] However, this method usually requires long reaction times (sometimes several hours up to several days) depending upon the factors including reaction solvent, reaction temperature, reagent concentrations, etc.[106]

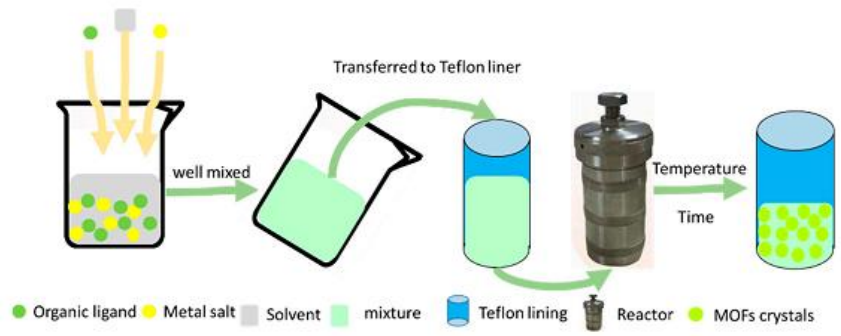

Figure 1.8 Schematic diagram for MOF synthesis by hydrothermal method or solvent heating method. Reproduced with permission from ref. 107. Copyright 2018, MDPI.

1.4.3 Microwave method

Solvothermal synthesis usually requires long reaction times (days to weeks), bulky equipment and high energy consumption. To overcome these limitations, microwave-assisted synthesis of MOFs has been developed.[108] Microwaves are normally produced by a magnetron which consists an oscillator converting high-voltage direct current into high-frequency radiation. In a typical laboratory instrument, waveguides transfer the generated energy from the magnetron to the sample chamber. Many solvent molecules, notably water, possess dielectric moments and rotate to align themselves with the alternating electric field of the microwaves. The heat generated due to the molecular movement and collision is dispersed in the molecules. The sample chamber is a Faraday cage which restricts the microwave radiation escaping into the environment. The main advantage of microwave synthesis is that energy is generated directly throughout the bulk of the material instead of by conduction from the external surface. Furthermore, microwave heating is almost instantaneous, occurs without heating the container and allows the use of temperatures above the boiling point of a used solvent. Microwave technique typically cannot produce single crystals but shape and size of particles can be finely controlled by this method.[109, 110]

1.4.4 Electrochemical method

Electrochemical method is predominantly applied for producing MOF powders on industrial scale.[111] The benefits of this method compared to solvothermal synthesis are low reaction temperature and quick reaction time. In bulk scale, there is limitation in crystallization for the in-situ production of the metal ions near the support surface, which actually diminish the unfavorable accumulation of crystals during the synthesis of membrane.[112] Furthermore, compared to solvothermal techniques, electrochemical synthesis method possesses more parameters for fine-tuning due to the simple adjustment of the voltage or imposing particular signals. Experimental set-up for electrochemical synthesis and coating of a ZIF (ZIF = zeolitic imidazolate framework) material is represented in Figure 1.9.[113]

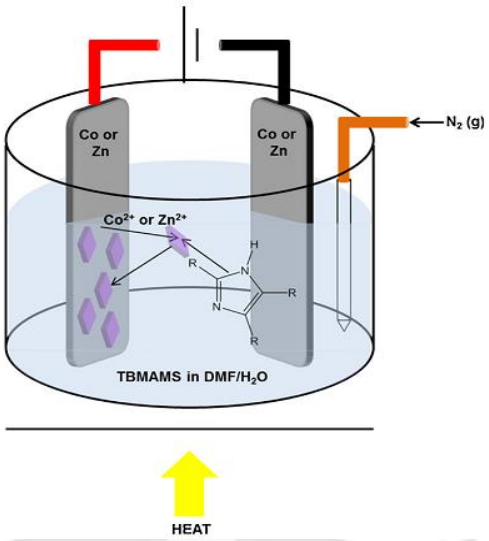

Figure 1.9 Illustration of the experimental setup used to synthesis ZIF coatings. Two Co or Zn electrodes are immersed in a tributylmethylammonium methyl sulphate (TBMAMS) in *N*,*N*-dimethylformamide (DMF):H_2O electrolyte solution containing an imidazolate linker. Heat is applied whilst deaerating the solution with gaseous N_2 and 2.5 V applied potential difference generates the ZIF coating on the anode. Reproduced with permission from ref. 113 . Copyright 2015, Elsevier.

1.4.5 Mechanochemical method

Mechanochemistry is basically a solvent free process in which grinding of two reactants with a pestle and mortar can produce the desired compound.[114] Ball mill process is actually a programmable mechanochemical process where no physical effort is required. Hence, it allows more systematic studies of the process.[115] The supplied kinetic energy has various effects on a crystalline solid including heating, reduction of particle size, local melting, phase changes to alternative polymorphs, formation of defects and dislocations in crystal lattices.[116] Different methods are adopted in mechanochemical synthesis which involves neat grinding, grinding-annealing, liquid assisted grinding, kneading, etc. It has been observed that solvent-free reactions produce very pure products and reduce the formation of solvated species.[117] Hence, this process has great importance for crystal engineers and solid-state chemists. Schematic presentation of mechanochemical synthesis of BIT-11 and BIT-11b (Ni-substituted ZIF-8 is denoted as BIT-11) is represented in Figure 1.10.[118]

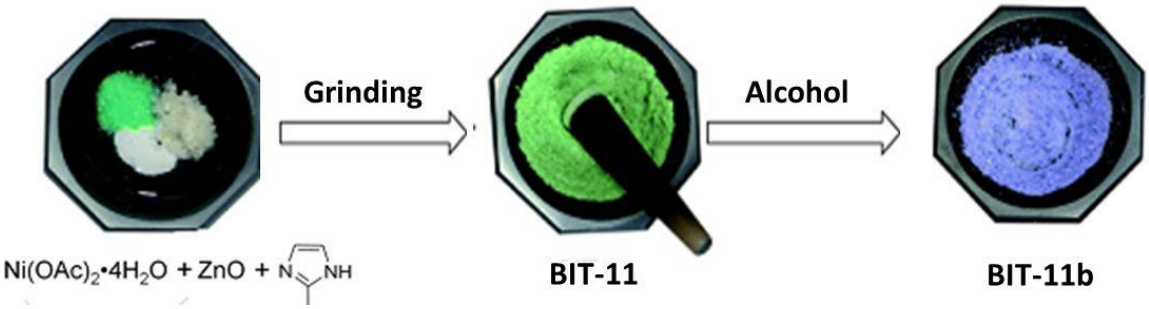

Figure 1.10 Schematic representation of the mechanochemical synthesis of BIT-11 and BIT-11b. Reproduced with permission from ref. 118. Copyright 2014, Royal Society of Chemistry.

1.4.6 Sonochemistry method

In sonochemistry method, high-energy ultrasound is utilized to a reaction mixture to obtain the product.[119] The dissolution of starting compounds can be enhanced by ultrasonication. Recently, the syntheses of organic compounds and nanomaterials are carried out through the application of sonochemistry.[120] In the field of MOF science, the main reason to adopt sonochemical synthesis is that it is quick, energy-efficient, environment friendly, easy to handle and can be applied at ambient temperature.[121] Special interest can be taken in future for scaling up of MOFs by this method.

1.4.7 Post-synthetic modification

The introduction of a particular functional group in MOFs for a special application is sometimes difficult due to the high sensitivity and reactivity of the additional functionality during the formation of MOFs. An efficient route to obtain MOFs having desired functionality is post-synthetic modification (PSM) .[122] This method was originally suggested by Hoskins and Robson in 1990.[50] Actually, in PSM, a MOF can be synthesized and modified in a heterogeneous manner after the formation of the solid lattice instead of synthesis of functionalized MOFs directly (Figure 1.11).[123] PSM is advantageous compared to the pre-functionalization approach because of greater control over the types and number of functional groups that can be incorporated into the framework. Furthermore, by using PSM, both the metal and organic species can be functionalized without affecting the overall stability of the framework.[124] Hence, PSM is regarded as an excellent tool for preparing topologically identical, but functionally diverse frameworks.

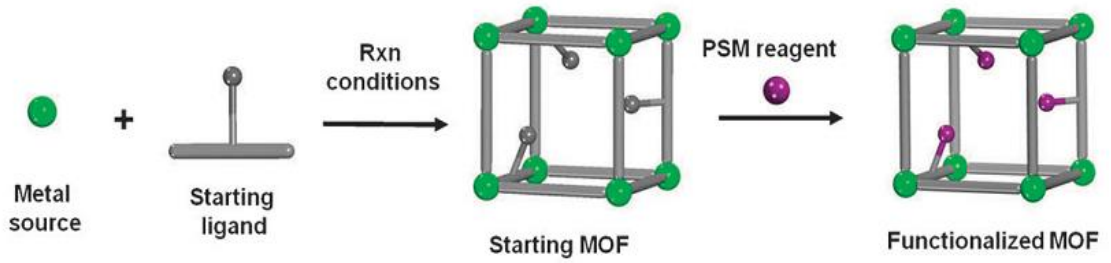

Figure 1.11 A generic scheme for the post-synthetic modification (PSM) of MOFs. Reproduced with permission from ref. 125. Copyright 2011, Royal Society of Chemistry.

Covalent modification is considered as the most popular route of PSM, in which functionalization of MOFs are performed for specific applications. PSM of amino group functionalized MOFs by aldehydes, anhydrides, isocyanates, acyl chlorides and alkyl bromides have been reported.[126] Moreover, covalent modification of azide-functionalized MOFs through click reactions is also possible. The reactive azide groups in the MOF cavity undergo quantitative click reactions with alkynes to form various MOFs having tailored pore surfaces.[127]

Besides covalent modification, dative modification of MOFs through post-synthetic metalation was also developed. MOF with 2,2′-bipyridine (bpy) sites can be post-synthetically metalated with soft metal Cu^{2+} and Pd^{2+}.[128] The coordinatively unsaturated metal sites in MOFs can be modified by additional ligands. For instance, the vacant coordination sites in some Cr and Cu-based MOFs could be modified with alkane amines to improve CO_2 uptake.[129, 130] The coordinatively unsaturated Zr_6-clusters can also bind with carboxylates through simple acid/base reactions. For example, the solvent-assisted ligand incorporation (SALI) method was developed for modifying the coordinatively unsaturated Zr-cluster of NU-1000 to enhance CO_2 uptake.[58]

Post-synthetic ligand and metal ion exchange have been developed as efficient methods to gain new MOFs with various ligands and metal ions.[131] Actually, the inert metal-ligand bonds in stable MOFs will significantly obstruct the process of the ligand and metal ion exchange. However, recent studies on the ligand and metal ion exchange of several stable MOFs prove that the robustness of such metal-ligand bonds was overestimated. Post-synthetic metal and ligand ion exchange processes were applied for several stable MOFs such as ZIFs, MIL series and UiO series.[132]

1.5 Characteristic features of aqua stable MOFs

For the successful application of MOF materials in fluorescence detection of environmental and biological chemical species under real conditions, the materials should be highly aqua stable. Hence, the design and synthesis of new aqua stable MOFs are highly desirable for practical applications. Different types of strategies have been used for the synthesis of water-stable MOFs. A brief description about the characteristic features of aqua-stable MOFs are discussed here.

1.5.1 High connectivity and bond strength of metal and ligands

Higher connectivity of the metal node with ligand provides greater stability to the framework. Actually, higher connectivity between metal node and ligand repairs the structural defect. Hence, probability of structural decomposition becomes lesser.[133] From a kinetic point of view, the decomposition of MOFs in solutions mainly occurs due to successive replacement of coordination moieties by small molecules. During this process, structural defects occur, which finally lead to the decomposition of overall framework. On the other side, framework with higher connectivity suppresses the ligand dissociation process and at the same time enhances the ligand association rate, leading to faster defect repairment. For example, in PCN-601, a 4,12-connected network is observed. The connectivity of both Ni_8 and pyrazolate-based porphyrinic ligand (a 4-connected linker) is relatively high among the reported inorganic clusters and organic ligands (a 12-connected node).[134] Not only connectivity but also strength of the metal–ligand bond plays crucial roles for the stability of MOF. According to the HSAB principle, stable MOFs are mostly developed from carboxylate-based ligands (hard Lewis bases) and high-valency metal ions (hard Lewis acids), or azolate-based ligands (soft Lewis bases) and low-valency transition metal ions (soft Lewis acids). Following this strategy, a huge number of aqua stable MOFs have been reported.[135]

1.5.2 Rigidity of ligand molecule

The rigidity of ligand molecules plays crucial roles to determine the robustness of the framework. It has been observed that the length of the ligand molecule is directly related to the activation energy of ligand dissociation and thus influences the stability of MOFs.[136] If we compare two isoreticular frameworks having long and short ligands, in transition state, ligands coordinated with the inorganic clusters are required to be bent. Assuming the displacements of the ligand terminals in the transition states are equal in the

two cases ($d_s = d_l$), the short and rigid ligand would be bent to a larger angle ($\theta s > \theta_l$) (Figure 1.12). This phenomenon enhances the activation energy of decomposition. That means greater energy will be required to decompose the framework. Hence, frameworks with short and rigid ligands show greater stability.[134]

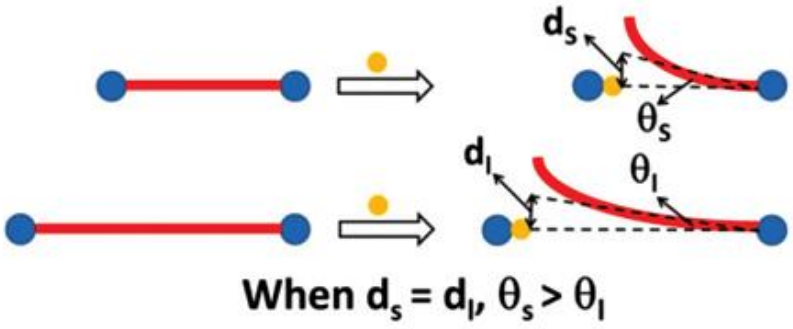

Figure 1.12 Illustration of the kinetic stability of MOFs with ligands of different lengths. Reproduced with permission ref. 134. Copyright 2016, American Chemical Society.

1.5.3 Hydrophobicity of ligand

Electrophilic metal centers of MOFs can be attacked by nucleophilic water molecules and can decompose the framework if the energy of this interaction is greater than the activation energy of the hydrolysis reaction.[137] Hence, the stability of MOFs in aqueous medium can be enhanced by installing hydrophobic functional groups in the ligands. The presence of hydrophobic groups in the MOFs enhances the pore hydrophobicity and repeals the water molecules, which protects the framework from further interactions with water molecules.[138] Methyl, ethyl, phenyl or long chain alkyl groups including fluorinated functional groups are commonly used for the design of hydrophobic ligands.[139] The water adsorption capacity gradually decreases with pore hydrophobicity, which can be directly measured by performing the water adsorption isotherms on the sample. ZIF-8 is a typical example where the methyl group on the ligand resists the water molecules from attacking the [ZnN_4] units.[140]

The transformation of hydrophilic to hydrophobic MOFs *via* PSM method was also applied. This transformation can be achived by mainly two methods. In one method, the ligand present in MOFs can be functionalized by hydrophobic groups by PSM method.[141] For example, Zhang et al. carried out diffusion controlled PSM wherein they observed ~9% loading of octadecanamine (C_{18} amine). This led to a drastic change in the water contact angle (WCA) of ZIF-90 from hydrophilic region to hydrophobic region, i.e. ~130°

after 16 h. Drastic change in water adsorption cpacity was also visualised. Furthermore, no change in XRPD patterns was observed after PSM (Figure 1.13).[142] Secondly, the surface of the MOF material can be coated by hydrophobic materials to enhance the moisture stability.[143]

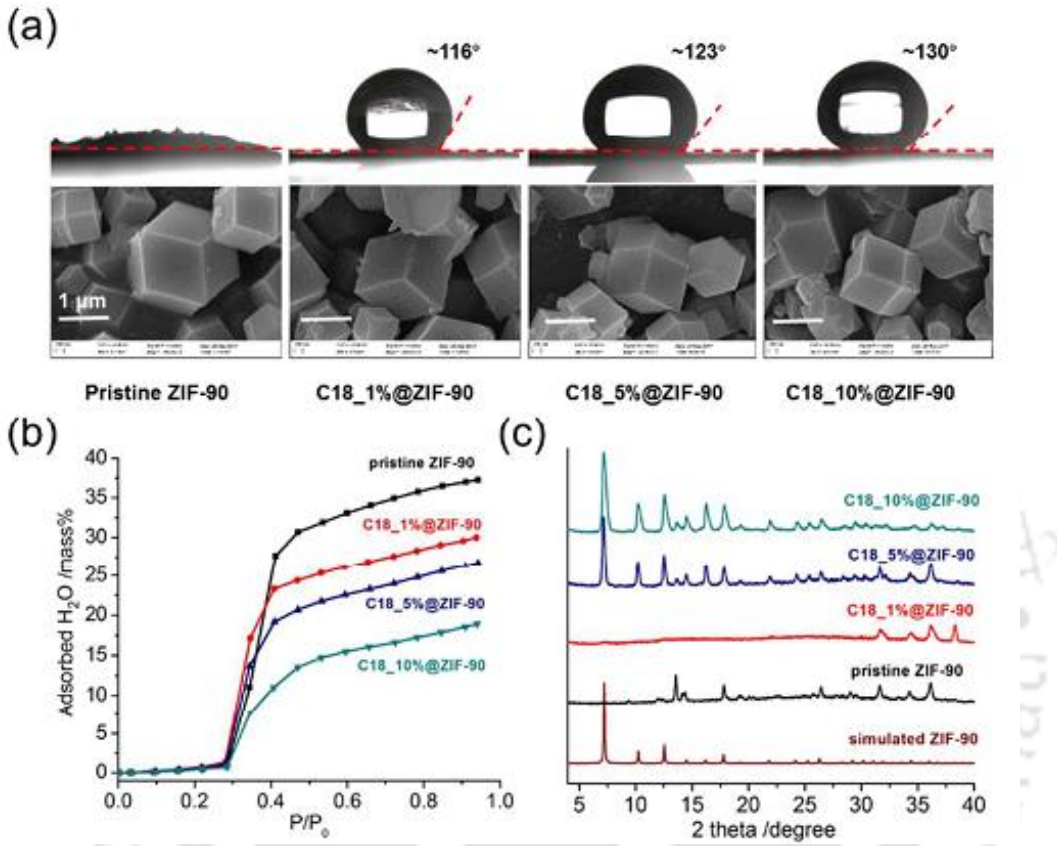

Figure 1.13 Performance evaluation after functionalization. (a) Surface hydrophobicity: SEM images (bottom) and corresponding relative contact angles of water (top). (b) Water adsorption: vapour adsorption isotherms at 298 K. (c) Hydrothermal stability: XRPD patterns after treating the samples in boiling water for 24 h. Reproduced with permission from ref. 142. Copyright 2018, Royal Society of Chemistry.

1.6 Key features of MOFs for fluorescence sensing and bio-imaging

A fluorescent sensor must have desired selectivity, sensitivity, fast response time, material stability and reusability. MOFs exhibit unique characteristic features to become excellent chemical sensors. The porous structures of MOFs can potentially preconcentrate the analytes to gain enhanced sensitivity towards particular analyte. The key features of MOFs to act as a luminescent sensor material is described below:

1.6.1 Predictable structures

Fluorescence properties of MOFs greatly depended on the structural arrangement and intermolecular packing of the compounds for their energy transfer. Hence, it is very much important to control the three-dimensional structure and intermolecular packing at the molecular level. However, during construction of solid-state inorganic materials, the chemical driving force is ionic bonding which is very strong and thus the solid-state syntheses of inorganic materials at high temperatures generally lead to the formation of inorganic solid materials without predictable structures. Hence, the preparation methods for inorganic solid materials have been criticized as the "shake and bake", "mix and wait", and "heat and beat" methodology.[144] The bond connectivity within organic molecules and metal-organic complexes is predictable but the overall three-dimensional packing structures of such types of compounds are still not predictable because some weak intermolecular interactions such as hydrogen bonding, van der Waals interactions and aromatic π-π interactions are there to control the overall 3D molecular packing.[145] The bond energy of the coordination bonds in MOF materials is moderate, which allows the reversible formation and breaking of chemical bonds during the syntheses of MOFs, allowing the formation of thermodynamically stable MOFs. In situ formed metal-containing clusters (generally termed as secondary building units (SBUs)) have some preferential co-ordination geometries. Moreover, the 3D connectivity of these metal ions and/or metal-containing clusters (as the nodes) with organic linkers of predetermined shapes has led to the construction of MOFs with a higher degree of predictable structures.[146]

1.6.2 Processability in nanoscale

Nanoscale MOFs are needed for the application in the fields of biology, drug delivery and biomedical imaging.[147] Actually, without nanoscale dimension, the internalization of the material into cells is not possible. The nano-MOFs show different or at least enhanced properties compared to bulk materials due to the high surface-to-volume ratio and quantum size effects. In addition, unique size-dependent optical, electrical and magnetic properties are also shown by nano-MOFs.

The nano-MOFs cannot be achieved by using conventional synthetic routes such as hydrothermal/solvothermal methods or slow diffusion method. Moreover, the conventional routes have several limitations on scaling up. Therefore, alternative methods such as the microwave assisted method, sonochemical and electrochemical methods have

been successfully introduced for synthesis of nano-MOFs.[148] Actually, microwave radiation and ultrasounds accelerate the nucleation process and increase the seed number which basically inhibits the growth of MOF crystals. Moreover, self-assembly of nano-MOFs can be confined into droplets by microemulsion and can have great control on the surface of substrates by templates.

Typically, sizes of nano-MOFs lie on the 100 nm scale, with few extending below 20 nm.[149] But, it has been well established that particles having size nanometer to micro-meter can be taken up by mammalian cells.[150, 151] In the earlier time, nano-MOFs were mainly focused for drug delivery and bioimaging.[152, 153] As the nano-MOF science progresses, more functional nano-MOFs are developed for medical applications. For example, the porphyrin or porphyrin derivatives-based nano-MOFs are proved to be very efficient in photodynamic therapy (PDT) of cancers, which can overcome the self-aggregation of porphyrin molecules in physiological conditions.[154, 155] Although the nano-MOFs for biomedical applications are still in the preclinical stage, some Fe and Zn-based nano-MOFs have shown good response in medical application due to their low toxicity and high therapeutic effect.[156] We expect the development of excellent nano-MOFs for clinical applications in near future.

1.6.3 Biocompatibility of MOFs

Biocompatibility is a property of a material, which means a material is not harmful for living tissue.[157] Biocompatibility is an important factor in design and synthesis of MOFs for biomedical applications. Biocompatible MOFs should have endogenous linkers which are bio-friendly and non-toxic in nature.[158] In addition to the choice of non-toxic ligands, choice of metal ions is also an important factor for the synthesis of biocompatible MOFs. According to the toxicological studies, some metals (e.g. Ca, Mn, Fe, Zn, Mg and Zr) are regarded as biocompatible ions for biological applications due to their considerable high lethal-dose levels of at least 1g kg^{-1}.[159-161]

Biocompatible MOFs are generally applied in the field of bioimaging and drug delivery. Some Gd^{3+}-, Mn^{2+}- and Fe^{3+}-containing MOFs showed great efficiency for bioimaging.[156] Due to the relatively greater biological toxicity of Gd ions, Mn^{2+}-based MOF contrast agents have been gradually developed because of the lower toxicity of Mn^{2+} than that of Gd^{3+}.[162, 163] Furthermore, two kinds of MOFs with UiO-66 structure containing high contents of Zr (37 wt%) and Hf (57 wt%) were reported. They are functionalized by silica and PEG, and exhibited high performance as CT contrast agents for spleen (131 HU)

or liver (86 HU) imaging.[164] MOF materials are also excellent candidates to deliver drugs due to their good biological safety and inherent porosity. In addition, the biggest advantage of MOFs as drug carrier agent is not only the high drug loading capacity, but also the long drug release time. Ferey et al. first encapsulated ibuprofen in a MOF in the year 2006. Ibuprofen has been utilized as a model drug in this study.[157] In 2010, Horcajada et al. reported the use of a series of non-toxic porous Fe(III)-MOFs, i.e. MIL-53, MIL-88A, MIL-88Bt, MIL-89, MIL-100 and MIL-101-NH_2, as carriers of antineoplastic and retroviral drugs, including busulfan, azidothymidine triphosphate, doxorubicin, cidofovir, ibuprofen, caffeine, urea etc.[165] Despite the concern on the stability of MOFs, the stability was reported to be significantly improved by coating polymer materials. For example, coating polydimethysiloxane (PDMS) on the surface of MOF materials can greatly enhance their moisture or water resistance. However, some of MOFs are also focused for oral administration and in-vivo application.[166] In future, continuous efforts need to be focused on biostability, biocompatibility and practicability to realize the full clinical applications of MOFs.

1.6.4 Collaborative luminescence properties

Fluorescent MOF materials are somehow different from other traditional inorganic and organic luminescent compounds for their potentially collaborative multifunctionalities. The organic moieties, metal centers, metal-organic charge transfer and guest molecules within MOFs can potentially generate luminescence.[167] All such interesting features help to develop MOFs as great luminescent materials. The permanent porosities and collaborative luminescent properties of MOFs are particularly useful to develop luminescent sensing materials for recognition of partcular analytes.[168, 169] Actually, judicial choice of metal ions and fine tuning of functional groups in MOFs can bring special properties in MOFs which enhance the detection abiliy of MOFs towards particular analyte. Several luminescent MOFs have been successfully employed for sensing and bioimaging applications.[170-172]

1.7 Origin of fluorescence in MOFs

When light is produced by absorption of energy, it is called luminescence. Now, luminescence has been clssified in two basic forms based on multiplicity of spin state during the radiative relaxation process. Those are fluorescence and phosphorescence. In fluorescence, emission occurs due to transition of electron between energy states having

the same spin multiplicity. This process generally occurs not more than about 10 ns. However, in phosphorescence, emission arises due to transition of electron between states with different spin multiplicity. The lifetime of this process is much greater than fluorescence (microsecond to second). Examples of MOFs having phosphorescence properties are very rear.[173] But, a variety of MOFs have been developed exhibiting fluorescence properties and subsequently applied for different purposes. Fluorescence can arise from organic ligands present in MOFs (specially from highly conjugated ligands), metal ions (widely observed in lanthanide based MOFs through antenna effect) and charge-transfer i.e. ligand-to-metal charge transfer (LMCT) and metal-to-ligand charge transfer (MLCT). Furthermore, the guest molecules can bring fluorescence property in MOFs (Figure 1.14).

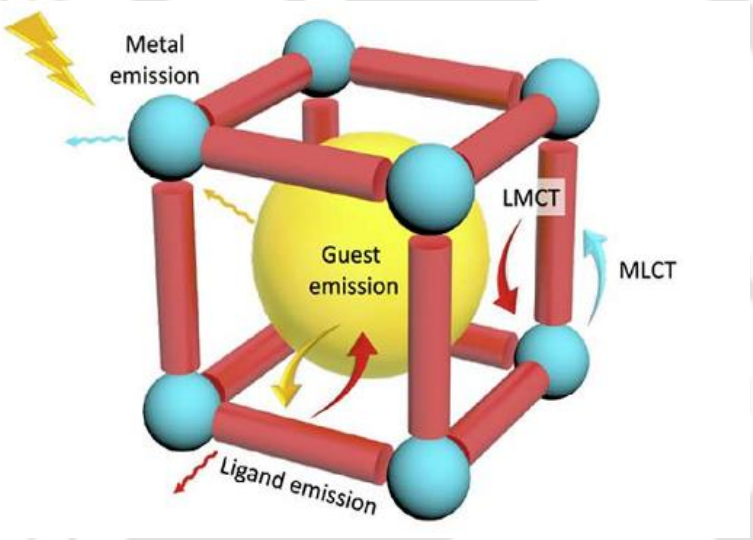

Figure 1.14 Representation of possible emission modes in MOFs. Inorganic SBUs, blue sphere; organic ligands, red cylinders; guest chromophores, yellow sphere inside. Reproduced with permission from ref. 174. Copyright 2018, Elsevier.

1.7.1 Ligand based fluorescence

When an organic molecule is excited by photon of appropriate energy, several photophysical events happen, which include internal conversion or vibrational relaxation, inter-system crossing, fluorescence and phosphorescence (Figure 1.15). The fluorescence property of organic molecules arises due to the radiative transition from its first singlet state excited state S_1 to the ground singlet state S_0, which is spin-allowed. The fluorescence properties can be characterized by the following parameters: (1) fluorescence spectrum,

which is defined as fluorescence intensity as a function of wavelength, (2) quantum yield, which reveals the efficiency of the fluorescence process. Generally, it is defined as the ratio of the number of photons emitted in the process to the number of photons absorbed and (3) lifetime, which signifies the average time spent by the molecule in its excited state before emitting a photon.[175]

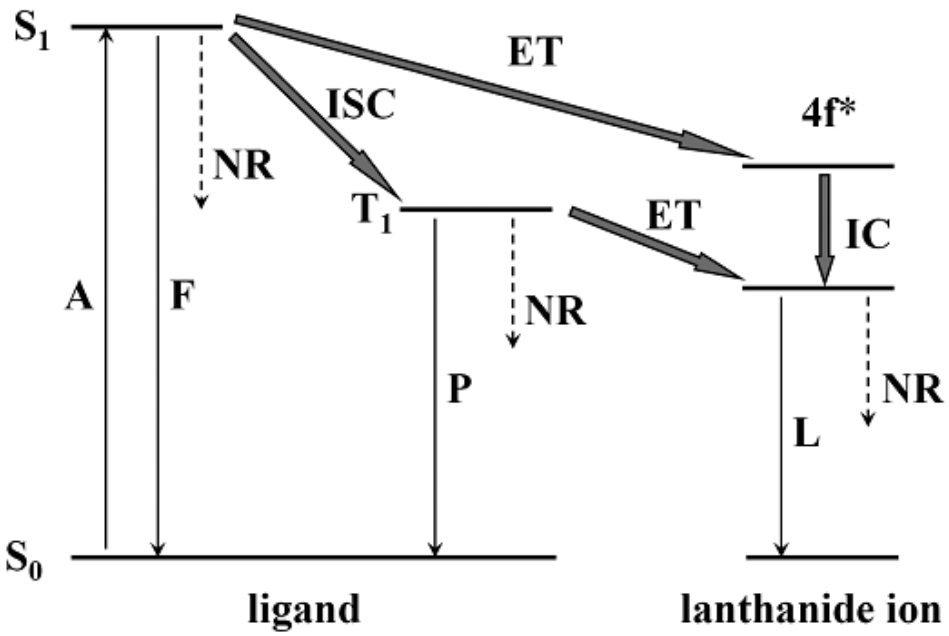

Figure 1.15 Jablonski diagram displaying the energy absorption and emission in MOFs. Abbreviations: A = absorption; F = fluorescence; P = phosphorescence; L = lanthanide-centered luminescence; ISC = intersystem crossing; ET = energy transfer; IC = internal conversion; S = singlet; T = triplet. Plain arrows indicate radiative transitions; dotted arrows indicate non-radiative transitions. Reproduced with permission from ref. 22. Copyright 2012, American Chemical Society.

In luminescent MOFs, π-conjugated rigid organic molecules with multi-carboxylate groups or heterocyclic groups are commonly employed as linkers. The fluorescence properties such as maximum emission wavelength and lifetime in solid MOFs are often different from the free ligands used for MOF formation. This is because the organic ligands are stabilized within MOFs, thus reduces the nonradiative decay rate which leads to increament in fluorescence intensity, lifetimes and quantum efficiencies. In the solid state, molecular interactions bring the molecules close together, which enable charge transfer among the organic ligands resulting in shift of spectra, broadening of

emission band and loss of fine structure. Furthermore, the spatial orientation and arrangement of linkers and overall coordination environment within MOFs can have influence on the fluorescence properties of the organic linkers. Actually, these factors may induce different intramolecular or intermolecular interactions among organic ligand molecules.[167] Hence, by controlling these interactions, tuning of the luminescence properties of MOFs can be possible. For example, a Zn-MOF constructed from 2,4,6-pyridine tricarboxylate ligand showed emission maxima at 467 nm, whereas free ligand showed emission maximum at 417 nm when excited at 338 nm. The red shift of emission band clearly suggested the formation of MOF structure which maximized the intramolecular/intermoleculear interactions among the organic linkers for their energy transfer and decreased the intraligand HOMO-LUMO energy gap.[176]

In excited state, fluorescence of organic ligand molecules can also be influenced by reversible changes of electronic distribution. The two important processes are excited-state electron transfer (ESET) and proton transfer (ESPT). The electrons in the excited state can move from the electron-rich donor to the electron acceptor during ESET process, while in ESPT process, the protons move instead of electron in the excited state to depart or join the molecule. ESPT is a very fast process as compared to fluorescence emission. The intramolecular proton transfer is much faster than intermolecular transfer process.[175] Jayaramulu et al. showed the luminescence change induced by excited-state intramolecular proton transfer (ESIPT) for both free H_2DHT organic linker and resulting MOF $Mg(DHT)(DMF)_2$ (DHT = 2,5-dihydroxyterephthalate). Both of the ligand and MOF exhibited tunable emission in different solvents due to ESIPT-induced fluorescence changes in different solvents.[177]

1.7.2 Metal centered fluorescence

Metal centered fluorescence is mainly observed for lanthanide based MOFs. Gradual filling of 4f orbitals with electrons is observed for lanthanide ions. Each lanthanide ion shows narrow and charcteristics 4f-4f transition.[178] From ultraviolet (UV) to visible and near-infrared (NIR) ranges, luminescent f-f emission has been observed for lanthanide ions. The Eu^{3+}, Tb^{3+}, Sm^{3+} and Tm^{3+} ions emit red, green, orange and blue light, respectively, whereas the Yb^{3+}, Nd^{3+} and Er^{3+} ions exhibit the near-infrared luminescence. Due to forbidden f-f transitions, generally lanthanide ions display weak absorption. Hence, high-power laser excitation is utilized for the excitation of lanthanide ions. This difficulty can be overcome by coupling species which can participate in energy transfer processes,

known as "luminescence sensitization" or "antenna effect". Raymond et al. showed that 2-hydroxyisophthalamide (IAM) ligand can sensitize four Ln(III) cations such as Tb(III), Eu(III), Sm(III) and Dy(III) (Figure 1.16).[178] In MOFs, the mechanism of antenna sensitization mainly occurs in three steps: organic ligands present in MOFs first absorb the light, after that energy is transferred to the lanthanide ions from organic ligands, last of all luminescence is generated from the lanthanide ions. One of the main energy migration paths is ligand-centered absorption followed by intersystem crossing $S_1 \rightarrow T_1$, $T_1 \rightarrow Ln^{3+}$ transfer and metal-centered emission. This phenomenon can be explained by Jablonski diagram displayed in Figure 1.15. Another possibility is the direct energy transfer from the excited singlet state S_1 to the energy levels of the lanthanide ion, which is known for Eu^{3+} and Tb^{3+}.[179]

By the use of antenna effect of organic ligands, efficient lanthanide MOFs can be obtained. The lowest triplet state of the organic linkers should be located at an energy level nearly equal to or above the resonance level of the lanthanide ions. The energy of the triplet state must be finely tuned to maximize the transfer and minimize the back-transfer process. Thus, by choosing appropriate organic ligand, luminescence property of lanthanide MOFs can be tuned. For example, in the isostructural lanthanide (Sm^{3+}, Eu^{3+}, Gd^{3+}, Tb^{3+}, Dy^{3+}) MOFs containing 4,4′-disulfo-2,2′-bipyridine-*N*,*N*′-dioxide ligand, the triplet state energy levels of organic linker were calculated to be 24038 cm^{-1}.[180] Hence, the organic ligand is able to sensitize the trivalent ions and strong emissions have been observed in Eu^{3+} and Tb^{3+} incorporated MOFs.

Figure 1.16 Observed emission from Ln(III) cations sensitized by 2-hydroxyisophthalamide (IAM) ligand irradiated with a standard laboratory UV lamp (λ_{ex} = 365 nm). From left to right, ligand only, Tb(III), Eu(III), Dy(III) and Sm(III) complexes. Reproduced with permission from ref. 178. Copyright 2009, American Chemical Society.

1.7.3 Charge transfer fluorescence

Charge transfer fluorescence is an allowed process, in which transition occurs from excited state to ground state. There are two types of charge transfers found in MOFs: one is ligand-to-metal charge transfer (LMCT) and another one is metal-to-ligand charge transfer (MLCT). LMCT occurs due to electronic transition from localized orbital of organic ligand molecule to a metal-centered orbital. In case of MLCT, exactly opposite scenario is observed. That means electronic transition from a metal-centered orbital to an organic ligand-localized orbital is observed.

MLCT fluorescence has been found in a five-coordinated Mn-MOF named Mn(Hbidc) (H_3bidc = 1H-benzimidazole-5,6-dicarboxylic acid).[181] This MOF showed a strong red emission in the range of 625-850 nm. The strongest emission in Mn-(Hbidc) was observed at 726 nm, which was significantly red-shifted from the original emission of free organic linker (found at 440 nm). The strong emission of Mn(Hbidc) MOF was ascribed to MLCT luminescence in which the relatively large π-conjugated system of benzimidazole ring within $Hbidc^{2-}$ enhanced the charge transfer process from Mn^{2+} ion to the organic linker.

Fluorescence emission due to LMCT has been also reported in some MOFs. The Zn and Cd-based MOFs $[Zn(2,3\text{-pydc})(bpp)]_3{\cdot}2.5H_2O$ and $[Cd(2,3\text{-pydc})(bpp)\text{-}(H_2O)]_3{\cdot}3H_2O$ (2,3-pydcH_2 = pyridine-2,3-dicarboxylic acid)[182] showed intense fluorescent emissions at 436 and 438 nm upon excitation at 372 and 370 nm, respectively. But, the free ligand exhibited very weak photoluminescence property upon excitation at 370 nm, which suggested that ligand-to-metal charge transfer process was efficient in this system. Two copper MOFs namely $Cu_5\text{-}(SCN)_5(3\text{-Abpt})_2$ and Cu(SCN)(3-Abpt) consisting of 3-Abpt ligand (3-Abpt = 4-amine-3,5-bis(3-pyridyl)-1,2,4-triazole) displayed strong yellow LMCT fluorescence centered at 559 and 570 nm, respectively. The free 3-Abpt ligand exhibited a narrow emission band at 388 nm and a broad shoulder emission band at 441 nm.[183]

Sometimes, LMCT or MLCT fluorescence may compete with ligand-based fluorescence which result in both LMCT/MLCT and ligand-based emission bands. For example, when the zinc MOF $Zn_2(ATA)_3(ATA)_{2/2}$ was excited at 320 nm, a weak blue fluorescence emission at 485 nm was observed due to the LMCT or MLCT process and a strong emission at 392 nm appeared from ligand-based emission.[184]

1.7.4 Guest induced fluorescence

For the highly ordered structure and control over pore size, MOF materials can serve as potential hosts for the encapsulation of guest luminescent species such as lanthanide ions and fluorescent dyes. Generally, a huge change in photophysical property is observed for guest induced MOFs than the parent material, which is susequently utilized for different application purposes. A variety of lanthanide ion doped MOFs Ln^{3+}@bio-MOF-1 (Ln^{3+} = Tb^{3+}, Sm^{3+}, Eu^{3+} or Yb^{3+}) were synthesized by An et al. from the as-synthesized bio-MOF-1 through cation exchange process. The different cation-exchanged MOFs showed different colors (Eu^{3+}, red; Tb^{3+}, green; Sm^{3+}, orange-pink) in naked eye, when they were excited at 365 nm.[185] Moreover, the quantum yields of these lanthanide doped MOFs were quite high in aqueous medium, which suggested that the lanthanide ions were well protected within the pores and the energy transfers from MOFs to lanthanide ions occured in efficient way. Luo et al. prepared the Eu^{3+} and Tb^{3+} doped MOFs having tunable fluorescence properties, which were employed for detection of cations and anions.[186] Another MOF namely JUC-48 was encapsulated with Rh6G dye molecules which showed interesting temperature dependent fluorescent properties.[187] A Rhodamine B encapsulated MOF was reported for optical imaging purpose.[188] A fluorescent protein decorated MOF was also reported which showed interesting fluorescence property.[189] Furthermore, Karmakar et al. developed a cationic dye (3,6-diaminoacridinium cation (DAAC)) loaded bio-MOF-1 (i.e.bio-MOF-1⊃DAAC) which served as a selctive sensor for toxic CN^- anions.[190] Hence, it has been observed that encapsulation of fluorescent species in host MOFs brings interesting fluorescent property in comparison with unmodified MOFs, which helps in molecular detction.

1.8 Applications of MOFs

Presence of both organic and inorganic moieties within the structure of MOFs makes them a rapidly expanding class of materials of great interest with a wide variety of applications such as gas storage and separation, catalysis, chemical and physical sensing, drug delivery, proton conduction, optoelectronics and imaging (Figure 1.17).[2, 20, 32, 86] This thesis is mainly focused on the the fluorescence sensing applications of MOFs.

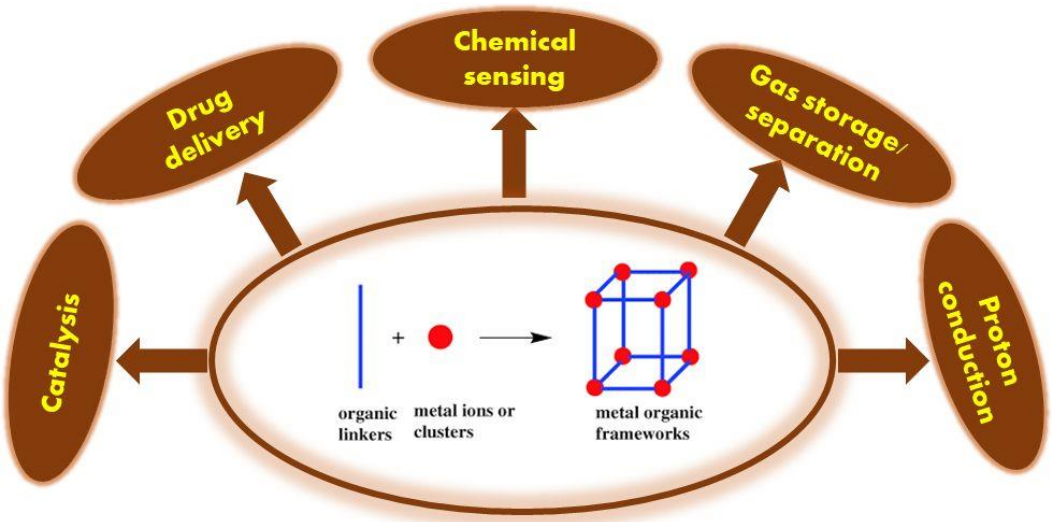

Figure 1.17 Various representative applications of MOFs.

1.8.1 Fluorescence sensing

A considerable amount of study was carried out by employing MOFs as a sensory materials in aqueous media based on the luminescence property of MOFs. Luminescence occurs when electrons in excited singlet states return to the ground state with emission of photon. This results to bring the luminescence property in MOFs, which may be quenched upon the absorption of analyte and it is known as the ‘‘turn-off’’ mechanism. Moreover, luminescence enhancement of MOFs is also possible after interaction with analytes which is described as a ‘‘turn-on’’ mechanism. The quantitative and qualitative analyses of targeted analytes can be performed by the luminescence enhancement, quenching or the movement of the emission wavelength. Till date, MOFs have widely been used for sensing purpose of ions, nitro explosives, volatile organic compounds, toxic compounds, gases, biomolecules, temperature, pH, humidity, etc.[2, 42] We will provide a brief discussion about the sensing study of toxic compounds and biomolecules in the next section as our study is entirely based on the fluorogenic detection of H_2S, formaldehyde (toxic species) and bilirubin (biomolecule).

1.8.1.1 Sensing of toxic compounds

Rapid, selective, sensitive and cost-effective fluorescent based detetcion of toxic compounds has drawn great attention because toxic species may cause severe environmental problems and create acute threats to the ecosystem. Environmental Protection Agency (EPA) has set up a number of optimum detection limits for the harmful toxic species. A huge variety of MOFs have been explored for the successful detection of

toxic compounds. Hydrogen sulphide (H_2S), formaldehyde, cyanide, phosphate, aniline, ammonia, amines etc. are principally reported as toxic compounds.

H_2S is regarded as a well-known gasotransmitter toxic gas. Misregulation of endogenous H_2S concentration may cause several diseases like Down syndrome, Alzheimer's disease, Parkinson's disease and even cancer.[191, 192] Hence, real time monitoring of H_2S is a highly challenging task. Ghosh et al. first reported a post-synthetically modified azide functionalized Zr-UiO-66 MOF for selective "turn-on" detection of H_2S under physiological conditions (Figure 1.18).[193] They also showed live cell imaging of H_2S by the material. Actually, H_2S mediated reduction of azide group to auxo-chromic amine functionality is the principal reason behind the "turn-on" response of the material in presence of H_2S. Following this mechanism, Ghosh and co-workers also reported a nitro functionalized Zr-UiO-66 framework for "turn-on" detection of H_2S. Here, nitro group is converted into amine during H_2S treatment.[9] Biswas and co-workers reported both azide and nitro functionalized Ce-UiO-66 MOFs capable to detect H_2S under biological conditions.[29] Later on, the same group explored the detection of H_2S by Zr-DUT-52-$(NO_2)_2$ MOF in aqueous medium and as well as in live cells.[194] An aluminium based azide functionalized MOF called Al-MIL-53-N_3 was reported for nanomolar level detection (detection limit = 90.47 nM) of H_2S.[195] Furthermore, detection capability of intracellular H_2S has also been demonstrated by the same material through live-cell imaging studies. Qian and co-workers developed a post-synthetically modified MOF (IRMOF-3-N_3) for selective detection of H_2S with detection limit of 28.3 µM.[196] The same group reported a Eu^{3+} and Cu^{2+} loaded framework called Eu^{3+}/Cu^{2+}@UiO-66-$(COOH)_2$ for selective detection of H_2S.[197] Yang group reported a post-synthetically modified Tb^{3+}@Cu-MOF for "turn-on" ratiometric detection of H_2S.[198] Wang group showed that malononitrile (MN) functionalization can induce a notable enhancement in the emission intensity of MN-ZIF-90 in presence of H_2S and biothiol-based amino acids (such as cysteine).[199] Tang et al. reported a MOF called Al-TCPP-Cu for selective detection of H_2S by H_2S-mediated precipitation of copper(II) sulphide.[200] Fe^{III}-MIL-88-NH_2 was also reported as an H_2S sensor material with a detection limit of 10 µM.[201] Recently, vinyl group incorporated Zr-UiO-66[202] and CAU-10 MOFs[192] are employed for "turn-off" detection of H_2S. Nucleophilic addition of H_2S on vinyl group is the reason behind the quenching of emission intensity of the MOF materials.

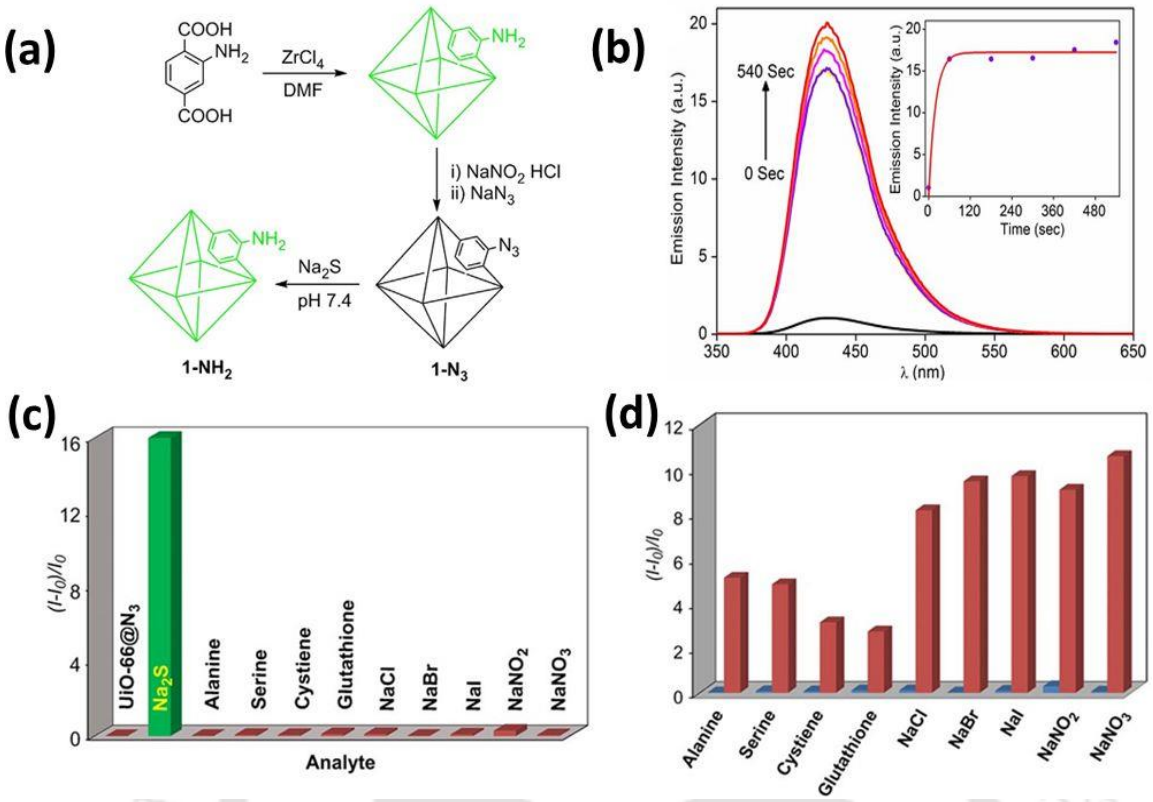

Figure 1.18 Fluorescence sensing of H_2S by UiO-66-N_3 (**1-N₃**) (a) Post-synthetic modification of **1-NH₂** to **1-N₃** via diazotization route. Reduction of **1-N₃** to **1-NH₂** upon addition of Na_2S at physiological pH giving rise to fluorescence turn-on response, (b) Fluorescence response of **1-N₃** towards addition of Na_2S after 0, 60, 180, 300, 420 and 540 s. Inset: Time dependence of emission intensity at 436 nm, (c) Relative fluorescence response of **1-N₃** towards various analytes (10 equivalents of azide group) after 540 seconds of analyte addition, (d) Turn-on response of probe **1-N₃** at 436 nm in presence of respective analyte (blue), followed by addition of Na_2S in solution containing analyte (red). Reproduced with permission from ref. 193. Copyright 2014, Nature publishing group.

Formaldehyde is a carcinogenic compound which is commonly regarded as a major component of sick building syndrome (SBS).[203] Formaldehyde is widely employed in household goods like adhesives, cosmetic items, particle boards, paints, textiles, etc. From these materials, formaldehyde can emit as a volatile species into the indoor environment which may cause strong irritation of mucous membranes and eyes.[204] According to World Health Organization (WHO), the permissible limit of exposure to formaldehyde is 0.08 ppm for 30 min.[205] On the other hand, the US National Institute for Occupation Safety and Health (NIOSH) has set a maximum of 0.016 ppm as the long term exposure limit for

formaldehyde.[206] In 2014, Dong et al. reported a porous Cu(I) MOF (MOF-2) which was constructed by Cu_2I_2 SBUs linked via four 2-(3,5-di(pyridin-4-yl)phenyl)-1H-benzo[d]imidazole ligands that was capable of the fluorescent and colorimetric detection of formaldehyde in the vapor phase through single-crystal-to-single-crystal transition.[207] In the same year, Zhao and co-workers developed a ZIF-8 based platform for the sensitive detection of formaldehyde vapor with a detection limit 0.057 ppm.[208] Yan et al. reported a dual emitting Ag^+ and Eu^{3+} loaded Zr-UiO-66 MOF for the ratiometric detection of formaldehyde.[209] The LOD value for this MOF towards formaldehyde was 0.051 ppm. Afterward, a dual emitting Eu^{3+} doped Zr-MOF was also reported for fluorimetric detection of forrmaldehyde in ethyl acetate medium having detection limit value of 0.20 ppm.[210] Vellingiri et al. discovered that Zr-UiO-66-NH_2 MOF can directly detect formaldehyde in trizma buffer medium without any post-synthetic modificaion or metal encapsulation.[211] The MOF showed great selectivity towards formaldehyde out of several aldehydes like propionaldehyde, butyraldehyde and valeraldehyde (Figure 1.19). The detection limit value for formaldehyde was 4 ppm for this material.

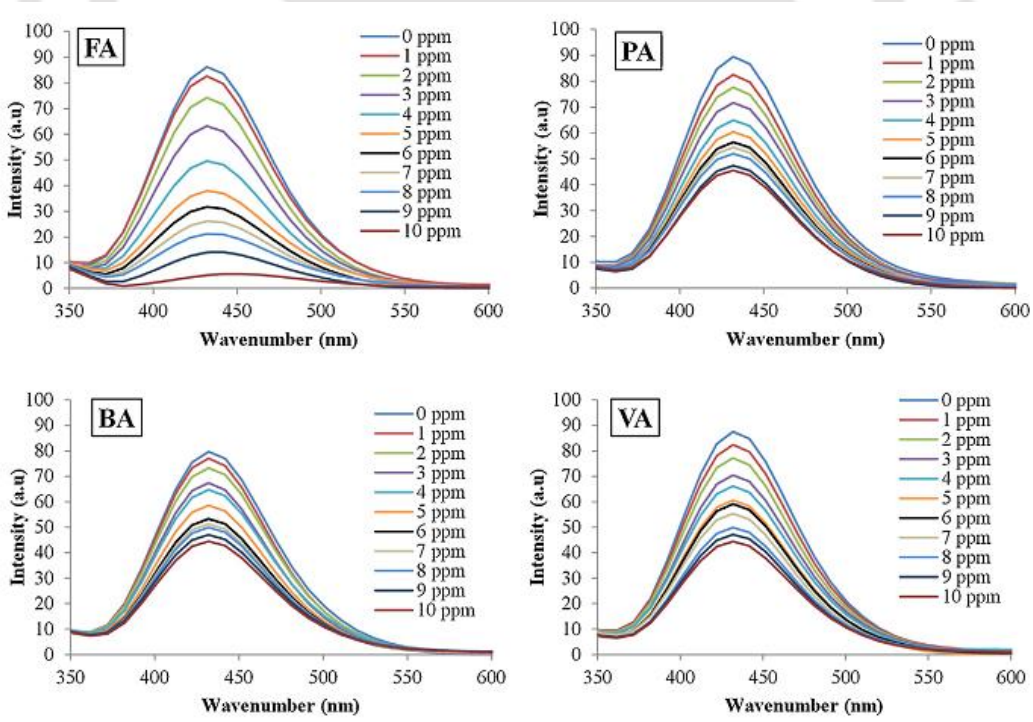

Figure 1.19 Fluorescence quenching of UiO-66-NH_2 in Trizma base buffer solution (50 mg L^{-1}, pH = 7.20) towards formaldehyde (FA), propionaldehyde (PA), butyraldehyde (BA) and valeraldehyde (VA). Reproduced with permission from ref. 211. Copyright 2017, Elsevier.

Cyanide is regarded as one of the lethally poisonous contaminants. It has dreadful impact on living beings. World Health Organization (WHO) has recommended the permissible limit of cyanide concentration in drinking water as low as 2 μM. Ghosh et al. first developed a post-synthetically modified ZIF-90 MOF having dicyanovinyl-functionalization.[212] This material showed great potential for selective cyanide sensing with a remarkable detection limit (2 μM) in DMSO/H_2O medium. Afterward, from the same group, a cationic dye (3,6-diaminoacridinium cation (DAAC)) loaded bio-MOF-1 (i.e. bio-MOF-1⊃DAAC) was reported for selective sensing for CN^- anions in pure aqueous medium with a detection limit of 5.2 ppb.[190] Biswas group has developed two MOFs, i.e. carbazole-functionalized Zr(IV) MOF[213] and CAU-10-N_2H_3 MOF[214] having detection capability of cyanide in pure aqueous medium with detection limit values of 0.14 and 0.48 μM, respectively. A Tb-MOF with nanomolar detection limit for cyanide was also reported.[215]

Anionic phosphate (PO_4^{3-}) is a major water pollutant which causes water eutrophication. Eutrophication is a severe threat to the aquatic animals. Qian et al. first used a Tb(III) based framework containing nitrilotriacetate ligand for the detection of PO_4^{3-} in aqueous medium.[216] Zhao et al. also developed ZnO QDs and MOF-5 for the recognition of PO_4^{3-} with limit of detection value of 53 nM.[217] Amine functionalized and hydrazine functionalized Zr-based UiO-66 frameworks were reported for efficient "turn-on" sensing of PO_4^{3-} with detection limit values of 1.25 μM and 0.196 μM, respectively.[218, 219] Most of the MOFs were not regenarable after the sensing event. A water-stable (pH range of stability: 2-12) 3D-MOF Eu–BTB (H_3BTB = 1,3,5-benzenetrisbenzoic acid) was explored for selective phosphate detection with good recyclable property.[220]

Organic amine vapours are toxic compounds which may cause contamination in food staff, water and soil. Chen et al. used a solvothermally prepared H-bonded three-dimensional Eu(III)-coordination polymer for "turn-on" detection of organic amines.[221] Chen and co-workers developed a 3D microporous Tb-MOF for efficient, selective and sensitive detection of aniline.[222] In this MOF, Tb^{3+} acted as the luminescent center. The fluorescence appeared through the antenna effect with the absorption of energy by the ligand, followed by energy transfer to the lanthanide ion. Emission of methanol suspension of the MOF was strongly quenched after exposing it with aniline. Li et al. explored a new Cd-based MOF called MOF1 for the detection of aniline in acetonitrile solution and also in vapor phase.[223] MOF1 was exposed to various aromatic amines in acetonitrile solution such as: nitroaniline, aniline, 4-methylaniline and diphenylamine. Strong quenching of

emission of the MOF was observed in presence of nitroaniline, whereas aniline showed moderate quenching. 4-Methylaniline caused slight enhancement in emission intensity and strong emission enhancement was shown by diphenylamine. Naphthalenediimide (NDI) unit based photochromic Mg-NDI MOF exhibited both naked eye based colorimetric as well as fluorogenic quenching response towards amines.[224] Another NDI-based MOF $ZnSiF_6(DPNDI)_2$ (DPNDI = *N*,*N*′-di(4-pyridyl)-1,4,5,8-naphthalene diimide) was also reported to sense trace amounts of organic amines.[225]

Furthermore, sensing of large molecule toxic species such as mycotoxin, organophosphate, antibiotics and dipicolinic acid (DPA) were also reported by several research groups. Deep and co-workers showed that pesticides such as parathion, methylparathion, paraoxon and fenitrothion bring quenching effect on emission intensity of MOF-5 suspension in ethanol.[226] Limit of detection for all four pesticides were approximately 5 ppb. The same group reported another MOF called $Cd(bdc\text{-}NH_2)$ (bdc-NH_2 = 2-aminobenzene-1,4-dicarboxylate) for the detection of same pesticides with better detection limit value (~1 ppb).[227] Zhou and co-workers developed two Zr-based isoreticular MOFs called BUT-12 and BUT-13 for efficient detection of antiboitics and nitraroamtic compounds.[228] Out of several antibiotics, these MOFs were able to selectively detect nitro functional NZF (nitrofurazone) and NFT (nitrofurantoin). Li group reported a Zn-based MOF called LMOF-241, which was employed to selectively detect mycotoxin aflatoxin B_1, a highly carcinogenic toxic compound produced by common food-contaminating fungi.[229] DPA is a dreadful toxin present in bacterial spore, which is produced by *Clostridium perfringes*. Presence of DPA generally indicates bacterial contamination. Lin et al. first reported a surface functionalized Tb-MOF which was used for DPA sensing.[230] Afterward, Deep et al. used another MOF $Tb(btc)(H_2O)_6$ (btc = benzene-1,3,5-tricarboxylate) for direct detection of DPA,[231] where no surface functionalisation was reported. Furthermore, the sensing study revealed that the MOF was selective towards DPA even in the presence of potentially interfering isonicotinic acid and *p*-phenylene diacetic acid. The detection limit (~0.4 nM) was also low enough. Some representative fluorescence-based detection of toxic species by MOFs are listed in Table 1.3.

Table 1.3 Summary of some MOFs employed for fluorimetric detection of environmental toxic species.

Targeted Analyte	MOFs	Medium Used	Detection Limit	Mode of Sensing	Ref.
H_2S	Zr-UiO-66-N_3	HEPES buffer	118 µM	turn-on	193
	Zr-UiO-66-NO_2	HEPES buffer	188 µM	turn-on	9
	Ce-UiO-66-N_3	HEPES buffer	12.2 µM	turn-on	29
	Ce-UiO-66-NO_2	HEPES buffer	34.84 µM	turn-on	29
	DUT-52-$(NO_2)_2$	HEPES buffer	20.0 µM	turn-on	194
	Al-MIL-53-N_3	HEPES buffer	90.47 nM	turn-on	195
	CAU-10-V-H	HEPES buffer	1.65 µM	turn-off	192
	UiO-66-CH=CH_2	HEPES buffer	6.46 µM	turn-off	202
HCHO	Zr-UiO-66-NH_2	Trizma base buffer	4.0 ppm	turn-off	211
	Eu/Zr-UiO-66-NH_2	ethyl acetate	0.20 ppm	turn-on	210
	Ag^+/Eu^{3+}-UiO-66	solid state	0.051 ppm	turn-on	209
	ZIF-8	solid state	0.057 ppm	turn-on	208
CN^-	M-ZIF-90	DMSO/H_2O	2 µM	turn-off	212
	carbazole-functionalized Zr-UiO-67	water	0.14 µM	turn-on	213
	CAU-10-N_2H_3	water	0.48 µM	turn-on	214
	bio-MOF-1⊃DAAC	HEPES buffer	5.2 ppb	turn-on	190
	Tb-ADP-Bipy MOF	water	30 nM	turn-on	215
PO_4^{3-}	UiO-66-NH_2	water	1.25 µM	turn-on	218
	Zr-UiO-66-N_2H_3	HEPES buffer	0.196 µM	turn-on	219
	TbNTA1	water	-	turn-off	216
	ZnO QDs & MOF	water	53 nM	turn-on	217
	Eu–BTB	water	10^{-5} mol/L,	turn-off	220
organic amine	EuL	2-propanol	-	turn-off	221
	Tb–BCB	methanol	-	turn-off	222
	MOF1	acetonitrile	-	turn-off	223

Targeted Analyte	MOFs	Medium Used	Detection Limit	Mode of Sensing	Ref.
organic amine	Mg–NDI	solid state	-	turn-off	224
	1a⊃naphthalene	ethanol	-	turn-on	225
pesticides	MOF-5	ethanol	5 ppb	turn-off	226
	NMOF1	ethanol	1 ppb	turn-off	227
antibiotics	BUT-12 and BUT-13	water	58 and 90 ppb	turn-off	228
mycotoxin	LMOF-241	dichloromethane	46 ppb	turn-off	229
dipicolinic acid	3′-Tb-EDTM	Tris buffer	48 nM	turn-on	230
	Tb-MOF	water	0.04 nM	turn-off	231

1.8.1.2 Sensing of biomolecules

Molecules which are produced from biological origin are regarded as biomolecules. So far, several MOFs have been expolored for fluorescence sensing of various biomarkers and biomolecules such as hippuric acid, bilirubin, amino acid, histidine, nucleic acid (DNA, RNA), HIV-1 U5 and thrombin.

Detection of biomarker is an important way for clinical diagnosis. Various highly selective and sensitive fluorescent probes based on MOFs have been developed for the detection of several biological indicators. Yan and co-workers utilized Eu^{3+} ion loaded MIL-121 to develop a fluorescent probe for the detection of hippuric acid in urine which is a biological indicator of toluene exposure.[232] The fluorescent colour of the sensor changed from bright red to dark red when it was exposed to hippuric acid spiked urine sample. Zaworotko and co-workers reported a lanthanide zeolite-like MOF (MZMOF-3), which was applied for fluorimetric detection of lysophosphatidic acid, which is a biomarker of ovarian cancer.[233] Bilirubin is a breakdown product of hemoglobin, which is regarded as a key biomarker for jaundice. Du and co-workers prepared UiO-66-PSM by aldimine condensation reaction between UiO-66-NH_2 and 2,3,4-trihydroxybenzaldehyde, which was employed for the detection of bilirubin under biological conditions.[234] The material showed strong fluorescence quenching in presence of bilirubin solution. Furthermore, great selectivity was observed towards bilirubin out of several biomolecules and biologically important ions (Figure 1.20). Interestingly, picomolar level detection (detection limit = 0.59 pM) of bilirubin was achieved by this material.

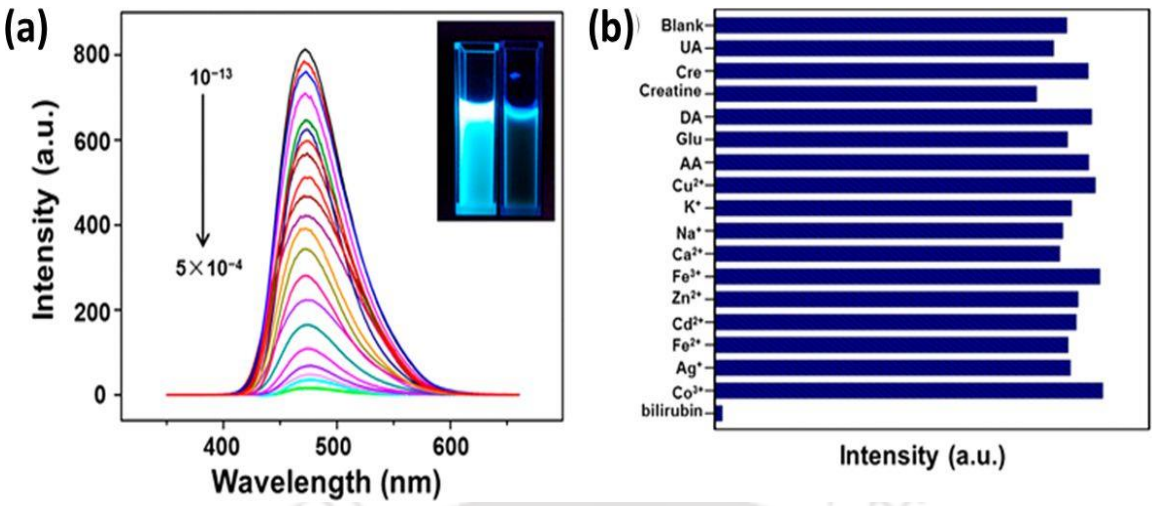

Figure 1.20 (a) Fluorescence spectra of UIO-66-PSM toward various concentrations of free bilirubin. Inset: Naked eye detection of bilirubin. (b) Fluorescence quenching effects of UIO-66-PSM toward interfering chemicals. Biomolecules: UA, uric acid; Cre, creatinine; DA, dopamine; Glu, glucose; AA, ascorbic acid. Reproduced with permission from ref. 234. Copyright 2017, American Chemical Society.

Moorthy et al. developed a water-stable homochiral Zn-PLA MOF (PLA = pyrene-tetralactic acid) which showed fluorescence quenching based enantioselective differentiation among analgous chiral amino acids (D-(+)- and L-(-)-isomers of histidine).[235] Kong et al. showed that a Cu-MOF was also able to detect amino acid by quenching the emission intensity of the material.[236]

Chen and co-workers developed a MOF called Cu(H_2DTOA) (H_2DTOA = dithiooxamide) which was highly effective and reliable for the detection of HIV-1 DNA sequences and thrombin.[237] Afterward, the same group reported a number of aqua stable Cu^{2+}, Dy^{3+} and Zn^{2+} based MOFs for the sensing of DNA or RNA. Several other functional MOFs such as MIL-101, MIL-88A and UiO-66-NH_2 were also employed as fluorescent sensing platforms for DNA/RNA detection.[238-243] In addition, these MOFs were able to distinguish complementary and mismatched target sequences with good sensitivity and selectivity. Some representative fluorescence-based detection of biomolecules by MOFs are listed in Table 1.4.

Table 1.4 Summary of some MOFs employed for fluorimetric detectiom of biomolecules.

Targeted Analyte	MOFs	Medium Used	Detection Limit	Mode of Sensing	Ref.
hippuric acid	Eu^{3+}@1	water	9 µg/mL	turn-off	232
lysophosphatidic acid	MZMOF-3	methanol	-	turn-on	233
bilirubin	UIO-66-PSM	PBS	0.59 pM	turn-off	234
histidine	Zn-PLA	water	-	turn-off	235
amino acid	[Cu(mal)(bpy)]·$2H_2O$	PBS	10.8 µM for glycine 14.4 µM for serine	turn-on	236
HIV DNA and thrombin	Cu(H_2dtoa)	Tris-HCl buffer	3 nM for ssDNA 1.3 nM for thrombin	turn-on	237
HIV ds-DNA and Sudan virus RNA	compound 1 (Cu-MOF)	Tris-HCl buffer	196 pM for HIV ds-DNA and 73 pM for SUDV RNA	turn-on	238
Ebolavirus RNA	compound 1 (Dy-MOF)	Tris-HCl buffer	160 pM	turn-on	239
HIV-1 ds-DNA	P-DNA@**2**	Tris-HCl buffer	10 pM	turn-on	240
HIV-1 DNA	MIL-101	Tris-HCl buffer	73 pM	turn-on	241
DNA	UiO-66-NH_2	Tris-HCl buffer	-	turn-on	243

1.9 Conclusions and outlook

As described in this Chapter, MOFs possess highly crystalline structures with predictable structures, tunable and functionalizable pores, which make them eligible materials for gas adsorption, gas separation, catalysis, drug delivery, chemical sensing, etc. Fluorometric detection of environmental and biological threats by MOFs has become a hot topic in recent days. Straight forward synthesis, predictable structures, great stability, collaborative functionality and predictable host-guest interactions make MOFs potential candidates for fluorogenic detection purpose. Great efforts have been observed to employ MOFs for sensing of several analytes so far. But, still some further work is needed for sharpening the features of sensitivity, selectivity, response time, stability and reusability. Stability of MOFs under moisture/aqueous conditions is also an important factor, particularly for those functional MOFs which are employed for real time detection purpose. Apart from hydrolytic stability, robustness of the material under biological conditions is also a crucial factor for developing MOFs for the sensing of biologically relevant molecules. Furthermore, for widespread application purpose, the development of synthetic routes using greener technology and cheaper starting materials without destroying the features of compound is a great challenge in this field, which has received considerable attention in current time. Considering the above stated facts, this thesis work mainly deals with the aqua stable functional MOFs which have been mainly prepared through well-known pre-functionalization or PSM route. Keeping the focus on the aqua stability and bio-compatiblility of MOFs, metal ions with higher oxidation states and low cytotoxicity (i.e. Zr^{4+} and Al^{3+}) and functional carboxylate ligands (terephthalate and isophthalate) have been employed fot the construction of MOFs. Functionalized CAU-10, MIL-53 and UiO-66 frameworks have been prepared in this thesis for their great aqua stable characteristics. Proper functional groups have been incorporated in the frameworks to make the MOFs suitable candidates for specific detection purpose. Hence, this thesis work basically presents the design, synthesis and charcterization of Zr(IV) and Al(III) based aqua stable MOFs for fluorimetric detection of environmental and biological threats under real conditions.

1.10 References

1. World Urbanization Prospects, UN Department of Economic and Social Affairs, 2014.
2. W. P. Lustig, S. Mukherjee, N. D. Rudd, A. V. Desai, J. Li and S. K. Ghosh, *Chem. Soc. Rev.*, 2017, **46**, 3242-3285.
3. G. Elias and W. F. Bauer, *J. Sep. Sci.*, 2006, **29**, 460-464.
4. A. R. Ivanov, I. V. Nazimov and L. A. Baratova, *J. Chromatogr., A*, 2000, **870**, 433-442.
5. M. A. Khan, F. Qazi, Z. Hussain, M. U. Idrees, S. Soomro and S. Soomro, *Int. J. Electrochem. Sci.*, 2017, **12**, 1711-1733.
6. N. S. Lawrence, J. Davis, L. Jiang, T. G. J. Jones, S. N. Davies and R. G. Compton, *Electroanal.*, 2000, **12**, 1453-1460.
7. M. Murata, T. A. Ivandini, M. Shibata, S. Nomura, A. Fujishima and Y. Einaga, *J. Electroanal. Chem*, 2008, **612**, 29-36.
8. Y. Jin, H. Wu, Y. Tian, L. Chen, J. Cheng and S. Bi, *Anal. Chem.*, 2007, **79**, 7176-7181.
9. S. S. Nagarkar, A. V. Desai and S. K. Ghosh, *Chem. Eur. J.*, 2015, **21**, 9994-9997.
10. S. Achmann, G. Hagen, J. Kita, I. M. Malkowsky, C. Kiener and R. Moos, *Sensors*, 2009, **9**, 1574-1589.
11. P. Falcaro, R. Ricco, A. Yazdi, I. Imaz, S. Furukawa, D. Mas-poch, R. Ameloot, J. D. Evans and C. J. Doonan, *Coord. Chem. Rev.*, 2016, **307**, 237-254.
12. O. Moldovan, B. Iniguez, M. J. Deen and L. F. Marsal, *IET Circuits Devices Syst.* , 2015, **9**, 446-453.
13. H. Zhu, H. Xu, Y. Yan, K. Zhang, T. Yu, H. Jiang and S. Wang, *Sens. Actuators B*, 2014, **202**, 667-673.
14. C. Jung, J. Heo, J. Han, N. Her, S.-J. Lee, J. Oh, J. Ryu and Y. Yoon, *Sep. Purif. Technol.*, 2013, **106**, 63-71.
15. A. Umar, M. M. Rahman, S. H. Kim and Y.-B. Hahn, *Chem. Commun.*, 2008, 166-168.
16. S. K. Das, C. S. Lim, S. Y. Yang, J. H. Han and B. R. Cho, *Chem. Commun.*, 2012, **48**, 8395-8397.
17. Y. Dong, G. Li, N. Zhou, R. Wang, Y. Chi and G. Chen, *Anal. Chem.*, 2012, **84**, 8378-8382.

18. H. Sohn, M. J. Sailor, D. Magde and W. C. Trogler, *J. Am. Chem. Soc.*, 2003, **125**, 3821-3830.
19. Y. Xu, Q. Yang, Z. Shen, X. Chen, X. Fan and Q. Zhou, *Macromolecules*, 2009, **42**, 2542-2550.
20. K. Müller-Buschbaum, F. Beuerle and C. Feldmann, *Microporous Mesoporous Mater.*, 2015, **216**, 171-199.
21. H. Furukawa, K. E. Cordova, M. O'Keeffe and O. M. Yaghi, *Science*, 2013, **341**, 1230444.
22. Y. Cui, Y. Yue, G. Qian and B. Chen, *Chem. Rev.*, 2012, **112**, 1126-1162.
23. B. Li, H.-M. Wen, W. Zhou and B. Chen, *J. Phys. Chem. Lett.*, 2014, **5**, 3468-3479.
24. C. Orellana-Tavra, R. J. Marshall, E. F. Baxter, I. A. Lázaro, A. Tao, A. K. Cheetham, R. S. Forgan and D. Fairen-Jimenez, *J. Mater. Chem. B*, 2016, **4**, 7697-7707.
25. P. Horcajada, C. Serre, M. Vallet-Regı´, M. Sebban, F. Taulelle and G. Fe´rey, *Angew. Chem., Int. Ed.*, 2006, **45**, 5974-5978.
26. W. Huang, J. Jiang, D. Wu, J. Xu, B. Xue and A. M. Kirillov, *Inorg. Chem.*, 2015, **54**, 10524-10526.
27. X. Li, H. Xu, F. Kong and R. A. Wang, *Angew. Chem. Int. Ed.*, 2013, **52**, 13769-13773.
28. J. M. Taylor, K. W. Dawson and G. K. H. Shimizu, *J. Am. Chem. Soc.*, 2013, **135**, 1193-1196.
29. A. Buragohain and S. Biswas, *CrystEngComm*, 2016, **18**, 4374-4381.
30. R. Dalapati and S. Biswas, *Sens. Actuators, B.*, 2017, **239**, 759-767.
31. R. Lv, J. Wang, Y. Zhang, H. Li, L. Yang, S. Liao, W. Gu and X. Liu, *J. Mater. Chem. A*, 2016, **4**, 15494-15500.
32. Q. Zhang, J. Wang, A. M. Kirillov, W. Dou, C. Xu, C. Xu, L. Yang, R. Fang and W. Liu, *ACS Appl. Mater. Interfaces*, 2018, **10**, 23976-23986.
33. J. Heine and K. Muller-Buschbaum, *Chem. Soc. Rev.*, 2013, **42**, 9232-9242.
34. A. Das, N. Anbu, A. Dhakshinamoorthy and S. Biswas, *Microporous Mesoporous Mater.*, 2019, **284**, 459-467.
35. R. Liang, F. Jing, L. Shen, N. Qin and L. Wu, *J. Hazard. Mater.*, 2015, **287**, 364-372.
36. K. M. Park, H. Kim, J. Murray, J. Koo and K. Kim, *Supramol. Chem.*, 2017, **29**, 441-445.

37. D. M. Liu, K. D. Lu, C. Poon and W. B. Lin, *Inorg. Chem.*, 2014, **53**, 1916-1924.
38. A. Chidambaram and K. C. Stylianou, *Inorg. Chem. Front.*, 2018, **5**, 979-998.
39. Y. Liu, X.-Y. Xie, C. Cheng, Z.-S. Shao and H.-S. Wang, *J. Mater. Chem. C*, 2019, **7**, 10743-10763.
40. H.-S. Wang, *Coord. Chem. Rev.*, 2017, **349**, 139-155.
41. P. Kumar, A. Deep and K.-H. Kim, *Trends Anal. Chem.*, 2015, **73**, 39-53.
42. D. Liu, K. Lu, C. Poon and W. Lin, *Inorg. Chem.*, 2014, **53**, 1916-1924.
43. B. J. Deibert and J. Li, *Chem. Commun.*, 2014, **50**, 9636-9639.
44. A. Douvali, A. C. Tsipis, S. V. Eliseeva, S. Petoud, G. S. Papaefstathiou, C. D. Malliakas, I. Papadas, G. S. Armatas, I. Margiolaki, M. G. Kanatzidis, T. Lazarides and M. J. Manos, *Angew. Chem., Int. Ed.*, 2015, **54**, 1651-1656.
45. X. Liu, S. Akerboom, M. d. Jong, I. Mutikainen, S. Tanase, A. Meijerink and E. Bouwman, *Inorg. Chem.*, 2015, **54**, 11323-11329.
46. J. L. Atwood, J. E. D. Davies and D. D. MacNicol, *Inclusion compounds: Structural aspects of inclusion compounds formed by inorganic and organometallic host lattices*, Oxford University Press, London ; Oxford, 1984.
47. T. Iwamoto, T. Nakano, M. Morita, T. Miyosh, T. Miyamoto and Y. Sasaki, *Inorg. Chim. Acta*, 1968, **2**, 313-316.
48. H. J. Buser, D. Schwarzenbach, W. Petter and A. Ludi, *Inorg. Chem.*, 1977, **16**, 2704-2710.
49. B. F. Hoskins and R. Robson, *J. Am. Chem. Soc.*, 1989, **111**, 5962-5964.
50. B. F. Hoskins and R. Robson, *J. Am. Chem. Soc.*, 1990, **112**, 1546-1554.
51. O. M. Yaghi and H. Li, *J. Am. Chem. Soc.*, 1995, **117**, 10401-10402.
52. H. Li, M. Eddaoudi, M. O'Keeffe and O. M. Yaghi, *Nature*, 1999, **402**, 276-279.
53. S. R. Batten, N. R. Champness, X.-M. Chen, J. G. -Martinez, S. Kitagawa, L. Öhrström, M. O'Keeffe, M. P. Suh and J. Reedijk, *CrystEngComm*, 2012, **14**, 3001-3004.
54. H. Furukawa, K. E. Cordova, M. O'Keeffe and O. M. Yaghi, *Science*, 2013, **341**, 1230444.
55. J. H. Cavka, S. Jakobsen, U. Olsbye, N. Guillou, C. Lamberti, S. Bordiga and K. P. Lillerud, *J. Am. Chem. Soc.*, 2008, **130**, 13850-13851.
56. A. Schaate, P. Roy, A. Godt, J. Lippke, F. Waltz, M. Wiebcke and P. Behrens, *Chem. Eur. J.*, 2011, **17**, 6643-6651.

57. D. Feng, Z.-Y. Gu, J.-R. Li, H.-L. Jiang, Z. Wei and H.-C. Zhou, *Angew. Chem., Int. Ed.*, 2012, **51**, 10307-10310.
58. P. Deria, J. E. Mondloch, E. Tylianakis, P. Ghosh, W. Bury, R. Q. Snurr, J. T. Hupp and O. K. Farha, *J. Am. Chem. Soc.*, 2013, **135**, 16801-16804.
59. S. Yuan, W. Lu, Y.-P. Chen, Q. Zhang, T.-F. Liu, D. Feng, X. Wang, J. Qin and H.-C. Zhou, *J. Am. Chem. Soc.*, 2015, **137**, 3177-3180.
60. M. Zhang, Y.-P. Chen, M. Bosch, T. Gentle, K. Wang, D. Feng, Z. U. Wang and H.-C. Zhou, *Angew. Chem., Int. Ed.*, 2014, **53**, 815-818.
61. J. E. Mondloch, W. Bury, D. Fairen-Jimenez, S. Kwon, E. J. DeMarco, M. H. Weston, A. A. Sarjean, S. T. Nguyen, P. C. Stair, R. Q. Snurr, O. K. Farha and J. T. Hupp, *J. Am. Chem. Soc.*, 2013, **135**, 10294-10297.
62. P. Deria, W. Bury, J. T. Hupp and O. K. Farha, *Chem. Commun.*, 2014, **50**, 965-1968.
63. V. Bon, I. Senkovska, M. S. Weiss and S. Kaskel, *CrystEngComm.*, 2013, **15**, 9572-9577.
64. H. Furukawa, F. Gándara, Y.-B. Zhang, J. Jiang, W. L. Queen, M. R. Hudson and O. M. Yaghi, *J. Am. Chem. Soc.*, 2014, **136**, 4369-4381.
65. D. Feng, W.-C. Chung, Z. Wei, Z.-Y. Gu, H.-L. Jiang, Y.-P. Chen, D. J. Darensbourg and H.-C. Zhou, *J. Am. Chem. Soc.*, 2013, **135**, 17105-17110.
66. V. Guillerm, F. Ragon, M. Dan-Hardi, T. Devic, M. Vishnuvarthan, B. Campo, A. Vimont, G. Clet, Q. Yang, G. Maurin, G. Férey, A. Vittadini, S. Gross and C. Serre, *Angew. Chem., Int. Ed.*, 2012, **51**, 9267-9271.
67. P. Ji, K. Manna, Z. Lin, X. Feng, A. Urban, Y. Song and W. Lin, *J. Am. Chem. Soc.*, 2017, **139**, 7004-7011.
68. D. Feng, Z.-Y. Gu, Y.-P. Chen, J. Park, Z. Wei, Y. Sun, M. Bosch, S. Yuan and H.-C. Zhou, *J. Am. Chem. Soc.*, 2014, **136**, 17714-17717.
69. H. L. Jiang, D. Feng, K. Wang, Z. Y. Gu, Z. Wei, Y. P. Chen and H. C. Zhou, *J. Am. Chem. Soc.*, 2013, **135**, 13934-13938.
70. T. Loiseau, C. Serre, C. Huguenard, G. Fink, F. Taulelle, M. Henry, T. Bataille and G. Férey, *Chem. Eur. J.*, 2004, **10**, 1373-1382.
71. I. Senkovska, F. Hoffmann, M. Froba, J. Getzschmann, W. Bohlmann and S. Kaskel, *Microporous Mesoporous Mater.*, 2009, **12**, 93-98.
72. Q. Yang, S. Vaesen, M. Vishnuvarthan, F. Ragon, C. Serre, A. Vimont, M. Daturi, G. D. Weireld and G. Maurin, *J. Mater. Chem.*, 2012, **22**, 10210-10220.

73. S. H. Lo, C. H. Chien, Y. L. Lai, C. C. Yang, J. J. Lee, D. S. Raja and C. H. Lin, *J. Mater. Chem. A*, 2013, **1**, 324-329.
74. S. Biswas, T. Ahnfeldt and N. Stock, *Inorg. Chem.*, 2011, **50**, 9518-9526.
75. Z. W. Wang, M. Chen, C. S. Liu, X. Wang, H. Zhao and M. Du, *Chem. Eur. J.*, 2015, **21**, 17215-17219.
76. C. Volkringer, T. Loiseau, N. Guillou, G. Férey, M. Haouas, F. Taulelle, E. Elkaim and N. Stock, *Inorg. Chem.*, 2010, **49**, 9852-9862.
77. C. Volkringer, T. Loiseau, N. Guillou, G. Férey, M. Haouas, F. Taulelle, N. Audebrand, I. Margiolaki, D. Popov, M. Burghammer and C. Riekel, *Cryst. Growth Des.*, 2009, **9**, 2927-2936.
78. C. Volkringer, T. Loiseau, M. Haouas, F. Taulelle, D. Popov, M. Burghammer, C. Riekel, C. Zlotea, F. Cuevas, M. Latroche, D. Phanon, C. Knofelv, P. L. Llewellyn and G. Férey, *Chem. Mater.*, 2009, **21**, 5783-5791.
79. S. H. Yang, J. L. Sun, A. J. Ramirez-Cuesta, S. K. Callear, W. I. F. David, D. P. Anderson, R. Newby, A. J. Blake, J. E. Parker, C. C. Tang and M. Schroder, *Nat. Chem.*, 2012, **4**, 887-894.
80. A. Fateeva, P. A. Chater, C. P. Ireland, A. A. Tahir, Y. Z. Khimyak, P. V. Wiper, J. R. Darwent and M. J. Rosseinsky, *Angew. Chem., Int. Ed.*, 2012, **51**, 7440-7444.
81. T. Loiseau, L. Lecroq, C. Volkringer, J. Marrot, G. Férey, M. Haouas, F. Taulelle, S. Bourrelly, P. L. Llewellyn and M. Latroche, *J. Am. Chem. Soc.*, 2006, **128**, 10223-10230.
82. C. Volkringer, D. Popov, T. Loiseau, G. Férey, M. Burghammer, C. Riekel, M. Haouas and F. Taulclle, *Chem. Mater.*, 2009, **21**, 5695-5697.
83. D. W. Feng, T. F. Liu, J. Su, M. Bosch, Z. W. Wei, W. Wan, D. Q. Yuan, Y. P. Chen, X. Wang, K. C. Wang, X. Z. Lian, Z. Y. Gu, J. Park, X. D. Zou and H. C. Zhou, *Nat. Commun.*, 2015, **6**, 5979.
84. X. Z. Lian, Y. P. Chen, T. F. Liu and H. C. Zhou, *Chem. Sci.*, 2016, **7**, 6969-6973.
85. P. Serra-Crespo, E. V. Ramos-Fernandez, J. Gascon and F. Kapteijn, *Chem. Mater.*, 2011, **23**, 2565-2572.
86. D. Alezi, Y. Belmabkhout, M. Suyetin, P. M. Bhatt, L. J. Weselinski, V. Solovyeva, K. Adil, I. Spanopoulos, P. N. Trikalitis, A. H. Emwas and M. Eddaoudi, *J. Am. Chem. Soc.*, 2015, **137**, 13308-13318.
87. H. Reinsch, M. A. v. d. Veen, B. Gil, B. Marszalek, T. Verbiest, D. d. Vos and N. Stock, *Chem. Mater.*, 2013, **25**, 17-26.

88. T. Ahnfeldt, N. Guillou, D. Gunzelmann, I. Margiolaki, T. Loiseau, G. Férey, J. Senker and N. Stock, *Angew. Chem., Int. Ed.*, 2009, **48**, 5163-5166.
89. H. Reinsch, M. Feyand, T. Ahnfeldt and N. Stock, *Dalton Trans.*, 2012, **41**, 4164-4171.
90. B. J. Burnett, P. M. Barron and W. Choe, *CrystEngComm*, 2012, **14**, 3839-3846.
91. S. Kitagawa, R. Kitaura and S. I. Noro, *Angew. Chem. Int. Ed.*, 2004, **43**, 2334-2375.
92. S. Noro, S. Kitagawa, T. Akutagawa and T. Nakamura, *Prog. Polym. Sci.*, 2009, **34**, 240-279.
93. D. J. Collins and H.-C. Zhou, *J. Mater. Chem.*, 2007, **17**, 3154-3160.
94. B. L. Chen, C. D. Liang, J. Yang, D. S. Contreras, Y. L. Clancy, E. B. Lobkovsky, O. M. Yaghi and S. Dai, *Angew. Chem. Int. Ed.*, 2006, **45**, 1390-1393.
95. M. Eddaoudi, D. B. Moler, H. Li, B. Chen, T. M. Reineke, M. O'Keeffe and O. M. Yagi, *Acc. Chem. Res.*, 2001, **34**, 319-330.
96. Z. Hu, Y. Peng, Z. Kang, Y. Qian and D. Zhao, *Inorg. Chem.*, 2015, **54**, 4862-4868.
97. D. J. Tranchemontagne, J. L. Mendoza-Cortes, M. O'Keeffe and O. M. Yaghi, *Chem. Soc. Rev.*, 2009, **38**, 1257-1283.
98. O. M. Yaghi, M. O'Keeffe, N. W. Ockwig, H. K. Chae, M. Eddaoudi and J. Kim, *Nature*, 2003, **423**, 705-714.
99. T. Wittmann, C. B. L. Tschense, L. Zappe, C. Koschnick, R. Siegel, R. Stäglich, B. V. Lotsch and J. Senker, *J. Mater. Chem. A*, 2019, **7**, 10379-10388.
100. Q. Fang, G. Zhu, M. Xue, Z. Wang, J. Sun and S. Qiu, *Cryst. Growth Des.*, 2008, **8**, 319-329.
101. R. Abazari, A. R. Mahjoub and J. Shariati, *J. Hazard. Mater.*, 2019, **366**, 439-451.
102. N. Bakhtiari and S. Azizian, *ACS Omega*, 2018, **3**, 16954-16959.
103. R. M. Barrer, *J. Chem. Soc.*, 1948, 127-132.
104. S. Kitagawa, R. Kitaura and S.-I. Noro, *Angew. Chem. Int. Ed.*, 2004, **43**, 2334-2375.
105. X.-X. Zhao, J.-P. Ma, Y.-B. Dong, R.-Q. Huang and T. Lai, *Crystal growth & design*, 2007, **7**, 1058-1068.
106. X. Shi, G. S. Zhu, S. L. Qiu, K. L. Huang, J. H. Yu and R. R. Xu, *Angew. Chem. Int. Ed.*, 2004, **43**, 6482-6485.
107. Y. Bian, N. Xiong and G. Zhu, *Processes*, 2018, **6**, 122.

108. S. H. Jhung, J.-H. Lee, P. M. Forster, G. Férey, A. K. Cheetham and J.-S. Chang, *Chem. Eur. J.*, 2006, **12**, 7899-7905.
109. Z. Ni and R. I. Masel, *J. Am. Chem. Soc.*, 2006, **128**, 12394-12395.
110. G. A. Tompsett, W. C. Conner and K. S. Yngvesson, *ChemPhysChem*, 2006, **7**, 296-319.
111. U. Mueller, M. Schubert, F. Teich, H. Puetter, K. Schierle-Arndt and J. Pastre, *J. Mater. Chem.*, 2006, **16**, 626-636.
112. H. Al-Kutubi, J. Gascon, E. J. R. Sudhölter and L. Rassaei, *ChemElectroChem.*, 2015, **2**, 462-474.
113. S. D. Worrall, H. Manna, A. Rogers, M. A. Bissett, M. P. Attfield and R. A. W. Dryfe, *Electrochimica Acta*, 2016, **197**, 228-240.
114. A. L. Garay, A. Pichon and S. L. James, *Chem. Soc. Rev.*, 2007, **36**, 846-855.
115. M. Klimakow, P. Klobes, A. F. Thünemann, K. Rademann and F. Emmerling, *Chem. Mater.*, 2010, **22**, 5216-5221.
116. C. Suryanarayana, *Prog. Mater. Sci.*, 2001, **46**, 1-184.
117. A. Pichon, A. Lazuen-Garay and S. L. James, *CrystEngComm*, 2006, **8**, 211-214.
118. R. Li, X. Ren, H. Ma, X. Feng, Z. Lin, X. Li, C. Hu and B. Wang, *J. Mater. Chem. A*, 2014, **2**, 5724-5729.
119. C. G. Carson, A. J. Brown, D. S. Sholl and S. Nair, *Cryst. Growth Des.*, 2011, **11**, 4505-4510.
120. R. J. Wood, J. Lee and M. J. Bussemaker, *Ultrason. Sonochem.*, 2017, **38**, 351-370.
121. W.-J. Son, J. Kim, J. Kim and W.-S. Ahn, *Chem. Commun.*, 2008, 6336-6338.
122. Z. Wang and S. M. Cohen, *Chem. Soc. Rev.*, 2009, **38**, 1315-1329.
123. S. J. Garibay, Z. Wang, K. K. Tanabe and S. M. Cohen, *Inorg. Chem.*, 2009, **48**, 7341-7349.
124. Z. Wang, K. K. Tanabe and S. M. Cohen, *Inorg. Chem.*, 2009, **48**, 296-306.
125. K. K. Tanabe and S. M. Cohen, *Chem. Soc. Rev.*, 2011, **40**, 498-519.
126. S. M. Cohen, *Chem. Rev.*, 2012, **112**, 970-1000.
127. G. Tuci, A. Rossin, X. Xu, M. Ranocchiari, J. A. v. Bokhoven, L. Luconi, I. Manet, M. Melucci and G. Giambastiani, *Chem. Mater.*, 2013, **25**, 2297-2308.
128. E. D. Bloch, D. Britt, C. Lee, C. J. Doonan, F. J. Uribe-Romo, H. Furukawa, J. R. Long and O. M. Yaghi, *J. Am. Chem. Soc.*, 2010, **132**, 14382-14384.

129. A. Demessence, D. M. D'Alessandro, M. L. Foo and J. R. Long, *J. Am. Chem. Soc.*, 2009, **131**, 8784-8786.
130. Y. Hu, W. M. Verdegaal, S.-H. Yu and H.-L. Jiang, *ChemSusChem*, 2014, **7**, 734-737.
131. D. Denysenko, J. Jelic, K. Reuter and D. Volkmer, *Chem.Eur.J.*, 2015, **21**, 8188-8199.
132. M. Kim, J. F. Cahill, H. Fei, K. A. Prather and S. M. Cohen, *J. Am. Chem. Soc.*, 2012, **134**, 18082-18088.
133. T.-F. Liu, D. Feng, Y.-P. Chen, L. Zou, M. Bosch, S. Yuan, Z. Wei, S. Fordham, K. Wang and H.-C. Zhou, *J. Am. Chem. Soc.*, 2015, **137**, 413-419.
134. K. Wang, X.-L. Lv, D. Feng, J. Li, S. Chen, J. Sun, L. Song, Y. Xie, J.-R. Li and H.-C. Zhou, *J. Am. Chem. Soc.*, 2016, **138**, 914-919.
135. M. Ding, X. Cai and H.-L. Jiang, *Chem. Sci.*, 2019, **10**, 10209-10230.
136. N. M. Padial, E. Q. Procopio, C. Montoro, E. López, J. E. Oltra, V. Colombo, A. Maspero, N. Masciocchi, S. Galli, I. Senkovska, S. Kaskel, E. Barea and J. A. R. Navarro, *Angew. Chem. Int. Ed.*, 2013, **52**, 8290-8294.
137. N. C. Burtch, H. Jasuja and K. S. Walton, *Chem. Rev.*, 2014, **114**, 10575-10612.
138. D. Ma, Y. Li and Z. Li, *Chem. Commun.*, 2011, **47**, 7377-7379.
139. S. Mukherjee, S. Sharma and S. K. Ghosh, *APL Mater.*, 2019, **7**, 050701.
140. K. S. Park, Z. Ni, A. P. Côté, J. Y. Choi, R. Huang, F. J. Uribe-Romo, H. K. Chae, M. O'Keeffe and O. M. Yaghi, *Proc. Natl. Acad. Sci. USA*, 2006, **103**, 10186-10191.
141. J. G. Nguyen and S. M. Cohen, *J. Am. Chem. Soc.*, 2010, **132**, 4560-4561.
142. H.-F. Zhang, M. Li, X.-Z. Wang, D. Luo, Y.-F. Zhao, X.-P. Zhou and D. Li, *J. Mater. Chem. A*, 2018, **6**, 4260-4265.
143. W. Zhang, Y. Hu, J. Ge, H.-L. Jiang and S.-H. Yu, *J. Am. Chem. Soc.*, 2014, **136**, 16978-16981.
144. A. Stein, S. W. Keller and T. E. Mallouk, *Science*, 1993, **259**, 1558.
145. A. D. Buckingham and P. W. Fowler, *J. Chem. Phys.*, 1983, **79**, 6426.
146. M. Eddaoudi, J. Kim, N. Rosi, D. Vodak, J. Wachter, M. O'Keeffe and O. M. Yaghi, *Science*, 2002, **295**, 469-472.
147. S. Wang, C. M. McGuirk, A. d'Aquino, J. A. Mason and C. A. Mirkin, *Adv.Mater.*, 2018, **30**, 1800202.

148. A. Carné, C. Carbonell, I. Imaz and D. Maspoch, *Chem. Soc. Rev.*, 2011, **40**, 291-305.
149. J. Owen and L. Brus, *J. Am. Chem. Soc.*, 2017, **139**, 10939-10943.
150. S. E. A. Gratton, P. A. Ropp, P. D. Pohlhau, J. C. Luft, V. J. Madden, M. E. Napier and J. M. DeSimone, *Proc. Natl. Acad. Sci. U. S. A.*, 2008, **105**, 11613-11618.
151. B. Alberts, A. Johnson, J. Lewis, M. Raff, K. Roberts and P. Walter, *Molecular biology of the cell, 4th edition*, 2002, Garland Science, New York.
152. P. Horcajada, R. Gref, T. Baati, P. K. Allan, G. Maurin, P. Couvreur, G. Ferey, R. E. Morris and C. Serre, *Chem. Rev.*, 2011, **112**, 1232-1268.
153. C. He, D. Liu and W. Lin, *Chem. Rev.* , 2015, **115**, 11079-11108.
154. J. Park, Q. Jiang, D. Feng, L. Mao and H.-C. Zhou, *J. Am. Chem. Soc.*, 2016, **138**, 3518-3525.
155. K. Lu, C. He and W. Lin, *J. Am. Chem. Soc.*, 2014, **136**, 16712-16715.
156. X. Cai, Z. Xie, D. Li, M. Kassymova, S.-Q. Zang and H.-L. Jiang, *Coord. Chem. Rev.*, 2020, **417**, 213366.
157. I.Tibbetts and G. E. Kostakis, *Molecules*, 2020, **25**, 1291.
158. E. Gulcay and I. Erucar, *Ind. Eng. Chem. Res.*, 2019, **58**, 3225-3237.
159. R. C. Huxford, J. D. Rocca and W. Lin, *Curr. Opin. Chem. Biol.*, 2010, **14**, 262-268.
160. M. A. Haydar, H. R. Abid, B. Sunderland and S. Wang, *Drug Des. Devel. Ther.*, 2019, **13**, 23-35.
161. X. Leng, X. Dong, W. Wang, N. Sai, C. Yang, L. You, H. Huang, X. Yin and J. Ni, *Molecules*, 2018, **23**, 2490.
162. D. R. Broome, M. S. Girguis, P. W. Baron, A. C. Cottrell, I. Kjellin and G. A. Kirk, *Am. J. Roentgenol.*, 2007, **188**, 586-592.
163. L. Thunus and R. Lejeune, *Coord. Chem. Rev.*, 1999, **184**, 125-155.
164. K. E. deKrafft, W. S. Boyle, L. M. Burk, O. Z. Zhou and W. Lin, *J. Mater. Chem.*, 2012, **22**, 18139-18144.
165. P. Horcajada, T. Chalati, C. Serre, B. Gillet, C. Sebrie, T. Baati, J. F. Eubank, D. Heurtaux, P. Clayette, C. Kreuz, J.-S. Chang, Y. K. Hwang, V. Marsaud, P.-N. Bories, L. Cynober, S. Gil, G. Férey, P. Couvreur and R. Gref, *Nat. Mater.*, 2010, **9**, 172.
166. K. J. Hartlieb, D. P. Ferris, J. M. Holcroft, I. Kandela, C. L. Stern, M. S. Nassar, Y. Y.Botros and J. F. Stoddart, *Mol. Pharma.*, 2017, **14**, 1831-1839.

167. Y. Cui, Y. Yue, G. Qian and B. Chen, *Chem. Rev.*, 2012, **112**, 1126-1162.
168. B. Zhao, X.-Y. Chen, P. Cheng, D.-Z. Liao, S.-P. Yan and Z.-H. Jiang, *J. Am. Chem. Soc.*, 2004, **126**, 15394-15395.
169. H.-L. Jiang, Y. Tatsu, Z.-H. Lu and Q. Xu, *J. Am. Chem. Soc.*, 2010, **132**, 5586-5587.
170. H. Xu, F. Liu, Y. Cui, B. Chen and G. Qian, *Chem. Commun.*, 2011, **47**, 3153-3155.
171. W. J. Rieter, K. M. L. Taylor, H. An, W. Lin and W. Lin, *J. Am. Chem. Soc.*, 2006, **128**, 9024-9025.
172. K. M. L. Taylor, A. Jin and W. Lin, *Angew. Chem., Int. Ed.*, 2008, **47**, 7722-7725.
173. X. Yang and D. Yan, *Chem. Sci.*, 2016, **7**, 4519-4526.
174. Y. Zhang, S. Yuan, G. Day, X. Wang, X. Yang and H.-C. Zhou, *Coord. Chem. Rev.*, 2018, **354**, 28-45.
175. M. Y. Berezin and S. Achilefu, *Chem. Rev.*, 2010, **110**, 2641-2684.
176. X. Li, X.-W. Wang and Y.-H. Zhang, *Inorg. Chem. Commun.*, 2008, **11**, 832-834.
177. K. Jayaramulu, P. Kanoo, S. J. George and T. K. Maji, *Chem. Commun.*, 2010, **46**, 7906-7908.
178. E. G. Moore, A. P. S. Samuel and K. N. Raymond, *Acc. Chem. Res.*, 2009, **42**, 542-552.
179. S. V. Eliseeva and J.-C. G. B€unzli, *Chem. Soc. Rev.*, 2010, **39**, 189-227.
180. B. D. Chandler, D. T. Cramb and G. K. H. Shimizu, *J. Am. Chem. Soc.*, 2006, **128**, 10403-10412.
181. Y. Wei, Y. Yu and K. Wu, *Cryst. Growth Des.*, 2008, **8**, 2087-2089.
182. G.-H. Wang, Z.-G. Li, H.-Q. Jia, N.-H. Hu and J.-W. Xu, *CrystEngComm.*, 2009, **11**, 292-297.
183. M.-X. Li, H. Wang, S.-W. Liang, M. Shao, X. He, Z.-X. Wang and S.-R. Zhu, *Cryst. Growth Des.*, 2009, **9**, 4626-4633.
184. X. W. Wang, J.-Z. Chen and J.-H. Liu, *Cryst. Growth Des.*, 2007, **7**, 1227-1229.
185. J. An, C. M. Shade, D. A. Chengelis-Czegan, S. Petoud and N. L. Rosi, *J. Am. Chem. Soc.*, 2011, **133**, 1220-1223.
186. F. Luo and S. R. Batten, *Dalton Trans.*, 2010, **39**, 4485-4488.
187. Q.-R. Fang, G.-S. Zhu, Z. Jin, Y.-Y. Ji, J.-W. Ye, M. Xue, H. Yang, Y. Wang and S.-L. Qiu, *Angew. Chem., Int. Ed.*, 2007, **46**, 6638-6642.

188. K. M. L.Taylor, W. J. Rieter and W. Lin, *J. Am. Chem. Soc.*, 2008, **130**, 14358-14359.

189. S. Jung, Y. Kim, S.-J. Kim, T.-H. Kwon, S. Huh and S. Park, *Chem. Commun.*, 2011, **47**, 2904-2906.

190. A. Karmakar, B. Joarder, A. Mallick, P. Samanta, A. V. Desai, S. Basu and S. K. Ghosh, *Chem. Commun.*, 2017, **53**, 1253-1256.

191. S. Fiorucci, E. Antonelli, A. Mencarelli, S. Orlandi, B. Renga, G. Rizzo, E. Distrutti, V. Shah and A. Morelli, *Hepatology*, 2005, **42**, 539-548.

192. S. Nandi, H. Reinsch and S. Biswas, *Microporus Mesoporous Mater.*, 2020, **293**, 109790.

193. S. S. Nagarkar, T. Saha, A. V. Desai, P. Talukdar and S. K. Ghosh, *Sci. Rep.*, 2014, **4**, 7053-7058.

194. R. Dalapati, S. N. Balaji, V. Trivedi, L. Khamari and S. Biswas, *Sens. Actuator, B*, 2017, **245**, 1039-1049.

195. A. Das, S. Banesh, V. Trivedi and S. Biswas, *Dalton Trans.*, 2018, **47**, 2690-2700.

196. X. Zhang, J. Zhang, Q. Hu, Y. Cui, Y. Yang and G. Qian, *Appl. Surf. Sci.*, 2015, **355**, 814-819.

197. X. Zhang, Q. Hu, T. Xia, J. Zhang, Y. Yang, Y. Cui, B. Chen and G. Qian, *ACS Appl. Mater. Interfaces*, 2016, **8**, 32259-32265.

198. X. Zheng, R. Fan, Y. Song, A. Wang, K. Xing, X. Du, P. Wang and Y. Yang, *J. Mater. Chem. C*, 2017, **5**, 9943-9951.

199. H. Li, X. Feng, Y. Guo, D. Chen, R. Li, X. Ren, X. Jiang, Y. Dong and B. Wang, *Sci. Rep.*, 2014, **4**, 4366-4370.

200. Y. Ma, H. Su, X. Kuang, X. Li, T. Zhang and B. Tang, *Anal. Chem.*, 2014, **86**, 11459-11463.

201. Y.-Y. Cao, X.-F. Guo and H. Wang, *Sens. Actuators, B*, 2017, **243**, 8-13.

202. Y. Li, X. Zhang, L. Zhang, K. Jiang, Y. Cui, Y. Yang and G. Qian, *J. Solid State Chem.*, 2017, **255**, 97-101.

203. W. J. Kim, N. Terada, T. Nomura, R. Takahashi, S. D. Lee, J. H. Park and A. Konno, *Clin. Exp. Allergy*, 2002, **32**, 287-295.

204. A. J. Hemple, K. S. Kjaergaard, L. Molhave and H. K. Hundnell, *Arch. Environ. Health*, 1999, **54**, 416-424.

205. *Air Quality Guidelines, 2nd ed.*, WHO Regional Office for Europe: Copenhagen, Denmark, 2001.

206. *Occupational Safety and Health Guideline for Formaldehyde Potential Human Carcinogen*, U.S. Department of Health and Human Services, Washington, DC, USA, 1988.
207. Y. Yu, X.-M. Zhang, J.-P. Ma, Q.-K. Liu, P. Wang and Y.-B. Dong, *Chem. Commun.*, 2014, **50**, 1444-1446.
208. H. Zhao, X. Li, W. Li, P. Wang, S. Chen and X. Quan, *RSC Adv.*, 2014, **4**, 36444-36450.
209. J.-N. Hao and B. Yan, *Nanoscale*, 2016, **8**, 12047-12053.
210. C. Li, J. Huang, H. Zhu, L. Liu, Y. Feng, G. Hu and X. Yu, *Sens. Actuators, B*, 2017, **253**, 275-282.
211. K. Vellingiri, A. Deep, K.-H. Kim, D. W. Boukhvalov, P. Kumar and Q. Yao, *Sens. Actuators, B*, 2017, **241**, 938-948.
212. A. Karmakar, N. Kumar, P. Samanta, A. V. Desai and S. K. Ghosh, *Chem. - Eur. J.*, 2016, **22**, 864-868.
213. A. Das and S. Biswas, *Sens. Actuators, B.*, 2017, **250**, 121-131.
214. R. Dalapati, S. Nandi, H. Reinsch, B. K. Bhunia, B. B. Mandal, N. Stock and S. Biswas, *CrystEngComm.*, 2018, **20**, 4194-4201.
215. L. Wang, S. Wang and Y. Chen, *Microchim. Acta*, 2017, **184**, 4597-4602.
216. H. Xu, Y. Xiao, X. Rao, Z. Dou, W. Li, Y. Cui, Z. Wang and G. Qian, *J. Alloys Compd.*, 2011, **509**, 2552-2554.
217. D. Zhao, X. Wan, H. Song, L. Hao, Y. Su and Y. Lv, *Sens. Actuators, B*, 2014, **197**, 50-57.
218. J. Yang, Y. Dai, X. Zhu, Z. Wang, Y. Li, Q. Zhuang, J. Shi and J. Gu, *J. Mater. Chem. A*, 2015, **3**, 7445-7452.
219. A. Das, S. Das, V. Trivedi and S. Biswas, *Dalton Trans.*, 2019, **48**, 1332-1343.
220. H. Xu, C.-S. Cao and B. Zhao, *Chem. Commun.*, 2015, **51**, 10280-10283.
221. J. Chen, F.-Y. Yi, H. Yu, S. Jiao, G. Pang and Z.-M. Sun, *Chem. Commun.*, 2014, **50**, 10506-10509.
222. Z. Guo, X. Song, H. Lei, H. Wang, S. Su, H. Xu, G. Qian, H. Zhang and B. Chen, *Chem. Commun.*, 2015, **51**, 376-379.
223. F. Wang, C. Dong, Z. Wang, Y. Cui, C. Wang, Y. Zhao and G. Li, *Eur. J. Inorg. Chem.*, 2014, **2014**, 6239-6245.
224. A. Mallick, B. Garai, M. A. Addicoat, P. S. Petkov, T. Heine and R. Banerjee, *Chem. Sci.*, 2015, **6**, 1420-1425.

225. J.-J. Liu, Y.-B. Shan, C.-R. Fan, M.-J. Lin, C.-C. Huang and W.-X. Dai, *Inorg. Chem.*, 2016, **55**, 3680-3684.
226. P. Kumar, A. K. Paul and A. Deep, *Microporous Mesoporous Mater.*, 2014, **195**, 60-66.
227. P. Kumar, A. K. Paul and A. Deep, *Anal. Methods*, 2014, **6**, 4095-4101.
228. B. Wang, X.-L. Lv, D. Feng, L.-H. Xie, J. Zhang, M. Li, Y. Xie, J.-R. Li and H.-C. Zhou, *J. Am. Chem. Soc.*, 2016, **138**, 6204-6216.
229. Z. Hu, W. P. Lustig, J. Zhang, C. Zheng, H. Wang, S. J. Teat, Q. Gong, N. D. Rudd and J. Li, *J. Am. Chem. Soc.*, 2015, **137**, 16209-16215.
230. W. J. Rieter, K. M. L. Taylor and W. Lin, *J. Am. Chem. Soc.*, 2007, **129**, 9852-9853.
231. N. Bhardwaj, S. Bhardwaj, J. Mehta, K.-H. Kim and A. Deep, *Biosens. Bioelectron.*, 2016, **86**, 799-804.
232. J.-N. Hao and B. Yan, *Chem. Commun.*, 2015, **51**, 14509-14512.
233. S.-Y. Zhang, W. Shi, P. Cheng and M. J. Zaworotko, *J. Am. Chem. Soc.*, 2015, **137**, 12203-12206.
234. Y. Du, X. Li, X. Lv and Q. Jia, *ACS Appl. Mater. Interfaces*, 2017, **9**, 30925-30932.
235. P. Chandrasekhar, A. Mukhopadhyay, G. Savitha and J. N. Moorthy, *Chem. Sci.*, 2016, **7**, 3085-3091.
236. W. Li, X. Qi, C.-Y. Zhao, X.-F. Xu, A.-N. Tang and D.-M. Kong, *ACS Appl. Mater. Interfaces*, 2017, **9**, 236-243.
237. X. Zhu, H. Zheng, X. Wei, Z. Lin, L. Guo, B. Qiu and G. Chen, *Chem. Commun.*, 2013, **49**, 1276-1278.
238. S.-P. Yang, S.-R. Chen, S.-W. Liu, X.-Y. Tang, L. Qin, G.-H. Qiu, J.-X. Chen and W.-H. Chen, *Anal. Chem.*, 2015, **87**, 12206-12214.
239. L. Qin, L.-X. Lin, Z.-P. Fang, S.-P. Yang, G.-H. Qiu, J.-X. Chen and W.-H. Chen, *Chem. Commun.*, 2016, **52**, 132-135.
240. H.-Q. Zhao, G.-H. Qiu, Z. Liang, M.-M. Li, B. Sun, L. Qin, S.-P. Yang, W.-H. Chen and J.-X. Chen, *Anal. Chim. Acta*, 2016, **922**, 55-63.
241. J. M. Fang, F. Leng, X. J. Zhao, X. L. Hu and Y. F. Li, *Analyst*, 2014, **139**, 801-806.
242. R. Mejia-Ariza, J. Rosselli, C. Breukers, A. Manicardi, L. W. M. M. Terstappen, R. Corradini and J. Huskens, *Chem. Eur. J.*, 2017, **23**, 4180-4186.

243. H.-T. Zhang, J.-W. Zhang, G. Huang, Z.-Y. Du and H.-L. Jiang, *Chem. Commun.*, 2014, **50**, 12069-12072.

CHAPTER 2

Rapid and highly sensitive detection of extracellular and intracellular H_2S by an azide-functionalized Al(III)-based metal-organic framework

This chapter represents synthesis and characterization of a new azide-functionalized Al(III)-based metal-organic framework (MOF) namely CAU-10-N_3 (CAU = Christian-Albrechts-University) which consists of 5-azido-isophthalic acid (H_2IPA-N_3) ligand. The desolvated material was employed as a reaction-based fluorescent turn-on probe for the detection of H_2S in HEPES buffer medium (10 mM, pH = 7.4). The material retained its high selectivity towards H_2S even in the presence of possibly competing biological species. Macrophage cells loaded with probe exhibited blue fluorescence after Na_2S addition, indicating the suitability of the probe for intracellular H_2S detection.

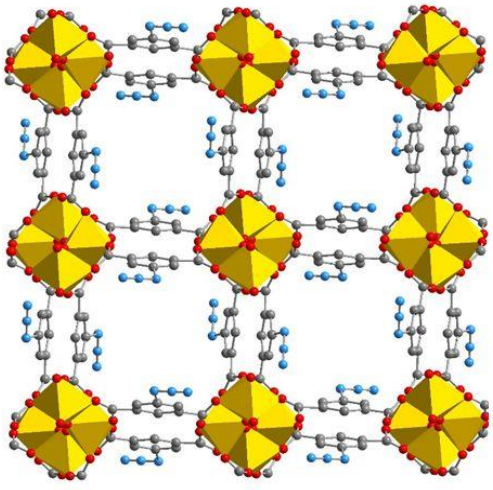

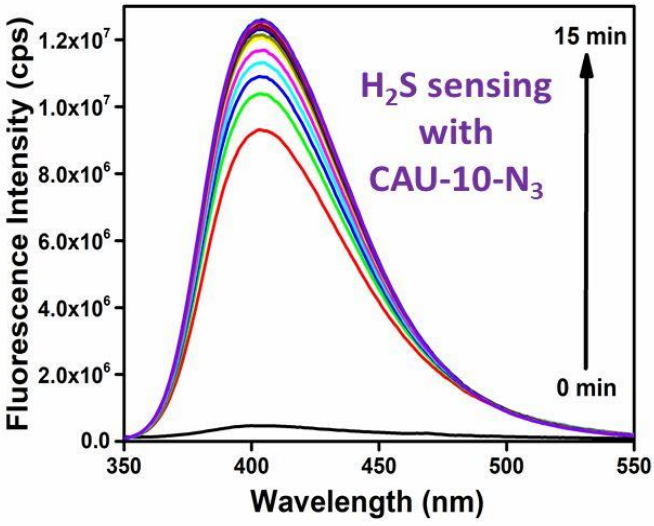

Dalton Transactions

S. Nandi, H. Reinsch, S. Banesh, N. Stock, V. Trivedi, S. Biswas, *Dalton Trans.*, 2017, **46**, 12856.

2.1 Introduction

Hydrogen sulphide (H_2S) is a colourless, flammable gas having characteristic foul odour like rotten eggs. It is commonly regarded as a poisonous gas.[1, 2] It is found in natural sources such as crude petroleum and natural gas. The disintegration of organic matters consisting of sulphur might result in the formation of H_2S. The higher concentration of H_2S in the physiological systems might cause several diseases including diabetes, Down's syndrome, Alzheimer's disease and liver cirrhosis.[3, 4] In spite of its poisonous effects, H_2S has been recently documented as the third member of the family of biological signalling molecules called gasotransmitters, after carbon monoxide (CO) and nitric oxide (NO). H_2S has been proposed to play crucial roles in numerous physiological and pathological processes including angiogenesis, neuroprotection, mediation of neurotransmission, cardioprotection, vasorelaxation, insulin release and control of inflammation.[5-7] Owing to its beneficial roles in physiological and pathological processes as well as fatal roles in living beings, we need to develop fast, selective and sensitive techniques for the practical detection of exogenous as well as endogenous H_2S.

A huge variety of techniques have been utilized until now for the detection and quantification of H_2S. Some of these include colorimetry, spectrophotometry, gas chromatography, high performance liquid chromatography, ion chromatography and electrochemical analysis.[8-10] However, these sensing methods suffer from severe drawbacks such as the necessity of complicated sample processing and the ruin of the cell lysates or tissues. Thus, they are not often found to be suitable for sensing applications in biological media. Compared to these traditional detection techniques, the fluorescence-based sensing method for H_2S has gained tremendous interests recently since it offers a number of benefits including high selectivity and sensitivity, straightforward operation, uncomplicated sample preparation, rapid response and non-damaging sensing of biological analytes.[11-13] A broad variety of materials have been studied so far for the sensing of H_2S. They include nanoparticles, quantum dots, conjugated polymers, small organic molecules, as well as metal-organic framework (MOF) materials.[14-26] However, many of these existing fluorescent probes for H_2S do not fulfil some essential criteria like quick response, high selectivity and sensitivity, etc.

MOFs possess versatile application potentials which range from gas storage/separation, heterogeneous catalysis and chemical sensing to biomedical imaging and drug delivery.[27-30] They are endowed with several important characteristics such as extraordinary physicochemical stability, adjustable porosity and highly conjugated ligands in their pore surfaces.[31, 32] These features make them excellent fluorescent probes for the detection of various categories of analytes. MOFs have several advantages over other luminescent materials. First of all, syntheses procedures of MOFs are much easier and straightforward than other luminescent probes.[33] Furthermore, The crystalline nature of the MOFs helps to determine the exact structure by X-ray diffraction, which is beneficial for describing the possible interaction of MOF with the desired analytes.[34] Due to inherent porosity of the MOF based sensors, the distance between MOF and analyte decreases, which can ensure a close interaction between them.[35] In addition, post-synthetic modification can be successfully executed in MOFs to incorporate new functional groups which can selectively interact with targeted species.[36] Furthermore MOFs are highly photostable and reusable for the detection of various analytes.[37, 38] However, only very few MOFs have been demonstrated thus far to exhibit fluorescence enhancement features in presence of H_2S.[17-22] Four different mechanisms can be identified for the sensing of H_2S by MOFs. They are: (1) H_2S-mediated reduction of nitro/azide groups into amines,[18, 19, 21, 22, 39, 40] (2) coordination of H_2S as the auxochromic group with Pb(II) ions,[41, 42] (3) cleavage of double bond,[17] and (4) H_2S-facilitated precipitation[20, 34] of copper(II) sulfide. Hitherto, only one Al(III)-based MOF has been shown to act as a fluorescent probe for H_2S detection.[22] Given that aluminium is highly abundant, less toxic and cheap, we have synthesized a new, azide-functionalized Al(III)-based MOF namely CAU-10-N_3 (**1**; CAU = Christian-Albrechts-University). In this work, we show that the fluorescence intensity of the thermally activated material (called **1′** henceforward) is enhanced after treatment with H_2S. Hence, it is capable of performing as a reaction-based fluorescent sensor for fast, and highly sensitive sensing of extracellular H_2S (in 10 mM HEPES buffer, pH = 7.4). The capability of the MOF probe to detect intracellular H_2S has been also demonstrated through live-cell imaging studies. We have used Na_2S as the source of H_2S in our sensing experiments.

2.2 Experimental section

2.2.1 Materials and physical measurements

All the reagents and solvents were procured from commercial sources and used without purification except the H_2IPA-N_3 ligand. The latter was prepared by following the previously reported procedure.[43] The Fourier transform infrared (FT-IR) spectra were collected in the region 440-4000 cm^{-1} on a Perkin Elmer Spectrum Two FT-IR spectrometer. The following notations were used in order for characterization of the bands: broad (br), strong (s), very strong (vs), medium (m) and weak (w). Thermogravimetric analyses (TGA) were accomplished with a SDT Q600 V20.9 Build 20 thermogravimetric analyzer in a temperature range of 25-700 °C in air atmosphere with a rate of 5 °C min^{-1}. X-ray powder diffraction (XRPD) patterns were collected with a Bruker D2 Phaser X-ray diffractometer (30 kV, 10 mA) or a STOE STADI MP diffractometer (40 kV, 40 mA) fitted with a Mythen detector, employing Cu-Kα_1 (λ = 1.5406 Å) radiation. FE-SEM images were accumulated with a Zeiss (Zemini) scanning electron microscope. The N_2 sorption isotherms were recorded by Quantachrome Autosorb iQ-MP volumetric gas adsorption equipment at −196 °C. The CO_2 adsorption experiments in the low-pressure range were performed by employing a Quantachrome iSorb-HP gas adsorption instrument at 25 °C. Before the sorption analysis, the degassing of the compound was carried out at 120 °C in high vacuum for 12 h. Fluorescence sensing studies were performed with a HORIBA JOBIN YVON Fluoromax-4 spectrofluorometer. A Bruker Avance III 600 spectrometer was used for recording ^{1}H-NMR at 600 MHz. Before the NMR measurements, the compound **1′** (10 mg) was digested in 450 µL of DMSO-d_6 and 50 µL of 48% HF (caution!). 10 mg of **1′** was treated with Na_2S solution (10 equivalents per azide group) then it was kept for 15 min after that it was filtered, washed and dried, then the resulting compound was digested in similar manner. The mass spectra were measured with an Agilent 6520 Q-TOF high-resolution mass spectrometer (HR-MS). Prior to the HR-MS measurement 10 mg of each **1′** and Na_2S treated **1′** separately added to 1.0 mL HPLC grade methanol then 100 µL of 48% HF (caution!) was introduced and sonicated for 5 min. The organic phase was separated and further diluted with HPLC grade methanol for HR-MS analysis.

2.2.2 Synthesis of [Al(OH)(IPA-N_3)]·3.2H_2O·0.4DMF (as-synthesized 1)

For the synthesis of **1**, 2(M) Al^{3+} solution was prepared by dissolving required quantity of $AlCl_3·6H_2O$ in water. A mixture of H_2IPA-N_3 ligand (0.20 g, 0.97 mmol), 2(M) Al^{3+} solution (0.48 mL, 0.97 mmol), DMF (0.55 mL) and H_2O (1.75 mL) was poured in a Teflon-lined steel autoclave and heated at 120 °C for 12 h. After cooling spontaneously to room temperature, the precipitate was collected by filtration and the solid was re-dispersed in water by sonication to achieve a homogeneous mixture. The suspension was further collected by filtration and the pale yellow crystalline solid was dried in a traditional oven at 100 °C for 4 h. The yield of **1** was 172 mg (0.51 mmol, 53%) related to the Al salt. Anal. cald. for $C_{9.2}H_{13.2}AlN_{3.4}O_{8.6}$ (336.00 g mol^{-1}): C, 32.88 H, 3.95 N, 14.17%. Found: C, 32.65 H, 3.74 N, 14.26%. FT-IR (KBr, cm^{-1}): 3417 (br), 3089 (w), 2919 (w), 2245 (w), 2120 (s), 1640 (s), 1570 (vs), 1457 (s), 1413 (vs), 1299 (m), 1198 (w), 1110 (w), 984 (m), 783 (s), 732 (s), 600 (s), 524 (m).

2.2.3 Activation procedure for the compound

Stirring of the as-synthesized **1** (100 mg) was carried out in methanol (20 mL) at ambient conditions for 12 h. After that the methanol-exchanged material was heated at 120 °C for 12 h under high vacuum. Hereafter, the thermally activated sample is termed as **1′**.

2.2.4 Rietveld refinement

The XRPD pattern of **1** could be successfully indexed using TOPAS academics[44] with a tetragonal *I*-centered cell, neglecting one peak of low intensity at $2\theta \approx 27°$ (a = 21.426(3) Å, c = 10.785(2) Å, extinction conditions suitable for space group $I4_1/a$). A suitable initial model for Rietveld refinement was established using the crystal structure of the CAU-10-OCH_3 material which crystallizes in the same space group.[45] The methoxy groups were replaced by azido groups and after imposing the indexed cell parameters, optimization of the structure was carried out by force-field calculation, using the universal force field as integrated in the Materials Studio software.[46] The refinement of the thus obtained model was performed by Rietveld method using TOPAS. The benzene ring of the ligand molecule and the azido group were refined as rigid bodies whereas all other atoms were freely refined. Residual electron density inside the pores was attributed to water molecules represented by oxygen atoms. However, these atoms should be rather considered placeholders for any kind of solvent molecules. It is worth mentioning that solely by the peak positions, the pattern

allows as well for higher symmetry (i.e. space group $I4_1/amd$). However, the models with higher symmetry were also set up and could not be refined.

2.2.5 Preparation of the medium for fluorescence investigations in HEPES buffer

10 mM HEPES buffer solution was prepared by dissolution of the required amount of HEPES in deionized water (100 mL). Then, NaOH solution (0.5 N) was added drop wise to this solution to maintain a pH of 7.4.

2.2.6 Fluorescence sensing experiments in HEPES buffer

We have performed all the fluorescence measurements with an excitation wavelength (λ_{ex}) of 330 nm. The fluorescence spectra were recorded in the range 340–550 nm. To carry out the fluorescence titration experiments, a suspension containing 0.5 mg of **1′** (1.78 μmol of azide functional group) in 2 mL of 10 mM HEPES buffer (pH = 7.4) was prepared in a fluorescence cuvette. To perform the time-dependent fluorescence sensing measurements, Na_2S (10 equivalents with respect to the azide functionality) was added to the suspension of **1′** and the fluorescence emission spectra were collected at a regular time interval (1 min) until saturation point was reached. We have also performed analogous experiments in which Na_2S was replaced by other competing analytes like alanine, glutathione, serine, cysteine, NaBr, NaCl, NaI, $NaNO_3$, $NaNO_2$, Na_2SO_4, $NaHSO_4$, $NaHSO_3$, Na_2SO_3 and $Na_2S_2O_3$. For determining the selectivity of **1′** for Na_2S in presence of other analytes, the interfering species (10 equivalents per azide group) and Na_2S (10 equivalents per azide group) were added consecutively to the suspension of CAU-10-N_3. Fifteen minutes after addition of these analytes, the fluorescence emission spectra were collected. For the purpose of concentration-dependent fluorescence sensing experiments, we have added 0 to 10 equivalents of Na_2S per azide group in an incremental manner to the suspension of CAU-10-N_3 in HEPES buffer and then the fluorescence emission intensity was monitored. Furthermore, a comparative time-dependent fluorescence sensing experiment was carried out with the aqueous suspension of **1′** instead of HEPES medium.

2.2.7 Culture of macrophage cells

The culture and maintenance of the macrophage cells were carried out according to a previously published procedure.[40]

2.2.8 Cellular imaging investigations

Cellular imaging experiment was performed as described previously with some modifications.[47] Ten thousand macrophage J774A.1 cells were loaded with 5 μM probe **1′** for 12 h at 37 °C. For removal of the probe present in the media, the cells were gently washed and consequently treated with Na_2S (10 μM) for 15 min to generate H_2S gas inside the cells. After this treatment, the cells were observed in the blue channel (λ_{ex} = 385 nm; λ_{em} = 431 nm) in Cytell cell imaging system (GE healthcare). The 10 random fields were selected and imaging was performed in the bright field and blue channel.

2.3 Results and discussion

2.3.1 Preparation and characterization

The conditions for the synthesis of the formerly reported isostructural, single as well as mixed-ligand CAU-10-X (X = -H, $-CH_3$, -OH, $-OCH_3$, $-NH_2$, $-NO_2$)[45, 48-50] materials were followed for the preparation of **1**. In brief, the solvothermal reaction of $AlCl_3 \cdot 6H_2O$ and H_2IPA-N_3 ligand having a 1:1 molar ratio in a DMF/H_2O solvent mixture resulted in the formation of **1** as a pale-yellow crystalline sample. As shown in Figure 2.1, the field emission-scanning electron microscopy (FE-SEM) images disclosed that the compound crystallized as a homogeneous crystalline phase.

For activating the material, the as-synthesized **1** was first stirred with methanol at ambient conditions. Subsequently, the methanol-exchanged **1** was heated in vacuum in order to remove the guest methanol molecules located in the pores. Thus, the thermally activated compound was obtained, which showed very similar XRPD pattern as its as-synthesized form (Figure 2.2). The retention of the structural robustness of the compound during the thermal activation period was confirmed from the XRPD experiment.

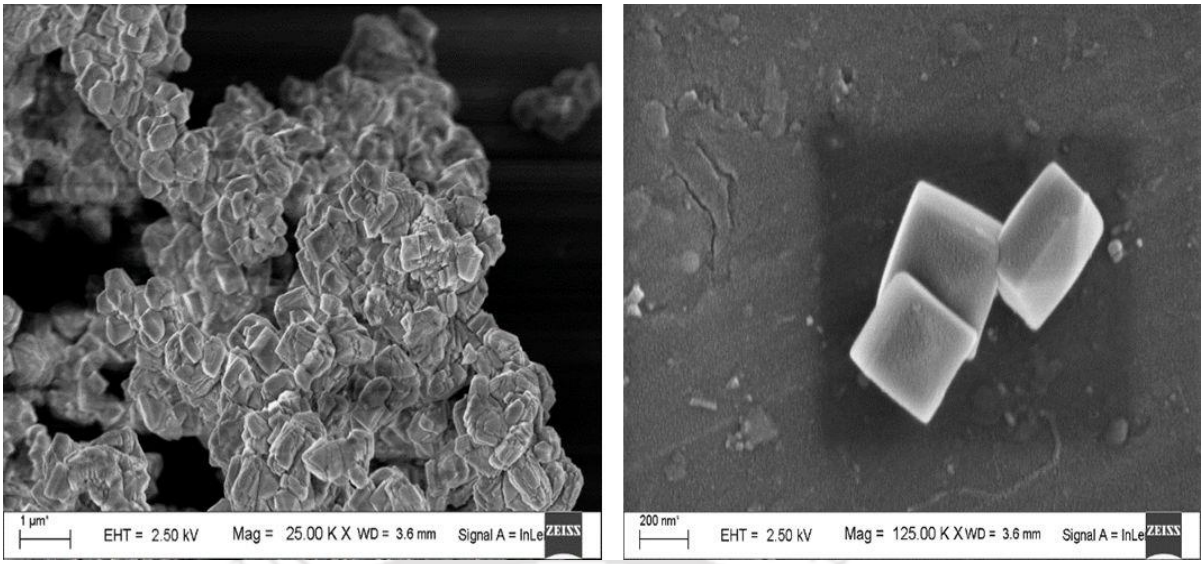

Figure 2.1 FE-SEM images of **1**.

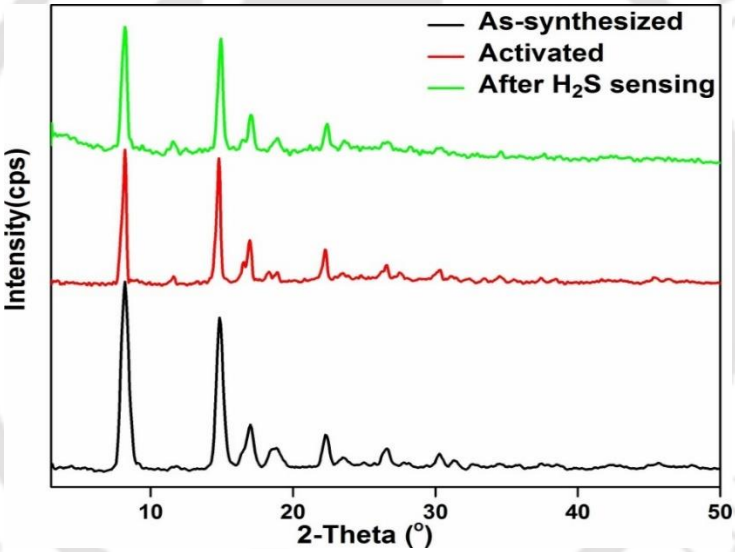

Figure 2.2 XRPD patterns of **1** in different forms: as-synthesized, thermally activated and after H_2S sensing experiment.

2.3.2 FT-IR spectroscopy

As displayed in Figure 2.3, the FT-IR spectra of as-synthesized and activated **1** contain strong absorption bands at about 1575 and 1410 cm^{-1}, which can be attributed to the asymmetric and symmetric $–CO_2$ stretching vibration of the coordinated H_2IPA-N_3 ligand molecules, respectively.[36, 39, 51] The strong absorption band at around 2120 cm^{-1} in the IR spectra of both as-synthesized and activated **1** is due to the azide functional group attached with the coordinated H_2IPA-N_3 ligand molecules. [39, 52]

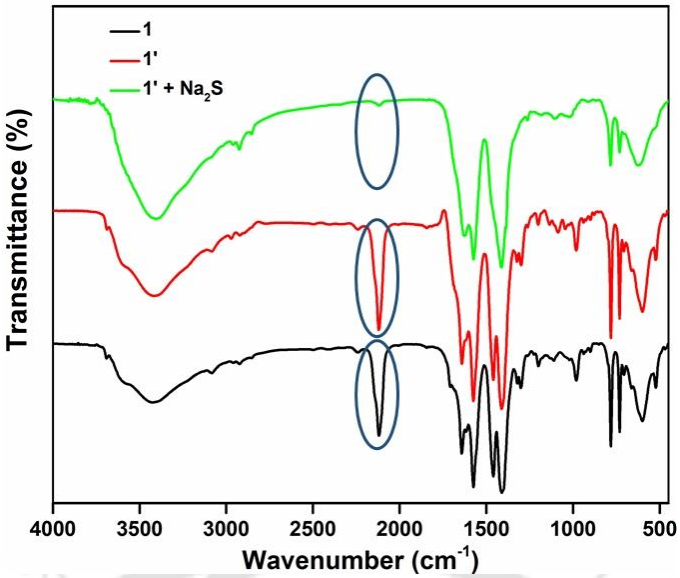

Figure 2.3 FT-IR spectra of as-synthesized (black) **1**, activated (red) **1'** and after treatment with Na_2S (green) **1'**+Na_2S.

2.3.3 Structure description

The room-temperature XRPD pattern of **1** was indexed in a tetragonal crystal system having the space group $I4_1/a$. Rietveld refinement (Figure 2.4) confirmed that **1** exhibits the same space group symmetry as the existing CAU-10-OCH_3 compound[45] (for details, see "Rietveld Refinement" sub-section under Experimental Section). Therefore, the presented MOF material possesses the CAU-10 framework topology. A brief description of the framework structure of **1** is presented here, since the structures of the isostructural, pristine and functionalized CAU-10-X (X = -H, -CH_3, -OH, -OCH_3, -NH_2, -NO_2)[45, 48-50] materials have been formerly described in the literature in detail. The framework of **1** (Figure 2.5) is built up of corner-sharing, *cis*-connected [AlO_6] polyhedra, which form helical chains. In the [AlO_6] polyhedra, four O atoms originate from four different carboxylate groups of the coordinated isophthalate (IPA) ligands whereas the other two O atoms stem from two bridging OH^- ions having *cis* configuration. In the framework, the adjacent helices having opposite handedness to each other are interconnected by the IPA ligands. The resulting network structure consists of sinusoidal, square-shaped channels, having a maximum diameter of 7 Å. The channel walls are decorated with the pendant azide groups of the coordinated IPA-N_3 ligands. The asymmetric unit

of **1** is displayed in Figure 2.6. Some relevant parameters are summarized in Table 2.1.

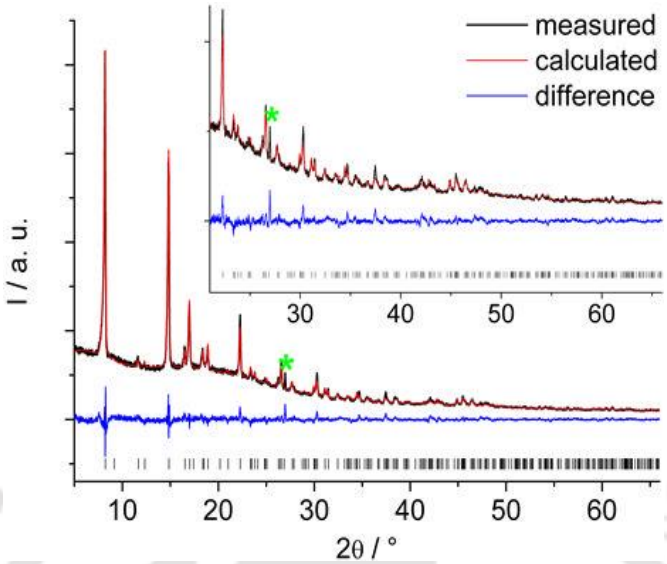

Figure 2.4 Final Rietveld plot for **1**. The black curve represents the measured data, the red curve is the theoretical data and the blue curve indicates the difference. Vertical black bars mark the allowed Bragg reflection positions. The green asterisks indicate a small crystalline impurity.

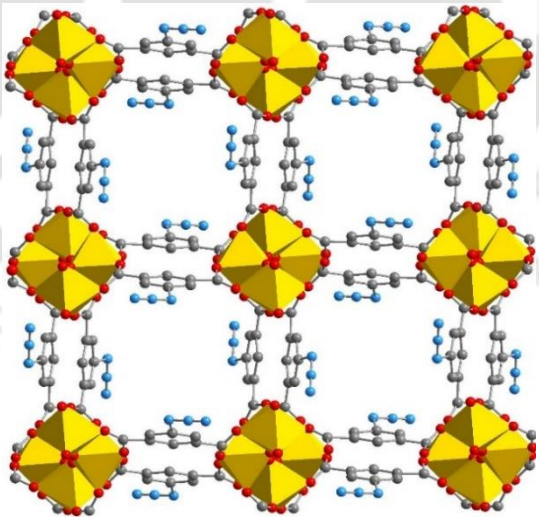

Figure 2.5 Framework structure of CAU-10-N_3 (**1**) in ball-and-stick representation. Color codes: Coordination environment of Al, yellow polyhedra; C, grey; N, blue; O, red. Guest molecules have been removed from the structural diagram for clarity.

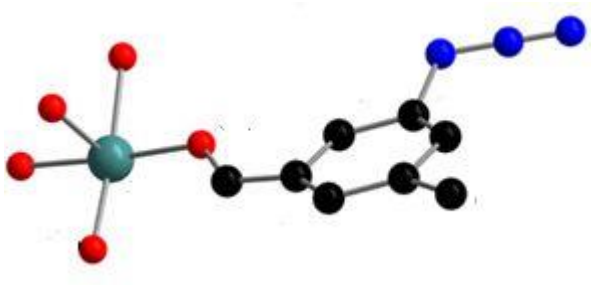

Figure 2.6 The asymmetric unit of **1**. Color codes: Al, sky blue; C, black; N, blue; O, red.

Table 2.1 Structural refinement parameters for **1**

formula	$AlO_5C_8H_3N_3$
crystal system	tetragonal
space group	$I4_1/a$
a / Å	21.4250(14)
c / Å	10.7954(11)
V/ Å^3	4955.4(7)
R_{wp} / %	4.7
R_p / %	3.5
R_{Bragg} / %	1.8
GoF	2.8

2.3.4 Thermal stability

Thermogravimetric (TG) analyses were accomplished for examining the thermal stability of the as-synthesized and activated compound. From Figure 2.7, it becomes unambiguous that that the material is thermally stable only up to 190 °C in an atmosphere. Afterwards, the compound starts to decompose slowly in a wide range of temperature because of the removal of the organic ligand molecules from the framework. Therefore, the material shows significantly lower thermal stability compared to the isostructural, functionalized CAU-10-X (X = -H, -CH_3, -OH, -OCH_3, -NH_2, -NO_2) compounds.[45, 48-50] Very recently, we have reported very low thermal stability for the azide-functionalized Ce-UiO-66 MOF.[39] The later exhibited thermal stability up to 200 °C.

The TG curve of as-synthesized **1** (Figure 2.7) reveals two weight loss steps. The first weight loss step of 17.2 wt% in the temperature range 30-130 °C can be attributed to the removal of 3.2 occluded H_2O molecules per formula unit (calcd.: 17.1 wt%). In the temperature range 130-190 °C, the second weight loss of 8.2 wt% can be related to the loss of 0.4 DMF molecules per formula unit (calcd.: 8.6 wt%).

For activated **1**, the first weight loss step of 7.5 wt% in the temperature range 30-130 °C can be attributed to the loss of adsorbed water molecules from the pores. The occurrence of this weight loss step can be linked to the hygroscopic nature of the activated material. Thus, the compound adsorbs moisture upon exposure to air during storage period.

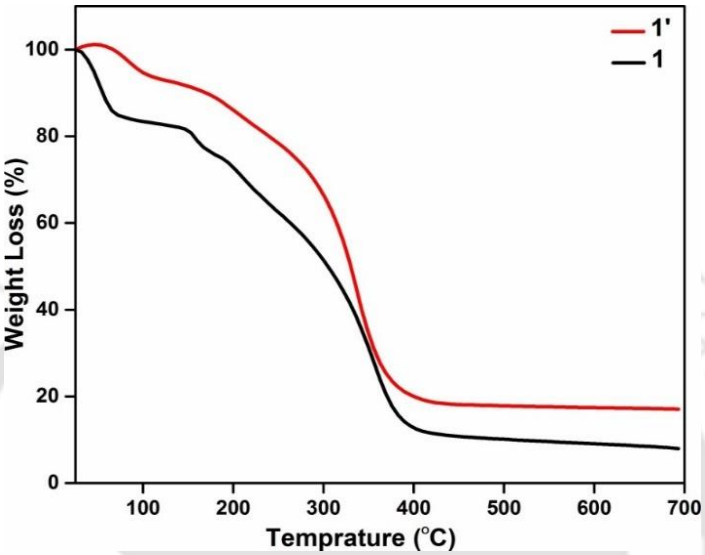

Figure 2.7 TG curves of as-synthesized **1** (black) and activated **1'** (red) recorded in an air atmosphere in the temperature range of 25-700 °C with a heating rate of 5 °C min^{-1}.

2.3.5 Gas adsorption properties

N_2 sorption isotherms were recorded for the thermally activated CAU-10-N_3 compound. The specific BET surface area of **1′**, which was determined from the N_2 adsorption isotherms (Figure 2.8a), was found to be 21 m^2 g^{-1}. This value suggests that the compound is almost non-porous towards N_2 molecules.

The permanent microporosity of the framework structure of **1′** was verified by carrying out CO_2 adsorption measurements in the low-pressure range. The CO_2 adsorption capacity of the MOF material at 1 bar and 25 °C was 1.0 mmol g^{-1} (Figure 2.8b). The CO_2 uptake value of CAU-10-N_3 falls in the ranges formerly reported for isostructural, functionalized CAU-10-X (X = -H, -CH_3, -OH, -OCH_3, -NH_2, -NO_2) compounds.[45, 48-50]

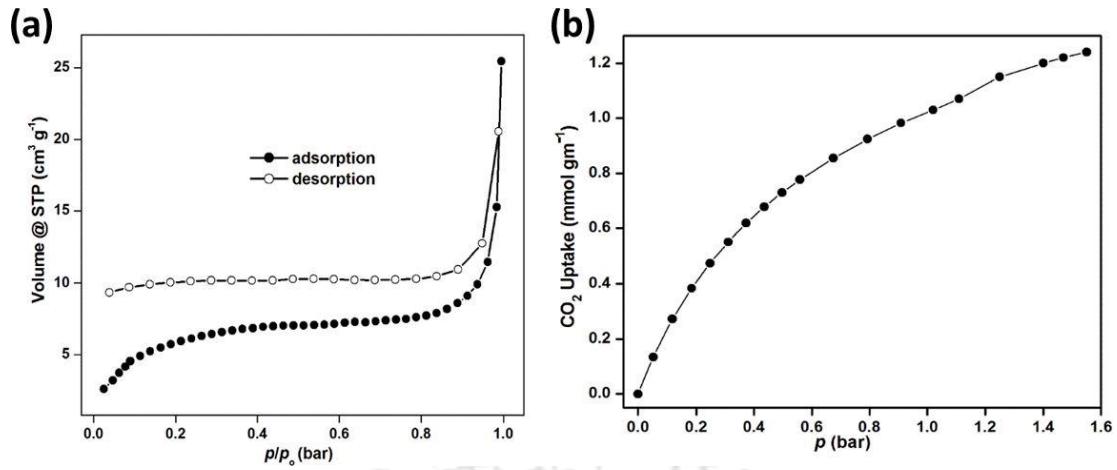

Figure 2.8 (a) N_2 adsorption (solid symbols) and desorption (empty symbols) isotherms of thermally activated **1'** recorded at –196 °C. (b) CO_2 adsorption isotherm of thermally activated **1'** recorded at 25 °C.

2.3.6 H_2S sensing behavior of probe 1′ in HEPES buffer

Al(III)-based MOFs are non-toxic as well as bio-compatible. Hence, several Al(III)-based MOFs have demonstrated huge potentials for biological and medical applications.[20, 53] Recently, we[39] and others[18, 19, 21] have demonstrated the ability of several Zn(II), Zr(IV) and Ce(IV)-based MOFs to detect extracellular as well as intracellular H_2S. More recently, the azide-functionalized Al(III)-based MIL-101 MOF material (which has been prepared by post-synthetic modification of the corresponding amine-functionalized MOF) has been used as a fluorescent turn-on sensor for the detection of H_2S with extraordinary sensitivity in physiological media.[22] Inspired by these facts, we have explored the potential of CAU-10-N_3 towards the rapid and sensitive sensing of both exogenous and endogenous H_2S.

We have performed fluorescence turn-on experiments for checking the sensing performance of CAU-10-N_3 compound for H_2S in physiological media. Before the treatment with H_2S, the azide-functionalized probe **1′** showed weak fluorescence. After the treatment of CAU-10-N_3 with H_2S, the azide groups are post-synthetically reduced to electron-donating amines. In the resulting amine-functionalized MOF material, the electron-donating amine groups push the electron density towards the benzene ring of the coordinated framework ligands. Consequently, the fluorescence emission intensity of the probe was enhanced when exposed to H_2S. It is noteworthy that the compound retained its structural integrity during this reaction-based fluorescence sensing process.

By employing the aqueous solution of Na_2S as the source of H_2S, the detection ability of the CAU-10-N_3 material was evaluated for the fluorimetric sensing of H_2S. Upon addition of Na_2S solution (10 equivalents for each azide group) to the suspension of **1′** in HEPES buffer (10 mM, pH = 7.4), the emission spectra were collected at a systematic time gap of 1 min up to 15 min. It can be seen from Figure 2.9 that the fluorescence emission intensity of **1′** increased nearly 20-fold after 1 min of addition of Na_2S solution. The saturation (with 26-fold increment in the fluorescent intensity) of the fluorescence emission intensity of the material occurred after 7 min of addition of Na_2S solution. Based on the time-dependent fluorescence data, it can be concluded that the CAU-10-N_3 material is a promising fluorescent probe for the real-time monitoring of extracellular H_2S.

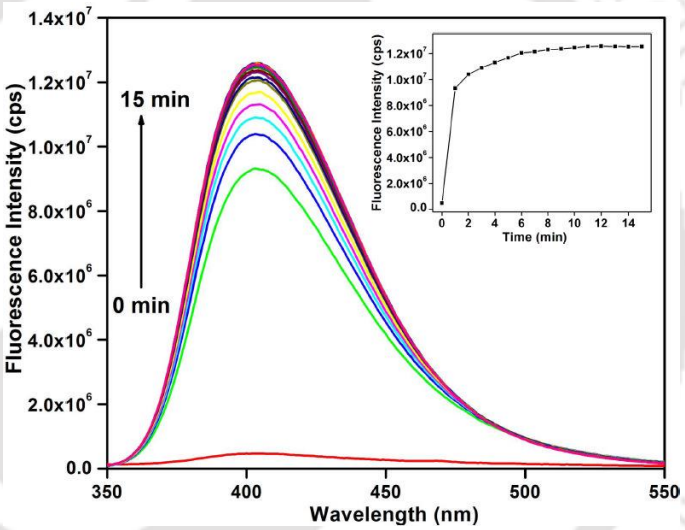

Figure 2.9 Fluorescence enhancement behavior of **1′** in HEPES buffer (10 mM, pH = 7.4) upon gradual addition of Na_2S at a systematic time gap (1 min) up to 15 min. Inset: plot of fluorescence intensity versus time (λ_{ex} = 330 nm and λ_{em} = 405 nm).

It should be noted that the response time of probe **1′** is similar with the formerly documented MOF-type fluorescence sensors for H_2S (Table 2.2).[17-22, 54] On the other hand, the detection capability of **1′** in terms of *n*-fold increase in the fluorescence intensity upon treatment with H_2S is slightly better than the previously reported Zr(IV) and Ce(IV)-based MOF probes.[18, 21, 39] In a comparative study, we have explored the fluorescence enhancement characteristic of CAU-10-N_3 in pure aqueous medium, instead of HEPES buffer. Interestingly, there was a 32-fold increase in the luminescence emission intensity of the MOF probe after 7 min of

H_2S addition in pure aqueous medium (Figure 2.10). Although the compound featured slightly higher increment in the florescence emission intensity (after 7 min of Na_2S addition) in water as compared to HEPES buffer, all the subsequent fluorescence sensing studies were performed in the latter medium since it mimics the physiological conditions. Moreover, the response time of **1′** for H_2S is shorter in HEPES buffer as compared to the aqueous medium, which encouraged us to choose HEPES buffer as the sensing medium.

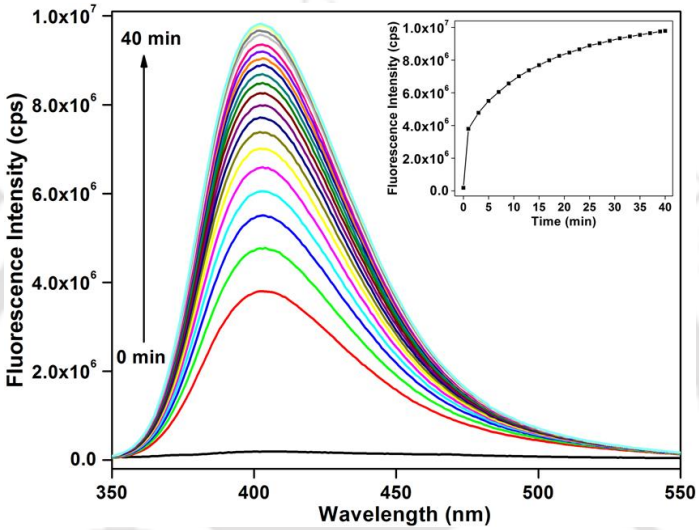

Figure 2.10 Fluorescence turn-on response of **1′** (in pure aqueous medium) towards gradual addition of Na_2S at a regular time interval of 1 min up to 40 min. Inset: time-dependence of the fluorescence emission intensity (λ_{ex} = 330 nm and λ_{em} = 405 nm).

For practical application purpose, a fluorescent sensor should feature high selectivity towards the target analyte when other interfering species co-exist in the biological media. Therefore, we have evaluated the selectivity of CAU-10-N_3 material towards H_2S over other competing biomolecules (serine, alanine, glutathione and cysteine) and usual anions (Cl^-, Br^-, I^-, NO_2^-, NO_3^-, $S_2O_3^{2-}$, SO_4^{2-}, SO_3^{2-}, HSO_3^- and HSO_4^-). To evaluate the selectivity, the fluorescence increment phenomena of **1′** were monitored in presence of these biological species in 10 mM HEPES buffer (pH = 7.4). A careful inspection of Figure 2.11 reveals that the fluorescence emission intensity of the MOF probe remains almost unaffected after treatment with the potentially interfering biochemical species. For most of the cases the increment in emission intensity is less than or nearly equal to 1.5 fold this may be due to the mild reducing nature of some analytes like NO_2^-, I^-, $S_2O_3^{2-}$, SO_3^{2-},

HSO_3^-, cysteine and glutathione[55, 56] but for serine and HSO_4^- the emission enhancement is 1.70 and 1.84 fold respectively, the reason behind this may be the cross reactivity or change in pH of the medium for the addition of analyte. Remarkably, the fold enhancements in presence of competing analytes are almost negligible as compared to Na_2S, which showed around 26-fold increment in emission intensity. Therefore, it can be inferred that CAU-10-N_3 is highly selective towards H_2S over other biological molecules and anions.

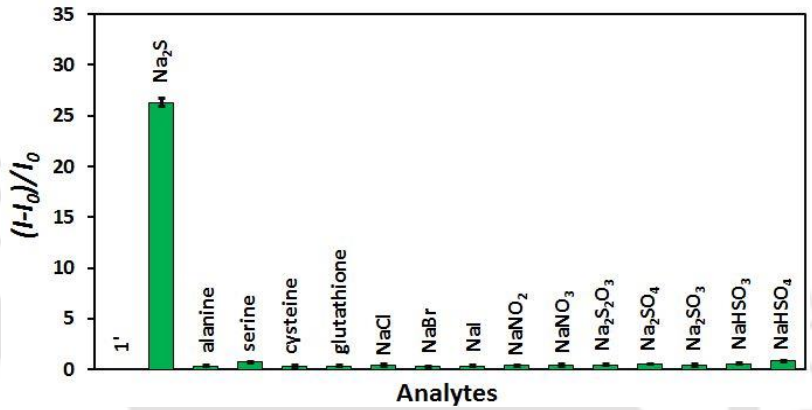

Figure 2.11 Comparative fluorescence enhancement behavior of **1′** in HEPES buffer (10 mM, pH = 7.4) towards different analytes (10 equivalents for each azide group) after 15 min of addition of analyte solution, error bar represents the standard errors of three experiments (λ_{ex} = 330 nm and λ_{em} = 405 nm).

A fluorescent sensor is expected to exhibit fluorescence enhancement properties towards H_2S even in the presence of other biochemical species, which will increase its sensing efficiency in complicated biological systems. Therefore, we have investigated the fluorescence increment behavior of CAU-10-N_3 compound towards H_2S in presence of other intrusive species. In the beginning, Na_2S (10 equivalents per azide functionality) was added to **1′** dispersed in HEPES buffer (10 mM, pH = 7.4), which also consisted of the competing biological species (10 equivalents per azide group). Fifteen minutes after the addition of Na_2S solution, the luminescence emission spectra of the resulting suspension were measured. It becomes evident from Figure 2.12 that the presence of the interfering analyes had negligible effects on the fluorescence turn-on features of the compound for H_2S. Hence, it can be concluded that the selectivity of CAU-10-N_3 for the sensing of H_2S is preserved despite in the existence of other intrusive biological species.

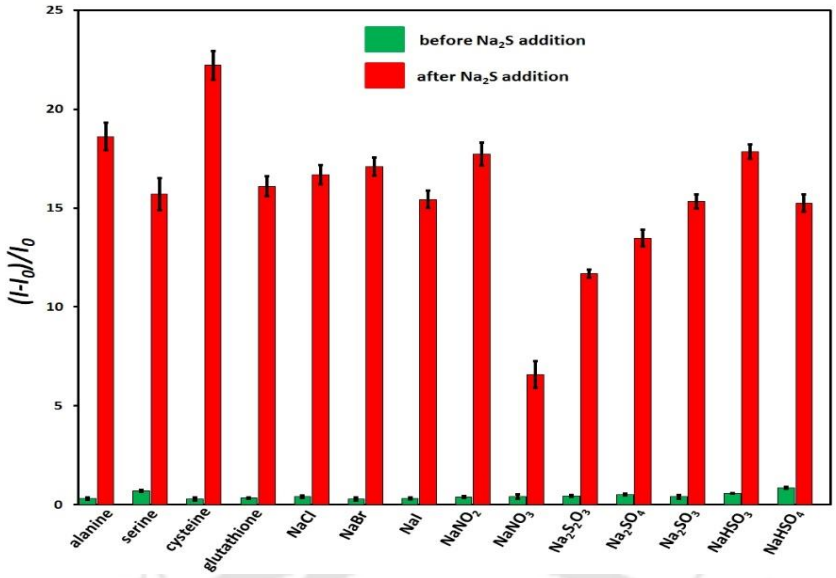

Figure 2.12 Fluorescence increment properties of **1'** in HEPES buffer (10 mM, pH = 7.4) upon addition of an intrusive analyte (green), followed by addition of Na_2S (red), error bar represents the standard errors of three experiments (λ_{ex} = 330 nm and λ_{em} = 405 nm).

The quantification of the fluorescence enhancement characteristics of the MOF probe in presence of H_2S was carried out by fluorescence titration experiments. In these experiments, we have measured the fluorescence emission spectra of the suspension of CAU-10-N_3 in HEPES buffer (10 mM, pH = 7.4) after addition of Na_2S (0 to 10 equivalents with regard to azide group) in an incremental manner. It can be observed from Figure 2.13 that the gradual addition of Na_2S solution resulted in progressive increment in the fluorescence emission intensity of the probe. At lower concentration of Na_2S, a linear curve (Figure 2.14) was obtained by plotting the fluorescence intensity of the probe versus the concentration of Na_2S. From this linear curve, the limit of detection (LOD) of CAU-10-N_3 for H_2S was deduced by using the following formula: LOD = $3\sigma/s$, where s symbolizes the slope of linear curve and σ represents the standard deviation for repetitive measurements of the blank solution.[57] For the present probe, the LOD value for H_2S has been calculated to be 2.65 μM. It should be noted that nanomolar to micromolar levels of H_2S concentration are normally found in the biological media.[58] This fact implies that the sensitivity of the probe can be utilized for the sensing of intracellular H_2S. The LOD value of CAU-10-N_3 for H_2S is lower than the literature values[17-22, 54] of other MOF sensors (Table 2.2). We have performed XRPD measurements for

checking the structural integrity of the probe after the H_2S sensing experiments. The XRPD pattern of **1′** recovered after the H_2S sensing experiments was very similar with that of the untreated **1′** (Figure 2.2), indicating its high structural robustness under the experimental conditions.

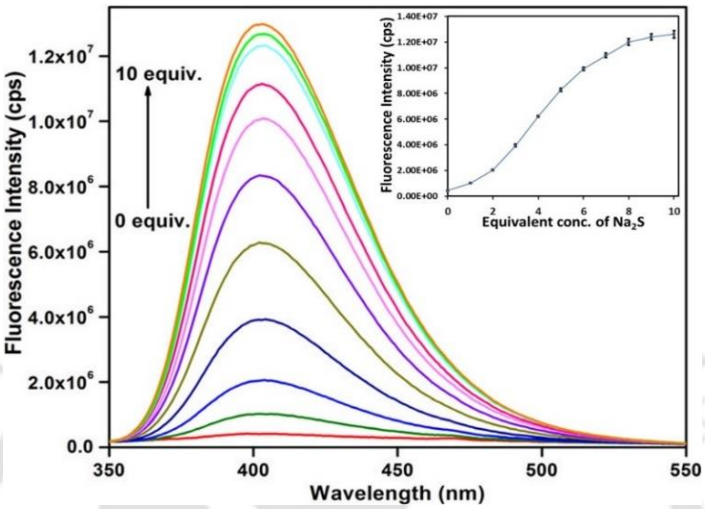

Figure 2.13 Fluorescence increment features of **1'** in HEPES buffer (10 mM, pH = 7.4) with increasing concentrations of Na_2S. (Incubation time: 1 min) Inset: concentration-dependence of the emission intensity, error bar represents the standard errors of three experiments (λ_{ex} = 330 nm and λ_{em} = 405 nm).

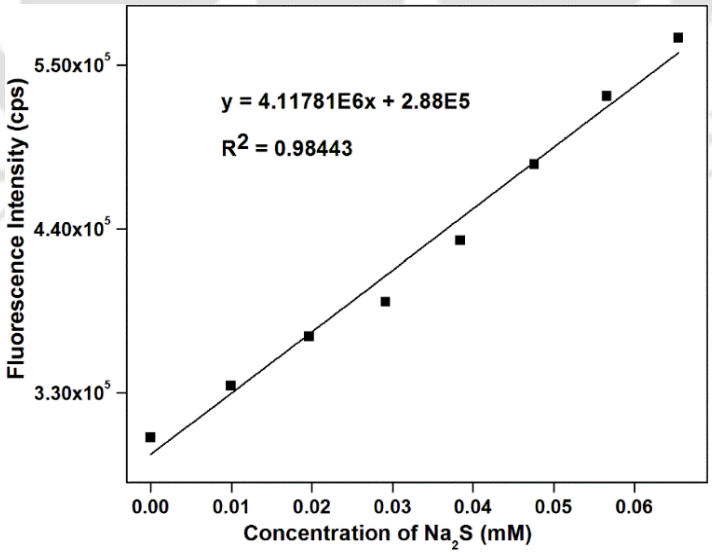

Figure 2.14 Change in the fluorescence intensity of **1′** in 10 mM HEPES buffer as a function of concentration of Na_2S.

Table 2.2 Comparison of the response time, detection limit and analyte used for the detection of H_2S by previously reported MOFs.

Sl. No.	MOF	Response Time (s)	Detection Limit (μM)	Analyte	Ref.
1	CAU-10-N_3	420	2.65	Na_2S	this work
2	DUT-52-$(NO_2)_2$	3300	20.0	Na_2S	47
3	Ce-UiO-66-N_3	760	12.2	NaSH	39
4	Ce-UiO-66-NO_2	760	34.84	NaSH	39
6	IRMOF-3-N_3	< 120	28.3	NaSH	59
7	Zr-UiO-66-NO_2	≈ 460	188	Na_2S	18
8	Zr-UiO-66-N_3	180	118	Na_2S	21
9	MN-ZIF-90	-	-	-	17
10	Al-TCPP-Cu	-	-	-	20
11	Al-MIL-101-N_3	-	100 (UV-lamp excitation); 0.1 (laser excitation)	Na_2S	22
12	Eu^{3+}/Cu^{2+}@UiO-66-$(COOH)_2$	30	5.45	NaSH	54

2.3.7 Mechanism for the detection of H_2S

For the determination of mechanism for the sensing of H_2S by **1'**, we performed FT-IR, mass and ^1H NMR spectroscopic analyses. In the FT-IR spectrum of Na_2S-treated **1'** (Figure 2.3), the characteristic absorption band for the azide group at 2120 cm^{-1} (found in as-synthesized and activated samples) was almost vanished. This observation signifies that the azide functionality has reacted with Na_2S. In the mass spectrum of the digested sample of un-treated **1'** (Figure 2.15), the most intense peak was found at m/z = 206.0684 (measured in negative ion mode), which corresponds to $(M{-}H)^-$ ion (M = mass of H_2IPA-N_3 ligand).The mass spectrum of the digested sample of Na_2S-treated **1'** (Figure 2.16) exhibits two intense peaks at m/z = 206.0657 and 180.0718 (measured in negative ion mode), which can be assigned to the $(M{-}H)^-$ ion of H_2IPA-N_3 and reduced H_2IPA-N_3 (i.e. H_2IPA-NH_2) ligands, respectively. Hence, it can be concluded that the azide functionality has been reduced to amine in presence of Na_2S during the sensing experiment.

In order to calculate the percentage conversion of azide into amine under experimental conditions for sensing, ^1H NMR analysis (Figure 2.17) was carried out with the digested samples of un-treated and Na_2S-treated **1'**. For un-treated **1'**, the peaks at 7.71 and 8.19 ppm correspond to two equivalent aromatic protons near azide functionality and one aromatic proton between two carboxyl groups of H_2IPA-N_3 ligand, respectively. In

case of Na_2S-treated **1'**, two new peaks at 7.96 and 8.28 ppm arise along with the signals for the aromatic protons of $H_2IPA\text{-}N_3$ ligand. The new peaks appear due to the aromatic protons of $H_2IPA\text{-}NH_2$ ligand. According to the peak area ratio between the protons of $H_2IPA\text{-}N_3$ and $H_2IPA\text{-}NH_2$ ligands, the calculated degree of conversion of the azide groups into amines is ~28% under the experimental conditions for sensing.

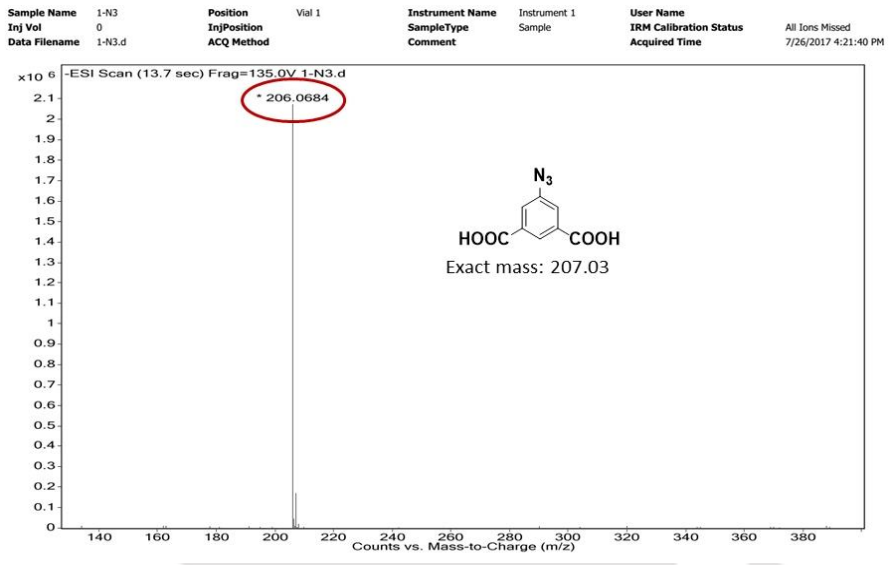

Figure 2.15 HR-MS spectrum of the digested **1′** showing m/z (negative ion mode) peak at 206.0684, which corresponds to $(M\text{-}H)^-$ ion (M = mass of $H_2IPA\text{-}N_3$ ligand).

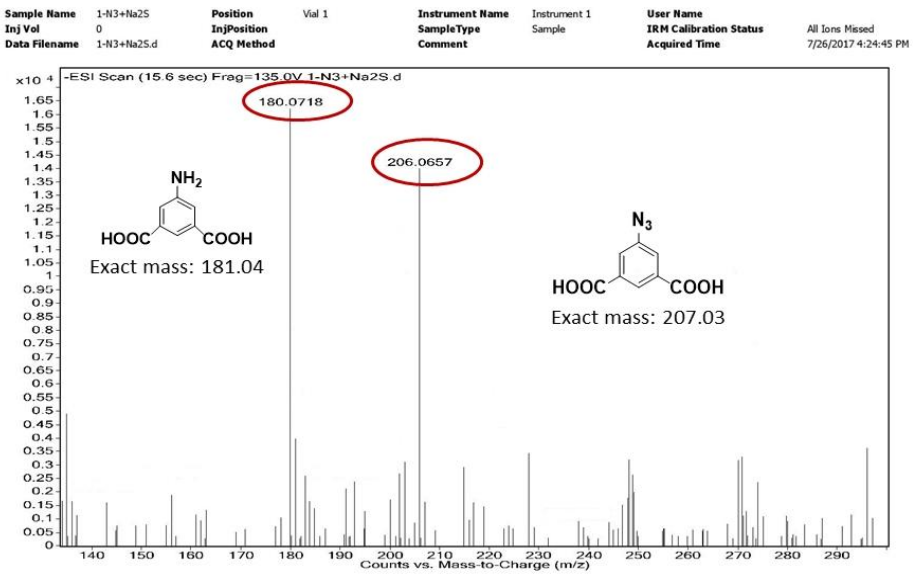

Figure 2.16 HR-MS spectrum of the digested Na_2S treated **1′** showing m/z (negative ion mode) peak at 206.0657 and 180.0718, which corresponds to $(M\text{-}H)^-$ ion of $H_2IPA\text{-}N_3$ ligand and reduced $H_2IPA\text{-}N_3$ ligand i.e $H_2IPA\text{-}NH_2$ respectively.

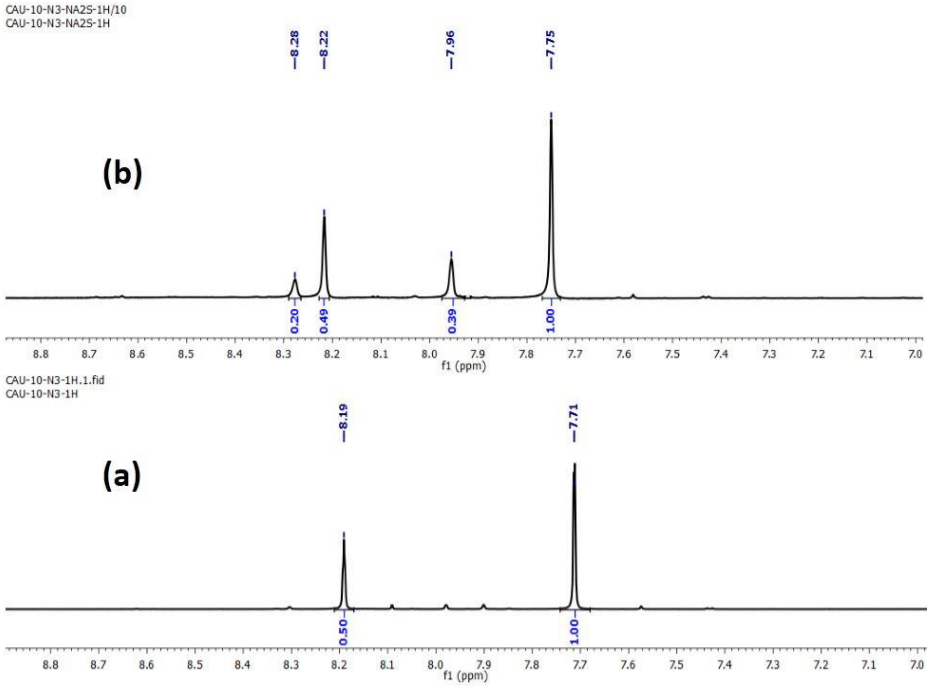

Figure 2.17 ^{1}H NMR spectrum of (a) **1′** and (b) Na_2S treated **1′** after digestion in DMSO-d_6/HF. New signals at 7.96 ppm and 8.28 ppm arises in case of Na_2S treated **1′** which prove the conversion of amine functionality from azide.

2.3.8 Suitability of probe 1′ for sensing H_2S in living cells

The quick response, selectivity and high sensitivity of CAU-10-N_3 towards sensing of exogenous H_2S encouraged us to explore its sensing performance for endogenous H_2S. In order to check the aptness of the material for sensing H_2S in biological systems, we have carried out live-cell imaging experiments in J774A.1 macrophage cells. The generation of intracellular H_2S was performed by first loading the macrophage cells with 5 µM probe and consequently incubating them with 10 µM Na_2S solution. Good morphology in the bright field was observed for the untreated cells, which did not exhibit any fluorescence in the blue channel (Figure 2.18a-b). When the cells were loaded with the probe only, low background fluorescence was noticed (Figure 2.18c-d). On the other hand, bright fluorescence signal was obtained for the cells which were loaded with **1'** and subsequently treated with Na_2S (Figure 2.18e-f). These cells also displayed healthy cellular morphology in the bright field. In this case, the fluorescence signal originated from all the cells but it was not uniform. Few cells glowed with brighter fluorescence than the others. The differential response in the cellular population can be mostly attributed to the age (young/old) and the capacity of these cells to uptake probe or analyte present in

the microenvironment.[60] From these observations, it can be concluded that the present probe is suitable for sensing intracellular H_2S.

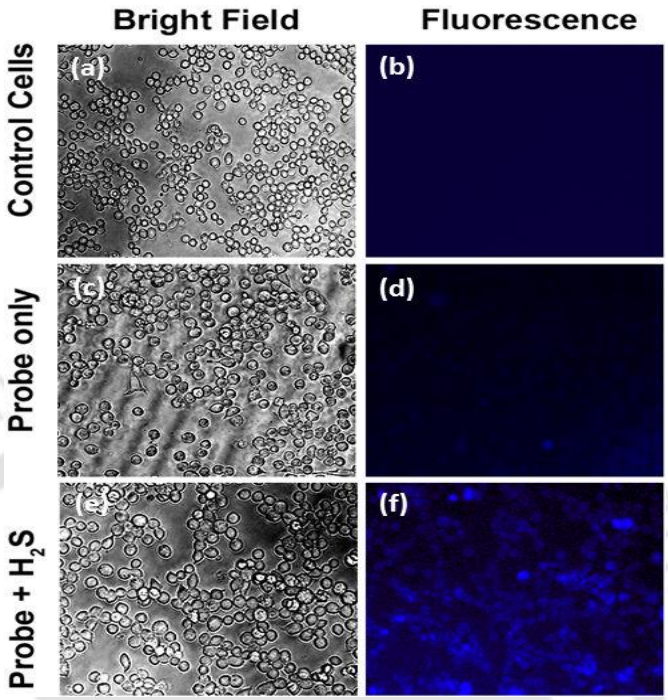

Figure 2.18 Ability of **1'** to detect H_2S in macrophage J774A.1 cells. Bright-field images of untreated cells (a), cells treated with 5 μM probe (c), and cells treated with 5 μM probe and 10 μM Na_2S (e). (b, d, f) are the fluorescence microscopy images of (a, c, e), respectively. Bright fluorescence was observed for H_2S-treated cells (f) only.

2.4 Conclusions

We have synthesized and comprehensively characterized the Al(III)-based, azide-functionalized MOF material called CAU-10-N_3 (**1**). The activated material **1′** has been demonstrated to detect extracellular H_2S (in 10 mM HEPES having pH of 7.4) with rapidness, selectivity and high sensitivity. The compound is capable of sensing H_2S even in the presence of other interfering biological molecules and anions commonly found in biological systems. The limit of detection of **1′** (2.65 μM) for H_2S is lower than for the existing MOF-type fluorescent probes for H_2S. The MOF compound shows very short response time and considerably high fold-increase in fluorescence emission intensity when treated with H_2S in HEPES buffer. Interestingly, probe **1′** is capable of detecting H_2S inside the macrophage cells with high sensitivity and short response time. Furthermore, the excellent detection

performance (in terms of short response time and extraordinary fold-increment in fluorescence intensity) in pure aqueous medium makes CAU-10-N_3 a possible candidate for the regulation of H_2S concentration in environmental (aqueous) samples.

2.5 References

1. R. Martínez-Máñez and F. Sancenón, *Chem. Rev.*, 2003, **103**, 4419-4476.
2. A. P. d. Silva, H. Q. N. Gunaratne, T. Gunnlaugsson, A. J. M. Huxley, C. P. McCoy, J. T. Rademacher and T. E. Rice, *Chem. Rev.*, 1997, **97**, 1515-1566.
3. K. Eto, T. Asada, K. Arima, T. Makifuchi and H. Kimura, *Biochem. Biophys. Res. Commun.*, 2002, **293**, 1485-1488.
4. S. Fiorucci, E. Antonelli, A. Mencarelli, S. Orlandi, B. Renga, G. Rizzo, E. Distrutti, V. Shah and A. Morelli, *Hepatology*, 2005, **42**, 539-548.
5. O. Kabil and R. Banerjee, *J. Biol. Chem.*, 2010, **285**, 21903-21907.
6. G. Yang, L. Wu, B. Jiang, W. Yang, J. Qi, K. Cao, Q. Meng, A. K. Mustafa, W. Mu, S. Zhang, S. H. Snyder and R. Wang, *Science*, 2008, **322**, 587-590.
7. A. Papapetropoulos, A. Pyriochou, Z. Altaany, G. Yang, A. Marazioti, Z. Zhou, M. G. Jeschke, L. K. Branski, D. N. Herndon, R. Wang and C. Szabó, *Proc. Natl. Acad.Sci. USA*, 2009, **106**, 21972-21977.
8. D. Jimenez, R. Martinez-Manez, F. Sancenon, J. V. Ros-Lis, A. Benito and J. Soto, *J. Am. Chem. Soc.*, 2003, **125**, 9000-9001.
9. D. G. Searcy and M. A. Peterson, *Anal. Biochem.*, 2004, **324**, 269-275.
10. P. R. Berube, P. D. Parkinson and E. R. Hall, *J. Chromatogr. A*, 1999, **830**, 485-489.
11. F. B. Yu, X. Y. Han and L. X. Chen, *Chem. Commun.*, 2014, **50**, 12234-12249.
12. W. Zhang, P. Li, F. Yang, X. Hu, C. Sun, W. Zhang, D. Chen and B. Tang, *J. Am. Chem. Soc.*, 2013, **135**, 14956-14959.
13. C. Zong, X. Liu, H. Sun, G. Zhang and L. Lu, *J. Mater. Chem.*, 2012, **22**, 18418-18425.
14. P. Wu, J. Zhang, S. Wang, A. Zhu and X. Hou, *Chem. Eur. J.*, 2014, **20**, 952-956.
15. Z. Zhang, Z. Chen, S. Wang, C. Qu and L. Chen, *ACS Appl. Mater. Interfaces*, 2014, **6**, 6300-6307.

16. A. Zhu, Z. Luo, C. Ding, B. Li, S. Zhou, R. Wang and Y. Tian, *Analyst*, 2014, **139**, 1945-1952.
17. H. Li, X. Feng, Y. Guo, D. Chen, R. Li, X. Ren, X. Jiang, Y. Dong and B. Wang, *Sci. Rep.*, 2014, **4**, 4366-4370.
18. S. S. Nagarkar, A. V. Desai and S. K. Ghosh, *Chem. Eur. J.*, 2015, **21**, 9994-9997.
19. X. Zhang, J. Zhang, Q. Hu, Y. Cui, Y. Yang and G. Qian, *Appl. Surf. Sci.*, 2015, **355**, 814-819.
20. Y. Ma, H. Su, X. Kuang, X. Li, T. Zhang and B. Tang, *Anal. Chem.*, 2014, **86**, 11459-11463.
21. S. S. Nagarkar, T. Saha, A. V. Desai, P. Talukdar and S. K. Ghosh, *Sci. Rep.*, 2014, **4**, 7053-7058.
22. A. Legrand, A. Pastushenko, V. Lysenko, A. Geloen, E. A. Quadrelli, J. Canivet and D. Farrusseng, *ChemNanoMat.*, 2016, **2**, 866-872.
23. K. Sun, X. Liu, Y. Wang and Z. Wu, *RSC Adv.*, 2013, **3**, 14543-14548.
24. V. S. Lin, W. Chen, M. Xian and C. J. Chang, *Chem. Soc. Rev.*, 2015, **44**, 4596-4618.
25. J. Li, C. Yin and F. Huo, *RSC Adv.*, 2015, **5**, 2191-2206.
26. H. A. Henthorn and M. D. Pluth, *J. Am. Chem. Soc.*, 2015, **137**, 15330-15336.
27. W. P. Lustig, S. Mukherjee, N. D. Rudd, A. V. Desai, J. Li and S. K. Ghosh, *Chem. Soc. Rev.*, 2017, **46**, 3242-3285.
28. A. H. Chughtai, N. Ahmad, H. A. Younus, A. Laypkov and F. Verpoort, *Chem. Soc. Rev.*, 2015, **44**, 6804-6849.
29. B. Li, H.-M. Wen, W. Zhou and B. Chen, *J. Phys. Chem. Lett.*, 2014, **5**, 3468-3479.
30. J. D. Rocca, D. Liu and W. Lin, *Acc. Chem. Res.*, 2011, **44**, 957-968.
31. Y. Cui, Y. Yue, G. Qian and B. Chen, *Chem. Rev.*, 2012, **112**, 1126-1162.
32. K. Müller-Buschbaum, F. Beuerle and C. Feldmann, *Microporous Mesoporous Mater.*, 2015, **216**, 171-199.
33. Y. Cui, Y. Yue, G. Qian and B. Chen, *Chem. Rev.*, 2012, **112**, 1126-1162.
34. Y. Cui, F. Zhu, B. Chen and G. Qian, *Chem. Commun.*, 2015, **51**, 7420-7431.
35. Z. Hu, K. Tan, W. P. Lustig, H. Wang, Y. Zhao, C. Zheng, D. Banerjee, T. J. Emge, Y. J. Chabal and J. Li, *Chem. Sci.*, 2014, **5**, 4873-4877.
36. R. Dalapati and S. Biswas, *Sens. Actuators., B*, 2017, **239**, 759-767.
37. S. S. Nagarkar, B. Joarder, A. K. Chaudhari, S. Mukherjee and S. K. Ghosh, *Angew. Chem. Int. Ed.*, 2013, **52**, 2881-2885.

38. A. Buragohain, M. Yousufuddin, M. Sarma and S. Biswas, *Cryst. Growth Des.*, 2016, **16**, 842-851.
39. A. Buragohain and S. Biswas, *CrystEngComm*, 2016, **18**, 4374-4381.
40. R. Deshmukh and V. Trivedi, *PLoS One*, 2014, **9**, 103706-103718.
41. X. Xin, J. Wang, C. Gong, H. Xu, R. Wang, S. Ji, H. Dong, Q. Meng, L. Zhang, F. Dai and D. Sun, *Sci. Rep.*, 2016, **6**, 21951-21959.
42. J. Cui, Y.-L. Wong, M. Zeller, A. D. Hunter and Z. Xu, *Angew. Chem. Int. Ed.*, 2014, **53**, 14438-14442.
43. M. Trigo-López, J. L. Barrio-Manso, F. Serna, F. C. García and J. M. García, *Macromol. Chem. Phys.*, 2013, **214**, 2223-2231.
44. A. Coelho, *Topas Academics 4.2, Coelho Software*, 2007.
45. H. Reinsch, M. A. v. d. Veen, B. Gil, B. Marszalek, T. Verbiest, D. d. Vos and N. Stock, *Chem. Mater.*, 2013, **25**, 17-26.
46. G. Siest, *Accelrys Materials Studio Version 5.0*, 2009.
47. R. Dalapati, S. N. Balaji, V. Trivedi, L. Khamari and S. Biswas, *Sens. Actuators., B*, 2017, **245**, 1039-1049.
48. N. Reimer, B. Bueken, S. Leubner, C. Seidler, M. Wark, D. D. Vos and N. Stock, *Chem. Eur. J.*, 2015, **21**, 12517-12524.
49. H. Reinsch, S. Waitschat and N. Stock, *Dalton Trans.*, 2013, **42**, 4840-4847.
50. H. Reinsch, F. M. Hinterholzinger, P. Jaeker, F. Hesse, B. Reimer, T. Bein, M. Položij, D. Nachtigallova, P. Nachtigall and N. Stock, *J. Phys. Chem. C*, 2015, **119**, 26401-26408.
51. R. Dalapati, B. Sakthivel, A. Dhakshinamoorthy, A. Buragohain, A. Bhunia, C. Janiak and S. Biswas, *CrystEngComm*, 2016, **18**, 7855-7864.
52. D. L. Pavia, G. M. Lampman, G. S. Kriz and J. A. Vyvyan, *Introduction to Spectroscopy*, Thomson Brooks/Cole Stamford, USA, 5th edn., 2015.
53. N. J. Hinks, A. C. McKinlay, B. Xiao, P. S. Wheatley and R. E. Morris, *Microporous Mesoporous Mater.*, 2010, **129**, 330-334.
54. X. Zhang, Q. Hu, T. Xia, J. Zhang, Y. Yang, Y. Cui, B. Chen and G. Qian, *ACS Appl. Mater. Interfaces*, 2016, **8**, 32259-32265.
55. L. Xun, E. Topp and C. S. Orser, *Biochem. Biophys. Res. Commun.*, 1992, **182**, 361-366.
56. N. W. Nairn, P. A. Bariola, T. J. Graddis, M. P. VanBrunt, A. Wang, G. Li and K. Grabstein, *Bioconjugate Chem.*, 2015, **26**, 2070-2075.

57. A. R. Lippert, E. J. New and C. J. Chang, *J. Am. Chem. Soc.*, 2011, **133**, 10078-10080.

58. J. Zhang and W. Guo, *Chem. Commun.*, 2014, **50**, 4214-4217.

59. X. Zhang, J. Zhang, Q. Hu, Y. Cui, Y. Yang and G. Qian, *Appl. Surf. Sci.*, 2015, **355**, 814.

60. J. M. Besterman and R. B. Low, *Biochem. J.*, 1983, **210**, 1-13.

CHAPTER 3

A dinitro-functionalized metal-organic framework featuring visual and fluorogenic sensing of H_2S in living cells, human blood plasma and environmental samples

This chapter describes a new dinitro-functionalized Zr(IV) MOF (MOF = metal-organic framework) having UiO-66 (UiO = University of Oslo) framework topology called UiO-66-$(NO_2)_2$. It shows fluorescence turn-on behavior towards H_2S in simulated biological medium (HEPES buffer, pH = 7.4). The compound not only displays highly sensitive fluorometric sensing of H_2S but also exhibits visually detectable colorimetric change towards H_2S under day light. Moreover, the high selectivity of the material towards H_2S is retained even when several other biologically intrusive species co-exist in the sensing medium. Fluorescence microscopy studies in J774A.1 cell revealed the efficacy of the probe for imaging H_2S in living cells. This material can detect H_2S in human blood plasma (HBP) and monitor sulfide concentration in real water samples.

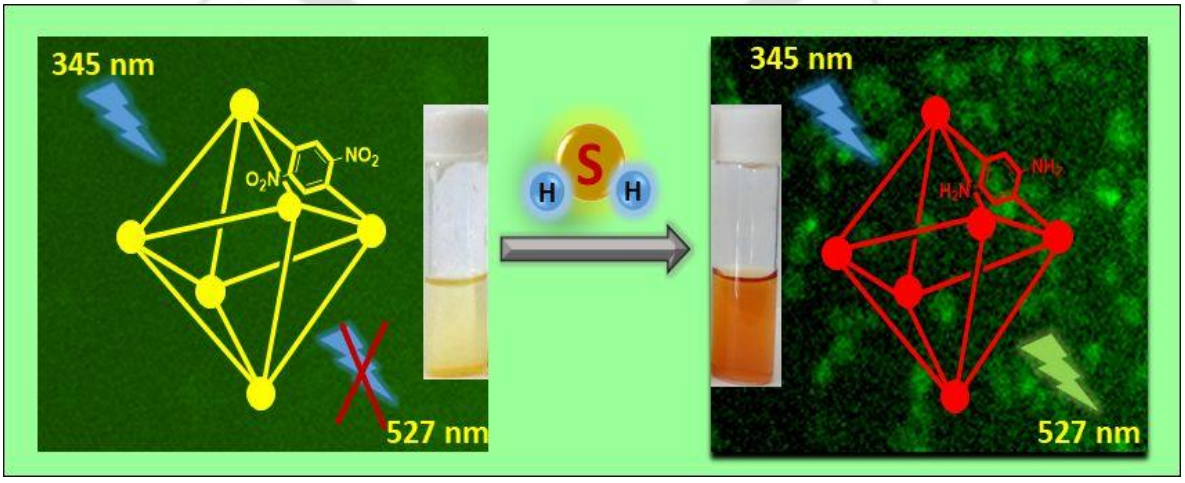

Analyst

S. Nandi, S. Banesh, V. Trivedi, S. Biswas, *Analyst*, 2018, **143**, 1482.

3.1 Introduction

Hydrogen sulphide (H_2S) has drawn more attention than other reactive sulphur species (RSS) due to its hazardous nature on environment as well as on living beings.[1] This gas can be released in the environment as by-product from several industrial processes and petroleum industry as well as from biological sources due to the decomposition of sulphur-containing organic molecules. Although H_2S has several detrimental roles, its ability to function as the third most crucial gasotransmitter has been recognized recently, the other two being CO and NO.[2] This gas performs crucial activity in regulation of blood pressure,[3] anti-inflammatory action,[3] neurotransmission,[4] angiogenesis,[5] anti-oxidation[6] and apoptosis[7]. In enzymes, H_2S can be produced with the help of several endogenous processes.[8, 9] In the biological medium, the concentration of this gas varies from nanomolar to micromolar levels.[10] But, higher concentration of H_2S in the bloodstream may cause several physiological disorders like Alzheimer's disease,[11] diabetes,[12] liver cirrhosis,[13] Down's syndrome[14] and cancer[15]. Therefore, it becomes obvious that H_2S is a potential target for identifying and curing these diseases. Since H_2S is fatal as well as beneficial for living organisms, it is a very important and challenging research task to invent new methods for the rapid and selective sensing as well as controlling the levels of H_2S in biological medium.

The precise detection of H_2S is a very difficult task since it is a highly volatile and reactive gas. Several conventional methods exist for the detection of H_2S levels including gas chromatography,[10, 16] high performance liquid chromatography,[17, 18] electrochemical analysis[19] and colorimetry[20, 21]. But, all these methods are unsuited for the identification of H_2S in living cells because they result in destruction of the cells and tissues.[22] Alternatively, the fluorometric detection technique has aroused significant research interests recently owing to its non-destructive characteristics, high selectivity and sensitivity, fast response, great spatial sampling capability, real-time monitoring and easy sample preparation.[23] Fluorescent "turn-on" probes are advantageous over "turn-off" probes. In case of the former, no false response is obtained, since the bright signal is obtained over a dark background and the signal-to-noise ratio is quite high.[24] Hence, high sensitivity, good selectivity,[25] fast response and cell permeability[26] should be the primary requirements of a proficient fluorescent turn-on sensor for endogenous H_2S.

Though several fluorescent turn-on sensors for H_2S have been documented to date,[27-35] it is still a difficult task to get a novel fluorescent probe having all the above-mentioned features. Many of these sensors do not satisfy essential requirements like rapid detection, selectivity and large fold increment in fluorescence intensity. Now-a-days, reaction-based fluorescent turn-on probes having pendant nitro/azide functionalities have drawn immense attention for the sensitive and selective sensing of H_2S.[28, 30, 31]

Metal-organic frameworks (MOFs),[36] made of metal ions/clusters and bridging ligands, have shown versatile application potentials in chemical sensing,[37-39] gas storage and separation,[40] heterogeneous catalysis[41, 42] and drug delivery[43]. Owing to the extraordinary thermal and chemical stability, adjustable pore size and pore surface functionalities, MOFs have been extensively used for the sensing of various types of analytes.[38] Nevertheless, a very few number of MOFs have been so far demonstrated to exhibit fluorescence turn-on response in presence of H_2S.[27-35, 44] Depending upon the reaction mechanism involved in H_2S sensing, they can be classified in the below mentioned types: (i) reduction of azide/nitro functionality into amine by H_2S causing increment in fluorescence intensity,[27-31, 44] (ii) fluorescent enhancement due to coordination of H_2S to central Pb(II) ions in Pb(II) based MOFs,[45, 46] (iii) precipitation of CuS in presence of H_2S and release of fluorescent MOF having Cu(II)-metalated porphyrin ligands,[47] and (iv) cleavage[48] of double bond by H_2S. Recently, we and other groups have reported Zr(IV) and Ce(IV) based mononitro-functionalized MOFs[28, 30] for selective detection of H_2S. However, the mononitro-functionalized UiO-66 type probes did not exhibit any visually detectable color change after H_2S addition and their applicability to live-cell imaging was not investigated. More recently, we have examined a dinitro-functionalized MOF bearing DUT-52 (DUT = Dresden University of Technology) framework topology for the highly selective sensing of both in vitro and in vivo H_2S.[27] Herein, we present a new dinitro-functionalized MOF with UiO-66 framework topology denoted as UiO-66-$(NO_2)_2$ (**2**). The MOF compound has shown great efficiency for the naked-eye as well as fluorogenic sensing of H_2S (Scheme 3.1) under simulated biological conditions (HEPES buffer, pH = 7.4). The material exhibits highly sensitive and selective sensing characteristics towards H_2S over other competing biological species. In addition, live-cell imaging experiments have been conducted with the non-toxic compound for demonstrating its efficacy to function as a fluorescent turn-on probe for the sensing of intracellular H_2S. Furthermore, the UiO-66-$(NO_2)_2$ material has been successfully applied

to detect H_2S in human blood plasma (HBP) and analyze sulfide concentration in environmental water samples.

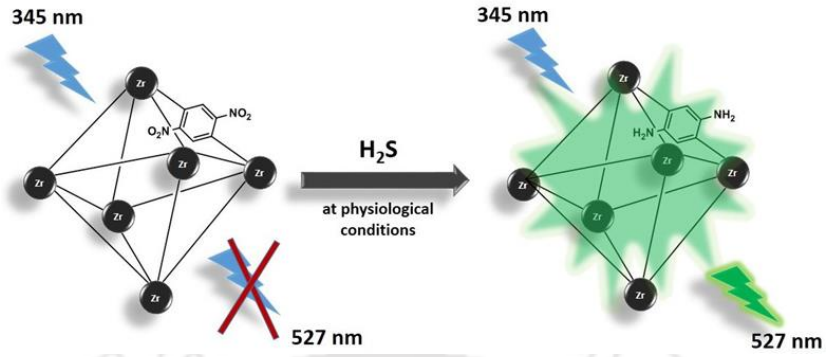

Scheme 3.1 Fluorescence increment behaviour of activated UiO-66-$(NO_2)_2$ MOF (**2'**) due to reduction of nitro groups into amines by H_2S at physiological conditions.

3.2 Experimental section

3.2.1 Materials and characterization methods

The synthesis of the H_2BDC-$(NO_2)_2$[49, 50] and H_2BDC-$(NH_2)_2$[51, 52] (prepared for mechanistic studies) ligands was accomplished as reported in the literature. In Figure 3.1-3.4, the ^{1}H NMR and mass spectra of these two ligands are shown. Other chemicals were obtained from commercial suppliers. Fourier transform infrared (FT-IR) spectra were collected with a Perkin Elmer Spectrum two FT-IR spectrometer in the region 440-4000 cm^{-1} with KBr pellet. The below-mentioned indications were used to represent the absorption peaks: broad (br), shoulder (sh), weak (w), strong (s), very strong (vs) and medium (m). A Netzsch STA449F3A00 thermogravimetric analyzer was used to conduct the thermogravimetric analyses (TGA) in the temperature range 25-700 °C at a heating rate of 10 °C min^{-1} under air atmosphere. The collection of the X-ray powder diffraction (XRPD) patterns at room temperature was conducted with a Bruker D2 Phaser X-ray diffractometer (30 kV, 10 mA) diffractometer, employing Cu-Kα_1 (λ = 1.5406 Å) radiation. The recording of the fluorescence emission spectra was accomplished with a HORIBA JOBIN YVON Fluoromax-4 spectrofluorometer. A Quantachrome Autosorb iQ-MP volumetric gas sorption analyzer was utilized to record the N_2 sorption isotherms at −196 °C. The MOF sample was degassed under high vacuum at 120 °C for overnight. ^{1}H-NMR spectra of **2′** and Na_2S-treated **2′** were recorded by a Bruker Avance III 600 spectrometer. Prior to the experiment, 10 mg of both **2′** and Na_2S-treated **2′** were

digested in 470 µL of DMSO-d_6 and 30 µL of 48% HF (caution!). An Agilent 6520 Q-TOF high-resolution mass spectrometer (HR-MS) was used for mass spectrometry. Before the HR-MS measurement, 15 mg of each of **2′** and Na_2S-treated **2′** were individually digested in 2 mL of HPLC grade methanol by treatment with 150 µL of 48% HF (caution!). After sonication for 10 min, the organic phase was collected by filtration. It was diluted by the addition of HPLC grade methanol for HR-MS measurement.

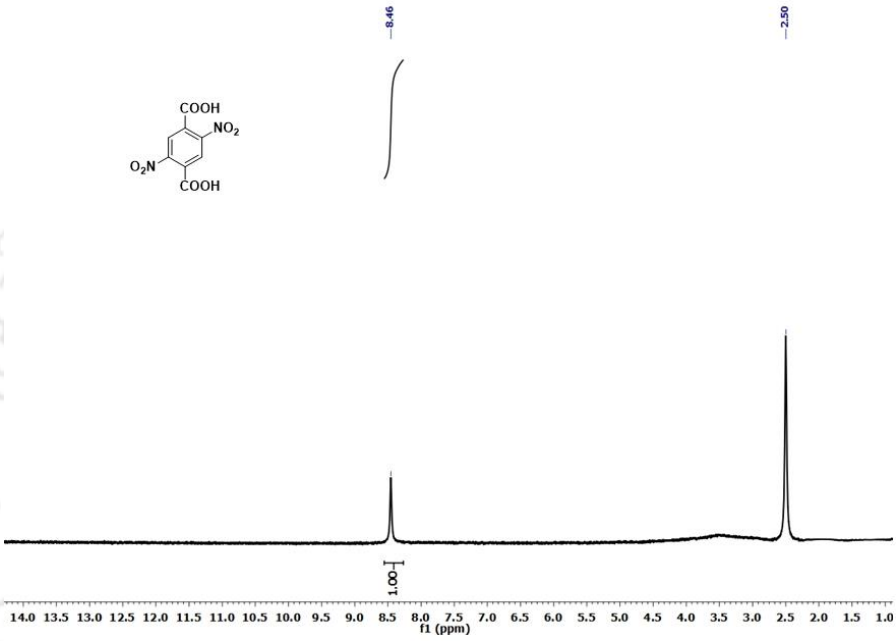

Figure 3.1 ^{1}H NMR spectrum of H_2BDC-$(NO_2)_2$ ligand.

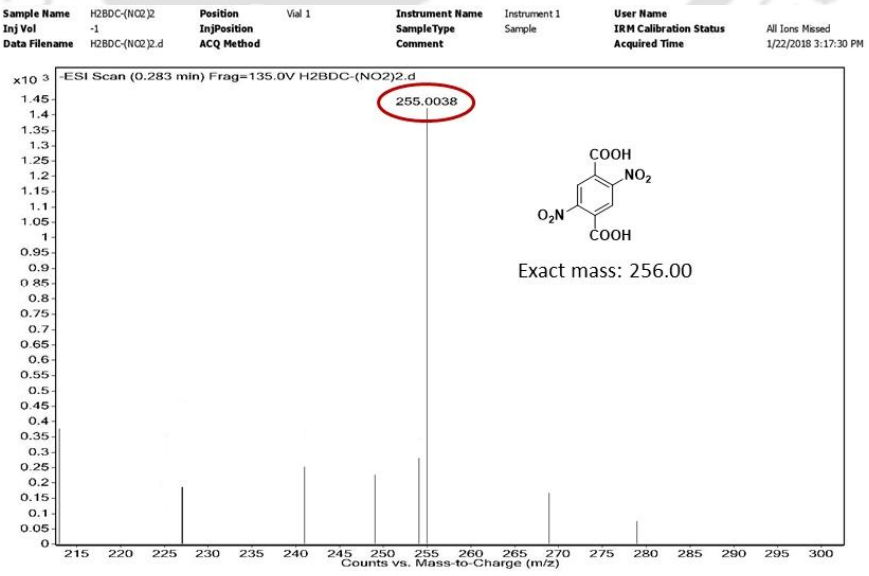

Figure 3.2 HR-MS spectrum of H_2BDC-$(NO_2)_2$ ligand.

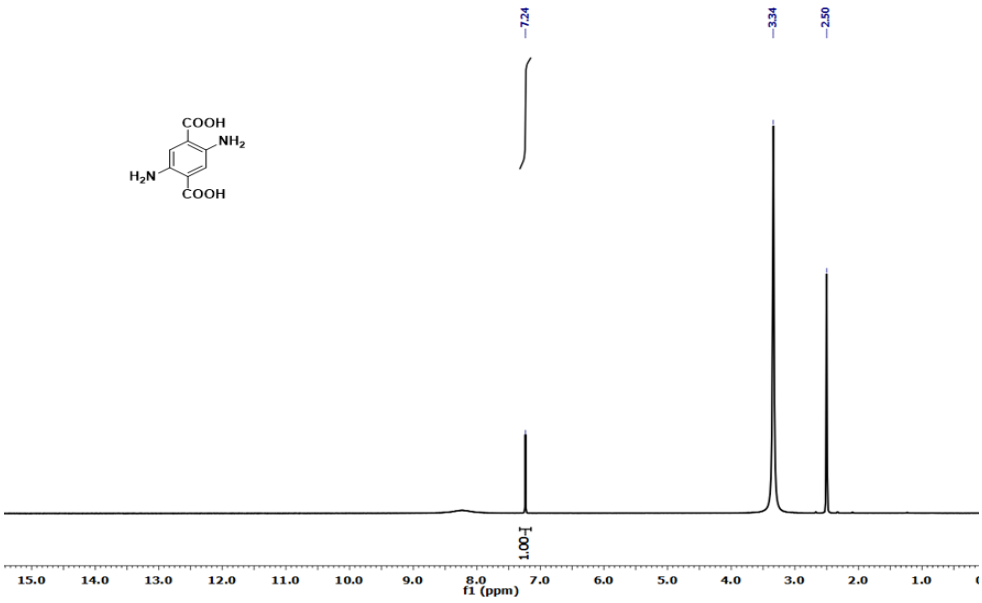

Figure 3.3 ^{1}H NMR spectrum of $H_2BDC\text{-}(NH_2)_2$ ligand.

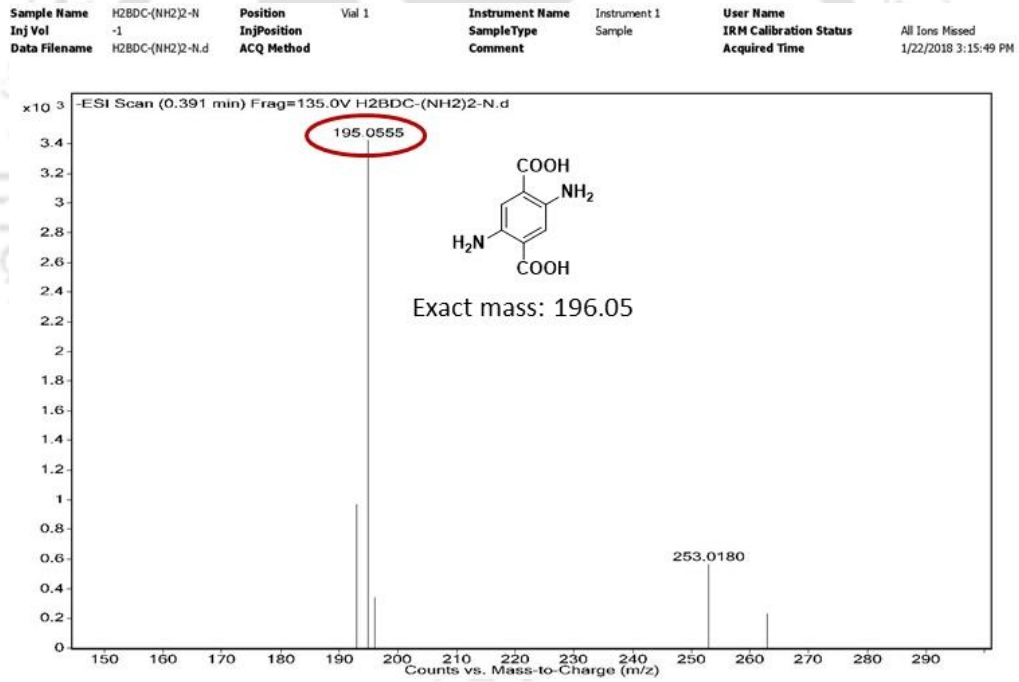

Figure 3.4 HR-MS spectrum of $H_2BDC\text{-}(NH_2)_2$ ligand.

3.2.2 Synthesis of $[Zr_6O_4(OH)_4(BDC\text{-}(NO_2)_2)_6]\cdot 8H_2O\cdot 2DMF$ (UiO-66-$(NO_2)_2$) (2)

In a glass tube, a mixture of $H_2BDC\text{-}(NO_2)_2$ ligand (50 mg, 0.20 mmol), $ZrCl_4$ (46 mg, 0.20 mmol) and benzoic acid (238 mg, 1.95 mmol) was placed. Then, 3 mL of DMF was introduced to the tube. The resulting mixture was dissolved by 15 min of sonication. After sealing the tube tightly, it was heated in a dry block heater at 130 °C for 24 h. Then,

the tube was cooled down to room temperature naturally and the yellow precipitate was filtered off. The material was washed with acetone (2 × 5 mL). Consequently, the drying of the compound was conducted in a conventional oven at 60 °C for 1 h. The yield of **2** was 72 mg (0.03 mmol, 80%). Elemental analysis calcd. for $C_{54}H_{46}N_{14}O_{66}Zr_6$ (2494.29 g mol^{-1}): C 26.00, H 1.84, N 7.86%. Found: C 25.83, H 1.80, N 7.78%. FT-IR (KBr, cm^{-1}): 3420 (br), 3063 (w), 2967 (w), 2857 (w), 1717 (sh), 1655 (sh) 1600 (s), 1552 (m), 1497 (m), 1414 (vs), 1387 (s), 1312 (w), 1264 (w), 1167(w),1023 (w), 927 (w), 866 (w), 797 (w), 721 (m), 653 (s), 570 (w).

3.2.3 Activation of as-synthesized 2

In order to remove the unreacted starting materials and occluded solvent molecules from the voids, we have first stirred the as-synthesized material (200 mg) in methanol (50 mL) at room temperature for overnight. Afterwards, the compound was filtered off. The heating of the material was accomplished in high vacuum at 120 °C for overnight. The thermally activated material is denoted as **2′**.

3.2.4 Preparation of 10 mM HEPES buffer

We accomplished all the fluorescence titration experiments under simulated biological conditions (i.e., 10 mM HEPES buffer, pH = 7.4). The preparation procedure for the HEPES buffer has been described elsewhere by us.[27, 28]

3.2.5 H_2S detection experiments in HEPES buffer

We have measured all the fluorescence spectra in the range of 360–670 nm by exciting at a wavelength of 345 nm. For the fluorescence titration experiments, the UiO-66-$(NO_2)_2$ compound (0.5 mg, 1.36 µmol of BDC-$(NO_2)_2$) was suspended in 10 mM HEPES buffer (2.5 mL) at pH = 7.4 inside a quartz cuvette. In order to conduct the H_2S sensing experiments in a time-dependent manner, Na_2S (10 equiv. of BDC-$(NO_2)_2$) was introduced to the suspension of UiO-66-$(NO_2)_2$. Subsequently, the fluorescence spectra were recorded at a systematic interval (2 min) until the florescence intensity became saturated. Similar experiments were accomplished by the replacement of Na_2S with other potentially competing analytes such as alanine, cysteine glutathione, serine, $NaNO_2$, $NaNO_3$, NaBr, NaCl, NaI, NaSCN, Na_2SO_4, $NaHSO_4$, $NaHSO_3$, Na_2SO_3 and $Na_2S_2O_3$. For determination of the selectivity of **2′** for Na_2S over other analytes, the potentially intrusive analytes (10 equiv. of BDC-$(NO_2)_2$) and Na_2S (10 equiv. of BDC-$(NO_2)_2$) were added to

2′ (dispersed in HEPES buffer) in a consecutive manner and the fluorescence emission spectra were collected after 40 min of addition of these analytes. In case of concentration-dependent H_2S sensing experiments, 0 to 20 equiv. of Na_2S were added stepwise to the suspension of UiO-66-$(NO_2)_2$ in HEPES buffer. After the addition, the fluorescence emission intensity of the compound was monitored.

3.2.6 H_2S sensing experiments in human blood plasma

A human blood sample (4 mL) was collected from the left arm vain. It was poured in a tube consisting of ethylenediaaminetetraacetic acid (EDTA). After centrifugation of the blood at 3000 rpm for 5 min, the plasma was separated. The plasma obtained from this process was used for the sensing experiments. The sensing of H_2S in HBP was performed by utilizing Na_2S as an internal standard. In seven microcentrifuge tubes, 160 µL of HBP and 20 µL of $ZnCl_2$ (final concentration = 1 mM) were added and subsequently 20 µL of Na_2S (final concentrations of 0, 50, 100, 150, 200, 250 and 300 µM) was spiked. Then, the resulting mixtures were incubated at 37 °C for 5 min. After that, 200 µL of 60% (v/v) acetonitrile was added to these tubes to precipitate the proteins. Afterwards, the tubes containing the mixtures were centrifuged at 6000 rpm for 5 min to separate the proteins. After centrifugation, the supernatant liquid was used for the detection of H_2S. 100 µL of HBP was added to the suspension of **2′** (0.5 mg MOF in 2.5 mL HEPES buffer). This suspension was kept undisturbed for 40 min. After that, the fluorescence emission spectra were collected (λ_{ex} = 345 nm, λ_{em} = 527 nm). Note: informed consent was obtained from all human subjects for the collection of blood samples and experimental procedures were conducted in accordance with the ethical guidelines.

3.2.7 Culture of macrophage cells

We have cultured and maintained the macrophage cells by following the reported literature method.[27]

3.2.8 Cell viability assay

J774A.1 cells were seeded in 96 well plate at 50000 per well as described previously.[53] The cells were treated with **2′** with concentrations of 0-100 µM for 24 h in serum free medium. For each concentration of probe, cell images were collected to monitor morphological changes during the treatment with probe. In addition, cellular viability was

measured by MTT assay as described previously.[54] The untreated cells were considered as 100% viable to express the viability of probe-loaded cells.

3.2.9 Live-cell imaging experiments

We have conducted the live-cell imaging experiment by following the procedure described in the literature with few alterations.[27] The incubation of macrophage J774A.1 cells (twenty thousands) with 5 μM of UiO-66-$(NO_2)_2$ was carried out for 12 h at 37 °C. To get rid of the residual probe, we first washed the cells mildly with phosphate buffer saline (PBS) and then treated them with Na_2S (10 μM) for 15 min to produce H_2S within the cells. Subsequently, we have observed the cells in the green channel (λ_{ex} = 461 nm; λ_{em} = 525 nm) using Cytell cell imaging system of GE Healthcare. After choosing ten random fields, the imaging of the cells was accomplished both in the bright field and green channel. In a separate set of experiment, probe-loaded cells were permeabilized with 0.1 % Triton X-100 and then Na_2S sensing experiment was repeated as described.

3.2.10 Sulfide sensing experiments in real water samples

For evaluation of the detection capability of H_2S by **2′** in real water samples, three different types of water samples such as mineral water, tap water and lake water were collected. 'Bisleri' mineral water was used as mineral water, tap water of IIT Guwahati campus was utilized and water of serpentine lake of IIT Guwahati, India was used for lake water. In nine separate microcentrifuge tubes, each of the water samples was spiked with known amount of Na_2S (final concentrations = 50, 75 and 100 μM). The Na_2S-spiked water samples (100 μL each) having three different concentrations were added separately to **2′** (suspended in HEPES buffer). After 40 min of addition, their fluorescence emission spectra were measured (λ_{ex} = 345 nm, λ_{em} = 527 nm).

3.3 Results and discussion

3.3.1 Preparation and characterization

Compound **2** was synthesized by using $ZrCl_4$ as a source of metal. Benzoic acid was employed as a modulator. The synthesis involved solvothermal reaction (130 °C, 24 h) in DMF. The $ZrCl_4$ salt, H_2BDC-$(NO_2)_2$ ligand and benzoic acid were taken in 1:1:10 molar ratio to obtain the yellow microcrystalline powder of UiO-66-$(NO_2)_2$.

The encapsulated guest molecules inside the cages of the as-synthesized material were removed by an activation method comprising two steps. The stirring of as-synthesized **2** was first carried out in methanol at room temperature. Later, the heating of methanol-exchanged **2** was performed under vacuum for getting rid of the guest methanol molecules from the pores.

Figure 3.5 shows that two strong absorption peaks at about 1600 and 1410 cm^{-1} dominate in the FT-IR spectra of the activated and as-synthesized UiO-66-$(NO_2)_2$ material. These two peaks arise due to the asymmetric and symmetric carboxylate stretching vibration of the framework BDC-$(NO_2)_2$ linkers, respectively.[28, 37] In both the IR spectra, the asymmetric N=O stretching vibration due to the presence of $–NO_2$ groups linked with the ligands results in absorption peaks at around 1495 cm^{-1}.[55] The absorption band at 1655 cm^{-1} in the IR spectra of as-synthesized **2** appears due to the stretching vibration of carbonyl group connected with the entrapped DMF molecules.[27] The absence of this band in the activated compound clearly indicates that the DMF molecules have been totally eliminated from the voids of UiO-66-$(NO_2)_2$ framework.

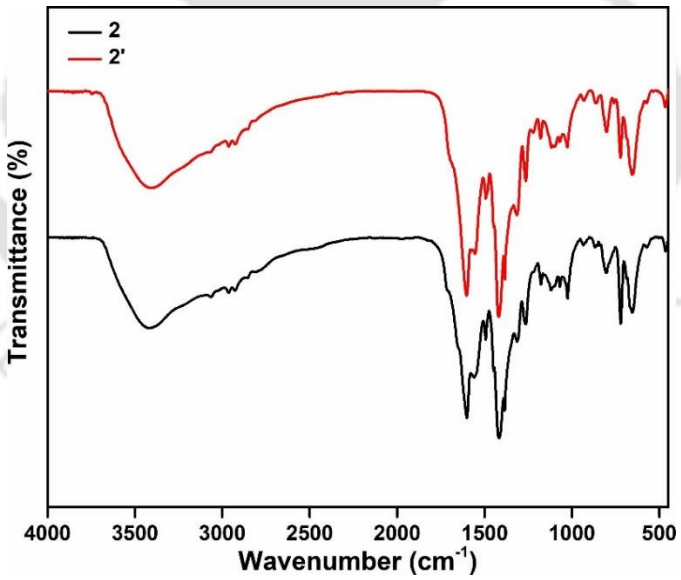

Figure 3.5 FT-IR spectra of as-synthesized **2** (black) and activated (red) **2'**.

As displayed in Figure 3.6, remarkable similarities can be observed between the experimental XRPD pattern of the as-synthesized UiO-66-$(NO_2)_2$ compound and the theoretical XRPD pattern of pristine UiO-66 compound.[56] From these similarities, it can be concluded that the framework of **2** is isostructural with the un-

functionalized UiO-66 material. According to the description by Lillerud's group,[56] UiO-66 framework contains hexanuclear $[Zr_6(OH)_4O_4]^{12+}$ building blocks. Similarly, compound **2** is constructed with hexanuclear $[Zr_6(OH)_4O_4]^{12+}$ building units in which μ_3-OH and μ_3-O groups reside on the triangular faces of the Zr_6 octahedron alternatively. In the Zr_6 octahedron, the carboxylate groups of twelve 1,4-benzenedicarboxylate (BDC) linkers are connected along the edges. This connectivity gives rise to the generation of a three-dimensional (3D), cubic framework, which has tetrahedral as well as octahedral cages (Figure 3.7). Eight tetrahedral cages are located at the corner of every central octahedral cage. These two types of cages are interconnected by constricted trigonal windows. The cages encapsulate guest molecules in the as-synthesized UiO-66 material. It is worthy to note that the BDC-$(NO_2)_2$ linkers replace the BDC linkers of UiO-66 in the presented compound, leading to the UiO-66-$(NO_2)_2$ framework.

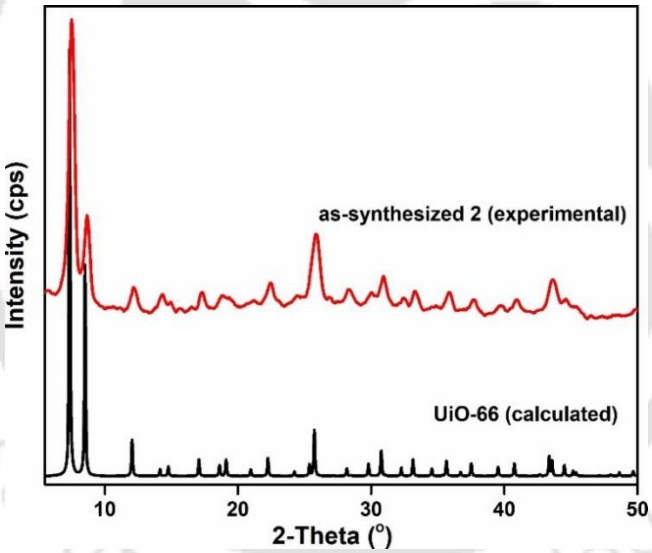

Figure 3.6 Theoretical (black) XRPD pattern of the UiO-66 compound and experimental (red) XRPD pattern of the as-synthesized UiO-66-$(NO_2)_2$ material.

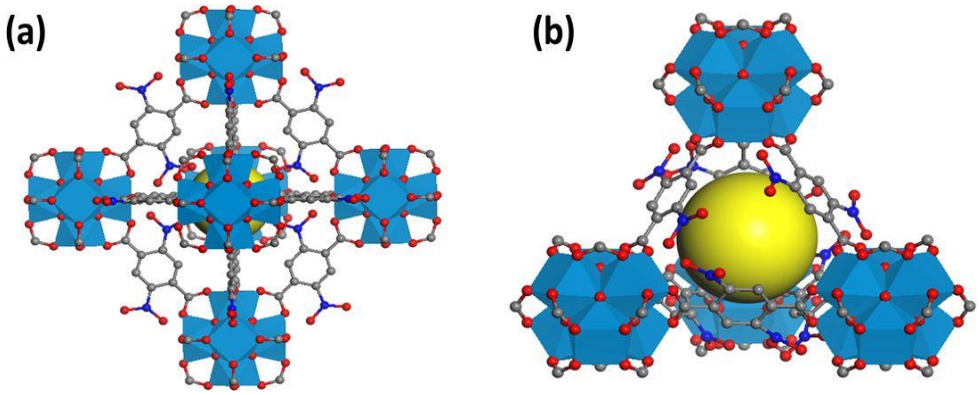

Figure 3.7 Spatial arrangement of the (a) octahedral and (b) tetrahedral cages in cubic UiO-66-$(NO_2)_2$. Color codes: Zr, sky blue polyhedra; C, grey; N, blue; O, red.

For demonstrating the permanent microporosity of the UiO-66-$(NO_2)_2$ compound, N_2 adsorption studies were conducted by employing the activated material. The material displayed N_2 adsorption isotherms of type-I (Figure 3.8a), which revealed its microporosity. As derived from the N_2 sorption isotherms, **2′** possesses a specific BET surface area of 385 $m^2 g^{-1}$. The micropore volume of the material at p/p_0 = 0.5 corresponds to 0.21 $cm^3 g^{-1}$. As expected, **2′** has lower micropore volume specific and BET surface area than the un-functionalized[56] and some other functionalized[57, 58] UiO-66 compounds. It may be related to the partial blockage of cages by the two bulky -NO_2 groups grafted with each linker molecule.

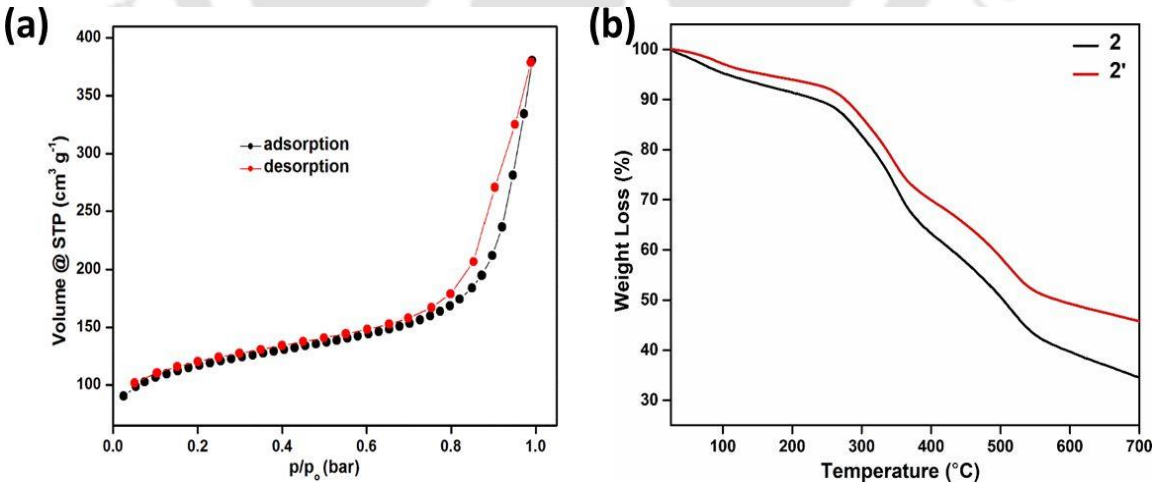

Figure 3.8 (a) N_2 adsorption (black circles) and desorption (red circles) isotherms of thermally activated **2'** recorded at –196 °C. (b) TG curves of as-synthesized **2** (black) and activated **2'** (red) recorded in an air atmosphere in the temperature range of 25-700 °C with a heating rate of 10 °C min^{-1}.

3.3.2 Thermal stability

The thermal stability of the activated and as-synthesized material was investigated by conducting thermogravimetric (TG) analyses under air atmosphere. The TG analyses (Figure 3.8b) show that the compound is stable up to 255 °C under air atmosphere. Then, the decomposition of the compound begins due to loss of organic ligands from the framework. It is noteworthy that **2** shows lower thermal stability than the un-functionalized UiO-66 and few other functionalized[57, 59] UiO-66 compounds. The thermal stability of UiO-66-$(NO_2)_2$ is similar with the UiO-66-$(OH)_2$ material.[57]

Two weight loss steps are found in the TG trace (Figure 3.8b) of as-synthesized UiO-66-$(NO_2)_2$ compound. The weight loss of 5.9% in the temperature range of 25-125 °C shows good agreement with the removal of eight occluded H_2O molecules (calcd.: 5.8%) per formula unit. In the temperature range of 125-255 °C, another weight loss of 5.3% is observed which compares well with the calculated value (5.8%) for the removal of two guest DMF molecules per formula unit. In case of activated UiO-66-$(NO_2)_2$ compound, the first weight loss of 3.7% in the temperature range of 25-125 °C occurs due to the elimination of H_2O molecules from the voids. It is noteworthy that the activated material adsorbs moisture during its storage under air atmosphere.

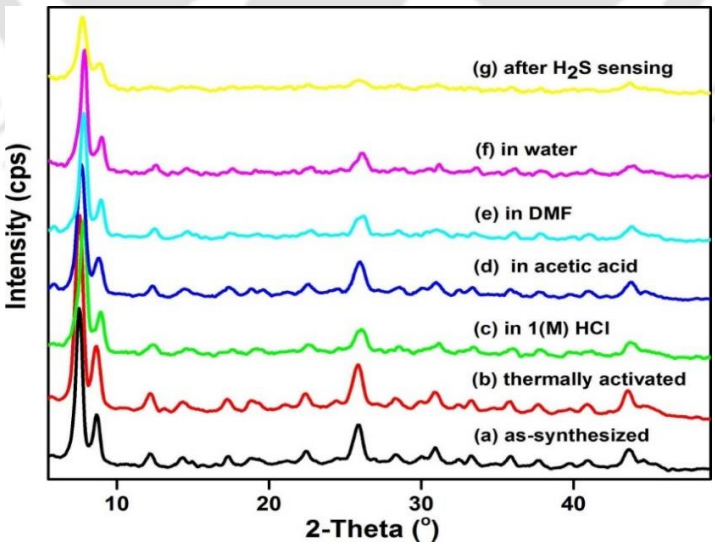

Figure 3.9 XRPD patterns of **2** in different forms: as-synthesized (a), thermally activated (b), after treatment with 1(M) HCl (c), acetic acid (d), DMF (e), water (f) and after H_2S sensing experiment (g).

3.3.3 Chemical stability

To examine the chemical stability, the samples of activated UiO-66-$(NO_2)_2$ compound was stirred for 4 h in different liquids (H_2O, DMF, 1(M) HCl and acetic acid) at room temperature. Then, the compounds were filtered off and XRPD measurements were performed (Figure 3.9). The XRPD pattern of the compound was almost unchanged after the treatment with the above mentioned liquids. Therefore, it becomes clear that the structural robustness of the compound is retained when it is exposed to these liquids. Hence, it can be concluded that UiO-66-$(NO_2)_2$ shows similar chemical stability with un-functionalized UiO-66 and structurally related compounds.[56, 57] As the compound is highly stable in water, we have selected HEPES buffer (pH = 7.4) as the sensing medium for H_2S.

3.3.4 Sensing of H_2S in HEPES buffer

Due to their non-toxicity and bio-friendly nature, Zr(IV)-based MOFs have been progressively used in the field of drug delivery and cellular imaging study.[60, 61] Previously, two mononitro-functionalized[30,28] MOFs namely Zr-UiO-66-NO_2 and Ce-UiO-66-NO_2 have shown highly selective and sensitive detection performance for H_2S under physiological conditions. Recently, a dinitro-functionalized Zr(IV) MOF called DUT-52-$(NO_2)_2$ was investigated by us for the sensing of both extracellular and intracellular H_2S.[27] Inspired by these facts, we have designed and prepared the new dinitro-functionalized Zr(IV)-based UiO-66 MOF. The UiO-66-$(NO_2)_2$ compound has been investigated for the rapid and selective sensing of H_2S in simulated biological fluid (HEPES buffer, 10 mM, pH = 7.4) as well as in living cells. Initially, ***2′*** is in fluorescence turn-off state, since it contains two electron-withdrawing nitro groups per BDC-$(NO_2)_2$ ligand molecule. However, the nitro groups are converted to amine groups by reduction in presence of H_2S, causing increment in the fluorescence emission intensity.

The sensing behavior of the MOF compound towards H_2S was explored by conducting fluorescence turn-on experiments (λ_{ex} = 345 nm) in HEPES buffer (10 mM, pH = 7.4). The dinitro-functionalized **2′** exhibited very weak fluorescence. Na_2S was employed as a source of H_2S.[62, 63] After addition of Na_2S solution, the nitro groups were reduced to electron donating amine groups and hence increment in the fluorescence intensity was noticed.[27, 30] During the H_2S sensing experiment, the compound retained its structural integrity (Figure 3.9). It is due to the fact that

only the functional groups undergo changes during the sensing event, but the framework structure remains intact.

For checking the potential of the MOF material for the fluorometric sensing of H_2S, we have added ten equivalents (for each nitro group) of Na_2S (as aqueous solution) to **2′** (dispersed in HEPES buffer). After the completion of addition, the fluorescence spectra were recorded at a regular interval of 2 min up to 60 min. As displayed in Figure 3.10, the increment in the fluorescence intensity was nearly 5-fold after 5 min and the saturation occurred after 40 min with 35-fold increase in the fluorescence intensity. These fluorescence spectra clearly imply that UiO-66-$(NO_2)_2$ compound is highly efficient in sensing H_2S in physiological medium. The response time for this probe is slower than most of the previously published MOF-based H_2S sensors (Table 3.2), but it is faster than the dinitro-functionalized, Zr(IV)-based DUT-52 material.[27] It is noteworthy that the fold-enhancement in the fluorescence intensity of **2′** (35-fold at saturation) is higher than many of the previously employed MOF-based sensors for H_2S,[29-31, 33, 48] but it is significantly lower than the DUT-52-$(NO_2)_2$ compound (68-fold at saturation).[27]

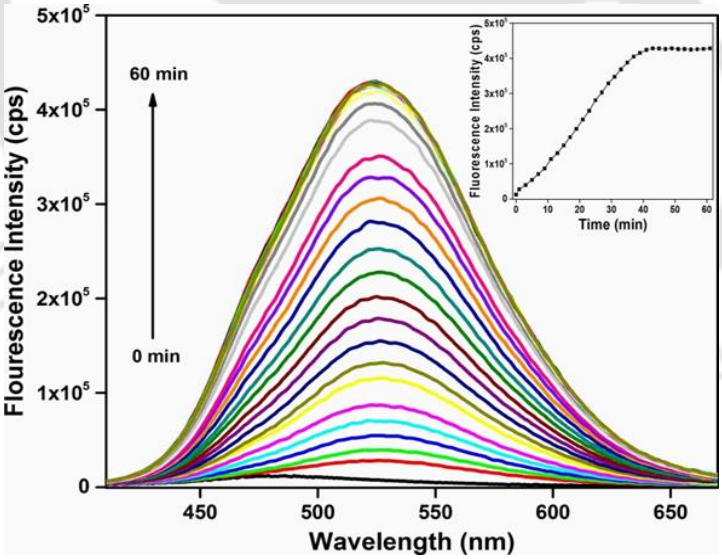

Figure 3.10 Fluorescence increment behavior of the HEPES suspension of **2'** after the addition of Na_2S as a function of time. The inset shows variation in the fluorescence intensity of **2'** (monitored at 527 nm) with time.

For real world applications, the probe should be highly selective towards the target analyte over other competing biochemical analytes in fluorescence turn-on

experiment. In order to investigate the selectivity of **2′** towards H_2S over other intrusive biological molecules (serine, alanine, glutathione cysteine) and anions (I^-, Br^-, Cl^-, NO_2, NO_3^-, $S_2O_3^{2-}$, SO_3^{2-}, SO_4^{2-}, HSO_3^-, HSO_4^-), the fluorescence response of **2′** was recorded after 40 min of addition of these species (10 equiv. of BDC-$(NO_2)_2$) separately in the sensing medium (10 mM HEPES buffer, pH = 7.4). It can be clearly seen from Figure 3.11 that a thiol-containing biomolecule (glutathione) and two biological anions (SO_3^{2-} and HSO_4^-) showed slight increment in the fluorescence intensity. For other interfering analytes, no observable change in the fluorescence intensity was detected. Moreover, it is quite obvious from the inset photograph of Figure 3.11 that **2′** showed visually detectable change in color (from bright yellow to orange) in presence of H_2S only Hence, UiO-66-$(NO_2)_2$ is highly selective towards H_2S over other interfering analytes in HEPES buffer medium.

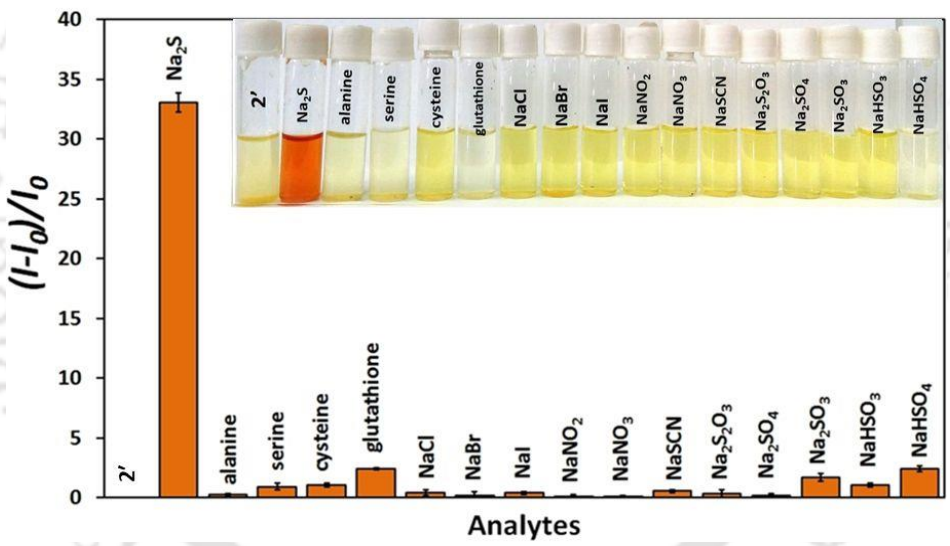

Figure 3.11 Comparative fluorescence response of the HEPES suspension of **2'** towards different analytes (10 equiv. of BDC-$(NO_2)_2$) after 40 min of the addition of analytes. Inset shows the corresponding visual change in color upon addition of each analyte. The error bars show the standard deviations of three measurements.

For efficient sensing of a fluorescent probe in complicated biological medium, it should exhibit fluorescence increment phenomena towards H_2S even in presence of other potentially interfering congeners. Hence, we carried out fluorescence experiments after addition of ten equivalents of Na_2S (10 equiv. of BDC-$(NO_2)_2$) solution to a HEPES suspension of **2′** containing other competing biological analytes. The fluorescence spectra were measured after 40 min of addition of Na_2S solution. It becomes unambiguous from

Figure 3.12 that the enhancement in the fluorescence intensity of **2′** was considerably high after the addition of Na_2S, even in presence of intrusive analytes. These results confirm that the existence of other interfering biochemical analytes does not significantly affect the selectivity of UiO-66-$(NO_2)_2$ towards the detection of H_2S.

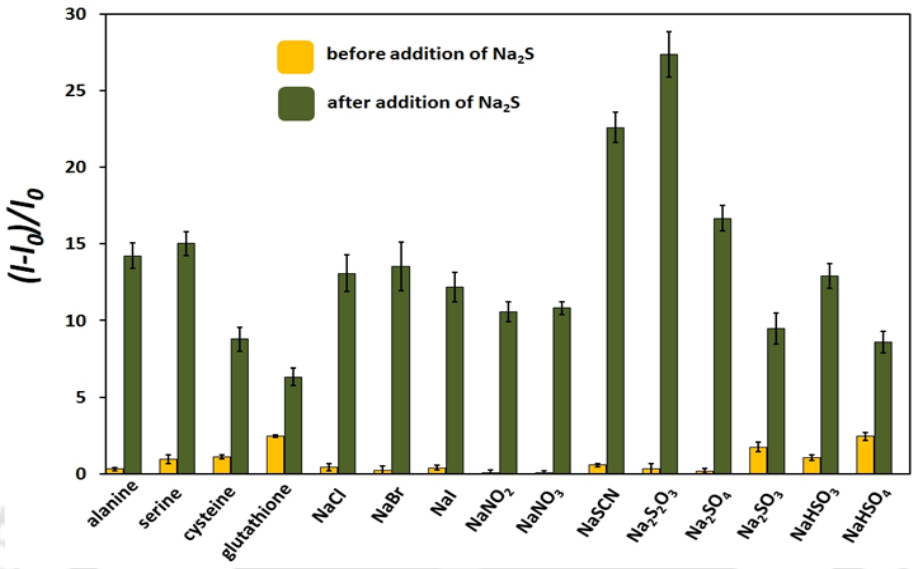

Figure 3.12 Fluorescence increment properties of the suspension of **2'** (in HEPES buffer) after the addition of an intrusive biological species (yellow) and subsequent addition of Na_2S solution (green). The error bars indicate the standard deviations of three measurements.

For quantification of the fluorescence enhancement features of UiO-66-$(NO_2)_2$ in presence of H_2S, fluorescence titration studies were performed. To perform this experiment, zero to ten equivalents of Na_2S solution (10 equiv. of BDC-$(NO_2)_2$) were incrementally introduced to the dispersion of **2′** in HEPES buffer. After that, the fluorescence spectra were collected. The fluorescence intensity (Figure 3.13) of the probe increased progressively upon the gradual addition of Na_2S solution. The naked-eye colorimetric response of **2′** towards incremental introduction of Na_2S solution is displayed in Figure 3.14. Such visual colorimetric responses demonstrate that UiO-66-$(NO_2)_2$ is an excellent colorimetric and fluorogenic probe for the selective sensing of H_2S in simulated biological medium. After the sensing experiment, the material was recovered and its XRPD pattern was recorded. It was found that the XRPD pattern (Figure 3.9) was very much similar with the un-reacted **2′**. The XRPD experiments clearly confirm the retention of structural integrity of the UiO-66-$(NO_2)_2$ probe during the sensing event.[28, 30, 48]

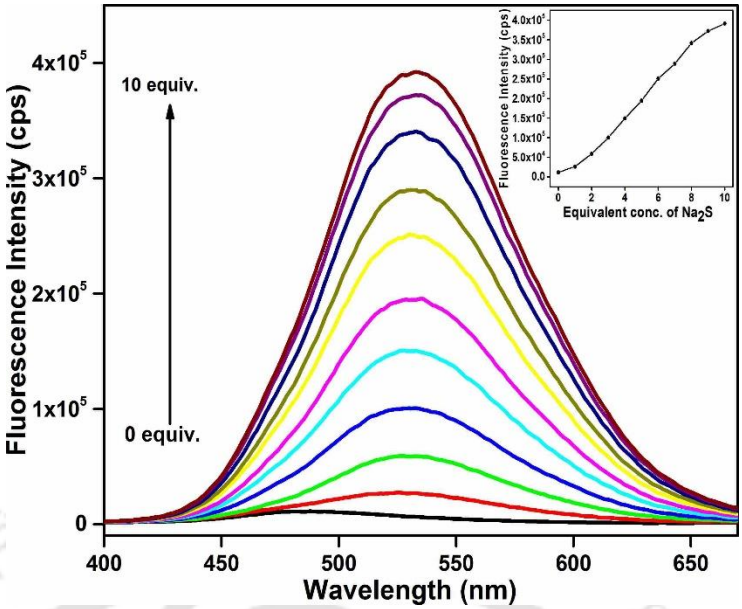

Figure 3.13 Fluorescence increment behavior of the HEPES suspension of **2'** with increasing concentration of Na_2S. The inset displays variation in the fluorescence intensity of **2'** with incremental introduction of Na_2S solution.

Figure 3.14 Naked-eye colorimetric detection behavior of the HEPES suspension of **2'** with increasing concentration of Na_2S under day light.

3.3.5 Analytical method validation for the sensing of H_2S in HEPES buffer

The method was evaluated by characterizing its analytical performance with regard to limit of detection (LOD), linearity and limit of quantification (LOQ). In the concentration range of 100-600 µM, the plot of the fluorescence intensity versus the concentration of Na_2S for the suspension of **2′** (in HEPES buffer) showed a remarkable linear curve having $R^2 = 0.9927$ (Figure 3.15). The regression equation for this calibration curve was $y = 57047x + 1.75\times10^4$. All the analytical parameters relevant to this equation are displayed in Table 3.1. This calibration curve was used

to derive the inter-day and intra-day precision and accuracy. It was also used for the quantification of Na_2S in real samples. The LOD and LOQ values were estimated at signal-to-noise ratio of three and ten, respectively. The calculated LOD of **2′** for H_2S was 14.14 μM. The detection limit is similar with the previously reported[27-31, 33, 48] MOF-type of probes for H_2S sensing (Table 3.2). Noticeably, falls within the H_2S concentration found in biological systems.[10, 64] The accuracy of the method was assessed by performing the recovery test. The reproducibility and precision were represented with regard to relative standard deviation (RSD). Intra-day precision was evaluated by measuring five replicate samples spiked with 100 μM of Na_2S in the same day and inter-day precision was deduced by running the experiments with the same sample in five different days. The obtained recovery (%) and RSD values demonstrate that the quantification is accurate and reproducible in this method.

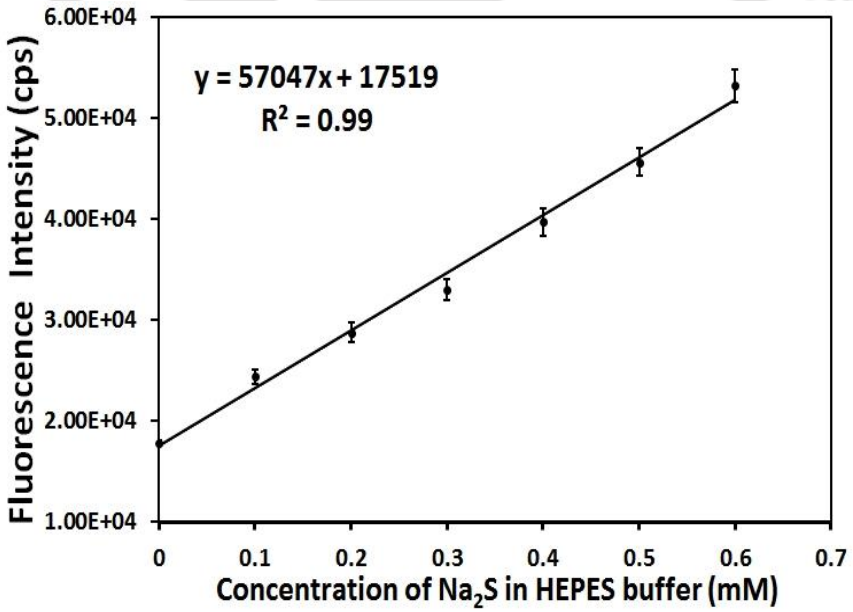

Figure 3.15 Change in the fluorescence intensity of **2′** in HEPES buffer as a function of Na_2S concentration. The error bars indicate the standard deviations of three measurements.

Table 3.1 Analytical parameters for the fluorogenic sensing of H_2S by **2'**.

Concentration Range (μM)	Regression Equation	Correlation Coefficient (R^2)	$S_{y/x}$[b]	Slope	LOD[c] (μM)	LOQ[d] (μM)	Intra-day Precision		Inter-day Precision	
							Found[e] (Mean ± RSD)	Recovery[f] (%)	Found[e] (Mean ± RSD)	Recovery[f] (%)
100-600	57047x+ 1.75×10^4	0.992	268.9	5.7×10^4	14.14	47.13	101.92 ± 2.49	101.92	96.03 ± 10.58	96.03

[a] Residual sum of squares

[b] Standard deviation of the residuals

[c] Limit of detection, 3RSD/slope

[d] Limit of quantification, 10RSD/slope

[e] Concentration of spiked Na_2S (100 μM)

[f] (Mean measured concentration/spiked concentration) ×100.

Table 3.2 Comparison of the response time, detection limit and analyte used of various existing probes for the fluorescence detection of H_2S.

Sl. No.	Sensor Material	Type of Material	Response Time (s)	Detection Limit (μM)	Analyte	Ref.
1	Zr-UiO-66-$(NO_2)_2$	MOF	2400	14.14 μM	Na_2S	this work
2	DUT-52-$(NO_2)_2$	MOF	3300	20.0 μM	Na_2S	65
3	Ce-UiO-66-N_3	MOF	760	12.2 μM	NaSH	66
4	Ce-UiO-66-NO_2	MOF	760	34.84 μM	NaSH	66
5	CAU-10-N_3	MOF	420	2.65 μM	Na_2S	44
6	IRMOF-3-N_3	MOF	< 120	28.3 μM	NaSH	67
7	Zr-UiO-66-NO_2	MOF	≈ 460	188 μM	Na_2S	68
8	Zr-UiO-66-N_3	MOF	180	118 μM	Na_2S	31
9	MN-ZIF-90	MOF	-	-	-	48
10	Al-TCPP-Cu	MOF	-	-	-	33
11	Al-MIL-101-N_3	MOF	-	100 μM (UV-lamp excitation); 0.1 μM (laser excitation)	Na_2S	34
12	Eu^{3+}/Cu^{2+}@UiO-66-$(COOH)_2$	MOF	30	5.45 μM	NaSH	69
13	NHS1	organic molecule	4800	20 nM	NaSH	26
14	Cy-N_3	organic molecule	1200	0.08 μM	NaSH	70
15	SFP-1, SFP-2	organic molecule	7200, 14400	-	Na_2S	71
16	SHS-M1, SHS-M2	organic molecule	-	0.2 μM, 0.4 μM	Na_2S	72

17	probe 1	organic molecule	≈ 3600	2.4 μM	NaSH	73
18	SF4	organic molecule	-	125 nM	NaSH	74
19	WSP5	organic molecule	-	47 nM	NaSH	75
20	NIR-H_2S	organic molecule	-	5×10^{-8} M	NaSH	76
21	probe 1	organic molecule	10800	-	Na_2S	77
22	Cy–NO_2	organic molecule	5400	2 μM	Na_2S	78
23	probe 1	organic molecule	2700	2.5 μM	Na_2S	79
24	RHP-2	organic molecule	2400	270 nM	Na_2S	80
25	HSN1, HSN2	organic molecule	5400, 2700	5-10 μM, 1-5 μM	H_2S	81
26	FS1	organic molecule	7200	5-10 μM	Na_2S	82
27	PI-N_3	organic molecule	180	8.79×10^{-7} M	NaSH	83
28	Probe 1	organic molecule	1800	3.05 μM	NaSH	84
29	Probe 1	organic molecule	180-600	0.78 nM	NaSH	85
30	Probe 4	organic molecule	600	259 nM	Na_2S	86
31	Probe 1	organic molecule	180	0.13 μM	NaSH	87
32	TPE-Az	organic molecule	120	-	NaSH	88
33	AzMB-coumarin	organic molecule	1200-2400	100 μM	NaSH	89
34	Lyso-AFP	organic molecule	1800	-	NaSH	90
35	SF1, SF2	organic molecule	3600	5-10 μM	NaSH	91
36	cpGFP-Tyr66pAzF	organic molecule	420	-	NaSH	92
37	CLSS-1, CLSS-2	organic molecule	-	0.7±0.3 μM, 4.6±2.0 μM	NaSH	93
38	DNS-Az	organic molecule	-	1 μM	Na_2S	94

3.3.6 Sensing of H_2S in human blood plasma

After achieving outstanding selectivity and sensitivity of **2′** towards H_2S in HEPES buffer, we decided to examine its sensing performance in a more complicated medium such as human blood plasma. For this experiment, Na_2S was used as an internal standard. We measured the fluorescence emission spectra after treatment of **2′** with Na_2S-spiked HBP samples possessing seven different concentrations (0, 50, 100, 150, 200, 250 and 300 μM). Figure 3.16 discloses a linear relationship between the fluorescence emission intensity and the concentration of Na_2S-spiked HBP solution added to **2′** dispersed in HEPES buffer. Hence, we can conclude that UiO-66-$(NO_2)_2$ is suitable for the detection and quantification of H_2S in HBP.

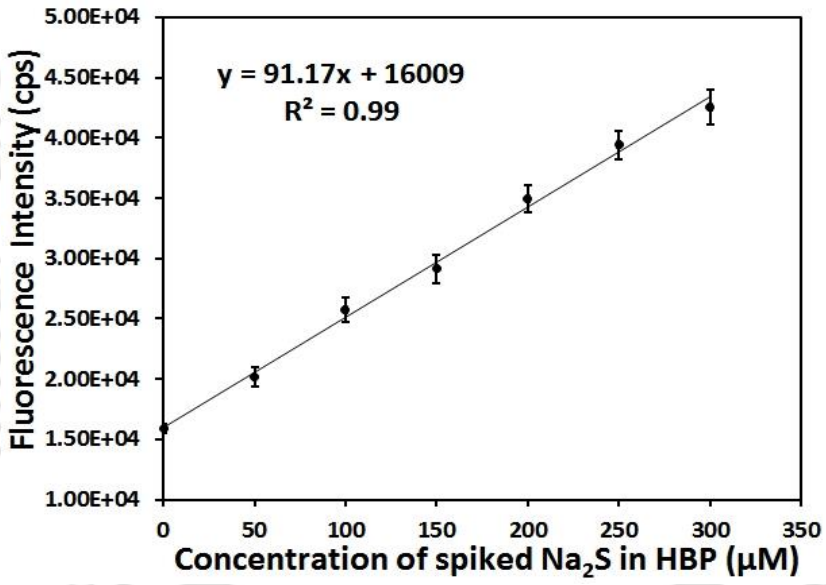

Figure 3.16 Fluorescence response of **2′** in presence of Na_2S-spiked human blood plasma. Na_2S was spiked as an internal standard. The error bars indicate the standard deviations of three measurements.

3.3.7 Sensing of H_2S in living cells

Inspired by the high selectivity, rapid response and excellent sensitivity of the UiO-66-$(NO_2)_2$ probe for the sensing of extracellular H_2S, we have investigated its detection capability for intracellular H_2S. The suitability of the compound for the detection of H_2S in biological medium was explored by conducting cellular imaging experiments in macrophage J774A.1 cells. Before the imaging experiment, cellular toxicity of **2′** towards

J774A.1 cells was evaluated. The cells treated with different concentrations of **2′** (0-100 µM) for 24 h did not affect the cellular morphology (Figure 3.17) and the probe-treated cells exhibited almost 100% viability (Figure 3.18). Hence, our probe was found to be suitable for performing cellular imaging experiment. Next, for the production of endogenous H_2S, at first we incubated the macrophage cells with the UiO-66-$(NO_2)_2$ material (5 µM) and later treated them with Na_2S solution (10 µM). The observation of the untreated cells in the bright field revealed very good morphology, whereas no fluorescence was noticed for the same cells in the green channel (Figure 3.19a-b). We observed negligible background fluorescence for the cells which were loaded only with the probe (Figure 3.19d-e). Very interestingly, we obtained bright green fluorescence signal when the cells incorporating the UiO-66-$(NO_2)_2$ material underwent treatment with the Na_2S solution (Figure 3.19h-i). Moreover, to ensure the loading of probe in the cells, we performed the following experiment. At first, the cells were loaded with probe and then permeabilized with Triton X-100 to make the cells leaky and loss of probe from intracellular sources. The level of permeabilization was almost more than 90% as the cells showed quick uptake of Trypan Blue (Figure 3.19j). These cells incubated with Na_2S did not show any significant fluorescence (Figure 3.19k). The loss of fluorescence signal from permeabilized cells indirectly proves that the probe is localized inside the cells and the fluorescence signal is originating from inside the cells instead of cell surface.

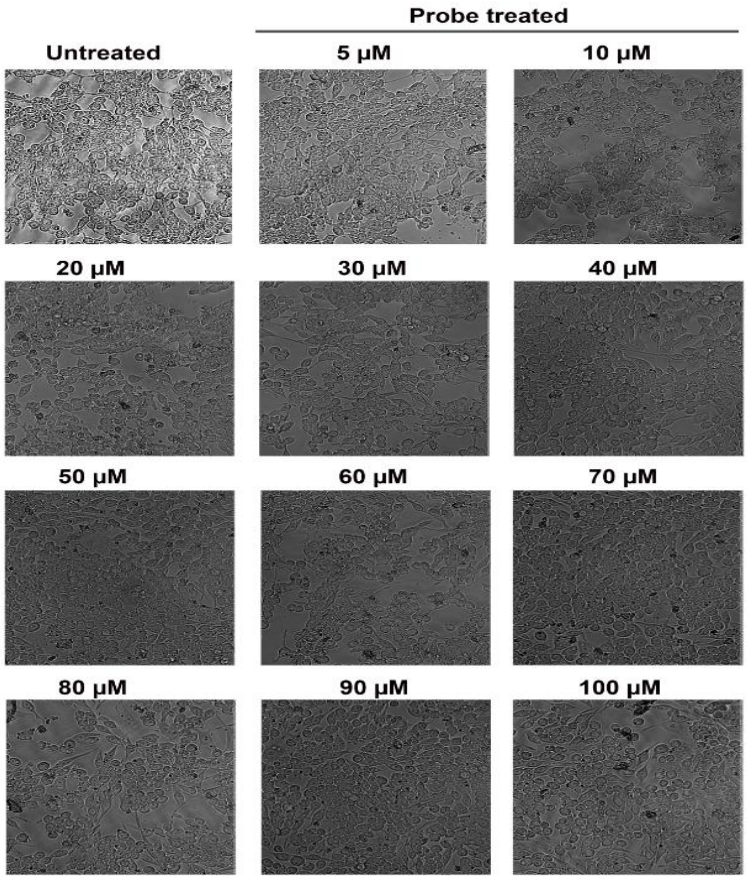

Figure 3.17 Morphological analysis of **2′**-treated J774A.1 cells. Macrophage J774A.1 cells were treated with different concentrations of probe (0-100 μM) for 24 h at 37 ºC and cells were observed with Cytell cell imaging system (GE Healthcare).

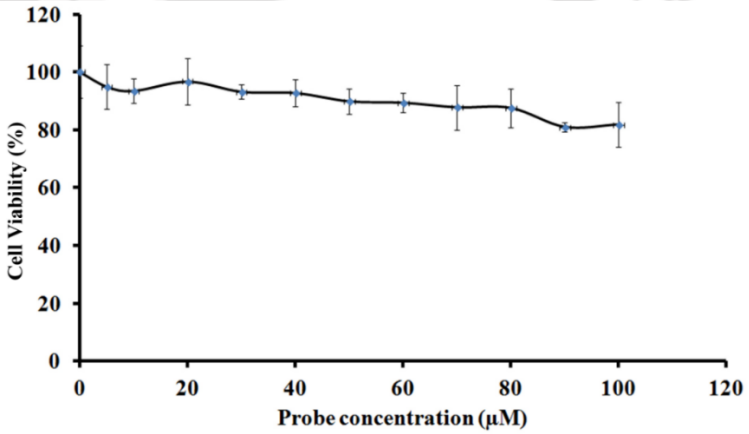

Figure 3.18 Cytotoxic effect of **2′** on J774A.1 survival. Ten thousand Macrophage J774A.1 cells were treated with different concentrations of probe (0-100 μM) for 24 h at 37 ºC and cellular viability was measured using MTT assay. ($n = 3$, $p < 0.001$).

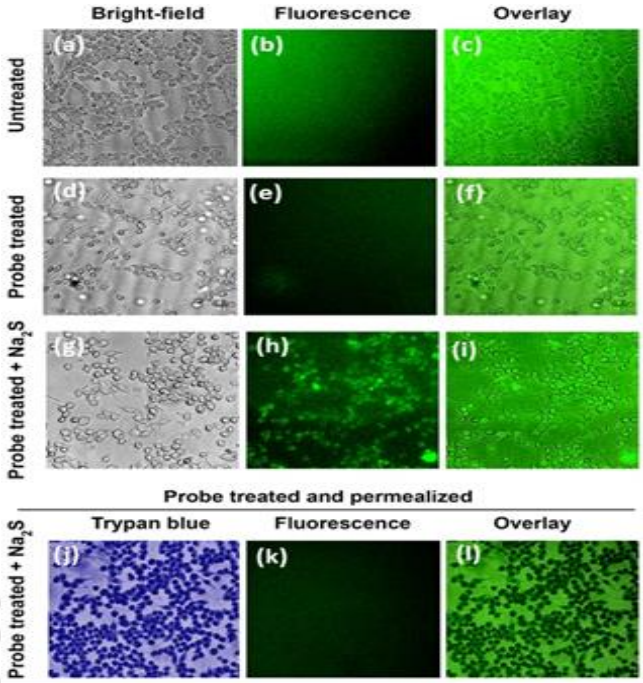

Figure 3.19 Fluorescence microscopic images showing the capability of UiO-66-$(NO_2)_2$ for sensing H_2S in macrophage J774A.1 cells. Bright-field images of (a) only cells, (d) cells after treatment with 5 µM probe, and (g) cells after treatment with 5 µM probe and 10 µM Na_2S. The fluorescence microscopy images (in green channel) of (a, d, g) correspond to (b, e, h), respectively. Upon treatment of the cells with H_2S, bright green fluorescence (h) was observed only after H_2S treatment. (c, f, i) are the overly images of bright field images (a, d, g) and fluorescent images (b, e, h). Cells (j-l) loaded with probe were permeabilized and H_2S sensing experiment was performed. Blue color cells (j) indicate permeabilized cells and these cells are not giving any fluorescence in green channel (k). (i) is the overlay image of (j) and (k).

3.3.8 Sensing of sulfide in real water samples

For investigating the Na_2S sensing behavior of UiO-66-$(NO_2)_2$ in real water samples, a total of nine water samples were utilized. They include three samples of the same the type (tap, mineral or lake water). The concentrations of Na_2S found and the recovery percentages in the environmental water samples are displayed in Table 3.3. The recovery percentages of Na_2S were found in the range of 91-107% for all the samples and the RSD values were in the range 3.01-6.75 (RSD = SD/mean value) × 100). The good recovery percentages and low RSD values obviously imply

that the probe can also provide adequate recoveries and good analytical precisions for real water samples.

Table 3.3 Detection performance of **2'** for Na_2S in real water samples.

Na_2S Spiked (μM)	Mineral Water		Tap Water		Lake Water	
	Na_2S Found[a] (μM)	Recovery (%)	Na_2S Found[a] (μM)	Recovery (%)	Na_2S Found[a] (μM)	Recovery (%)
50	46.88 ± 4.63	93.76	47.89 ± 3.01	96.60	53.54 ± 6.14	107.08
75	73.85 ± 5.38	98.46	70.49 ± 6.75	93.98	68.23 ± 5.96	90.97
100	95.55 ± 4.74	95.55	98.56 ± 3.75	98.56	99.26 ± 3.24	99.26

[a] Na_2S found ± RSD (n = 3)

3.3.9 Mechanistic study for the sensing of H_2S

During the sensing event, it is expected that the two attached nitro groups of the BDC-$(NO_2)_2$ ligand present in **2′** are reduced by H_2S and converted to the corresponding amine compound. Due to this reduction process, the fluorescence intensity of the compound is enhanced. This expected mechanism of H_2S sensing by **2′** has been successfully verified by mass spectrometry and ^{1}H NMR spectroscopic studies. The most intense peak at m/z = 254.9898 in the mass spectrum of digested **2′** (Figure 3.20) represents the $(M-H)^-$ ion of H_2BDC-$(NO_2)_2$ ligand (M = mass of H_2BDC-$(NO_2)_2$ ligand). The mass spectrum (Figure 3.21) of digested Na_2S-treated **2′** reveals two intense peaks at m/z = 254.9924 and 195.0440. These two peaks correspond to $(M-H)^-$ ion of H_2BDC-$(NO_2)_2$ ligand and reduced H_2BDC-$(NO_2)_2$ ligand (i.e. H_2BDC-$(NH_2)_2$), respectively. Hence, it becomes evident that the nitro groups are reduced to form amine functionalities in presence of Na_2S. Furthermore, the sensing mechanism has been corroborated by ^{1}H NMR analysis (Figure 3.22) of the digested **2′** and Na_2S-treated **2′**. For **2′**, the signal at 8.43 ppm arises due to the two equivalent aromatic protons present at 3- and 6-positions of the benzene ring of the H_2BDC-$(NO_2)_2$ ligand. In case of Na_2S-treated **2′**, the additional signal at 7.18 ppm is obviously for the two equivalent aromatic protons of the H_2BDC-$(NH_2)_2$ ligand since the peak position is closely matches with the peak position for the aromatic protons of H_2BDC-$(NH_2)_2$ ligand which arises at 7.24 ppm (Figure 3.22). For calculation of the degree of conversion from nitro to

amino compound, the peak corresponding to the two equivalent aromatic protons of $H_2BDC\text{-}(NO_2)_2$ ligand is set to an integration of 1 and consequently integration of the newly appeared peak is performed. Under the experimental conditions for H_2S sensing, the calculated extent of conversion from nitro to amine functionalities is ~48%. It was estimated from the peak area ratio between the protons of $H_2BDC\text{-}(NO_2)_2$ and $H_2BDC\text{-}(NH_2)_2$ ligands, which were observed in the ^1H NMR spectrum of the digested Na_2S-treated **2′**.

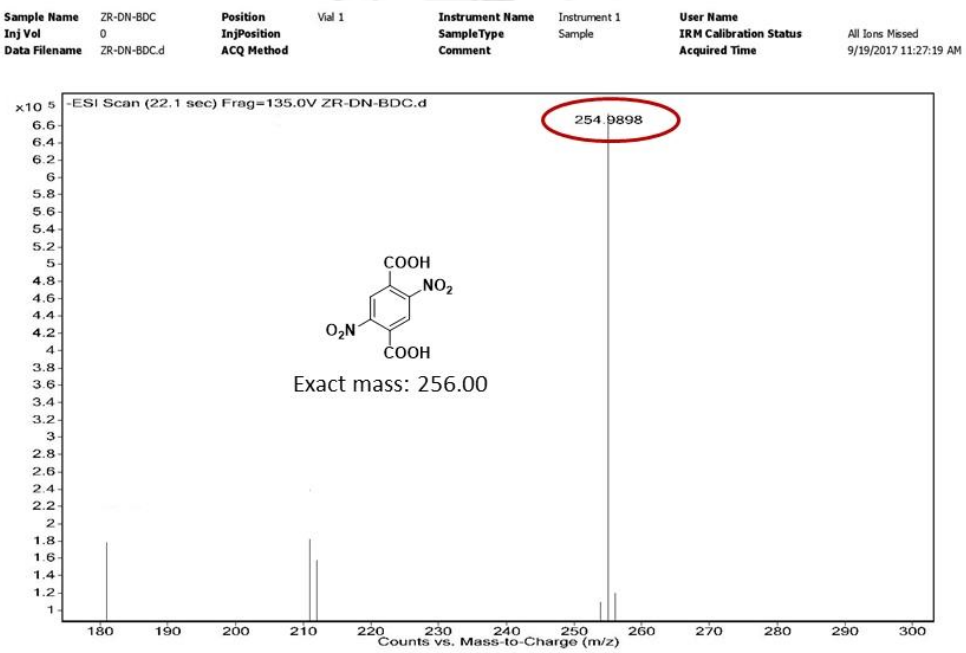

Figure 3.20 HR-MS spectrum of **2′** (digested in MeOH/HF) showing m/z peak at 254.9898 (negative ion mode), which corresponds to $(M\text{-}H)^-$ ion (M = mass of $H_2BDC\text{-}(NO_2)_2$ ligand).

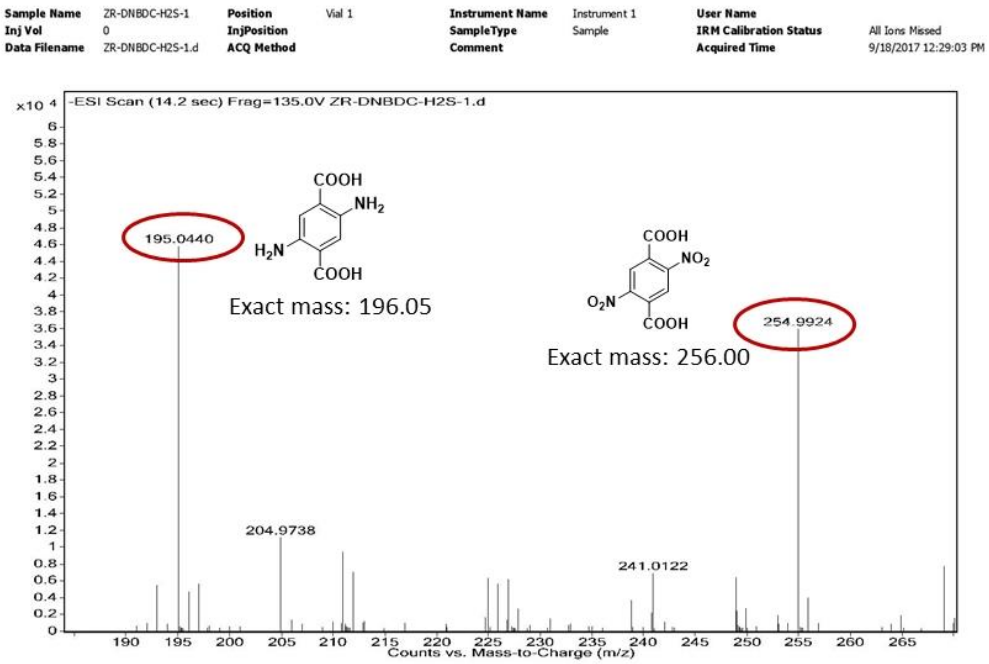

Figure 3.21 HR-MS spectrum of Na_2S-treated **2′** (digested in MeOH/HF) showing m/z (negative ion mode) peaks at 254.9924 and 195.0440, which correspond to $(M-H)^-$ ion of $H_2BDC\text{-}(NO_2)_2$ ligand and reduced $H_2BDC\text{-}(NO_2)_2$ ligand i.e. $H_2BDC\text{-}(NH_2)_2$, respectively.

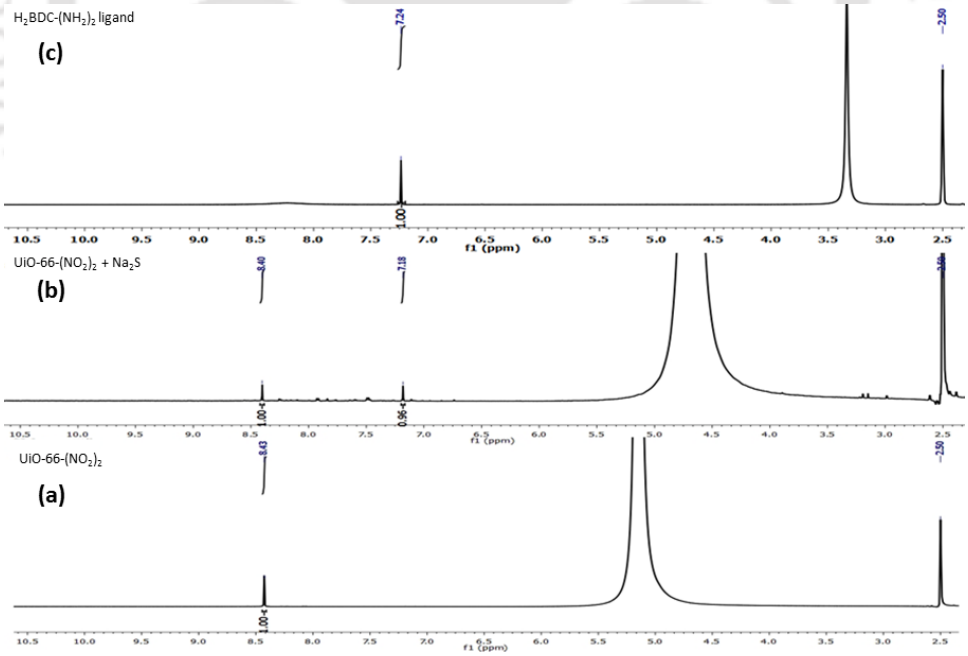

Figure 3.22 ^1H NMR spectra of (a) **2′**, (b) Na_2S-treated **2′** (digested in DMSO-d_6/HF) and (c) $H_2BDC\text{-}(NH_2)_2$ ligand. In the spectrum of Na_2S-treated **2′**, a new peak arises at 7.18 ppm closely matches with the peak (~7.24 ppm) of $H_2BDC\text{-}(NH_2)_2$ ligand, which clearly

signifies the formation of the diamine compound i.e. $H_2BDC\text{-}(NH_2)_2$ by reduction of the corresponding dinitro compound i.e. $H_2BDC\text{-}(NO_2)_2$.

3.4 Conclusions

In summary, the new dinitro-functionalized Zr(IV) MOF called UiO-66-$(NO_2)_2$ has been prepared successfully and characterized thoroughly. The material has excellent efficiency to detect H_2S selectively in the HEPES buffer medium with a detection limit of 14.14 μM. The fold increment (35-fold at saturation) in the fluorescence intensity of this material is remarkably higher than the formerly reported mononitro- and azide-functionalized Zr(IV) and Ce(IV) based UiO-66 MOFs. In addition, the compound is a promising platform for the naked-eye detection of H_2S under day light. In presence of other competing biomolecules, its selectivity towards H_2S remains unaltered. Apart from the sensing of extracellular H_2S, the presence of H_2S in living cells can be detected by this biocompatible, nontoxic MOF using live-cell imaging experiment. All the above discussions clarify that the presented UiO-66-$(NO_2)_2$ compound is a suitable probe for the selective and sensitive recognition of H_2S in biological medium. In addition, we have demonstrated the aptness of the probe for sensing H_2S in human blood plasma and analyzing sulfide concentration in environmental water samples. Therefore, we believe that our work will trigger substantial research interests in the field of MOF based H_2S sensors.

3.5 References

1. C. Szabo, C. Ransy, K. Módis, M. Andriamihaja, B. Murghes, C. Coletta, G. Olah, K. Yanagi and F. Bouillaud, *J. Pharmacol.*, 2014, **171**, 2099-2122.
2. R. Wang, *Antioxid. Redox Signal.*, 2010, **12**, 1061-1064.
3. L. Li, P. Rose and P. K. Moore, *Annu. Rev. Pharmacol. Toxicol.*, 2011, **51**, 169-187.
4. H. Kimura, *Mol. Neurobiol.*, 2002, **26**, 13-19.
5. C. Szabó and A. Papapetropoulos, *Br. J. Pharmacol.*, 2011, **164**, 853-865.
6. L. Xie, H. Feng, S. Li, G. Meng, S. Liu, X. Tang, Y. Ma, Y. Han, Y. Xiao, Y. Gu, Y. Shao, C.-M. Park, M. Xian, Y. Huang, A. Ferro, R. Wang, P. K. Moore, H. Wang and Y. Ji, *Antioxid. Redox Signal.*, 2016, **24**, 329-343.

7. D. Wu, Q. Hu, X. Liu, L. Pan, Q. Xiong and Y. Z. Zhu, *Nitric Oxide*, 2015, **46**, 204-212.
8. H. Kimura, *Amino Acids*, 2011, **41**, 113-121.
9. M. H. Stipanuk and I. Ueki, *J. Inherit. Metab. Dis.*, 2011, **34**, 17-32.
10. J. Furne, A. Saeed and M. D. Levitt, *Am. J. Physiol. Regul. Integr. Comp. Physiol.*, 2008, **295**, R1479-R1485.
11. K. Eto, T. Asada, K. Arima, T. Makifuchi and H. Kimura, *Biochem. Biophys. Res. Commun.*, 2002, **293**, 1485-1488.
12. W. Yang, G. Yang, X. Jia, L. Wu and R. Wang, *J. Physiol.*, 2005, **569**, 519-531.
13. S. Fiorucci, E. Antonelli, A. Mencarelli, S. Orlandi, B. Renga, G. Rizzo, E. Distrutti, V. Shah and A. Morelli, *Hepatology*, 2005, **42**, 539-548.
14. P. Kamoun, *Med. Hypotheses*, 2001, **57**, 389-392.
15. C. Szabo, C. Coletta, C. Chao, K. Modis, B. Szczesny, A. Papapetropoulos and M. R. Hellmich, *Proc. Natl. Acad. Sci. USA*, 2013, **110**, 12474-12479.
16. M. Ishigami, K. Hiraki, K. Umemura, Y. Ogasawara, K. Ishii and H. Kimura, *Antioxid. Redox Signal.*, 2009, **11**, 205-214.
17. A. R. Ivanov, I. V. Nazimov and L. A. Baratova, *J. Chromatogr., A*, 2000, **870**, 433-442.
18. Y. V. Tcherkas and A. D. Denisenko, *J. Chromatogr., A*, 2001, **913**, 309-313.
19. M. A. Khan, F. Qazi, Z. Hussain, M. U. Idrees, S. Soomro and S. Soomro, *Int. J. Electrochem. Sci.*, 2017, **12**, 1711-1733.
20. Z. Yuan, F. Lu, M. Peng, C.-W. Wang, Y.-T. Tseng, Y. Du, N. Cai, C.-W. Lien, H.-T. Chang, Y. He and E. S. Yeung, *Anal. Chem.*, 2015, **87**, 7267-7273.
21. S. Kang, J. Oh and M. S. Han, *Dyes Pigm.*, 2017, **139**, 187-192.
22. Z. Hai, Y. Bao, Q. Miao, X. Yi and G. Liang, *Anal. Chem.*, 2015, **87**, 2678-2684.
23. X. Wu, L. Li, W. Shi, Q. Gong, X. Li and H. Ma, *Anal. Chem.*, 2016, **88**, 1440-1446.
24. J. Zhang and W. Guo, *Chem. Commun.*, 2014, **50**, 4214-4217.
25. H. Peng, W. Chen, S. Burroughs and B. Wang, *Curr. Org. Chem.*, 2013, **17**, 641-653.
26. G.-J. Mao, T.-T. Wei, X.-X. Wang, S.-Y. Huan, D.-Q. Lu, J. Zhang, X.-B. Zhang, W. Tan, G.-L. Shen and R.-Q. Yu, *Anal. Chem.*, 2013, **85**, 7875-7881.
27. R. Dalapati, S. N. Balaji, V. Trivedi, L. Khamari and S. Biswas, *Sens. Actuator, B*, 2017, **245**, 1039-1049.

28. A. Buragohain and S. Biswas, *CrystEngComm*, 2016, **18**, 4374-4381.
29. X. Zhang, J. Zhang, Q. Hu, Y. Cui, Y. Yang and G. Qian, *Appl. Surf. Sci.*, 2015, **355**, 814-819.
30. S. S. Nagarkar, A. V. Desai and S. K. Ghosh, *Chem. Eur. J.*, 2015, **21**, 9994-9997.
31. S. S. Nagarkar, T. Saha, A. V. Desai, P. Talukdar and S. K. Ghosh, *Sci. Rep.*, 2014, **4**, 7053-7058.
32. P.-C. Chen, Y.-C. Li, J.-Y. Ma, J.-Y. Huang, C.-F. Chen and H.-T. Chang, *Sci. Rep.*, 2016, **6**, 24882-24890.
33. Y. Ma, H. Su, X. Kuang, X. Li, T. Zhang and B. Tang, *Anal. Chem.*, 2014, **86**, 11459-11463.
34. A. Legrand, A. Pastushenko, V. Lysenko, A. Geloen, E. A. Quadrelli, J. Canivet and D. Farrusseng, *ChemNanoMat*, 2016, **2**, 866-872.
35. X. Zhang, Q. Hu, T. Xia, J. Zhang, Y. Yang, Y. Cui, B. Chen and G. Qian, *ACS Appl. Mater. Interfaces*, 2016, **8**, 32259-32265.
36. N. Stock and S. Biswas, *Chem. Rev.*, 2012, **112**, 933-969.
37. M. SK and S. Biswas, *CrystEngComm*, 2016, **18**, 3104-3113.
38. K. Müller-Buschbaum, F. Beuerle and C. Feldmann, *Microporous Mesoporous Mater.*, 2015, **216**, 171-199.
39. R. Dalapati and S. Biswas, *Sens. Actuators, B.*, 2017, **239**, 759-767.
40. Z. Kang, L. Fan and D. Sun, *J. Mater. Chem. A*, 2017, **5**, 10073-10091.
41. R. Dalapati, B. Sakthivel, A. Dhakshinamoorthy, A. Buragohain, A. Bhunia, C. Jainak and S. Biswas, *CrystEngComm*, 2016, **18**, 7855-7864.
42. L. Ma, C. Abney and W. Lin, *Chem. Soc. Rev.*, 2009, **38**, 1248-1256.
43. C. Orellana-Tavra, R. J. Marshall, E. F. Baxter, I. A. Lázaro, A. Tao, A. K. Cheetham, R. S. Forgan and D. Fairen-Jimenez, *J. Mater. Chem. B*, 2016, **4**, 7697-7707.
44. S. Nandi, H. Reinsch, S. Banesh, N. Stock, V. Trivedi and S. Biswas, *Dalton Trans.*, 2017, **46**, 12856-12864.
45. X. Xin, J. Wang, C. Gong, H. Xu, R. Wang, S. Ji, H. Dong, Q. Meng, L. Zhang, F. Dai and D. Sun, *Sci. Rep.*, 2016, **6**, 21951-21959.
46. J. Cui, Y.-L. Wong, M. Zeller, A. D. Hunter and Z. Xu, *Angew. Chem. Int. Ed.*, 2014, **53**, 14438-14442.
47. Y. Ma, H. Su, X. Kuang, X. Li, T. Zhang and B. Tang, *Anal. Chem.*,, 2014, **86**, 11459-11463.

48. H. Li, X. Feng, Y. Guo, D. Chen, R. Li, X. Ren, X. Jiang, Y. Dong and B. Wang, *Sci. Rep.*, 2014, **4**, 4366-4370.
49. D. P. Arya and D. J. Jebaratnam, *Tetrahedron Lett.*, 1995, **36**, 4369-4372.
50. H. A. Staab and H. Hafner, *Eur. J. Inorg. Chem.*, 1977, **110**, 3358-3365.
51. J. Quinn, E. Jin and Y. Li, *Tet. Lett.*, 2015, **56**, 2280-2282.
52. M. Kim, J. A. Boissonnault, P. V. Dau and S. M. Cohen, *Angew. Chem. Int. Ed.*, 2011, **50**, 12193-12196.
53. R. Deshmukh and V. Trivedi, *PLoS One*, 2014, **9**, e103706.
54. R. Deshmukh and V. Trivedi, *Toxicol. In Vitro*, 2013, **27**, 16-23.
55. C. N. Banwell and E. M. McCash, McGraw-Hill, New York, 1994.
56. J. H. Cavka, S. Jakobsen, U. Olsbye, N. Guillou, C. Lamberti, S. Bordiga and K. P. Lillerud, *J. Am. Chem. Soc.*, 2008, **130**, 13850-13851.
57. S. Biswas and P. V. D. Voort, *Eur. J. Inorg. Chem.*, 2013, **2013**, 2154-2160.
58. G. E. Cmarik, M. Kim, S. M. Cohen and K. S. Walton, *Langmuir*, 2012, **28**, 15606-15613.
59. J. B. DeCoste, G. W. Peterson, H. Jasuja, T. G. Glover, Y. Huang and K. S. Walton, *J. Mater. Chem. A*, 2013, **1**, 5642-5650.
60. X. Zhu, J. Gu, Y. Wang, B. Li, Y. Li, W. Zhao and J. Shi, *Chem. Commun.*, 2014, **50**, 8779-8782
61. K. Jiang, L. Zhang, Q. Hu, Q. Zhang, W. Lin, Y. Cui, Y. Yang and G. Qian, *Chem. Eur. J.*, 2017, **23**, 10215-10221.
62. Y. Qian, B. Yang, Y. Shen, Q. Du, L. Lin, J. Lin and H. Zhu, *Sens. Actuators, B*, 2013, **182**, 498-503.
63. M. Ren, B. Deng, X. Kong, K. Zhou, K. Liu, G. Xu and W. Lin, *Chem. Commun.*, 2016, **52**, 6415-6418.
64. V. S. Lin, W. Chen, M. Xian and C. J. Chang, *Chem. Soc. Rev.*, 2015, **44**, 4596-4618.
65. R. Dalapati, S. N. Balaji, V. Trivedi, L. Khamari and S. Biswas, *Sens. Actuators., B*, 2017, **245**, 1039-1049.
66. A. Buragohain and S. Biswas, *CrystEngComm*, 2016, **18**, 4374-4381.
67. X. Zhang, J. Zhang, Q. Hu, Y. Cui, Y. Yang and G. Qian, *Appl. Surf. Sci.*, 2015, **355**, 814.
68. S. S. Nagarkar, A. V. Desai and S. K. Ghosh, *Chem. Eur. J.*, 2015, **21**, 9994-9997.

69. X. Zhang, Q. Hu, T. Xia, J. Zhang, Y. Yang, Y. Cui, B. Chen and G. Qian, *ACS Appl. Mater. Interfaces*, 2016, **8**, 32259–32265.
70. F. Yu, P. Li, P. Song, B. Wang, J. Zhao and K. Han, *Chem. Commun.*, 2012, **48**, 2852-2854.
71. Y. Qian, J. Karpus, O. Kabil, S.-Y. Zhang, H.-L. Zhu, R. Banerjee, J. Zhao and C. He, *Nat. Commun.*, 2011, **2**, 1-7.
72. S. K. Bae, C. H. Heo, D. J. Choi, D. Sen, E.-H. Joe, B. R. Cho and H. M. Kim, *J. Am. Chem. Soc.*, 2013, **135**, 9915-9923.
73. Y. Jiang, Q. Wu and X. Chang, *Talanta*, 2014, **121**, 122-126.
74. V. S. Lin, A. R. Lippert and C. J. Chang, *Proc. Natl. Acad. Sci. U.S.A.*, 2013, **110**, 7131-7135.
75. B. Peng, W. Chen, C. Liu, E. W. Rosser, A. Pacheco, Y. Zhao, H. C. Aguilar and M. Xian, *Chem. Eur. J.*, 2013, **20**, 1010-1016.
76. X. Cao, W. Lin, K. Zheng and L. He, *Chem. Commun.*, 2012, **48**, 10529-10531.
77. W. Xuan, R. Pan, Y. Cao, K. Liu and W. Wang, *Chem. Commun.*, 2012, **48**, 10669-10671.
78. R. Wang, F. Yu, L. Chen, H. Chen, L. Wang and W. Zhang, *Chem. Commun.*, 2012, **48**, 11757-11759.
79. M.-Y. Wu, K. Li, J.-T. Hou, Z. Huang and X.-Q. Yu, *Org. Biomol. Chem.*, 2012, **10**, 8342-8347.
80. L. Zhang, W. G. Meng, L. Lu, Y. S. Xue, C. Li, F. Zou, Y. Liu and J. Zhao, *Sci. Rep.*, 2014, **29**, 5870.
81. L. A. Montoya and M. D. Pluth, *Chem. Commun.*, 2012, **48**, 4767-4769.
82. S. K. Das, C. S. Lim, S. Y. Yang, J. H. Han and B. R. Cho, *Chem. Commun.*, 2012, **48**, 8395-8397.
83. K. Zheng, W. Lin and L. Tan, *Org. Biomol. Chem.*, 2012, **10**, 9683-9688.
84. W. Sun, J. Fan, C. Hu, J. Cao, H. Zhang, X. Xiong, J. Wang, S. Cui, S. Sun and X. Peng, *Chem. Commun.*, 2013, **49**, 3890-3892.
85. J. Zhang and W. Guo, *Chem. Commun.*, 2014, **50**, 4214-4217.
86. T. Saha, D. Kand and P. Talukdar, *Org. Biomol. Chem.*, 2013, **11**, 8166-8170.
87. Y. Liu and G. Feng, *Org. Biomol. Chem.*, 2014, **12**, 438-445.
88. Y. Cai, L. Li, Z. Wang, J. Z. Sun, A. Qin and B. Z. Tang, *Chem. Commun.*, 2014, **50**, 8892-8895.

89. Z. Wu, Z. Li, L. Yang, J. Han and S. Han, *Chem. Commun.*, 2012, **48**, 10120-10122.

90. Q. Qiao, M. Zhao, H. Lang, D. Mao, J. Cui and Z. Xu, *RSC Adv.*, 2014, **4**, 25790-25794.

91. A. R. Lippert, E. J. New and C. J. Chang, *J. Am. Chem. Soc.*, 2011, **133**, 10078-10080.

92. S. Chen, Z.-j. Chen, W. Ren and H.-w. Ai, *J. Am. Chem. Soc.*, 2012, **134**, 9589-9592.

93. T. S. Bailey and M. D. Pluth, *J. Am. Chem. Soc.*, 2013, **135**, 16697-16704.

94. H. Peng, Y. Cheng, C. Dai, A. L. King, B. L. Predmore, D. J. Leferand and B. Wang, *Angew. Chem. Int. Ed.*, 2011, **50**, 9672 -9675.

CHAPTER 4

A metal-organic framework showing selective and sensitive detection of exogenous and endogenous formaldehyde

This chapter presents synthesis and characterization of a new hydrazine functionalized Al(III) metal-organic framework (MOF) having MIL-53 (MIL = Material of Institute Lavoisier) framework topology. The activated material showed great potential for the selective sensing of formaldehyde in the existence of other potentially competitive aldehydes in both aqueous and 10 mM HEPES buffer (pH = 7.4) media. The fluorescence "turn-on" behavior of the reaction-based probe can be ascribed to the inhibition of photo-induced electron transfer (PET) process (from hydrazine group to phenyl ring) due to the formation of hydrazone moiety. The ability of the probe to detect formaldehyde in the vapor phase was also demonstrated. The material is also capable to detect endogenous formaldehyde in cancer cells.

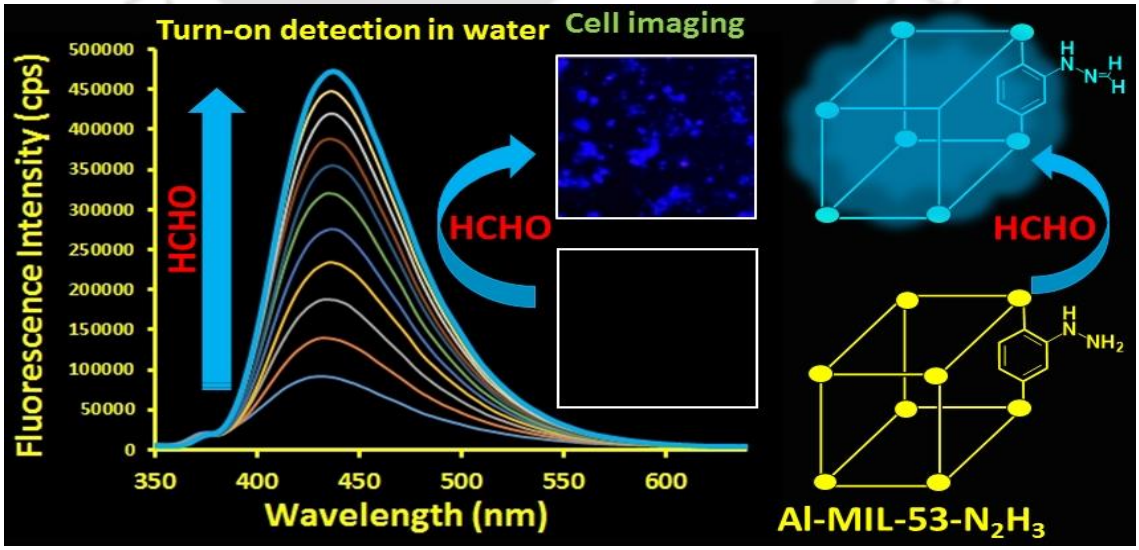

Inorganic Chemistry including bioinorganic chemistry

S. Nandi, E. Sharma, V. Trivedi, S. Biswas, *Inorg. Chem.*, 2018, **57**, 15149.

4.1 Introduction

Formaldehyde (FA) is the most simplest aldehyde among all the reactive carbonyl species (RCS).[1] It is involved in the methylation and demethylation of DNA and RNA.[2, 3] Hence, it plays beneficial roles in the activation and suppression of gene activities, brain function and memory formation.[4-6] Despite its beneficial roles, FA has been recognized as the most harmful RCS. It has been extensively utilized as a potent preservative. It is also widely employed in household goods like adhesives, cosmetic items, particle boards, paints, textiles, etc. From these materials, FA can emit as a volatile species into the indoor environment.[7-11] It can also be released into the environment by some natural processes (e.g., degradation of humic substances, emission by microbes, combustion of biomass, etc.) as well as by anthropogenic activities (e.g., tobacco smoke, automobile exhaust, etc.).[9, 12] Moreover, FA can be produced endogenously by the oxidase and demethylase enzymes such as JmjC domain-containing protein[13, 14] and lysine specific demethylase 1 (LSD1).[15, 16] Due to the degradation reaction by formaldehyde dehydrogenase, the physiological concentration of FA can range from 100 to 400 μM.[4, 17] Moreover, in cancer cells, the endogenous concentration of FA can reach up to 1000 μM.[18] Owing to its high electrophilic nature, FA can easily bind with nucleophilic site of DNA and proteins, which causes cellular dysfunction. The abnormal concentration of FA in human body is responsible for various types of diseases such as cancer,[18, 19] diabetes,[20] cirrhosis, cardiovascular and neurological disorders.[21] In recent years, FA is identified as major component for sick building syndrome (SBS).[22-24] It can cause strong irritation of mucous membranes and eyes.[24] According to World Health Organization (WHO), the permissible limit of exposure to FA is 0.08 ppm for 30 min.[25] On the other hand, the US National Institute for Occupation Safety and Health (NIOSH) has set a maximum of 0.016 ppm as the long term exposure limit for FA.[26]

After taking the above-mentioned facts into account, the detection of FA has been explored in the last few years. A variety of techniques have been employed such as spectrophotometry,[27] colorimetry,[28] gas chromatography (GC),[29] high-performance liquid chromatography,[30] ion chromatography [31] and polarography[32] for the quantification and detection of FA. Unfortunately, all of these methods demand well-trained operators, bulky and expensive instrumentation, high power consumption and destruction of bio-specimens. Hence, these traditional methods are unsuitable for the spatiotemporal sensing of FA. Recently, fluorescence sensing technique has drawn more attention than the

conventional methods due to its simple operation, high selectivity, sensitivity, fast response and non-destructive detection of bio-specimens.[33] Generally, two types of mechanisms have been reported for the fluorometric sensing of FA. In one kind of mechanism, the fluorescent properties of the fluorogenic core present in the molecule can be restored by disrupting the photo-induced electron transfer (PET) process,[34, 35] either via condensation reaction or via 2-aza-Cope reaction after the initial condensation reaction.[36, 37] In the second type of mechanism, a drastic fluorescence enhancement is observed due to the condensation reaction between FA and primary amine which cause a rhodamine unit transformation from spiro to open-ring conformation through a cyclisation reaction.[38] A variety of fluorescent probes have been explored for the purpose of sensing FA which includes organic small molecules,[39] organic-inorganic hybrid materials[40] and metal-organic framework (MOF) compounds.[41-44]

MOFs are a new class of functional porous materials having extended crystalline frameworks, and comprising metal ions and organic linkers.[45] Due to tunable functionality and porosity, chemical stability as well as highly conjugated backbones, MOF materials have been widely employed in chemical sensing,[46, 47] gas storage and separation,[48] catalysis,[49, 50] drug delivery.[51] Till now, only four MOF materials have been employed for the fluorogenic sensing of FA.[41-44] Here, we report the synthesis, comprehensive characterization and fluorescence sensing properties of a new Al(III) MOF (**1**) having MIL-53 (MIL = Material of Institute Lavoisier) framework topology and containing the hydrazine-functionalized $H_2BDC\text{-}N_2H_3$ ($H_2BDC\text{-}N_2H_3$ = 2-hydrazinyl-1,4-benzenedicarboxylic acid) ligand. In its thermally activated form (**3′**), the material acts as an efficient probe for detecting FA (in aqueous, HEPES buffer media and vapor phase) with remarkable sensitivity and selectivity (Scheme 4.1). The endogenous FA in breast cancer cells can be efficiently detected by this MOF probe. Moreover, the compound has the potential to detect the change in concentration of FA in cancer cells. It should be noted that the $H_2BDC\text{-}N_2H_3$ ligand has never been utilized for the preparation of any MOF material. Therefore, **3′** is the first example of a hydrazine-functionalized Al(III) MOF which possesses the $BDC\text{-}N_2H_3$ ligand and exhibits selective fluorescence sensing properties towards FA. Though several MOF compounds were utilized previously for the sensing of FA (Table 4.1), some of them require the incorporation of guest metal ions (i.e., Ag^+, Eu^{3+}, etc.) for the sensing of FA. However, **3′** can successfully detect FA by functional group interconversion without incorporation of any metal ion. Moreover, some of the MOF materials were employed for the aqueous-phase sensing and few of them were

utilized for the vapor-phase sensing of FA. However, **3′** was successfully employed for both aqueous- and gas-phase sensing of FA. The capability of none of the MOF materials was examined for the detection of FA in living cells, whereas **3′** has the ability to detect FA in cancer cells. Furthermore, **3′** showed selectivity toward FA over a wide number of other aldehydes (oxaldehyde, acetaldehyde, butyraldehyde, propionaldehyde, valeraldehyde, crotonaldehyde, benzaldehyde, 4-chlorobenzal-dehyde, and anisaldehyde). Such a vast number of competitive aldehydes were not utilized during the selectivity study for the other reported MOF materials. In addition, the response time (60 s) of **3′** toward FA is also lower than the other MOF-based FA sensors. Hence, an easy synthetic procedure, sensing of FA in a versatile medium and fast response and high selectivity toward FA over other aldehydes make **3′** a superior FA sensor over the reported MOF probes.

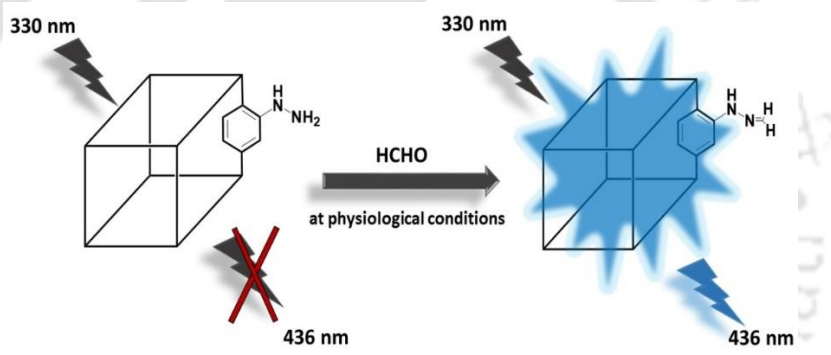

Scheme 4.1 Fluorogenic "turn-on" sensing of formaldehyde by activated Al-MIL-53-N_2H_3 (**3′**) probe at physiological conditions.

Table 4.1 Comparison of the results of various formaldehyde sensors.

A.	Fluorescent sensors						
Sl. No.	Sensor Material	Type of Material	Response Time (s)	Detection Limit	Medium Used	Mode of Sensing	Ref.
1	Al-MIL-53-$NHNH_2$	MOF	60	8.37 µM	HEPES buffer	Turn-on	this work
2	Zr-UiO-66-NH_2	MOF	120	4.0 ppm	Trizma base buffer	Turn-off	41

3	Eu/Zr-UiO-66-NH_2	MOF	-	0.20 ppm	ethyl acetate	Turn-on	42
4	Ag^{+}/Eu^{3+}-UiO-66	MOF	360	0.051 ppm	solid state	Turn -on	44
5	ZIF-8	MOF	300	0.057 ppm	solid state	Turn -on	43
6	compound **1**	organic molecule	480	0.78 µM	PBS buffer	Turn-on	52
7	aniline-substituted BODIPY motif (**AnB**)	organic molecule	-	165 nM	CH_3OH	Turn-on	34
8	FAP-1	organic molecule	7200	5 µM	PBS buffer	Turn-on	36
9	Na-FA	organic molecule	1800	7.1×10^{-7} M	PBS buffer	Turn-on	35
10	FP1	organic molecule	10800	0.01 mM	PBS buffer	Turn-on	37
11	FAP	organic molecule	7200	0.5 µM	PBS buffer	Turn-on	39
12	RFAP	organic molecule	7200	0.3 µM	PBS buffer	Turn-on	53
13	probe **1**	organic molecule	-	900 nM	water	Turn-on	54
14	2-amidyl-3-(3-amidly-1H-benzo[d] imidazolyl)-pyridine	organic molecule	48	6 µM	water	Turn-on	55
B.	Electrochemical sensors						
Sl. No.	Sensor Material	Type of Material		Linear Range		Detection Limit	Ref.

15	$SPC_{Pt}Es$	screen-printed carbon electrodes	60-460 µM L^{-1}	60 µM L^{-1}	56
16	Pd NW arrays	nanowire	2 µM - 1 mM	0.5 µM	57
17	Pd-modified TiO_2 electrode	TiO_2 electrode	0 - 17.7 mM	0.015 mM	58
18	AgPd/Ch–IL	nanoparticles	0.060 - 20 mM	0.022 mM	59
19	PdSPE	screen-printed macroelectrodes	19.68 - 27.84 µM	2 µM	60
20	screen-printed carbon electrodes modified with gold clusters	gold clusters	1 - 10 mM	0.9 mM	61
C.	Enzymatic sensors				
21	thin-film planar electrodes and immobilised alcohol oxidase	conductometric enzyme biosensor	0.05 - 500 mM	0.05 mM	62
22	electrodes-formaldehyde-dehydrogenase	Dehydrogenase enzyme-based sensor	30 ng mL^{-1} - 1.5 µg mL^{-1}	30 ng mL^{-1}	63

4.2 Experimental section

4.2.1 Materials and characterization methods

All the required chemicals were procured from commercial sources and used without purification, except the $H_2BDC\text{-}N_2H_3$ ligand. Fourier transform infrared (FT-IR) spectra were collected with a Perkin Elmer Spectrum two FT-IR spectrometer in the range 440-4000 cm^{-1} with KBr pellet. The below mentioned indications were employed for the characterization of the absorption bands: medium (m), weak (w), broad (br), very strong (vs), strong (s) and shoulder (sh). Ambient temperature X-Ray powder diffraction (XRPD) patterns were measured on a Bruker D2 Phaser X-ray diffractometer (30 kV, 10 mA) using Cu-*K*α (λ = 1.5406 Å) radiation. FE-SEM images were collected with a Zeiss (Zemini)

scanning electron microscope. Dynamic light scattering (DLS) measurements were performed by a Zetasizer Nano ZS90 (model no. ZEN3690) instrument. Thermogravimetric analyses (TGA) were collected under air atmosphere at a heating rate of 10 °C min^{-1} in a temperature region of 25-800 °C by employing a Netzsch STA-409CD thermal analyzer. Fluorescence emission behavior was analyzed by a HORIBA JOBIN YVON Fluoromax-4 spectrofluorometer. The excitation wavelength (λ_{ex}) was 330 nm for all the fluorescence experiments. The nitrogen sorption isotherms were performed employing a Quantachrome Autosorb iQ-MP gas sorption analyzer at -196 °C. Prior to the sorption measurement, degassing of the material was performed at 130 °C for 12 h under dynamic vacuum. A Bruker Avance III 600 spectrometer was used for recording ^{1}H-NMR and ^{13}C-NMR spectra at 600 MHz. Before the NMR measurements, the ligand (5 mg) was dissolved in 500 µL of DMSO-*d*$_6$. The mass spectrum (in ESI mode) was measured with an Agilent 6520 Q-TOF high-resolution mass spectrometer. Prior to the ESI-MS measurement, 15 mg of **3′** and FA-treated **3′** were separately digested in 2 mL of HPLC grade methanol by the treatment with 200 µL of 48% HF (caution!). For FA-treated **3′**, required amount of $NaHCO_3$ was added to the medium to attain neutral pH (as imine bond is unstable in acute acidic medium), filtered and then FA was introduced in the filtrate. For both samples, the organic layer was collected by filtration after 15 min of sonication. Then, the samples were further diluted by adding HPLC grade methanol for the ESI-MS measurements. Fluorescence lifetime measurements were carried out using time correlated single-photon counting (TCSPC) method by an Edinburgh Instrument Life-Spec II instrument.

4.2.2 Preparation of H_2BDC-N_2H_3 ligand

In a 100 mL round-bottom flask, a mixture of 2-amino-1,4-bezenedicarboxylic acid (1.81 g, 10 mmol) and 20 mL conc. HCl was placed. This mixture is cooled to 0 °C and stirred at this temperature for full dissolution. Then, an ice-cold solution of $NaNO_2$ (0.7 g) dissolved in water (5 mL) was introduced. The resulting mixture was stirred for 2 h, maintaining the temperature at 0 °C. Afterward, an ice-cold mixture containing $SnCl_2{\cdot}2H_2O$ (4.5 g) and conc. HCl (15 mL) was introduced. The stirring was continued for another 3 h at ambient conditions. A light yellow colored precipitate was obtained. It was filtered off and washing was carried out several times with water until neutral pH is attained. Finally, drying of the precipitate was conducted in an air oven at 60 °C for 6 h. The yield was 1.2 g (6.1 mmol, 61 %). ^{1}H-NMR (600 MHz, DMSO-*d*$_6$): δ = 7.50 (d, 1H),

7.69 (s, 1H), 7.99 (d, 1H), 9.15 (s, 1H) ppm. ^{13}C NMR (150 MHz, DMSO-d_6): δ = 168.36, 166.58, 147.26, 135.79, 131.91, 120.42, 117.07, 114.63 ppm. ESI-MS (m/z): 195.0331 for $(M-H)^-$ ion (M = mass of $H_2BDC\text{-}N_2H_3$ ligand). In Figures 4.1-4.3 the NMR and mass spectra of the $H_2BDC\text{-}N_2H_3$ ligand are shown.

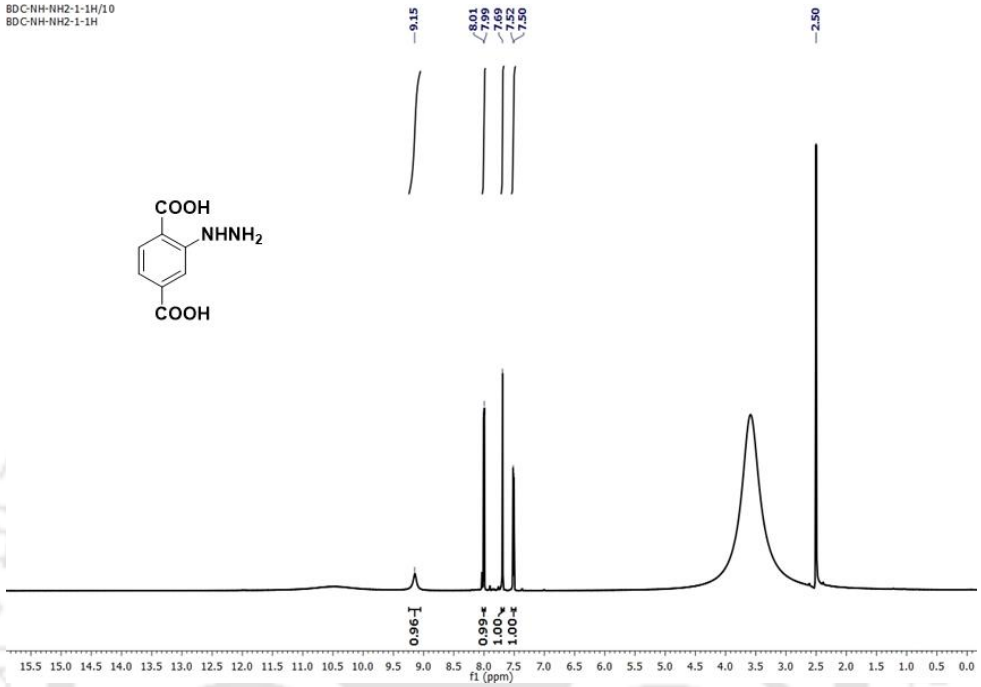

Figure 4.1 ^{1}H NMR spectrum of $H_2BDC\text{-}N_2H_3$ ligand measured in DMSO-d_6.

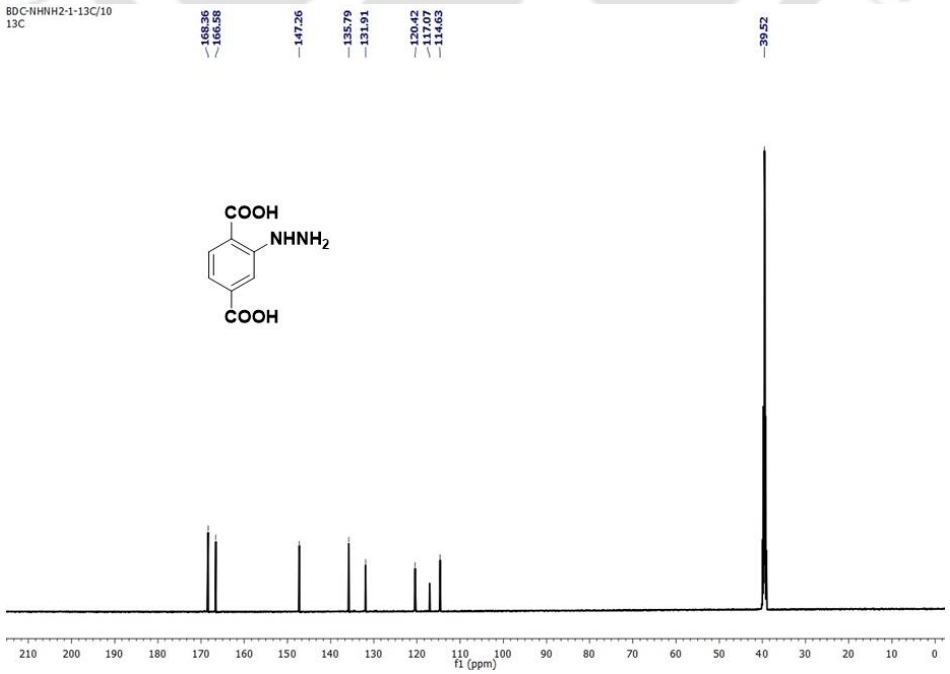

Figure 4.2 ^{13}C NMR spectrum of $H_2BDC\text{-}N_2H_3$ ligand measured in DMSO-d_6.

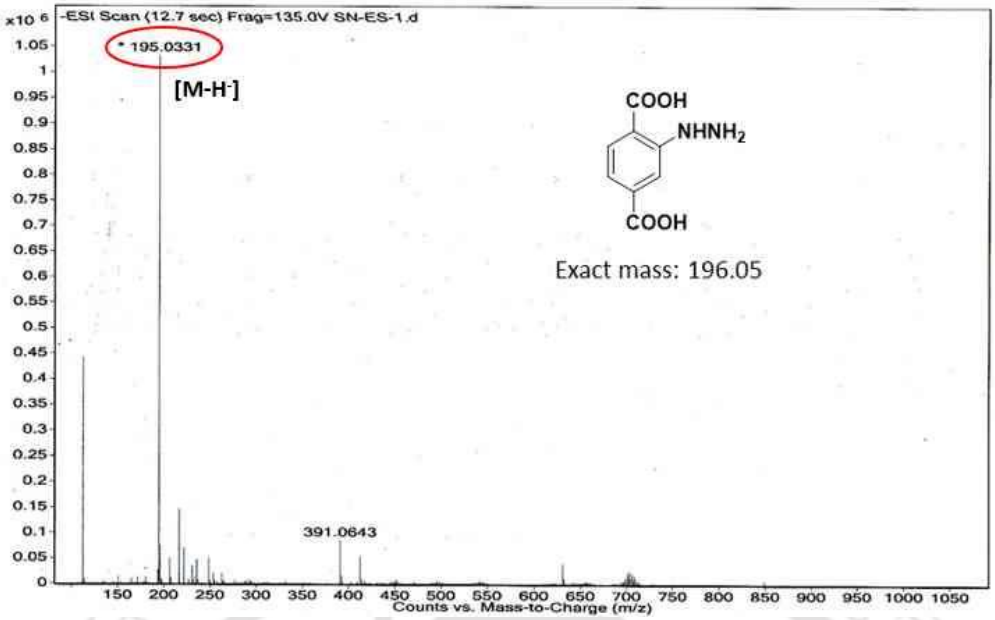

Figure 4.3 ESI-MS spectrum of $H_2BDC\text{-}N_2H_3$ ligand measured in methanol. The spectrum shows m/z peak at 195.0331, which corresponds to $(M\text{-}H)^-$ ion (M = mass of $H_2BDC\text{-}N_2H_3$ ligand).

4.2.3 Preparation of $[Al(OH)(BDC\text{-}N_2H_3)]\cdot 0.85DEF\cdot 1.0H_2O$ (Al-MIL-53-N_2H_3; 3)

In a Pyrex tube, $Al(NO_3)_3\cdot 9H_2O$ (57 mg, 0.15 mmol) and $H_2BDC\text{-}N_2H_3$ (30 mg, 0.15 mmol) ligand was placed. Then, 3 mL of DEF/H_2O (1 mL/2 mL) mixture was poured into the tube, which was sealed and sonicated for 15 min. Afterward, it was heated at 120 °C for 24 h using a block heater. The resulting yellow colored material was obtained by filtration and dried inside an air oven at 70 °C for 6 h. Yield: 30 mg (0.08 mmol, 53%). The yield was calculated on the basis of the aluminum salt. FT-IR (KBr, cm^{-1}): 3426 (br), 2968 (sh), 2934 (w), 2851 (w), 1657 (m), 1628 (sh), 1580 (vs), 1505 (w), 1430 (s), 1381 (sh), 1313 (w), 1265 (m), 1216 (w), 1098 (m), 1003 (m), 853 (w), 804 (m), 768 (m), 678 (m), 578 (br), 481 (br).

4.2.4 Activation of the material

At first, heating of the as-synthesized compound (100 mg) was conducted at 150 °C for overnight in 20 mL DMF by using a Teflon-lined stainless steel autoclave. Later, stirring of the filtered compound was carried out in acetone (50 mL) for overnight at room temperature. In the third step, heating of the filtered material at 130 °C for overnight was performed using high vacuum pump. The guest-free material is named as **3′**.

4.2.5 Fluorescence sensing experiments in aqueous medium

The probe (5 mg) was placed in a glass vial and water or 10 mM HEPES buffer (5 mL each) was added. The preparation protocol for the HEPES buffer solution has been reported by us previously.[47] The mixture was sonicated for 1 h. After keeping for one day at room temperature, a stable suspension was obtained.

The above-mentioned suspension (200 μL) of the probe (in water or HEPES buffer) was placed inside a quartz cuvette. Then, we have added 2800 μL of deionized water or HEPES buffer to the suspension. All the fluorescence titration measurements were carried out using the resulting suspension. These experiments involved addition of the solutions of various aldehydes (20 mM) to the suspension (3 mL) of the probe. Formaldehyde, oxaldehyde, acetaldehyde and 4-chlorobenzaldehyde are readily soluble in water. Therefore, 20 mM aqueous or HEPES buffer solutions of these aldehydes were prepared in pure deionized water. The other aldehydes (butyraldehyde, propionaldehyde, valeraldehyde, crotonaldehyde, benzaldehyde and anisaldehyde) are insoluble in water. For them, the required amount of an aldehyde (for 20 mM solution) was dissolved in minimum amount of distilled ethanol. Then, deionized water or HEPES buffer was added to fulfil the required volume.

4.2.6 Fluorescence sensing experiments in vapor phase

To examine the fluorescence detection performance of **3′** towards FA vapor, time-dependent fluorescence titration experiments were carried out. Prior to the experiment, a thin film of **3′** was fabricated on the quartz slide. At first, a suspension of **3′** was prepared by dispersing 50 mg of **3′** in 5 mL of ethanol. Before film deposition, the dispersion was sonicated for 30 min in an ultrasonic bath to get a homogeneous suspension of **3′**. The spin-coating method was applied to prepare the thin film of **3′** on the quartz slide. By maintaining the spin-coating speed at 2000 rpm for 1 min, the suspension of **3′** was dropped on the quartz slide which was fixed on a spin-coater. This spin-coating process was repeated for several times until a homogeneous coating was obtained. Afterward, the as-prepared film of **3′** on the quartz slide was dried at room temperature.

The film-coated quartz slide was fixed inside of a quartz cuvette in a suitable position (Figure 4.4). The solid-state emission spectra of the spin-coated sample were measured in the beginning. Then, 100 μL of FA was carefully introduced at the bottom of the cuvette by a pipette. After that the cuvette was quickly sealed by cap. After the introduction of FA, the emission spectra were recorded with 1 min interval until saturation

in intensity of the emission spectra was obtained. To ensure the selectivity of **3′** towards FA in the vapor phase, similar experiments were repeated with different liquid aldehydes (oxaldehyde, acetaldehyde, butyraldehyde, propionaldehyde, valeraldehyde, crotonaldehyde, benzaldehyde and anisaldehyde). It is worth to note that 4-chlorobenzaldehyde was excluded from the vapor phase sensing experiment as it is a solid compound.

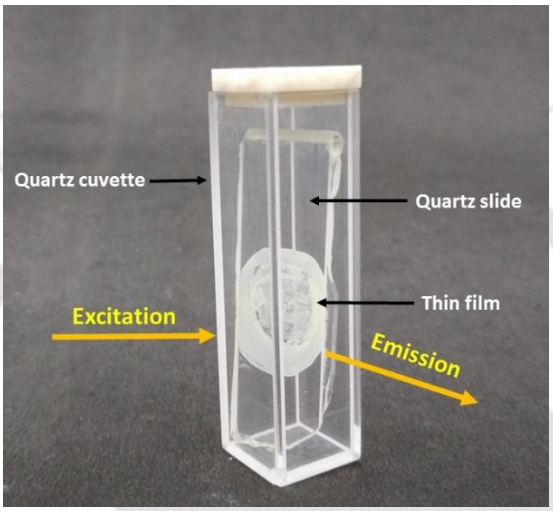

Figure 4.4 Custom-designed sensor set-up used for the vapor-phase sensing of FA.

4.2.7 Cell culture and imaging experiments

The culture of the MDAMB-231 breast cancer cells was performed in DMEM:F12 media consisting of 10% fetal bovine serum (FBS) and 1% antibiotic cocktail as described formerly.[64] Cells were loaded with **3′** (0.5 mg/mL) for 10 h in serum-containing media. To remove excess probe, the washing of the cells was carried out with phosphate buffered saline (PBS) thrice. Then, the cells were treated with FA (50 µM) for 60 min at 37 °C in PBS. The cancer cells were observed in the bright field and the blue channel (λ_{ex} = 390 nm, λ_{em} = 430 nm) using Cytell cell imaging system (GE Healthcare) and images were captured from randomly selected fields.

4.3 Results and discussion

4.3.1 FT-IR Spectroscopy

The FT-IR spectra (Figure 4.5) of the activated and as-synthesized forms of **3** were recorded to ensure the incorporation of the ligand in the MOF structure during the solvothermal reaction and the complete elimination of guest molecules from the voids of the MOF after thermal activation. In the FT-IR spectra of as-synthesized **3** and activated **3′**, strong absorption bands at around 1580 and 1430 cm^{-1} were noticed, which can be ascribed to the asymmetric and symmetric $–CO_2$ stretching vibrations of the coordinated BDC-N_2H_3 ligand, respectively.[65] The carbonyl stretching vibration of the trapped DEF molecules gives rise to medium absorption band at 1657 cm^{-1} in the IR spectrum of the as-synthesized form of the material.[66] This absorption band is totally vanished in the IR spectrum of activated **3′**, indicating entire elimination of DEF molecules from the pore of the material.

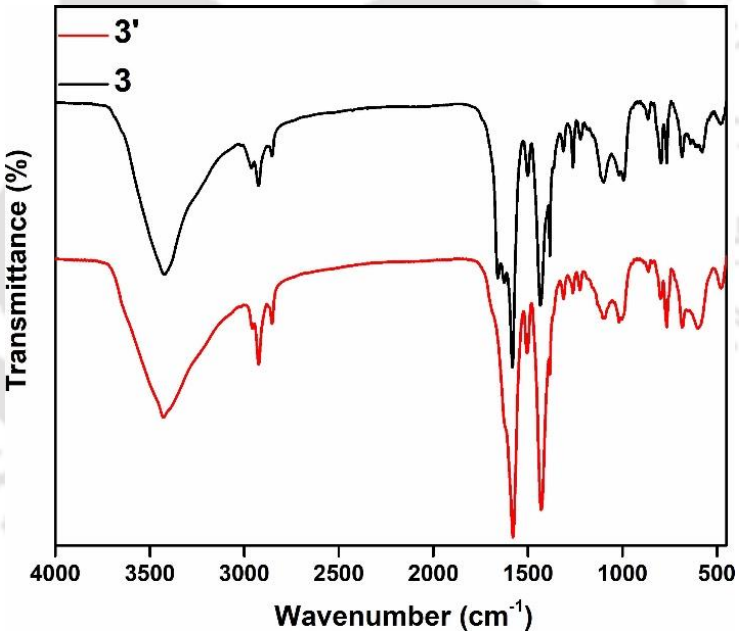

Figure 4.5 FT-IR spectra of as-synthesized **3** (black) and activated (red) **3′**.

4.3.2 Structure description

The hydrazine-functionalized Al-MIL-53 (**3**) exhibits the same framework topology as the un-functionalized compound. The framework structure of Al-MIL-53 has been previously described by Loiseau *et al.* [67] Briefly, the structure of Al-MIL-53 is constructed by the interconnection of infinite *trans* chains of corner-sharing (via OH

groups) [$AlO_4(OH)_2$] octahedra by the 1,4-benzenedicarboxylate (BDC) ligands to form a three-dimensional (3D) framework containing one-dimensional (1D) rhombic pores. For the presented compound (**3**), the BDC-N_2H_3 ligand molecules replace the BDC ligands of Al-MIL-53 framework. The as-synthesized form of **3** incorporates guest (DEF and water) molecules inside the pores under ambient conditions. Furthermore, the hydrazine groups attached with the coordinated BDC-N_2H_3 ligands point towards the interior of the pores.

From Figure 4.6, it is obvious that the experimental XRPD pattern of the as-synthesized title compound shows great similarity with the XRPD pattern of the un-functionalized Al-MIL-53 compound. Therefore, **3** is isostructural with un-functionalized Al-MIL-53. Furthermore, the XRPD pattern of the thermally activated **3′** (Figure 4.7) shows remarkable similarity with that of the as-synthesized **3**, which suggests that the structural integrity of the compound is retained after the thermal activation procedure. The XRPD pattern of **3′** was also recorded after the formaldehyde sensing process. As can be seen from the XRPD pattern, the crystallinity (and thus structural robustness) of **3′** remains intact after the sensing experiment, indicating that **3′** is efficient for practical sensing applications.

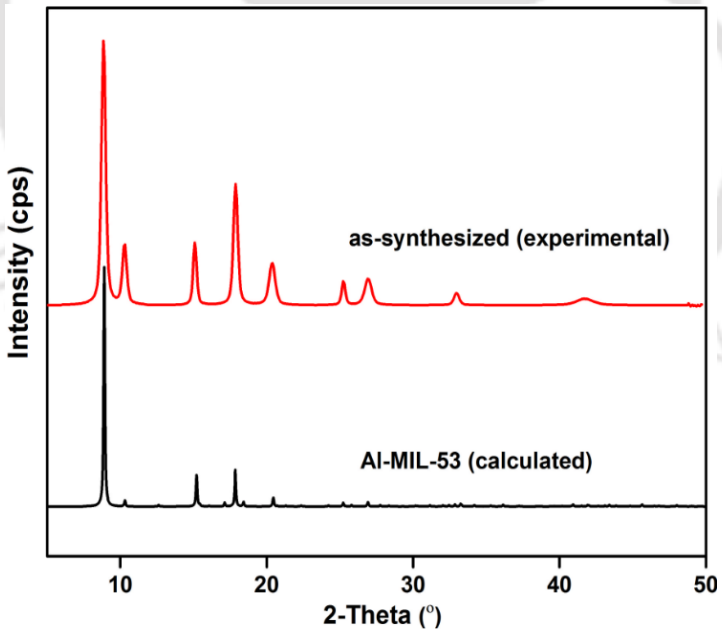

Figure 4.6 Calculated XRPD pattern of Al-MIL-53 (black) and experimental XRPD pattern of as-synthesized Al-MIL-53-N_2H_3 (red).

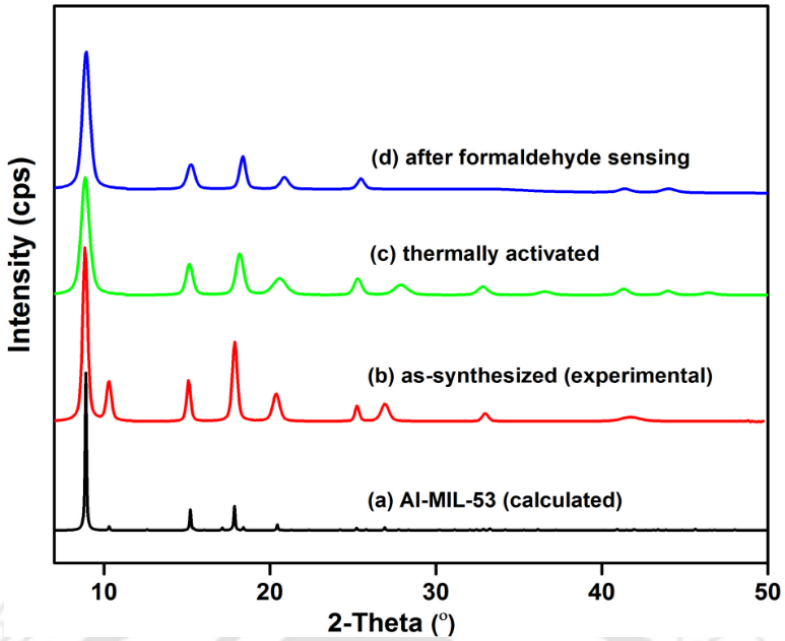

Figure 4.7 XRPD patterns of **3** in different forms: calculated (a), as-synthesized (b), thermally activated (c) and after formaldehyde sensing experiment (d).

4.3.3 Thermal stability

Thermogravimetric analyses (TGA) were carried out for investigation of the thermal stability of the as-synthesized and thermally activated forms of **3** in the temperature range of 25-800 °C under air atmosphere. According to the TG curve (Figure 4.8a), the compound displays high thermal stability up to 480 °C under air atmosphere.

In the TG trace of as-synthesized **3**, the first weight loss of 5.1 wt% in the temperature range of 25-130 °C can be attributed to the elimination of one guest water molecule per formula unit (calcd.: 5.2 wt%). The next weight loss of 25.3 wt% in the temperature range of 130-360 °C can be assigned to the removal of 0.85 DEF molecule per formula unit (calcd.: 25.1 wt%). After 480 °C, the compound starts to decompose due to the removal of coordinated ligand molecules from the framework.

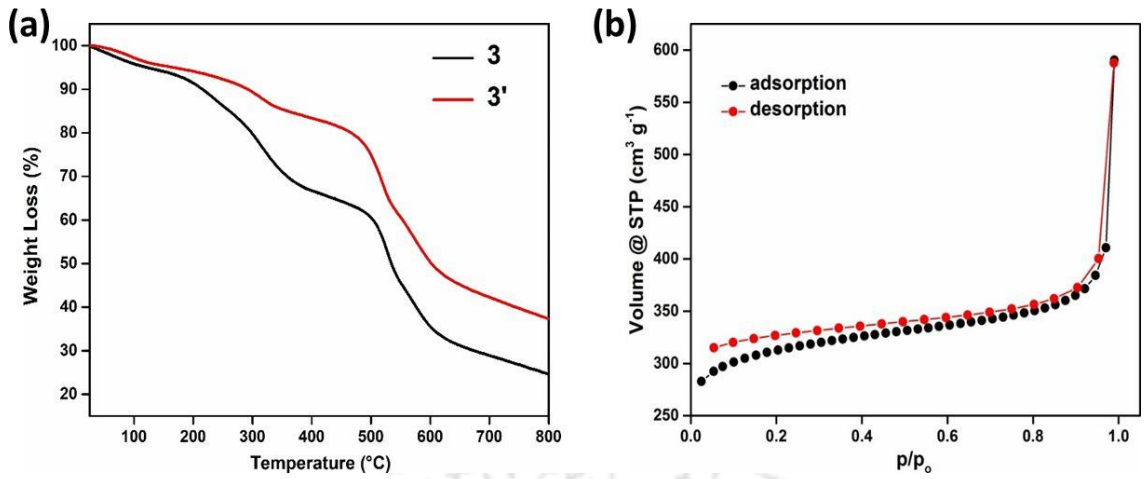

Figure 4.8 (a) TG curves of as-synthesized **3** (black) and activated **3′** (red) recorded in an air atmosphere in the temperature range of 25-800 °C with a heating rate of 10 °C min^{-1}. (b) N_2 adsorption (black circles) and desorption (red circles) isotherms of thermally activated **3′** recorded at –196 °C.

4.3.4 Surface area analysis

In order to prove permanent microporosity, N_2 sorption studies were carried out with **3′**. The compound showed type-I N_2 sorption isotherms (Figure 4.8b), which are characteristic of microporous materials. For the presented material, the BET surface area and micropore volume were found to be 958 m^2 g^{-1} and 0.51 cm^3 g^{-1} (at $p/p_0 = 0.50$), respectively. The BET surface area of **3′** is comparable with those of the other functionalized Al-MIL-53 compounds.[68, 69]

4.3.5 Particle size measurement

The morphology of **3′** was investigated using FE-SEM technique. The FE-SEM images (Figure 4.9a) reveal that the particles of **3′** display rod-like morphology and are almost uniform in size. The average diameter of the particles is about 600-700 nm. The shape and size of the particles are very similar with previously reported MIL-53(Al).[70]

The average particle size measured by the DLS method is 741 nm for the ethanolic dispersion of **3′** (Figure 4.9b). The poly-dispersion index (PDI, 0.31) value signifies narrow distribution of the particle size. Moreover, the average particle size obtained from the DLS study is in good agreement with the FE-SEM results.

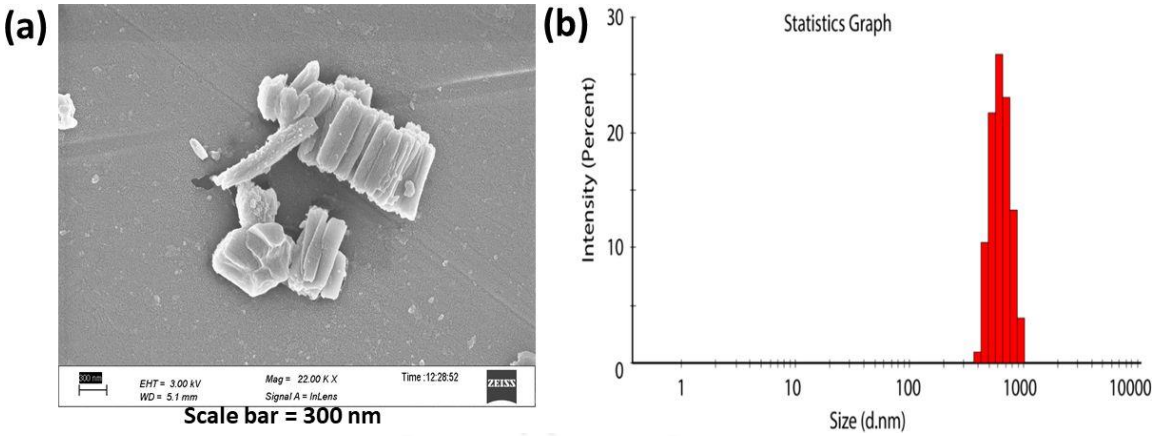

Figure 4.9 (a) FE-SEM images of **3′** under different magnification, (b) Particle size distribution of the ethanolic dispersion of **3′** measured by DLS method.

4.3.6 Sensing of FA in HEPES buffer medium

For the carcinogenic effect of FA, its real time detection has become a highly demanding task. As a result, a huge number of fluorescent probes based on small organic molecules have been developed in the last few years. [34-38, 52] Unfortunately, the number of existing MOF-based fluorescent probes for formaldehyde is very less (Table 4.1).[41-44] Al(III) based MOFs are always preferable to MOFs containing other metal ions for their high hydrolytic stability, non-toxic nature and bio-friendly behavior.[46] All the above facts motivated us to examine the efficacy of the new hydrazine functionalized Al(III) based MIL-53 compound for sensitive and selective sensing of FA in both aqueous and physiological media (HEPES buffer, pH = 7.4).

Fluorescence experiments were performed to evaluate the detection performance of FA by the presented material. Prior to the introduction of FA, the hydrazine functionalized **3′** was in fluorescent "turn-off" state due to photo-induced electron transfer (PET) from the hydrazine moiety to the phenyl ring.[34] But, after the addition of FA, the hydrazine functionality is transformed to hydrazone moiety, which suppresses the PET process and restores the fluorescence property of the fluorogenic core. Consequently, a drastic enhancement in fluorescent emission intensity was detected for the material in the presence of FA.

For time-dependent study, 500 μL of 20 mM FA was introduced to the suspension of **3′** in HEPES buffer medium and fluorescence spectra were collected upon excitation at 330 nm at a regular time interval of 1 min up to 10 min. Figure 4.10a reveals that saturation of the emission intensity occurred within 60 s with 4-fold increment as compared to the

initial intensity. Another fluorescence experiment was performed by replacing the HEPES buffer medium with aqueous medium (Figure 4.10b). In this case, the fluorescence intensity also attained saturation within 60 s but a remarkably higher fold increment (7 fold) was noticed for the aqueous medium than the HEPES buffer. It can be accounted for the higher stability of the hydrazone moiety at lower pH (water at pH = 7.0) than higher pH (HEPES at pH = 7.4) of the medium.[52] Though the fold increment in fluorescence intensity in aqueous medium is reasonably superior to HEPES buffer medium, we have employed HEPES buffer for the subsequent fluorescence experiments as the biological conditions are more accurately mimicked by the later medium.

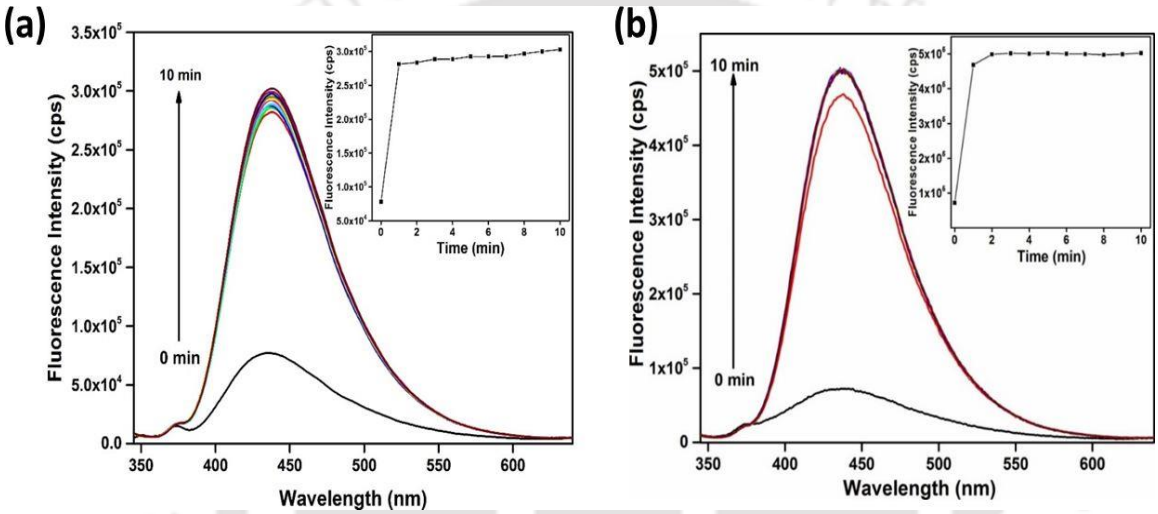

Figure 4.10 Increment in emission intensity of **3′** after the introduction of 20 mM formaldehyde (500 μL) from 1 min to 10 min in (a) HEPES buffer and (b) aqueous medium. Inset plot shows the enhancement in emission intensity as a function of time (monitored at 436 nm).

An ideal fluorescent sensor should exhibit high selectivity towards the desired analyte over other competing species. Hence, we have examined the selectivity of the MOF probe towards FA with respect to other common aldehyde compounds (oxaldehyde, acetaldehyde, butyraldehyde, propionaldehyde, valeraldehyde, crotonaldehyde, benzaldehyde, 4-chlorobenzaldehyde and anisaldehyde) in both HEPES buffer and aqueous media. From Figure 4.11 and 4.12, it becomes obvious that the fluorescence intensity (monitored at 436 nm) of the Al-MIL-53-N_2H_3 probe changed hardly in the presence of other aldehyde compounds. Only FA was capable of enhancing the emission intensity of the compound. As the bulky and polar hydrazine functionality is grafted with

the BDC ligand, a highly polar environment has been generated in the MOF structure. Moreover, the interconnection of infinite *trans* chains of corner-sharing (via OH groups) $[AlO_4(OH)_2]$ octahedra by the BDC-N_2H_3 ligands forms a 3D framework containing 1D channels. Furthermore, the hydrazine groups attached with the coordinated BDC-N_2H_3 ligands point towards the interior of the pores, which is not possible in discrete H_2BDC-N_2H_3 ligand. On the other hand, as FA is the smallest and highest electrophilic aldehyde among other competitive aldehydes, it can easily diffuse through the porous channel of the MOF material and react with the nucleophilic hydrazine functional group present to form hydrazone moiety. Other aldehyde molecules having larger sizes are unable to diffuse through the pore channel. These competitive aldehydes can hardly react with the hydrazine functional group owing to their lower electrophilic nature as compared to FA. A careful inspection of Figure 4.11 reveals that both oxaldehyde and acetaldehyde show similar enhancement in emission intensity which is lower than the emission intensity of **3′** in presence of FA. This is due to the larger size and lower electrophilic nature of acetaldehyde and oxaldehyde as compared to FA. Therefore, the selective response of FA towards **3′** can be assigned to the highly polar environment and porous structure of the MOF material as well as the smallest size and highest electrophilic character of FA over other aldehydes.[71]

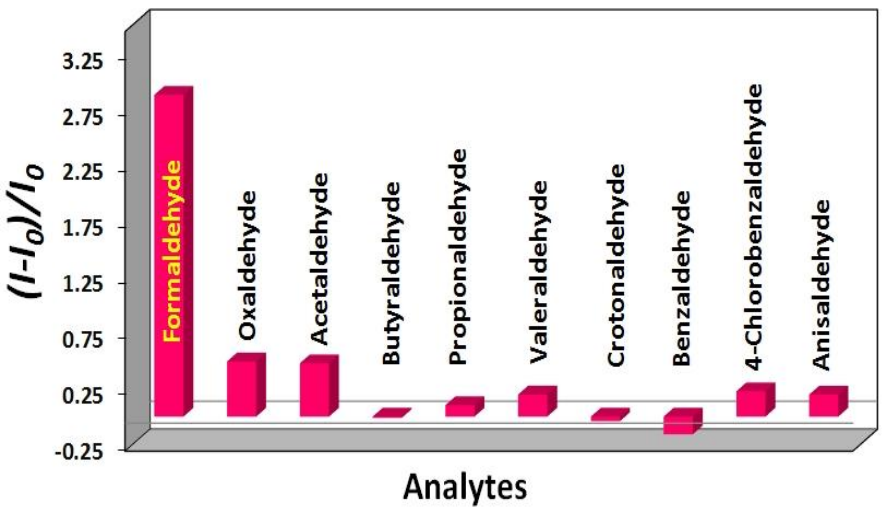

Figure 4.11 Relative fluorescence turn-on signal of **3′** towards the addition of different aldehydes (20 mM, 500 μL) in HEPES buffer.

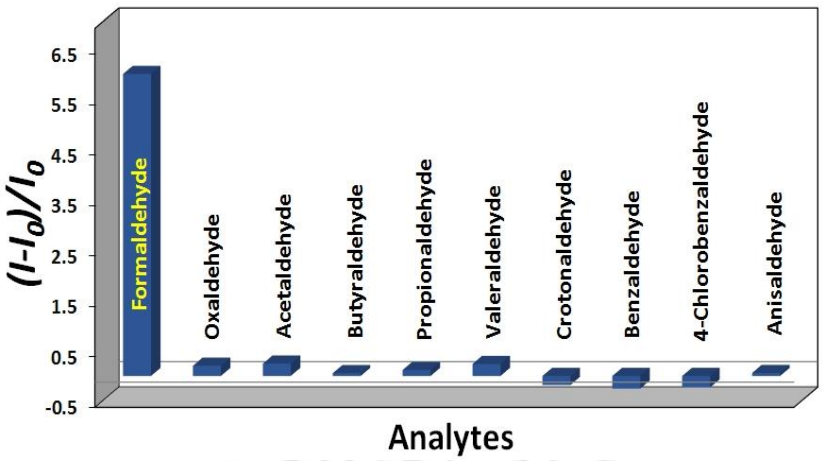

Figure 4.12. Relative fluorescence turn-on response of **3′** towards different aldehydes in aqueous medium.

Another set of fluorescence experiments was performed to examine the selectivity of the probe towards FA in the presence of other aldehyde compounds in both HEPES buffer and aqueous media. For these experiments, FA was added to the suspension of **3′** which already contained other competing aldehydes. From Figure 4.13 and 4.14, it becomes clear that FA is capable to enhance the emission intensity of the suspension of the probe in both HEPES buffer and aqueous media, even though other aldehydes exist in the system. Hence, we can conclude that the present probe has shown remarkable selectivity towards FA even in the existence of other competing aldehyde compounds.

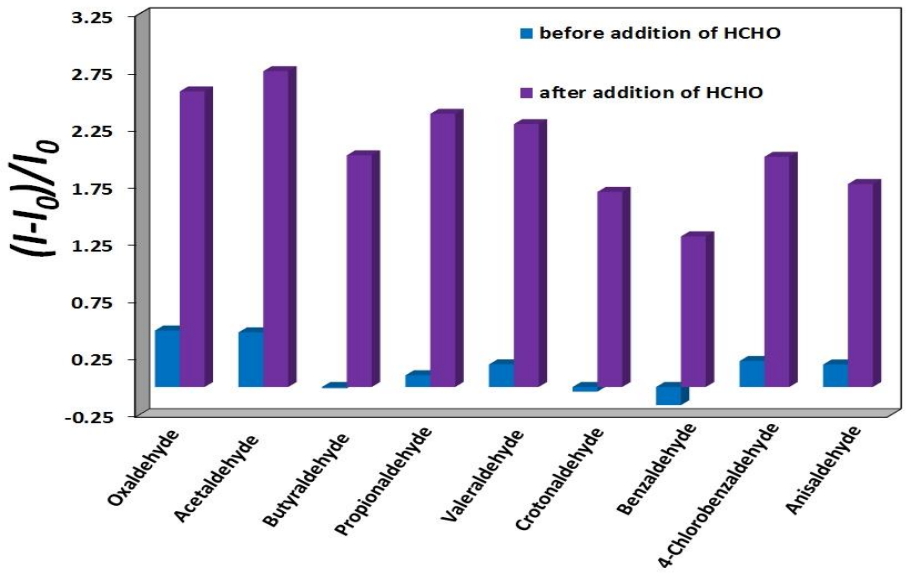

Figure 4.13 Relative fluorescence turn-on signal (monitored at 436 nm) of **3′** towards formaldehyde (20 mM, 500 μL) in presence of other possibly intrusive aldehydes (20 mM, 500 μL) in HEPES buffer.

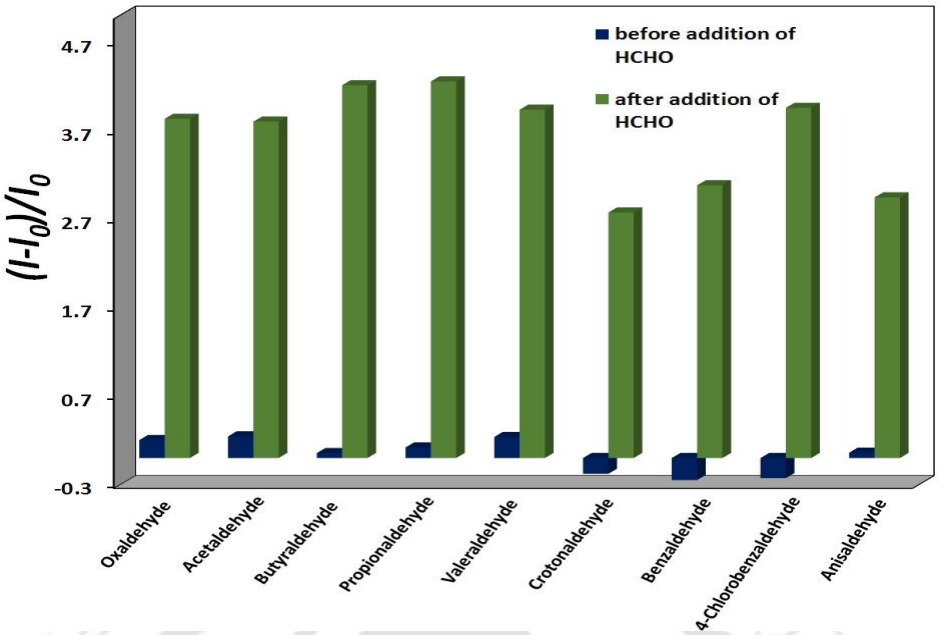

Figure 4.14 Relative fluorescence turn-on response of **3′** towards formaldehyde in presence of other potentially interfering aldehydes in aqueous medium.

To quantify the detection process of FA by the probe, a concentration-dependent fluorescence titration experiment was performed. Figure 4.15a reveals that with incremental introduction of FA in the HEPES buffer suspension of **3′**, the fluorescence intensity also enhanced gradually. Similar outcome was observed when the concentration-dependent fluorescence titration experiment was conducted with the aqueous suspension of the MOF material (Figure 4.15b).

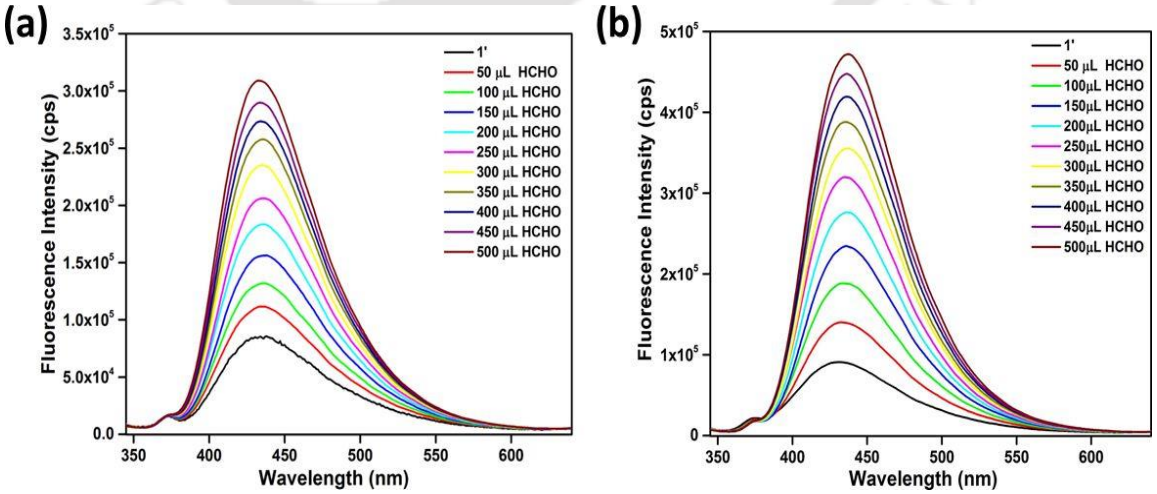

Figure 4.15 Enhancement of the fluorescence emission intensity of **3′** upon gradual addition of 20 mM formaldehyde solution in (a) HEPES buffer and (b) aqueous medium.

In order to determine the limit of detection (LOD) of **3′** towards FA, the fluorescence intensity of the HEPES buffer suspension of the compound was monitored upon incremental addition of very low concentrations of FA solution. When the emission intensity of **3′** versus the concentration of FA was plotted, a linear curve ($R^2 = 0.99$) having a slope (m) of 200262.98 was obtained (Figure 4.16a). The standard deviation (σ) was determined from eight blank measurements with the MOF probe. The LOD value was calculated by employing the formula: LOD = $3\sigma/m$. The calculated LOD value of **3′** for FA sensing in HEPES buffer was 8.37 μM (0.25 ppm). It is worthy to note that the LOD value of the probe for FA in the aqueous medium (Figure 4.16b) was estimated to be 2.14 μM (64.33 ppb). These values fall within the permissible limit of formaldehyde concentration in drinking water and food stuffs as set by WHO/EPA (86 μM). Moreover, the LOD values are lower than the intracellular concentration of FA (100-400 μM).[4, 17] It is interesting to note that the structural integrity of the MOF material was retained throughout the sensing event (Figure 4.7).

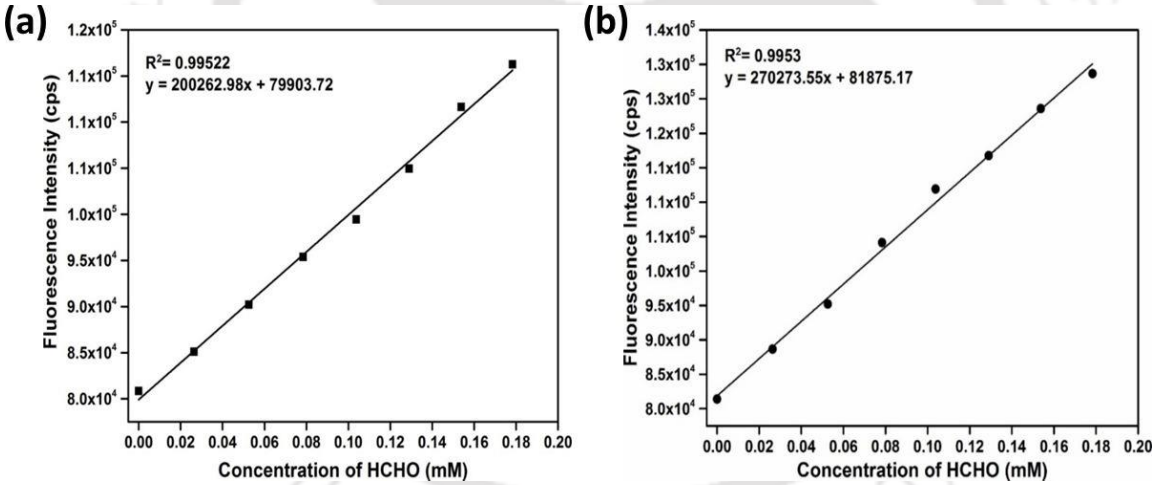

Figure 4.16 Change in the fluorescence intensity of **3′** in as a function of concentration of formaldehyde in (a) HEPES buffer and (b) aqueous medium.

To examine the retention of shape and size of the particles of the material in HEPES buffer, **3′** was soaked in HEPES buffer medium for 12 h (as the cells were loaded with **3′** for 10 h and afterward FA was treated and incubated for 1 h before imaging experiment). Then, **3′** was collected by filtration and dried in a conventional oven at 60 °C for 12 h. The FE-SEM images of the HEPES buffer soaked material (Figure 4.17a) reveal that the overall morphology of the material is very similar with the activated material (Figure 4.10). Hence, no alteration in shape and size of the particles of the material was detected

even after soaking the material in HEPES buffer. Moreover, we have recorded the XRPD pattern of **3′** obtained after soaking in HEPES buffer. Figure 4.17b suggests that framework topology of **3′** is unchanged even after soaking in HEPES buffer for 12 h.

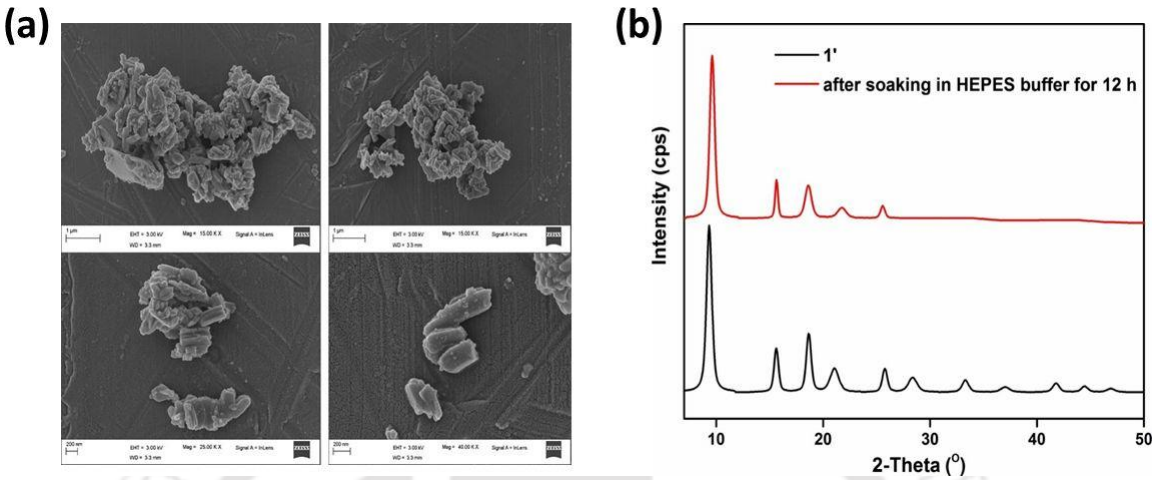

Figure 4.17 (a) FESEM images of **3′** after soaking in HEPES buffer for 12 h. (b) XRPD pattern of **3′** after soaking in HEPES buffer for 12 h.

4.3.7 Sensing of FA in vapor phase

The permanent porosity and efficient solid-state emission of **3′** inspired us to investigate the vapor-phase fluorimetric sensing of FA. The time-dependent fluorescence profile (Figure 4.18) of the **3′**-coated quartz slide clearly signifies that with gradual exposure of FA vapor, the emission intensity of the film-coated quartz slide increased and saturation in the fluorescence intensity occurred within 20 min of addition of FA. Moreover, around three-fold increment in the fluorescence emission intensity was noticed within 20 min of exposure (monitored at 486 nm). Noticeably, in the solid-state emission spectrum of **3′**, a large bathochromic shift (50 nm) in the λ_{max} value was observed as compared to the solution state. This large shift in the λ_{max} value may be attributed to the strong intermolecular interactions, i.e., hydrogen bonding, Van der Waals interactions etc. in the solid state.[72]

High selectivity towards FA vapor over the vapors of other competitive aldehydes is necessary for an ideal FA sensor. Hence, we have conducted selectivity test with other liquid aldehydes. The **3′**-coated film on quartz slide was first exposed to the vapors of different aldehydes for 20 min and then the fluorescence spectra were recorded. Figure 4.19 reveals that the vapors of all other aldehydes failed to enhance the emission intensity of the **3′**-coated film significantly as compared to FA. Only acetaldehyde was able to

enhance the emission intensity of the **3′**-coated film by 1.8 fold with respect to its initial intensity. The lower boiling point (20.2 °C) and smaller size of acetaldehyde as compared to other aldehydes may be the possible reason behind the higher fold increment in emission intensity of the **3′**-coated film in presence of acetaldehyde vapor. The **3′**-coated film showed higher fold increment (3 fold) towards FA vapor than acetaldehyde vapor (1.8 fold). It is important to mention that for the vapor-phase sensing of FA, the fold increment (3 fold) of emission intensity is lower and the response time (20 min) is considerably higher than the aqueous-phase sensing of FA, where increment in fluorescence intensity is 7 fold and response time is 1 min. Nevertheless, the vapor-phase sensing of FA by the **3′**-coated film is particularly interesting because of its high selectivity towards FA over the vapors of other aldehydes and application potential for real-world sensing of FA vapor.

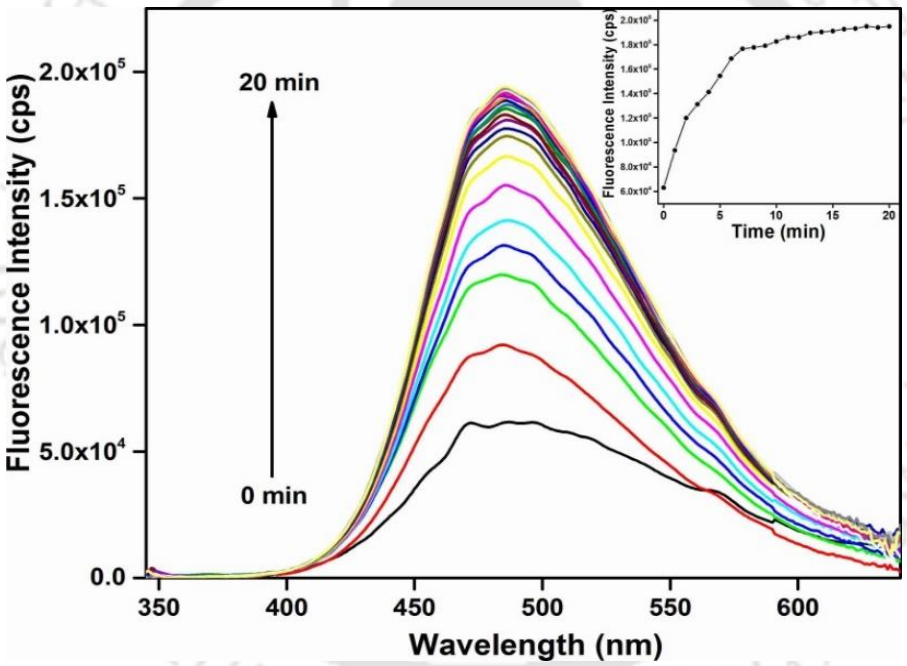

Figure 4.18 Increment in emission intensity of **3′** coated film on quartz slide after the introduction of formaldehyde (100 μL) in cuvette from 1 min to 20 min. Inset plot shows the enhancement in emission intensity as a function of time (monitored at 486 nm).

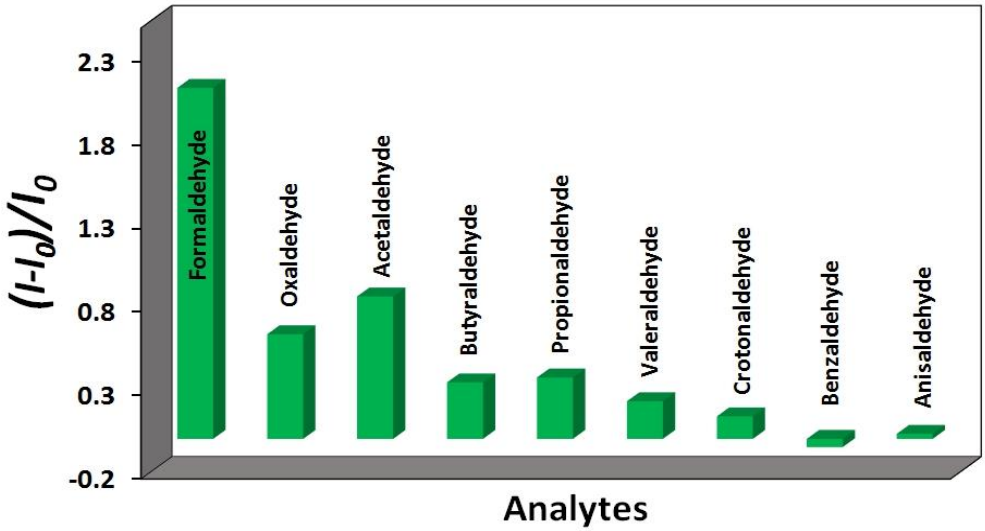

Figure 4.19 Relative fluorescence turn-on signal of **3′** coated film on quartz slide (after 20 min) towards the addition of different aldehydes (100 µL).

4.3.8 Sensing of FA in live cancer cells

After achieving excellent selectivity and sensitivity of **3′** for FA sensing in both HEPES buffer and aqueous media, we next examined its detection performance in more complicated and challenging medium like breast cancer cells. The cancer cells without the MOF probe were observed in both bright field and blue channel. These cells were found to be healthy and they did not exhibit any fluorescence (Figure 4.20a-c). When the cancer cells were incubated with the suspension of the fluorescent probe **3′**, it was taken up by the cells. The probe did not affect the cellular viability but the cellular morphology was affected due to uptake of the probe. Furthermore, it did not cause any morphological change to the mammalian cells, as evident from the bright field imaging (Figure 4.20d). Interestingly, the cells could detect endogenous FA in cancer cells and exhibited blue fluorescence signal (Figure 4.20e, 4.20f). The probe-loaded cells, after treatment with FA (50 µM) for 60 min, gave marginal increase in the blue fluorescence signal as compared to the probe-loaded cells (Figure 4.20h, 4.20i). Our results clearly indicate that the probe **3′** has the potential to detect the intracellular FA in cancer cells and could be able to respond to the change in intracellular FA levels.

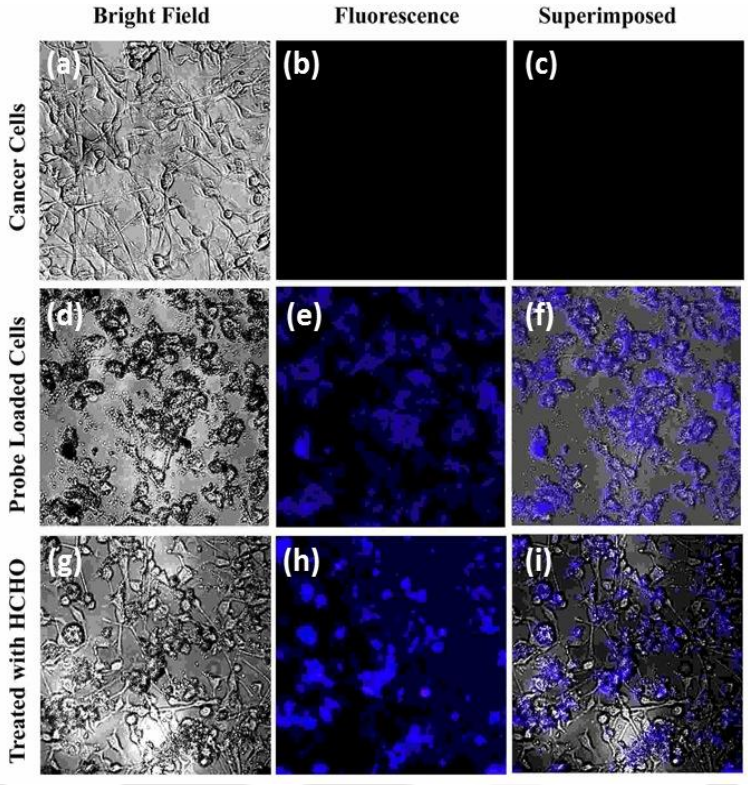

Figure 4.20 Detection of FA in MDAMB-231 breast cancer cells by Al-MIL-53-N_2H_3 probe. MDAMB-231 unloaded cells (a-c), probe-loaded cells (d-f) and probe-loaded cells treated with 50 µM FA (g-i) for 1 h at 37 °C in complete medium. The probe-loaded cancer cells display bright blue fluorescence whereas the addition of FA causes marginal increase in the fluorescence signal. The superposition of bright field and fluorescence indicates that the signal arises from the cell associated probe.

It is worthy to mention that we have carried out the imaging experiment by the MDAMB-231 cells. The mean diameter of these cells are in the range of 10-20 µM.[73-75] Hence, the probe with average particle size of 741 nm (as measured by DLS method) can easily be taken up by MDAMB-231 cells. Actually, the mammalian cells can take-up extracellular molecules in the range of nm to µm and the mode of their uptake depends on size.[76-78] Smaller objects (nm range) are mostly been taken-up by pinocytosis whereas large objects (1-3 µm) are been taken by phagocytosis.[79, 80]

4.3.9 Mechanism of FA sensing

As the mechanism for FA detection, we expected that the hydrazine functionality present in the BDC-N_2H_3 ligand of the MOF material is converted to the hydrazone moiety in presence of FA during the sensing process. Due to this functional group conversion, the photo-induced electron transfer (PET) process from hydrazine group to phenyl ring is

prohibited. As a result, dramatic enhancement in the emission intensity of the compound was observed, since the fluorogenic core restored its fluorescence property. The formation of the hydrazone moiety was verified by mass spectrometry. The peak at m/z = 195.0374, which was observed in the mass spectrum of digested **3′** (Figure 4.21), signifies the $(M-H)^-$ ion of $H_2BDC\text{-}N_2H_3$ ligand (M = mass of $H_2BDC\text{-}N_2H_3$ ligand). In the mass spectrum of digested FA-treated **3′** (Figure 4.22), the peak at m/z = 207.0586 represents the $(M{-}H)^-$ ion of the hydrazone functionalized H_2BDC ligand (i.e. $H_2BDC\text{-}NHNH{=}CH_2$). Hence, it can be concluded that during the detection process, FA is converted to hydrazone moiety from the hydrazine moiety. The reaction-based sensing mechanism for FA by **3′** was further investigated by an inhibition experiment with a quencher of FA such as $NaHSO_3$.[52, 81] From Figure 4.23a, it becomes evident that FA was unable to increase the emission intensity of the suspension of **3′** when it was pretreated with $NaHSO_3$. As $NaHSO_3$ is strongly nucleophilic in nature, it readily reacts with highly electrophilic FA and inhibits its reactivity towards the hydrazine-functionalized MOF compound. Therefore, negligible increment in the fluorescence intensity occurred for the $NaHSO_3$-pretreated suspension of **3′** as compared to the untreated suspension of **3′**. However, no inhibition in the activity of FA occurred when $NaHSO_3$ solution was added after the addition of FA to the suspension of **3′** (Figure 4.23b). This observation signifies that FA transformed the hydrazine group to hydrazone moiety and consequently the emission intensity of the compound was enhanced. Hence, the post-treatment by $NaHSO_3$ solution did not cause significant change in the emission intensity. To ensure that only hydrazine group is responsible for the interaction and enhancing the emission intensity in presence of FA, sensing experiment was carried out with un-functionalized and amine-functionalized Al-MIL-53. It can be observed from Figure 4.24 that no observable "turn on" response was obtained from un-functionalized and amine functionalized Al-MIL-53 in presence of FA. Hence, it can be inferred that only hydrazine group is responsible for the "turn on" response due to conversion to hydrazone moiety and consequently inhibition of photo-induced electron transfer process in presence of FA.

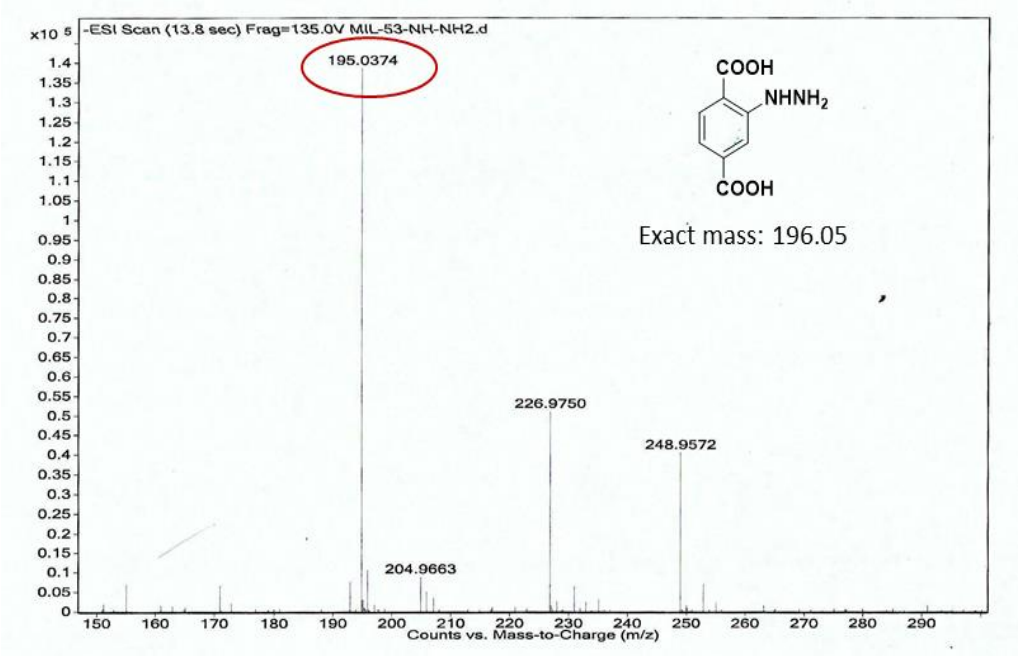

Figure 4.21 ESI-MS spectrum of the **3′** (digested in MeOH/HF). The spectrum shows m/z peak at 195.0374, which corresponds to $(M-H)^-$ ion (M = mass of $H_2BDC\text{-}NHNH_2$ ligand).

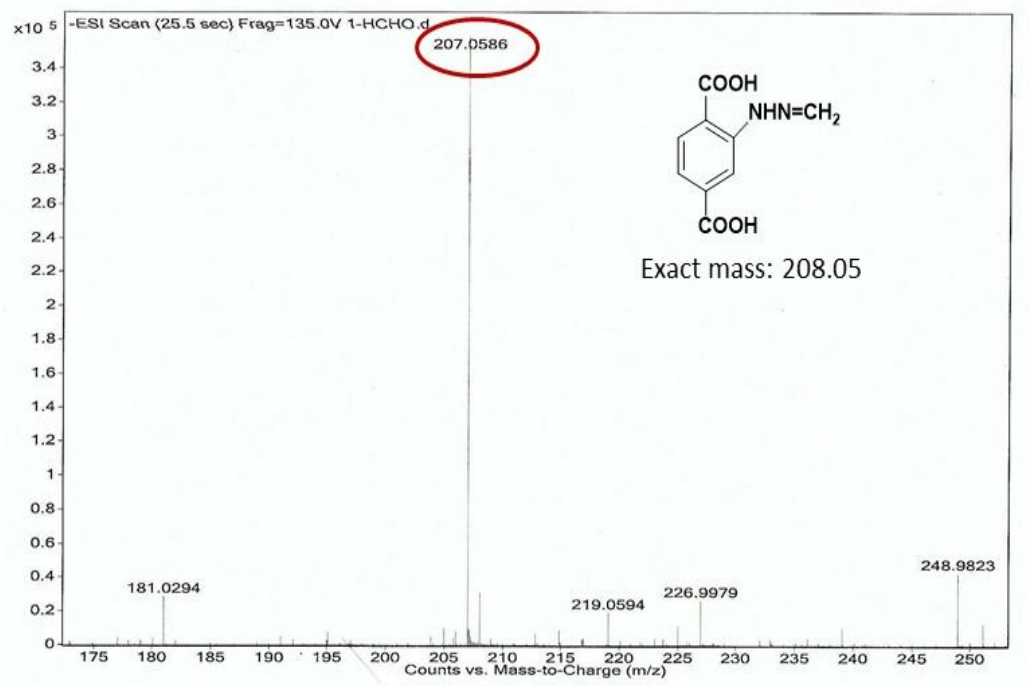

Figure 4.22 ESI-MS spectrum of the formaldehyde-treated **3′** (digested in MeOH/HF). The spectrum shows m/z peak at 207.0586, which corresponds to $(M-H)^-$ ion of $H_2BDC\text{-}NH\text{-}N{=}CH_2$ ligand.

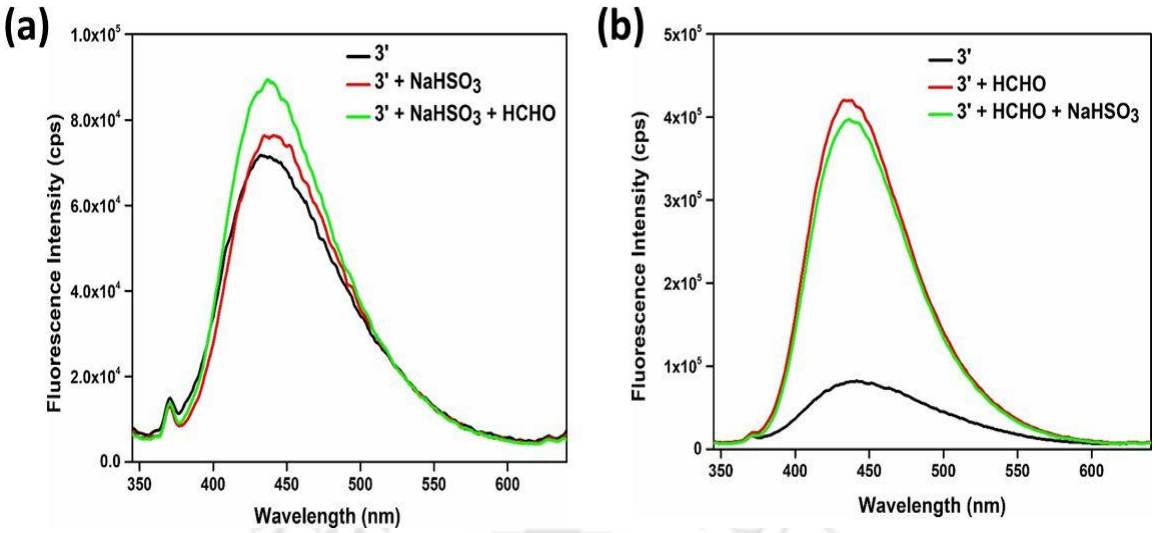

Figure 4.23 (a) Fluorescence spectra of **3′** (in HEPES buffer) under different conditions: only probe (black), in presence of 500 µL of 40 mM $NaHSO_3$ (red) and in presence of 500 µL of 20 mM formaldehyde pretreated with 500 µL of 40 mM $NaHSO_3$ (green). (b) Fluorescence spectra of **3′** (in HEPES buffer) under different conditions: only probe (black), in presence of 500 µL of 20 mM formaldehyde (red) and in presence of 500 µL of 20 mM formaldehyde post-treated with 500 µL of 40 mM $NaHSO_3$ (green).

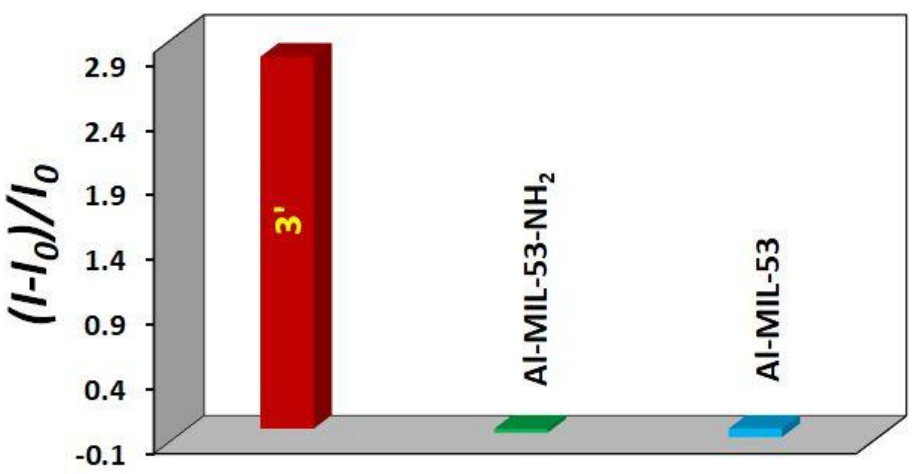

Figure 4.24 Relative fluorescence response of **3′**, Al-MIL-53-NH_2 and Al-MIL-53 towards 20 mM FA (500 µL) in HEPES buffer medium.

The recyclability of the reaction-based fluorescent probe was examined up to six cycles of sensing experiments. As shown in Figure 4.25, the fluorescence turn-on response of **3′** towards FA was significantly reduced after the first cycle and became almost negligible in the subsequent cycles. The poor recyclability of the MOF material for the detection of FA can be attributed to the fact that the hydrazine functional group was

converted to hydrazone moiety through the reaction with FA during the first cycle of sensing experiment. Therefore, the hydrazine-functionalized **3′** showed negligible fluorescence turn-on responses in the subsequent cycles of sensing experiments. Thus, the poor recyclability of the Al-MIL-53-N_2H_3 probe for FA sensing is consistent with the proposed sensing mechanism.

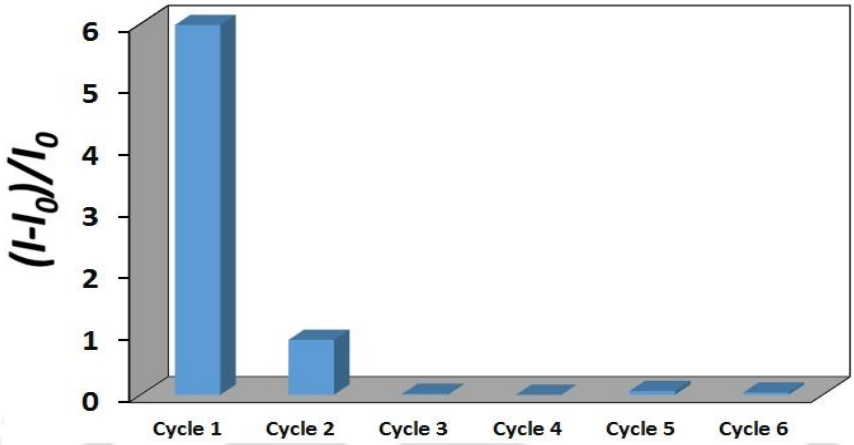

Figure 4.25 Recyclability test for the fluorescence turn-on response of **3′** towards formaldehyde.

4.3.10 Experimental support for PET mechanism

Time-resolved fluorescence experiments can provide invaluable information when more than one emitting species are present in the system.[82] To ensure the involvement of PET process from the hydrazine group to phenyl moiety in **3′**, we have performed fluorescence lifetime studies. Time-resolved fluorescence lifetime decay profiles of the aqueous suspension of **3′** were collected before and after the addition of FA (20 mM, 500 µL) at different emission wavelengths. The fluorescence lifetime decay profiles (Figure 4.26) and the fitted results (Table 4.2) clearly signify that before the addition of FA, the fluorescence decayed (λ_{em} = 436 nm) in three-exponential manner with lifetime values of 13.19 ns (63.06%), 0.39 ns (18.97%) and 4.31 ns (17.97%). Such a three-exponential decay profile indicates the contribution from three components. After addition of FA, the lifetime decay profiles were measured at different emission wavelengths (Table 4.2). Upon the addition of FA (λ_{em} = 436 nm), the two short-lived components almost completely disappeared and the percentage of the long-lived component increased with an increase of its lifetime value from 13.19 ns to 19.01 ns. In the presence of FA, the increase in lifetime value of the long-lived component and the disappearance of the two short-lived

components confirm the inhibition of the PET process.[83] Moreover, the large difference in the time-resolved fluorescence decay profiles (Figure 4.26) of **3′** before and after the addition of FA suggests the formation of imine bond.[55]

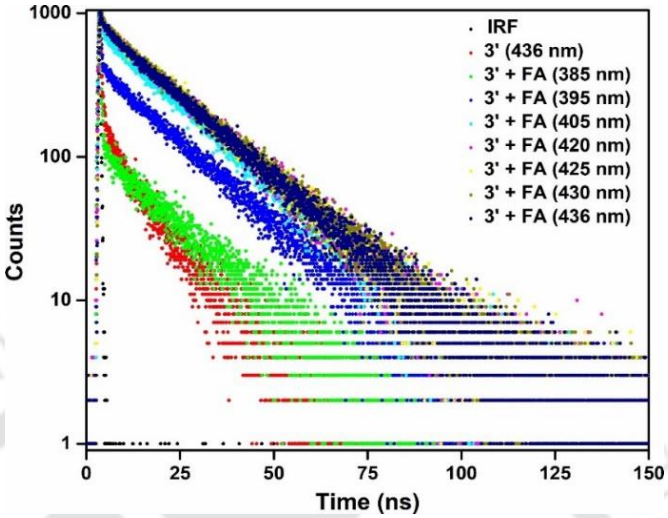

Figure 4.26 Time-resolved fluorescence decay profiles of the aqueous suspension of **3′** before and after the addition of FA at an excitation wavelength of 336 nm and at different emission wavelengths.

Table 4.2 Fluorescence lifetimes of **3′** before and after the addition of FA at different emission wavelengths (λ_{ex} = 336 nm, pulsed diode laser).

Condition	λ_{em} (nm)	τ_1 (ns)	τ_2 (ns)	τ_3 (ns)	A_1 (%)	A_2 (%)	A_3 (%)	χ^2
Before addition of FA	436	13.19	0.39	4.31	63.06	18.97	17.97	1.02
After addition of FA	385	18.65	0.31	5.01	80.21	16.25	3.54	1.07
	395	18.48	0.39	-	96.25	3.75	-	1.06
	405	18.87	0.62	-	98.65	1.35	-	1.02
	420	18.94	1.17	-	99.13	0.87	-	1.07
	425	18.99	1.09	-	99.09	0.91	-	1.04
	430	19.11	2.11	-	98.64	1.36	-	1.05
	436	19.01	1.62	-	98.40	1.60	-	1.04

4.4 Conclusions

We have judiciously designed, synthesized and comprehensively characterized a hydrazine functionalized Al(III) MOF material having MIL-53 topology. As confirmed by the thermogravimetric analysis, the compound shows high thermal stability up to 480 °C in air atmosphere. According to the N_2 sorption measurements, the compound after activation (**3′**) possesses a BET surface area of 958 m^2 g^{-1}. Compound **3′** can be utilized as a fluorescence turn-on probe for the selective detection of FA (in aqueous, HEPES buffer media and vapor phase), even in the presence of potentially intrusive species. The fluorescence turn-on phenomenon can be explained by the inhibition of PET event (from hydrazine group to phenyl ring) owing to hydrazone formation. The anticipated mechanism has been confirmed by mass analyses as well as by the specially designed inhibition experiments. The Al-MIL-53-N_2H_3 probe exhibits short response time (1 min) for FA in 10 mM HEPES buffer. It is also highly sensitive for FA having a detection limit of 8.37 μM (0.25 ppm) in HEPES buffer. In addition to the solution phase, the probe is capable of detecting FA in the vapor phase. Moreover, intracellular FA in breast cancer cells can be efficiently sensed by the material. As corroborated by the XRPD experiments, the crystallinity (and hence structural robustness) of **3′** remains intact after the fluorescence sensing experiments. Therefore, **3′** is a potential probe for the real-time detection of FA in aqueous, vapor and simulated physiological media as well as inside cancer cells.

The fluorescence turn-on sensing of FA by MOFs is still in the stage of infancy. There is a huge scope for the development of new MOF probes and evaluation of their performances in terms of detection limit, fold increment, response time, etc. Hence, we believe that our work will stimulate tremendous research interests in the field of MOF-related sensors for FA.

4.5 References

1. V. J. Cogliano, Y. Grosse, R. A. Baan, K. Straif, M. B. Secretan and F. E. Ghissassi, *Environ. Health Perspect.*, 2005, **113**, 1205-1208.
2. R. M. Kohli and Y. Zhang, *Nature*, 2013, **502**, 472-479.
3. G. Jia, Y. Fu, X. Zhao, Q. Dai, G. Zheng, Y. Yang, C. Yi, T. Lindahl, T. Pan, Y.-G. Yang and C. He, *Nat. Chem. Biol.*, 2012, **13**, 885-887.
4. Z. Tong, C. Han, W. Luo, X. Wang, H. Li, H. Luo, J. Zhou, J. Qi and R. He, *Age*, 2013, **35**, 583-596.

5. S. K. Patra, A. Patra, F. Rizzi, T. C. Ghosh and S. Bettuzzi, *Cancer Metastasis Rev.*, 2008, **27**, 315-334.
6. C. A. Miller, S. L. Campbell and J. D. Sweatt, *Neurobiol. Learn. Mem.*, 2008, **89**, 599-603.
7. J. Y. An, S. Kim, H. J. Kim and J. Seo, *Build. Environ.*, 2010, **45**, 1826-1833.
8. J. Liu, W. Wang, S. Li, M. Liu and S. He, *Sensors*, 2011, **11**, 11871-11884.
9. Z. He, Y. Zhang and W. Wei, *Build. Environ.*, 2012, **47**, 197-204.
10. N. Lu, J. Pei, Y. Zhao, R. Qi and J. Liu, *Build. Environ.*, 2012, **57**, 253-258.
11. X. Wang, Y. Si, J. Wang, B. Ding, J. Yu and S. S. Al-Deyab, *Sens. Actuators, B*, 2012, **163**, 186-193.
12. K. Kawamura, K. Kerman, M. Fujihara, N. Nagatani, T. Hashiba and E. Tamiya, *Sens. Actuators, B*, 2005, **105**, 495-501.
13. J. R. Whetstine, A. Nottke, F. Lan, M. Huarte, S. Smolikov, Z. Chen, E. Spooner, E. Li, G. Zhang, M. Colaiacovo and Y. Shi, *Cell*, 2006, **125**, 467-481.
14. R. J. Klose, K. Yamane, Y. Bae, D. Zhang, H. Erdjument-Bromage, P. Tempst, J. Wong and Y. Zhang, *Nature*, 2006, **442**, 321-316.
15. S. M. Kooistra and K. Helin, *Nat. Rev. Mol. Cell Biol.*, 2012, **13**, 297-311.
16. Y. Shi, F. Lan, C. Matson, P. Mulligan, J. R. Whetstine, P. A. Cole, R. A. Casero and Y. Shi, *Cell*, 2004, **119**, 941-953.
17. M. E. Andersen, H. J. Clewell, E. Bermudez, D. E. Dodd, G. A. Willson, J. L. Campbell and R. S. Thomas, *Toxicol. Sci.*, 2010, **118**, 716-731.
18. Z. Tong, W. Luo, Y. Wang, F. Yang, Y. Han, H. Li, H. Luo, B. Duan, T. Xu, Q. Maoying, H. Tan, J. Wang, H. Zhao, F. Liu and Y. Wan, *PLoS One*, 2010, **5**, e10234.
19. R. Baan, Y. Grosse, K. Straif, B. Secretan, F. E. Ghissassi, V. Bouvard, L. Benbrahim-Tallaa, N. Guha, C. Freeman, L. Galichet and V. Cogliano, *Lancet Oncol.*, 2009, **10**, 1143-1144.
20. P. H. Yu, *J Neural Transm Suppl.*, 1998, **52**, 201-216.
21. K. Tulpule and R. Dringen, *J. Neurochem.*, 2013, **127**, 7-21.
22. Y. I. Korpan, M. V. Gonchar, A. A. Sibirny, C. Martelet, A. V. El'skaya, T. D. Gibson and A. P. Soldatkin, *Biosens. Bioelectron.*, 2000, **15**, 77-83.
23. W. J. Kim, N. Terada, T. Nomura, R. Takahashi, S. D. Lee, J. H. Park and A. Konno, *Clin. Exp. Allergy*, 2002, **32**, 287-295.

24. A. J. Hemple, K. S. Kjaergaard, L. Molhave and H. K. Hundnell, *Arch. Environ. Health*, 1999, **54**, 416-424.
25. *WHO Regional Office for Europe: Copenhagen, Denmark*, 2001.
26. *U.S. Department of Health and Human Services: Washington, DC, USA*, 1988.
27. G. R. Mohimann, *Appl. Spectr.*, 1985, **39**, 98-101.
28. L. Feng, C. J. Musto and K. S. Suslick, *J. Am. Chem. Soc.*, 2010, **132**, 4046-4047.
29. T. Dumas, *J. Chromatogr.*, 1982, **247**, 289-295.
30. B. Mann and M. L. Grajeski, *J. Chromatogr.*, 1987, **386**, 149-158.
31. J. M. Lorrain, C. R. Fortune and B. Dellinger, *Anal. Chem.*, 1981, **53**, 1302-1305.
32. J. C. Septon and J. C. Ku, *Am. Ind. Hyg. Assoc. J.*, 1982, **43**, 845-852.
33. G.-J. Mao, T.-T. Wei, X. X. Wang, S. Huan, D.-Q. Lu, J. Zhang, X.-B. Zhang, W. Tan, G.-L. Shen and R.-Q. Yu, *Anal. Chem.*, 2013, **85**, 7875-7881.
34. H. Song, S. Rajendiran, N. Kim, S. K. Jeong, E. Koo, G. Park, T. D. Thangadurai and S. Yoon, *Tetrahedron Lett.*, 2012, **53**, 4913-4916.
35. Y. Tang, X. Kong, A. Xu, B. Dong and W. Lin, *Angew. Chem.*, 2016, **55**, 3356-3359.
36. T. F. Brewer and C. J. Chang, *J. Am. Chem. Soc.*, 2015, **137**, 10886-10889.
37. A. Roth, H. Li, C. Anorma and J. Chan, *J. Am. Chem. Soc.*, 2015, **137**, 10890-10893.
38. L. He, X. Yang, Y. Liu, X. Kong and W. Lin, *Chem. Commun.*, 2016, **52**, 4029-4032.
39. Z. Li, Y. Xu, H. Zhu and Y. Qian, *Chem. Sci.*, 2017, **8**, 5616-5621.
40. T. Itoh, I. Matsubara, W. Shin, N. Izu and M. Nishibori, *Sens. Actuators, B*, 2008, **128**, 512-520.
41. K. Vellingiri, A. Deep, K.-H. Kim, D. W. Boukhvalov, P. Kumar and Q. Yao, *Sens. Actuators, B*, 2017, **241**, 938-948.
42. C. Li, J. Huang, H. Zhu, L. Liu, Y. Feng, G. Hu and X. Yu, *Sens. Actuators, B*, 2017, **253**, 275-282.
43. H. Zhao, X. Li, W. Li, P. Wang, S. Chen and X. Quan, *RSC Adv.*, 2014, **4**, 36444-36450.
44. J.-N. Hao and B. Yan, *Nanoscale*, 2016, **8**, 12047-12053.
45. N. Stock and S. Biswas, *Chem. Rev.*, 2012, **112**, 933-969.
46. S. Nandi, H. Reinsch, S. Banesh, N. Stock, V. Trivedi and S. Biswas, *Dalton Trans.*, 2017, **46**, 12856-12864.

47. A. Buragohain and S. Biswas, *CrystEngComm*, 2016, **18**, 4374-4381.
48. Z. Bao, G. Chang, H. Xing, R. Krishna, Q. Ren and B. Chen, *Energy Environ. Sci.*, 2016, **9**, 3612-3641.
49. R. Dalapati, B. Sakthivel, A. Dhakshinamoorthy, A. Buragohain, A. Bhunia, C. Jainak and S. Biswas, *CrystEngComm*, 2016, **18**, 7855-7864.
50. R. Dalapati, B. Sakthivel, M. K. Ghosalya, A. Dhakshinamoorthy and S. Biswas, *CrystEngComm*, 2017, **19**, 5915-5925.
51. A. R. Chowdhuri, D. Bhattacharya and S. K. Sahu, *Dalton Trans.*, 2016, **45**, 2963-2973.
52. Y. H. Lee, Y. Tang, P. Verwilst, W. Lin and J. S. Kim, *Chem. Commun.*, 2016, **52**, 11247-11250.
53. T. F. Brewer, G. Burgos-Barragan, N. Wit, K. J. Patel and C. J. Chang, *Chem. Sci.*, 2017, **8**, 4073-4081.
54. C. Liu, C. Shi, H. Li, W. Du, Z. Li, L. Wei and M. Yu, *Sens. Actuators, B*, 2015, **219**, 185-191.
55. W. Zhou, H. Dong, H. Yan, C. Shi, M. Yu, L. Wei and Z. Li, *Sens. Actuators, B*, 2015, **209**, 664-669.
56. L. d. T.-d. Román, M. A. Alonso-Lomillo, O. Domínguez-Renedo, C. Merino-Sánchez, M. P. Merino-Amayuelas and M. J. Arcos-Martínez, *Talanta*, 2011, **86**, 324-328.
57. Y. Zhang, M. Zhang, Z. Cai, M. Chen and F. Cheng, *Electrochim. Acta*, 2012, **68**, 172-177.
58. Q. Yi, F. Niu and W. Yu, *Thin Solid Films*, 2011, **519**, 3155-3161.
59. Q. Wang, J. Zheng and H. Zhang, *J. Electroanal. Chem.*, 2012, **674**, 1-6.
60. J. P. Metters, F. Tan and C. E. Banks, *J. Solid State Electrochem.*, 2013, **17**, 1553-1562.
61. M. Baez-Gaxiola, C. Fernández-Sánchez and E. Mendoza, *Anal. Methods*, 2015, **7**, 538-542.
62. S. V. Dzyadevych, V. N. Arkhypova, Y. I. Korpan, V. Anna, A. P. Soldatkin, N. Jaffrezic-Renault and C. Martelet, *Anal. Chim. Acta*, 2001, **445**, 47-55.
63. Y. Herschkovitz, I. Eshkenazi, C. Campbell and J. Rishpon, *J. Electroanal. Chem.*, 2000, **491**, 182-187.
64. S. J. Deka, A. Roy, V. Ramakrishnan, D. Manna and V. Trivedi, *Chem Biol Drug Des.*, 2017, **89**, 953-963.

65. M. SK and S. Biswas, *CrystEngComm*, 2016, **18**, 3104-3113.
66. R. Dalapati, S. N. Balaji, V. Trivedi, L. Khamari and S. Biswas, *Sens. Actuator, B*, 2017, **245**, 1039-1049.
67. T. Loiseau, C. Serre, C. Huguenard, G. Fink, F. Taulelle, M. Henry, T. Bataille and G. Férey, *Chem. Eur. J*, 2004, **10**, 1373-1382.
68. M. Pera-Titus, T. Lescouet, S. Aguado and D. Farrusseng, *J. Phys. Chem. C*, 2012, **116**, 9507-9516.
69. T. Ahnfeldt, D. Gunzelmann, T. Loiseau, D. Hirsemann, J. Senker, G. Férey and N. Stock, *Inorg. Chem.*, 2009, **48**, 3057-3064.
70. E. Rahmani and M. Rahmani, *Ind. Eng. Chem. Res.*, 2018, **57**, 169-178.
71. S. E. Sayed, L. Pascual, M. Licchelli, R. M. Mañez, S. Gil, A. M. Costero and F. Sancenón, *ACS Appl. Mater. Interfaces*, 2016, **8**, 14318-14322.
72. E. B. Faulkner and R. J. Schwartz, *Journal*, 2009, 538.
73. R. Khojah, R. Stoutamore and D. D. Carlo, *Lab Chip*, 2017, **17**, 2542-2549.
74. U. Kim, C.-W. Shu, K. Y. Dane, P. S. Daugherty, J. Y. J. Wang and H. T. Soh, *Proc. Natl. Acad. Sci. U. S. A.*, 2007, **104**, 20708-20712
75. A. Meunier, J. A. Hernández-Castro, K. Turner, K. Li, T. Veres and D. Juncker, *Anal. Chem.*, 2016, **88**, 8510–8517.
76. A. M. Bannunah, D. Vllasaliu, J. Lord and S. Stolnik, *Mol. Pharmaceutics*, 2014, **11**, 4363-4373.
77. H. Suzuki, T. Toyooka and Y. Ibuki, *Environ. Sci. Technol.*, 2007, **41**, 3018-3024.
78. Q. Mu, G. Su, L. Li, B. O. Gilbertson, L. H. Yu, Q. Zhang, Y.-P. Sun and B. Yan, *ACS Appl. Mater. Interfaces*, 2012, **4**, 2259-2266.
79. S. E. A. Gratton, P. A. Ropp, P. D. Pohlhaus, J. C. Luft, V. J. Madden, M. E. Napier and J. M. DeSimone, *Proc. Natl. Acad. Sci. U. S. A.*, 2008, **105**, 11613-11618.
80. B. Alberts, A. Johnson, J. Lewis, M. Raff, K. Roberts and P. Walter, *Molecular biology of the cell, 4th edition*, Garland Science, New York, Fourth edn., 2002.
81. H. R. Lotfy and I. G. Rashed, *Water Res.*, 2002, **36**, 633-637.
82. P. Ashokkumar, V. T. Ramakrishnan and P. Ramamurthy, *J. Phys. Chem. A*, 2011, **115**, 14292-14299.
83. V. Thiagarajan, C. Selvaraju, E. J. P. Malar and P. Ramamurthy, *ChemPhysChem*, 2004, **5**, 1200-1209.

CHAPTER 5

A recyclable post-synthetically modified Al(III) based metal-organic framework for fast and selective fluorogenic recognition of bilirubin in human biofluids

This chapter describes fast and selective detection of bilirubin by a recyclable Al(III) based post-synthetically modified MIL-53 metal-organic framework (MOF). Post-synthetic modification was achieved by the aldimine condensation reaction between MIL-53-NH_2 and 2,3,4-trihydroxy benzaldehyde. The material has huge potential to detect bilirubin in HEPES buffer medium (pH=7.4) by fluorescence "turn-off" mechanism. The probe displayed ultra-fast response (30 s), low detection limit (1.26 pM) and high selectivity towards bilirubin in the co-existence of several metal ions and biomolecules. The real field application of the probe was thoroughly investigated in human bio-fluids (blood serum and urine samples) by standard addition method. The quenching ability of the MOF material by bilirubin was also explored on portable paper strip device.

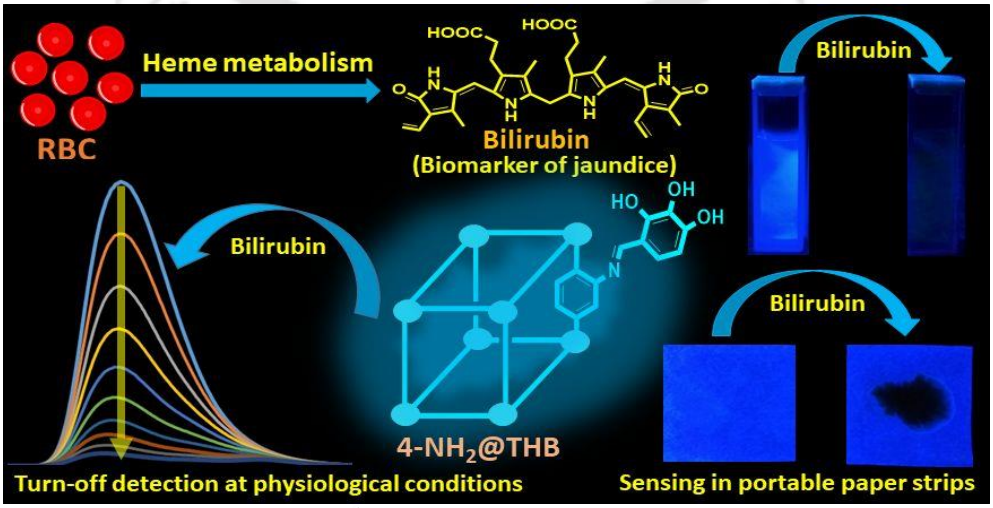

Dalton Transactions

S. Nandi, S. Biswas, *Dalton Trans.*, 2019, **48**, 9266.

5.1 Introduction

Bilirubin is a yellow-red pigment which is produced by the catabolism process of hemoglobin present in the red blood cells.[1, 2] Although bilirubin is considered as a waste product which is excreted through urine and bile, it has several crucial physiological activities.[3] Bilirubin has antioxidant and anti-inflammatory properties which can assist the protection of lipids from oxidation.[4, 5] It can play major role to defend against oxidative stress.[6] Moreover, for cerebral,[7] pulmonary,[8] hepatobiliary,[9] cardiovascular,[10] and immunological systems,[11] it has vital protective roles. Due to dysfunction of liver or biliary obstruction, the concentration of bilirubin in human blood increase from regular level of <25 μmol (<1.2 mg/dL) to >50 μmol/L (>2.5 mg) which indicates the condition of jaundice.[12] Excessive concentration of bilirubin in blood is dreadful towards human health because the accumulation of bilirubin in organs may cause organ failure, brain damage or even death.[13, 14] Hence, the detection of bilirubin in blood is important for the diagnosis of jaundice. Generally, in acute condition, jaundice can be identified by the yellow coloration of urine, stool, mucous membrane and sclera (protective outer layer of the eye).[15] To prevent the condition reaching its serious level, prior identification and treatment is required. Therefore, fast and selective detection and exact quantification of bilirubin in human biofluids is essential for the proper diagnosis of jaundice.

During past few years, a lot of methods have been explored for the detection and quantification of bilirubin.[16-24] Clinical detection of bilirubin in blood plasma is performed by monitoring the colour change during diazotization reaction of bilirubin and sulphanilic acid.[3] But, this technique suffers from several drawbacks such as slow response (30 min is required to obtain intense colour), less stability and degradation.[25] Moreover, various types of enzymatic and non-enzymatic electrochemical bio-sensors have been developed with different bio-compatible platforms for the detection of bilirubin.[26, 27] But, the above mentioned techniques suffer from several disadvantages like costly instrumentation, huge power utilization and spoliation of cell lytes. Hence, these methods are not appropriate for real field detection and quantification of bilirubin. Fluorimetric detection of biomolecules is highly desirable as it offers fast response, high selectivity, amplified sensitivity with a wide range of concentration and non-destructive nature of

sensing.[28, 29] Till now, a very few fluorescent probes were utilized for the detection of bilirubin, which include nanomaterials,[27] organic small molecules,[30] conjugate polymers,[31] as well as metal-organic frameworks.[32] Unfortunately, they are unable to fulfil the criteria of an effective sensor like instant response, high selectivity and sensitivity, recyclability, etc.

Metal-organic frameworks (MOFs) are auspicious candidates for fluorescence detection applications because of their fluorescence property, adjustable porosity, high surface area and high physicochemical stability.[33] MOFs have drawn much attention over other conventional sensors because of their straightforward synthesis, well-defined structural property, predictable interactions between MOF and targeted analyte, high photo-stability and reusability.[34, 35] Till date, a huge number of MOFs have been employed for the sensing purpose of organic molecules,[36] metal ions,[37] explosives,[38] biomolecules,[39] pH, temperature, humidity,[34, 40, 41] etc. But, still MOFs having great sensitivity and selectivity towards the desired analyte are rear.[42] Hence, the introduction of specific site to ensure the interactions with targeted analyte is highly desirable. In recent days, post-synthetic modification (PSM) has become an outstanding process to incorporate new functional groups without harming the structural integrity of the MOF material.[43, 44] The newly introduced functional groups can play as a recognition site for the desired analyte.[45, 46] Here, we have prepared a post-synthetically modified Al(III) based MOF (**4-NH_2@THB)** by the reaction between MIL-53-NH_2 and 2,3,4-trihydroxy benzaldehyde (Scheme 5.1). The enrichment of hydroxyl groups in **4-NH_2@THB** provides recognition sites for bilirubin.[30, 47] Moreover, the aromatic ring of bilirubin can interact with π-electron abundant **4-NH_2@THB** via π-π interactions.[48] Till date, only one Zr-based MOF material has been reported in the literature for the sensing of bilirubin.[32] But, detailed study of the material for the sensing of bilirubin in human biofluids (i.e. urine) and reusability of the probe were not investigated. Herein, we have reported a bio-compatible Al(III) based post-synthetically modified recyclable MOF material, which can detect bilirubin by quenching its bright blue fluorescence in HEPES buffer medium. Moreover, economical portable paper test strips were prepared by dip coating method and used for the rapid detection of bilirubin. Furthermore, the ability of the MOF material to detect bilirubin in human blood serum and urine was also investigated.

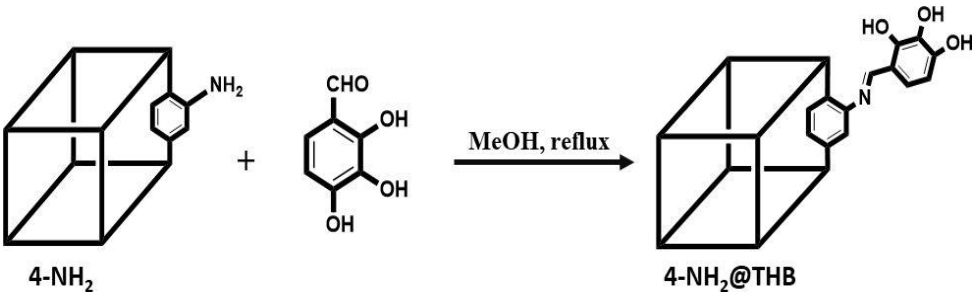

Scheme 5.1 Synthesis scheme of **4-NH$_2$@THB**.

5.2 Experimental section

5.2.1 Materials and characterization methods

All the required chemicals were purchased from commercial sources and used without purification. Fourier transform infrared (FT-IR) spectra were recorded with a Perkin Elmer Spectrum two FT-IR spectrometer in the range of 440-4000 cm^{-1} with KBr pellet. The below mentioned indications were employed for the characterization of the absorption bands: medium (m), weak (w), broad (br), very strong (vs), strong (s) and shoulder (sh). Ambient temperature X-Ray powder diffraction (XRPD) patterns were collected on a Bruker D2 Phaser X-ray diffractometer (30 kV, 10 mA) using Cu-*K*α (λ = 1.5406 Å) radiation. FE-SEM images were captured with a Zeiss (Zemini) scanning electron microscope. Thermogravimetric analyses (TGA) were collected under air atmosphere at a heating rate of 10 °C min^{-1} in a temperature region of 25-800 °C by employing a Netzsch STA-409CD thermal analyzer. Fluorescence emission behavior was recorded by a HORIBA JOBIN YVON Fluoromax-4 spectrofluorometer. The excitation wavelength (λ_{ex}) was 325 nm for all the fluorescence experiments. The nitrogen sorption isotherms were performed employing a Quantachrome Autosorb iQ-MP gas sorption analyzer at -196 °C. Prior to the sorption measurement, degassing of the material was performed at 120 °C for 12 h under dynamic vacuum. A Bruker Avance III 600 spectrometer was utilized for recording ^{1}H-NMR at 600 MHz. The mass spectrum (in ESI mode) was measured with an Agilent 6520 Q-TOF high-resolution mass spectrometer. Fluorescence lifetime measurements were performed by time correlated single-photon counting (TCSPC) method by an Edinburgh Instrument Life-Spec II instrument. The fluorescence decays were analyzed by reconvolution method using the FAST software provided by Edinburgh Instruments. Zeta potential was measured with a Zetasizer Nano ZS90 (model no. ZEN3690) instrument. X-ray photoelectron spectroscopy (XPS)

measurement was carried out at room temperature using a custom-built near-ambient pressure photoelectron spectrometer (Prevac, Poland). It is equipped with an R3000HP analyser (Scienta) with a twin-anode source and a monochromatic (Al-Kα) X-ray source.

5.2.2 Preparation of MIL-53-NH_2 (4-NH_2)

Synthesis of **4-NH_2** was carried out by following the previously reported method.[49] In a nutshell, a mixture of $AlCl_3 \cdot 6H_2O$ (493.6 mg), H_2BDC-NH_2 ligand (375.6 mg) and 5 mL deionized water was taken in a hydrothermal autoclave reactor and heated for 5 h at 150 °C in a conventional oven. After cooling down to room temperature, the light yellow coloured solid compound was filtered and washing was done by deionized water. Yield: 62% based on H_2BDC-NH_2 ligand. The as-synthesized form contains free H_2BDC-NH_2 ligand. For the removal of the unreacted H_2BDC-NH_2 ligand, the as-synthesized compound was heated in DMF solvent at 150 °C for 12 h. Then, DMF molecules were exchanged by low boiling solvent like methanol for 12 h. Thereafter, the methanol-exchanged light-yellow material was heated at 120 °C under dynamic vacuum to get activated **4-NH_2**.

5.2.3 Post-synthetic modification of 4-NH_2

A mixture of **4-NH_2** (100 mg, 0.4 mM) and 60 mg (0.4 mM) of THBA (2,3,4-trihydroxy benzaldehyde) was poured in a 100 mL round-bottom flask containing 30 mL dry methanol. The resulting mixture was sonicated for 10 min and then 30 µL glacial acetic was dropped into the above mixture. Then, the suspension was refluxed for 3 days under nitrogen atmosphere. The obtained solid was filtered and washed with DMF. The filtered solid was stirred for 24 h in methanol at room temperature. The resulting orange coloured solid was filtered and dried at 70 °C for 24 h in oven (yield: 56 mg). The Schiff base modified compound was denoted as **4-NH_2@THB** hereafter.

5.2.4 Fluorescence detection experiments in HEPES buffer

Compound **4-NH_2@THB** (10 mg) was taken in a glass vial and 10 mL of 10 mM HEPES buffer was introduced. The preparation method of HEPES buffer solution was previously reported.[50] The resulting suspension was sonicated for 30 min. A stable suspension was obtained after keeping for overnight at room temperature. The resulting suspension (100 µL) of the probe in HEPES buffer was

poured inside a quartz cuvette containing 2900 μL of HEPES buffer. All the fluorescence titration experiments were performed using the resulting suspension. For all the titration experiments, emission intensity was monitored at 429 nm whereas excitation wavelength was 325 nm. For selectivity study, initially 5 mL of 10 mM solutions of competitive analytes were prepared in 10 mM HEPES buffer solution. The analyte solutions of desired concentrations were prepared by proper dilution. It is worth to mention that due to lower solubility of bilirubin in aqueous phase, 5 μL of 1M NaOH solution was added in the HEPES buffer solution of bilirubin for the complete dissolution of bilirubin. For selectivity test, titration experiments were performed by stepwise introduction of 1 mM solution of different competitive analytes to a 3 mL HEPES buffer suspension of the probe. The quenching efficiency was derived by employing $(1\text{-}I/I_0) \times 100\%$, where I_0 is the initial fluorescence emission intensity of the probe dispersed in 10 mM HEPES and I is the fluorescence emission intensity in presence of analyte.

5.2.5 Fluorescence detection experiments in portable paper strips

Commercially available Whatman filter paper was immersed into the HEPES buffer suspension of **4-NH_2@THB** for 5 min. Thereafter, the filter paper was dried well and cut into 2 cm ×2 cm size to get fluorescent paper strips. These fluorescent paper strips were used for bilirubin detection.

5.2.6 Fluorescence detection experiments in human blood serum

From the left arm vain of a healthy volunteer, blood (6 mL) was collected. This blood sample was taken in a centrifuged tube. The collected blood sample was then immediately centrifuged for 10 min at 3000 rpm speed in order to separate the blood cells. The supernatant light yellow coloured serum was collected by a Pasteur pipette. After that the serum was immediately stored at 0 °C. Thereafter, different concentrations of free bilirubin were spiked in human blood plasma. After that different concentrations of bilirubin-spiked human blood serum were introduced into the HEPES buffer suspension of the probe and fluorescence spectra were recorded (λ_{ex} = 325 nm, λ_{em} = 429 nm). Note: informed consent was obtained from all human subjects for the collection of blood samples and experimental procedures were conducted in accordance with the ethical guidelines.

5.2.7 Fluorescence detection experiments in human urine samples

From a healthy volunteer, human urine sample (10 mL) was collected. Then, the urine sample was acidified with 500 µL of conc. HNO_3 and centrifuged at 5000 rpm for 10 min. The supernatant was collected. Then, different amounts of bilirubin were spiked into the urine samples to obtain different concentrations of bilirubin-spiked urine samples. These solutions were used for bilirubin detection in urine samples.

5.3 Results and discussion

5.3.1 Characterization of material

The post-synthetically modified metal-organic framework (**4-NH_2@THB**) was successfully characterized by employing a number of analytical techniques such as FT-IR spectroscopy, ESI-MS, NMR spectroscopy, XRPD, TG analysis, N_2 sorption analysis and FE-SEM measurement.

A drastic colour change (yellow to orange) of the material after post-synthetic modification (Figure 5.1) is an indirect proof for the formation of newly functionalized compound. Moreover, in the FT-IR spectrum of **4-NH_2** (Figure 5.2), the two teeth-like sharp bands at 3487 and 3388 cm^{-1} are due to the asymmetrical and symmetrical stretching vibrations of the N−H bond, respectively.[51, 52] These two bands were vanished and only one broad band was observed in that region of the FT-IR spectrum of **4-NH_2@THB**, which suggests the richness of hydroxyl group after post-synthetic modification.[32] The strong absorption band near 1633 cm^{-1} signifies the formation of imine bond between amine moiety of MIL-53-NH_2 and aldehyde functionality of 2,3,4-trihydroxy benzaldehyde, which was not observed in the FT-IR spectrum of **4-NH_2**.[53]

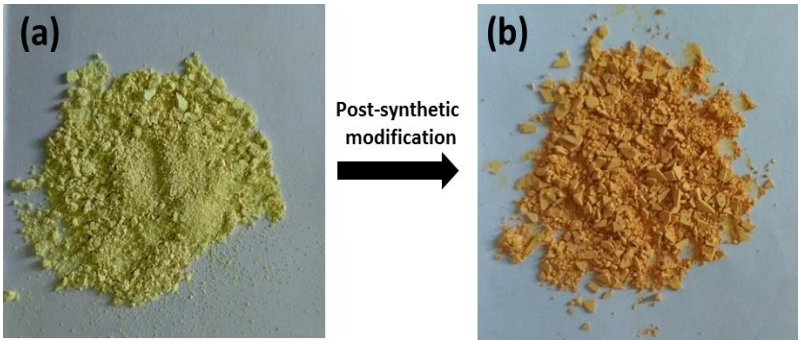

Figure 5.1 Digital images of (a) **4-NH_2** and (b) **4-NH_2@THB** in solid state.

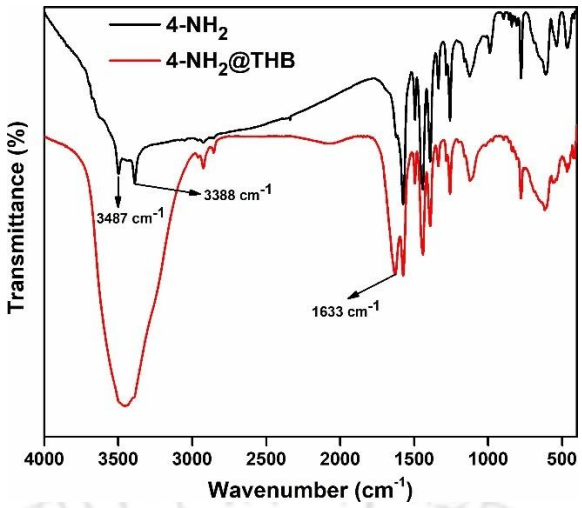

Figure 5.2 FT-IR spectra of **4-NH_2** (black) and **4-NH_2@THB** (red).

The ESI-MS spectrum of digested **4-NH_2@THB** material (Figure 5.3) exhibits two intense peaks at m/z = 182.0519 and 318.0697 (measured in positive ion mode), which can be ascribed to the $(M+H)^+$ ion of H_2BDC-NH_2 ligand and imine-functionalized ligand (i.e. product of condensation reaction between H_2BDC-NH_2 ligand and 2,3,4-trihydroxy benzaldehyde). Hence, it becomes evident that during post-synthetic modification reaction, partial conversion of amine functionality to imine functionality was successfully achieved.

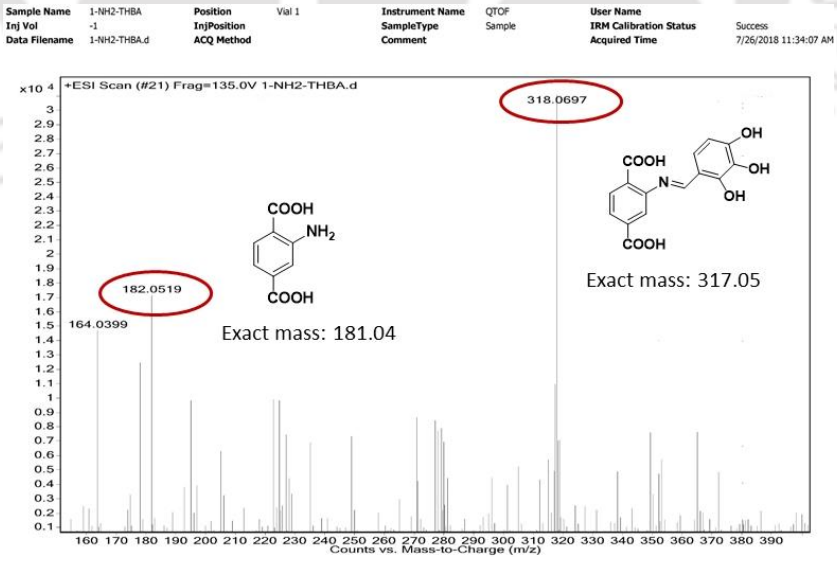

Figure 5.3 ESI-MS spectrum of the digested framework of **4-NH_2@THB** showing m/z (positive ion mode) peaks at 182.0519 and 318.0697, which correspond to $(M+H)^+$ ion (M = mass of ligands) of H_2BDC-NH_2 ligand and the imine-functionalized ligand, respectively.

To determine the percentage conversion of the amine moiety to imine functionality, ^{1}H NMR spectrum of digested **4-NH$_2$** and **4-NH$_2$@THB** material was compared (Figure 5.4). The new signals at δ = 8.11, 7.97.7.75, 7.11 and 6.50 ppm are due to the aromatic protons from imine-functionalized ligand, whereas the new signal at δ = 9.71 ppm is ascribed to the proton of the imine bond. On the basis of peak area ratio of aromatic protons of H_2BDC-NH_2 ligand and the imine-functionalized ligand of digested **4-NH$_2$@THB**, the calculated percentage conversion from amine to imine functionality is ~51%.

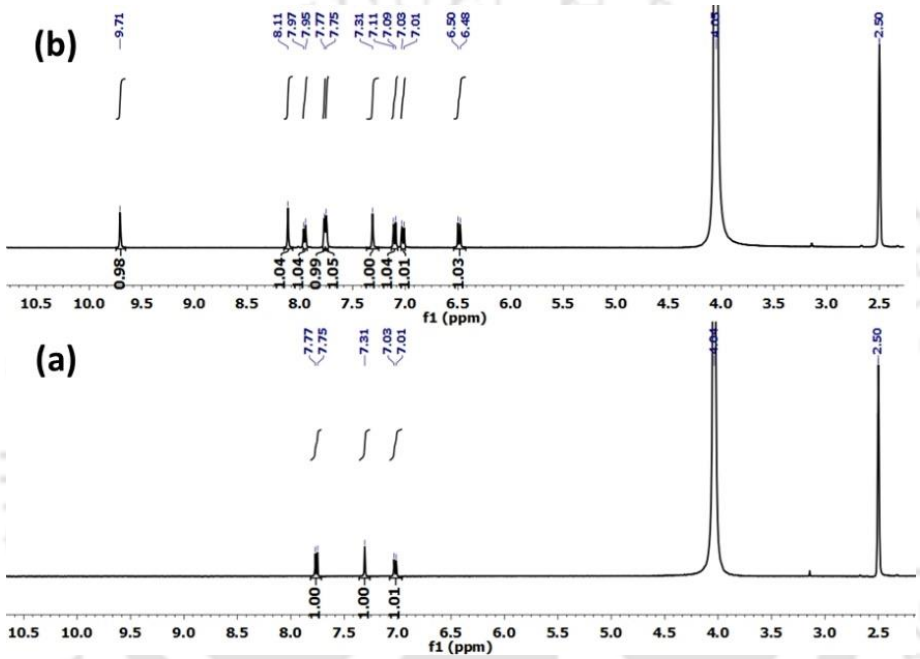

Figure 5.4 ^{1}H NMR spectra of (a) **4-NH$_2$** and (b) **4-NH$_2$@THB** after framework digestion in K_3PO_4/D_2O. The assignment of the NMR peaks for **4-NH$_2$@THB** was interpreted according to the presence of the new peaks observed for the phenyl and imine moiety. To calculate the percent of conversion, the aromatic proton peaks corresponding to H_2BDC-NH_2 ligand were set to an integration of 1 and all new peaks were integrated accordingly *Digestion protocol of the MOF sample for recording NMR spectra:* 10 mg of each MOF sample was added to 400 µL of DMSO-d_6. To this solution, 200 µL of saturated K_3PO_4 in D_2O was added. After shaking for 5 min, the MOF sample was totally dissolved and the organic phase was analyzed by ^{1}H NMR spectroscopy immediately.

Compounds **4-NH$_2$** and **4-NH$_2$@THB** show very similar X-ray diffraction patterns (Figure 5.5). The similar XRPD patterns of **4-NH$_2$** and **4-NH$_2$@THB**

clearly indicate that during post-synthetic modification, no loss in structural integrity was occurred.

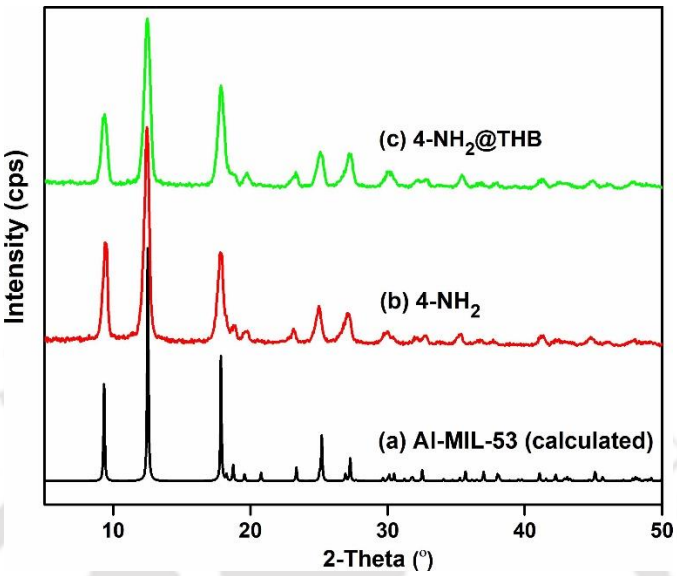

Figure 5.5 XRPD patterns of Al-MIL-53 (calculated) (a), **4-NH_2** (b) and **4-NH_2@THB** (c).

The TG traces of **4-NH_2** and **4-NH_2@THB** (Figure 5.6) show that the parent and post-synthetically modified materials have almost similar thermal stability up to 440 °C. Hence, the post-synthetically modified compound was achieved without harming the thermal stability of the material. During post-synthetic modification, the amine functionality grafted with the parent material is converted to imine functionality but the framework structure remains same. Therefore, the material after post-synthetic modification shows almost similar thermal stability as the unmodified compound.[54] In the TG trace of **4-NH_2**, the first weight loss of 5.0 wt.% in the temperature range 0-125 °C shows good agreement with the removal of 0.7 guest water molecule per formula unit (calcd.: 5.3 wt.%). After 440 °C, sudden break in the TG curve suggests the framework decomposition. Hence, the formula of **4-NH_2** is $[Al(OH)(C_8H_5NO_4)]\cdot 0.7H_2O$. On the other hand, in the TG trace of **4-NH_2@THB**, the first weight loss of 4.5 wt.% in the temperature range 0-125 °C is ascribed to the removal of 0.8 guest water molecule per formula unit (calcd.: 4.7 wt.%). The sudden weight loss near about 430 °C signifies the collapse of the structure of the material. Based on the above calculation and ^1H NMR study, the formula of the material is $[Al(OH)(C_{15}H_9NO_7)_{0.51}(C_8H_5NO_4)_{0.49}]\cdot 0.8H_2O$.

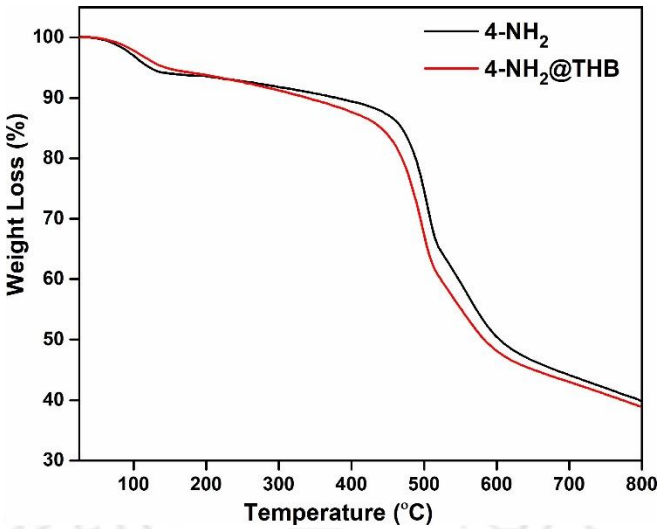

Figure 5.6 TG curves of **4-NH₂** and **4-NH₂@THB** recorded in the temperature range of 25-800 °C with a heating rate of 10 °C min^{-1}.

N_2 sorption isotherms of **4-NH₂** and **4-NH₂@THB** were measured at –196 °C to investigate the porosity and surface area of the materials (Figure 5.7). As derived from the sorption profiles of **4-NH₂**, the specific BET surface area is 1088 m^2 g^{-1} and the micropore volume is 0.72 cm^3 g^{-1} (calculated at p/p_0 = 0.5). On the other side, after post-synthetic modification, the specific surface area and micropore volume of the material become 52 m^2 g^{-1} and 0.05 cm^3 g^{-1}, respectively. Such drastic reduction of both surface area and micropore volume indicates the introduction of 2,3,4-trihydroxy benzaldehyde molecule in the framework. The incorporation of this bulky molecule blocks the pores of the material. Consequently, such lower surface area is obtained after post-synthetic modification.

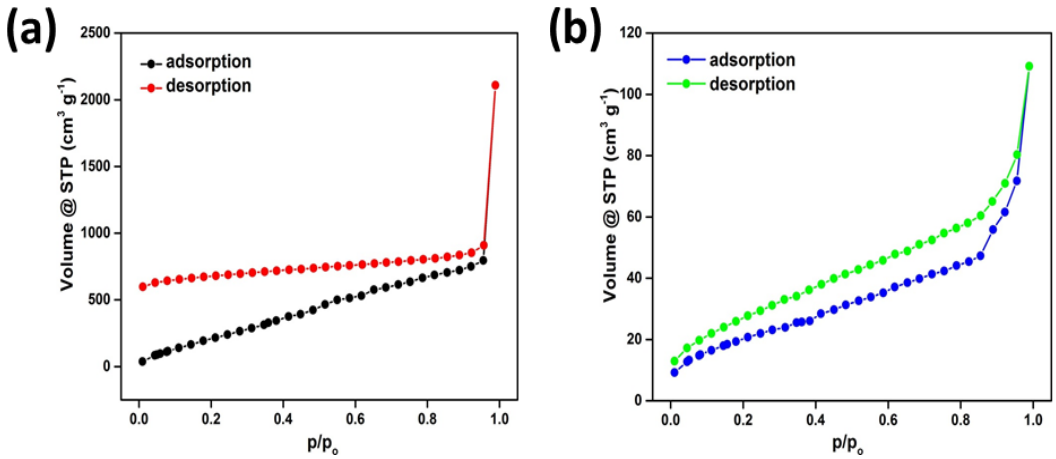

Figure 5.7 N_2 adsorption and desorption isotherms of (a) **4-NH₂** and (b) **4-NH₂@THB** recorded at –196 °C.

FE-SEM images were collected to ensure the retention in morphology after post-synthetic modification of **4-NH_2**. Figure 5.8 displayed that both **4-NH_2** and **4-NH_2@THB** crystals have similar size and shape. Hence, it can be concluded that during PSM process, no alteration in the morphology of the parent material occurred.

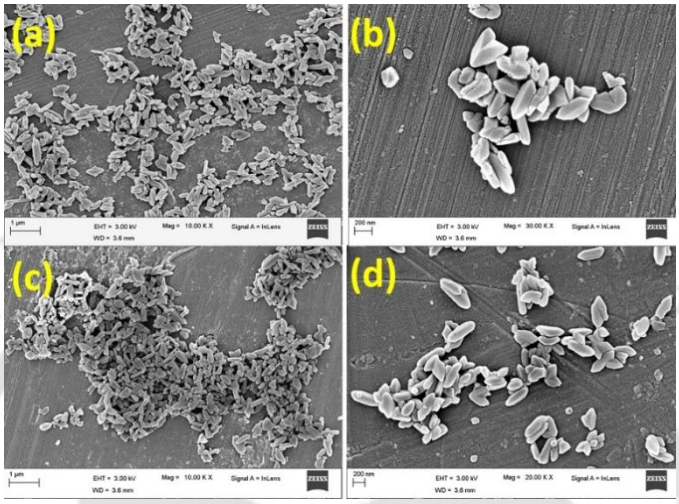

Figure 5.8 FE-SEM images of **4-NH_2** (a, b) and **4-NH_2@THB** (c, d).

5.3.2 Sensing of bilirubin in HEPES buffer medium

Bilirubin is a key biomarker for jaundice disease. Hence, the fast and sensitive detection of bilirubin has become a challenging task in the field of medical research. Some small molecule fluorescent probes, conjugate polymers and electrochemical sensors were developed to examine the detection performance towards bilirubin.[30, 31, 55-58] But, the number of efficient probes for the detection of bilirubin is quite less because of their tricky synthetic procedure, slow response, poor selectivity and sensitivity towards targeted analyte. On the other hand, MOF materials are highly advantageous over other probes for their easy and straight forward preparation, high physicochemical stability, high photosatblility and recyclability.[34] Regeneration and reusability are important features of a sensor material because they are directly related to the cost effectiveness of the detection process. Most of above-mentioned probes could not be reused because of their high solubility in the sensing medium. But, due to insoluble nature of the MOF material, it can be easily recovered from sensing medium and reused. All these facts motivated us to explore the sensing ability of bilirubin by the post-synthetically

modified Al(III) based MIL-53 compound. The high hydrolytic stability and bio-friendly nature of Al(III) based MOFs than the MOFs containing other metal ions make them superior sensor materials over other MOF materials.

The incorporation of electron rich 2,3,4-trihydroxy benzaldehyde moiety into the MIL-53-NH_2 framework via condensation reaction enhances the emission intensity around 2-fold as compared to the parent material (Figure 5.9). This highly fluorescent material was utilized for the detection of bilirubin via "turn-off" mechanism. Prior to the addition of bilirubin, **4-NH_2@THB** showed a bright blue fluorescence under UV lamp due to ligand-to-metal charge transfer process. But, as soon as the material came into contact with bilirubin, an instant quenching in the emission intensity was observed. This is due to inner filter effect as reabsorption of excitation and emission light took place by bilirubin.[59, 60] In addition, the molecular interactions between the hydroxyl group containing MOF material and -NH moiety rich bilirubin occurred which led to static quenching of fluorescence.[30, 31] These are the reasons behind the suppression of fluorescent emission signal of **4-NH_2@THB** in presence of bilirubin.

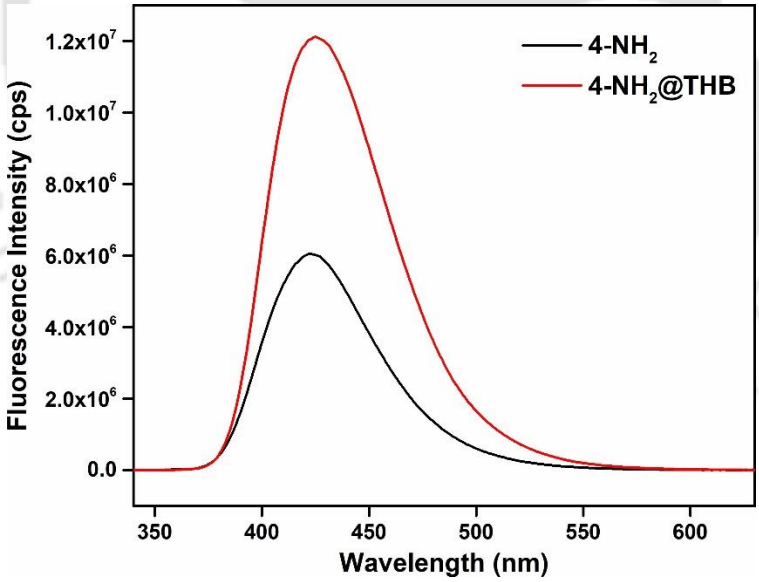

Figure 5.9 Fluorescence emission spectra of **4-NH_2** (black) and **4-NH_2@THB** (red).

In order to perform time-dependent detection of bilirubin, 200 µL of 1 mM bilirubin solution was introduced into the HEPES buffer suspension of **4-NH_2@THB** and emission spectra were collected with 1 min interval up to 10 min upon excitation at 325 nm. It can be noticed from Figure 5.10 that the strong fluorescence emission property of **4-NH_2@THB** suspension was instantly reduced

after coming into contact with bilirubin. Moreover, the probe (**4-NH_2@THB)** showed much better quenching behaviour in presence of bilirubin than the parent material (**4-NH_2)** (Figure 5.11). It is worth to mention that around 30 min of time is required for the clinical detection of bilirubin.[3, 25] Hence, the presented material could be utilized for instant diagnosis of jaundice through rapid detection of bilirubin.

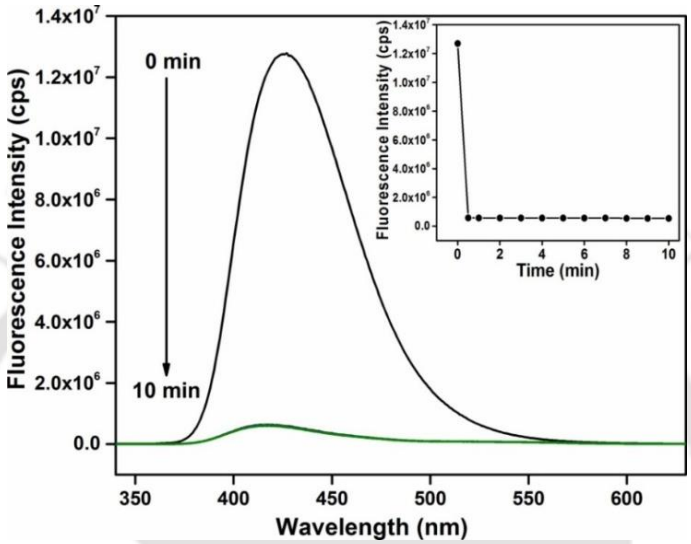

Figure 5.10 Quenching of the emission intensity of HEPES buffer suspension of **4-NH_2@THB** after the introduction of 1 mM bilirubin (200 μL) from 1 min to 10 min. The inset plot shows the suppression of emission intensity as a function of time (monitored at 429 nm).

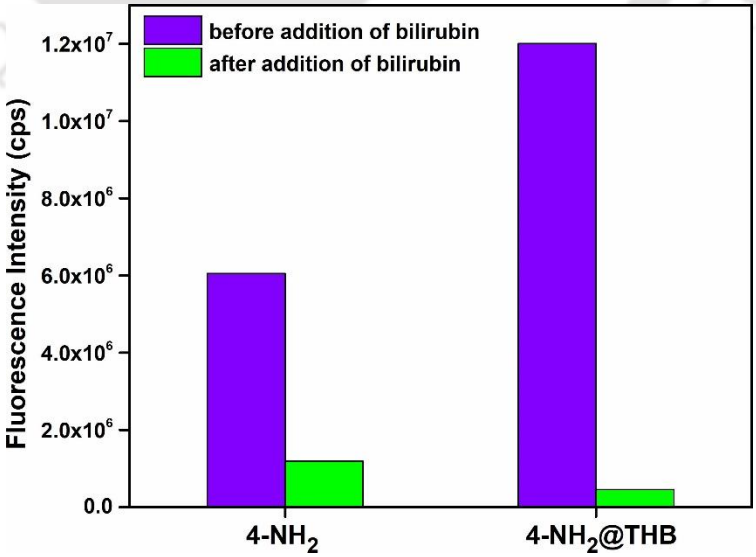

Figure 5.11 Fluorescence emission intensity of **4-NH_2** and **4-NH_2@THB** before and after addition of bilirubin.

A potential fluorescent sensor must retain its selectivity towards targeted analyte over other intrusive compounds. Therefore, several biomolecules (ascorbic acid, creatine, creatinine, dopamine, glucose, urea, uric acid) and metal ions (Ca^{2+}, Cd^{2+}, Co^{2+}, Cu^{2+}, Fe^{2+}, Fe^{3+}, K^{+}, Mg^{2+}, Na^{+}, Zn^{2+}) were utilized to confirm the selectivity of the probe towards bilirubin. Figure 5.12 discloses that out of 17 competitive analytes, **4-NH_2@THB** showed the highest quenching efficiency (~96%) towards bilirubin. A careful observation in Figure 5.12 revealed that Fe^{3+} showed around 22% quenching of emission intensity of **4-NH_2@THB**. This quenching behaviour can happen due to either cation exchange phenomenon or interactions of Fe^{3+} ions with the coordinated organic ligands of MOF.[37, 61] Interestingly, Na^{+}, Mg^{2+} and Cd^{2+} ions showed some "turn-on" response towards **4-NH_2@THB**. It has been well-documented that hydrated alkali and alkaline metal ions can boost the intersystem crossing (ISC) process and the population of the excited triplet state of the fluorophore is increased by cation-π interaction, which enhances the luminescence behaviour of the probe.[62] It has been reported that Cd^{2+} ion has tendency to form coordination bond with nitrogen atom of imine bond, which effectively reduces the non-radiative transition and enhances the ligand cantered charge transfer.[63] As a result, the fluorescence property of the probe is enhanced.

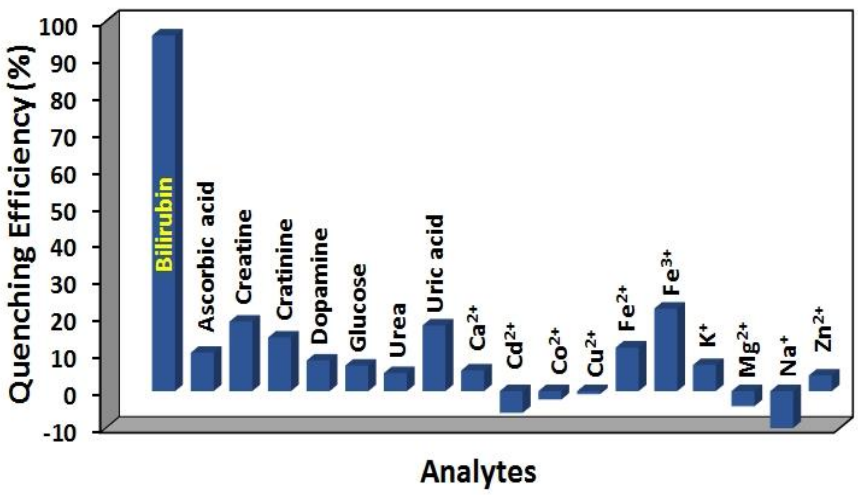

Figure 5.12 Fluorescence quenching effect of **4-NH_2@THB** towards the introduction of different intrusive analytes (1 mM, 200 μL) in HEPES buffer.

To ensure the specificity of the probe towards bilirubin in the co-existence of its congeners, bilirubin was introduced into the suspension of **4-NH_2@THB**

which already contained intrusive agents. After the addition of bilirubin solution, the emission spectra were collected. Figure 5.13 clearly imply that bilirubin can effectively reduce the emission intensity of the probe even in the co-existence of other intrusive biomolecules and metal ions. Hence, it becomes obvious that the presented material has remarkable selectivity towards bilirubin over other congeners.

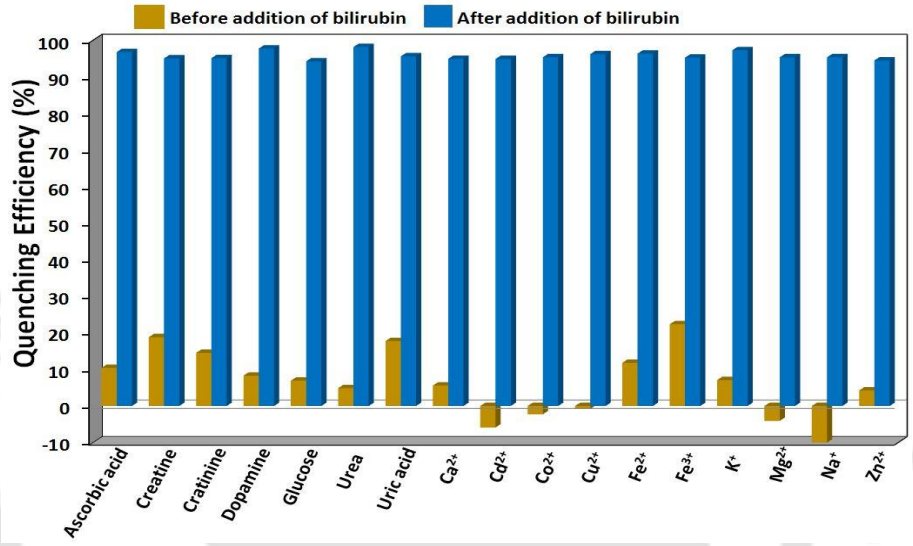

Figure 5.13 Quenching of the fluorescence emission intensity of HEPES buffer suspension of **4-NH_2@THB** towards bilirubin (1 mM, 200 µL) in the co-existence of other congeners (1 mM, 200 µL).

A compound should exhibit a distinct response to the targeted analyte at a specific concentration. Figure 5.14 shows the relation between the quenching efficiency of the probe and the concentration of various analytes. This figure reveals that considerable quenching of the fluorescence of **4-NH_2@THB** occurs at lower concentration of bilirubin and at higher concentration of bilirubin, significant increase in quenching efficiency occurs. But, for other analytes, negligible quenching efficiency is observed at lower concentration. Among them, the quenching efficiency increases slightly for few analytes at higher concentration.

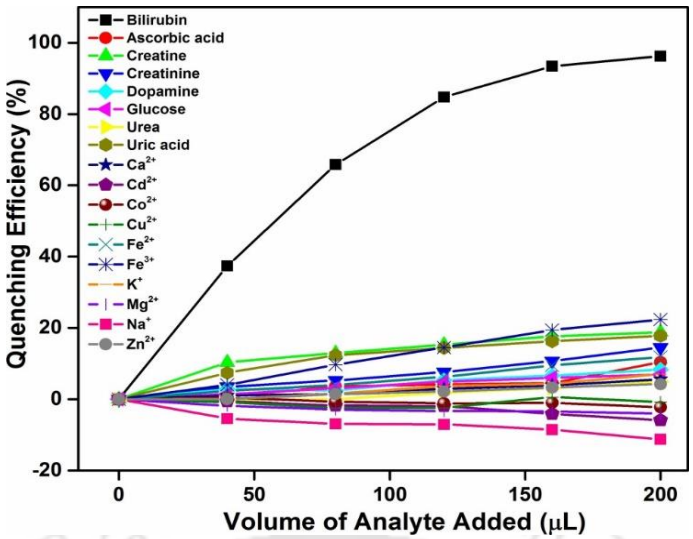

Figure 5.14 Variation of the fluorescence quenching efficiencies upon incremental addition of 1 mM solution of different competitive analytes to a 3 mL suspension of **4-NH_2@THB.**

For the estimation the Stern-Volmer (S-V) quenching constant the following equation was employed: $(I_0/I) = K_{sv}[Q] + 1$, where, I_0 is the initial fluorescence emission intensity of **4-NH_2@THB** and I represents the fluorescence emission intensity after the introduction of analyte, [Q] is the molar concentration of analyte and K_{sv} is the quenching constant. Figure 5.15 shows the S-V plots for the fluorescence emission suppression of **4-NH_2@THB** by different analytes. The luminescence quenching data obtained from the S-V equation helps to determine the nature of quenching process (static versus dynamic). At lower concentration of bilirubin, the linear nature of the S-V plot signifies that quenching process is occurring via static or dynamic manner. But, at higher concentration of bilirubin, the S-V plot deviates from linearity, which indicates the presence of both static and dynamic quenching processes.[64, 65] The calculated K_{sv} value for bilirubin is found to be 4.18×10^6 M^{-1} (Figure 5.16). This large quenching constant suggests that bilirubin is an excellent acceptor for **4-NH_2@THB** donor material.

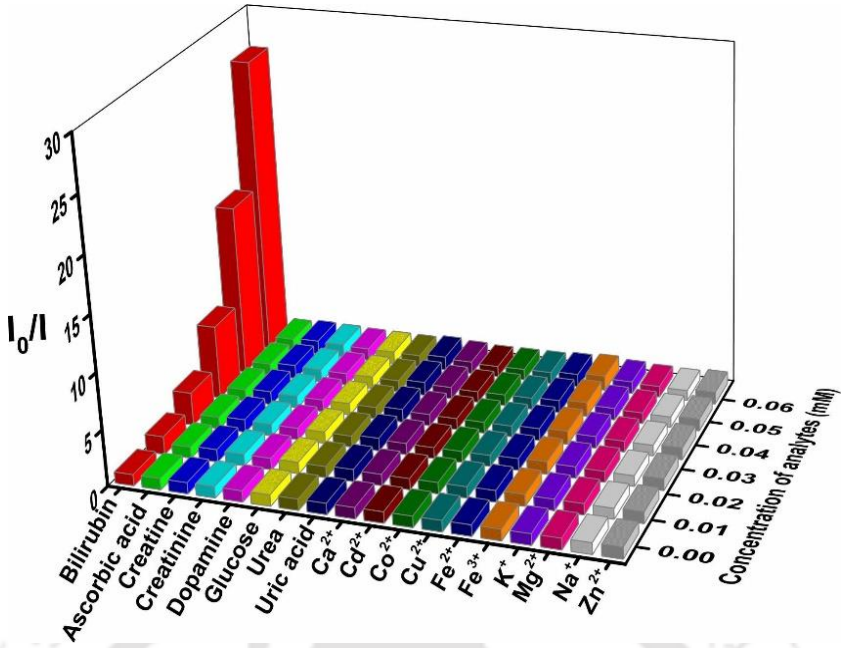

Figure 5.15 Stern-Volmer plots for the fluorescence quenching of **4-NH_2@THB** upon gradual addition of different intrusive analytes.

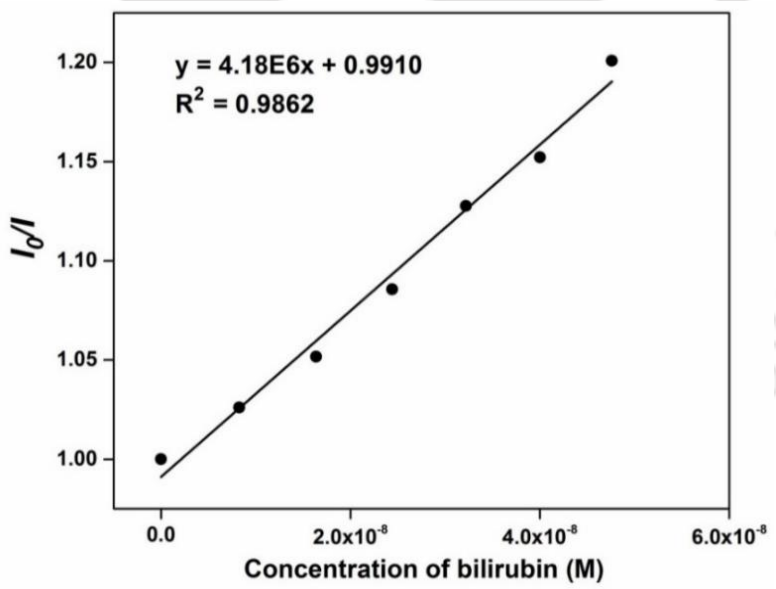

Figure 5.16 Stern-Volmer plot for the fluorescence emission quenching of **4-NH_2@THB** in presence of bilirubin solution.

For quantification of the sensing process of bilirubin by **4-NH_2@THB**, a concentration dependent fluorescence titration was carried out. Figure 5.17 shows that gradual suppression of the emission intensity of probe is observed with the incremental introduction of bilirubin with a distinct blue-shift ($\Delta\lambda$= 16 nm, 429 nm to 413 nm). The observed blue-shift suggests the formation of exciplexes (which

stabilize the excited state).[66] Exciplexes are generally formed by the interaction of an excited molecule with an unlike molecule.[67] In the present system, formation of exciplexes by the association of hydroxyl group containing **4-NH$_2$@THB** and -NH moiety rich bilirubin through hydrogen bonding interaction is the most probable reason behind the blue shift of emission band during concentration dependent fluorescence titration experiment.[68] Figure 5.18 shows nice linear relationships between the fluorescence emission intensity ratio I_0/I (where, I_0 represent initial fluorescence intensity and I signify the fluorescent intensity in presence of bilirubin) and the concentration of bilirubin in micro-, nano-, and picomolar levels. But, at milimolar concentration of bilirubin, the linearity is largely deviated. For the evaluation of limit of detection (LOD) of **4-NH$_2$@THB** towards bilirubin, fluorescence spectra of the probe were measured after the introduction of very less concentrated solution of bilirubin. A linear curve was acquired by plotting the fluorescence emission intensity of the material against the concentration of bilirubin solution (Figure 5.19). From this curve, LOD value was evaluated by applying the equation: 3σ/k (k = slope of the curve, σ = standard deviation obtained from blank measurements). The calculated LOD value is 1.26 pM (linear range = 10^{-12} – 1.2×10^{-5} M). This value is slightly higher than the recently reported MOF based fluorescent probe called UIO-66-PSM (LOD = 0.59 pM).[32] Interestingly, this value is lesser than the reported non-MOF based fluorescent probes (Table 5.1).

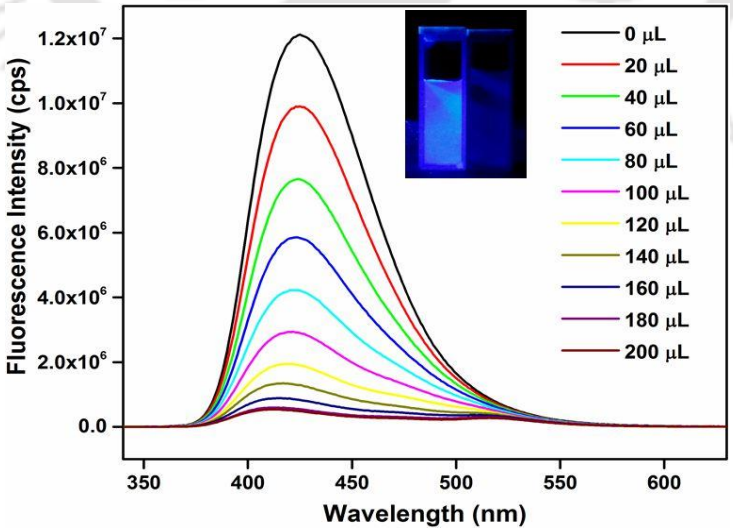

Figure 5.17 Suppression of the fluorescence emission intensity of HEPES buffer suspension of **4-NH$_2$@THB** upon stepwise addition of 1 mM bilirubin solution. Inset plot shows the naked eye detection of bilirubin under UV lamp.

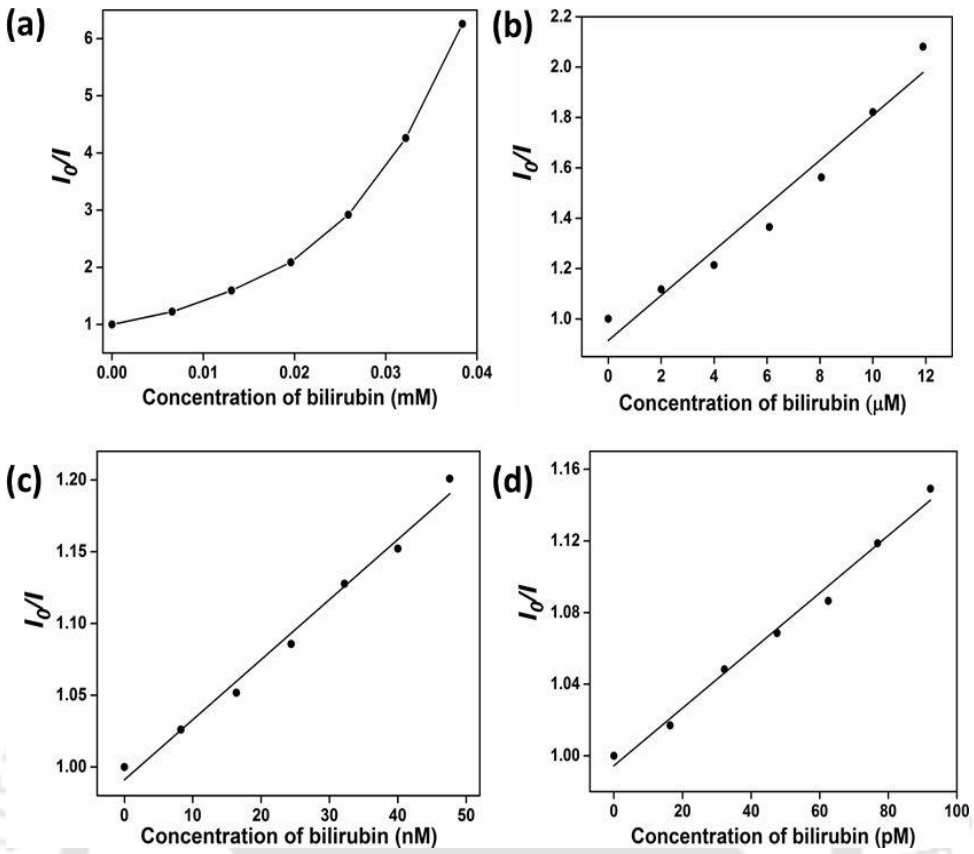

Figure 5.18 Relationships between I_0/I and concentrations of bilirubin in mili- (a), micro- (b), nano- (c), and picomolar (d) levels.

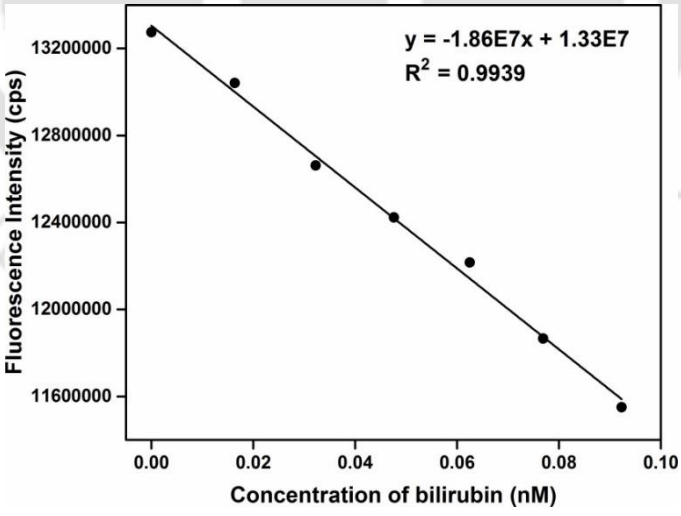

Figure 5.19 Change in the fluorescence emission intensity of **4-NH_2@THB** in HEPES buffer as a function of bilirubin concentration.

Table 5.1 Comparison of the results of various bilirubin sensors.

A.	Fluorescent sensors						
Sl. No.	Sensor Material	Type of Material	Medium Used	Response Time (s)	Linear Range (M)	Detection Limit	Ref.
1	Al-MIL-53-NH_2@THB	MOF	HEPES buffer	30	10^{-12} - 1.2×10^{-5}	1.26 pM	this work
2	UIO-66-PSM	MOF	PBS buffer	30	10^{-13} - 5×10^{-4}	0.59 pM	32
3	PDPPF-*co*-Ph	polymer	THF	-	10^{-6} - 10^{-5}	-	69
4	BAMD	organic molecule	phosphate buffer	600	10^{-12} - 5×10^{-4}	2.8 pM (pH = 7.4) 3.3 pM (pH = 9.0)	30
5	PF-Ph-GlcA	polymer	PBS buffer	-	-	150 nm	31
6	HSA-AuNCs	nanoclusters	phosphate buffer	-	10^{-6} - 5×10^{-5}	248 nM	70

B.	Electrochemical sensors				
Sl. No.	Sensor Material	Type of Material	Linear Range	Detection Limit	Ref.
7	SiO_2@ZrONPs/CHIT	nanoparticles	0.02- 250 µM	0.1 nM	26
8	CuO-CdO NCs	nanocomposite	10.0 pM -10.0 mM	1.0 ± 0.1 pM	57
9	HSA-AuNCs	nanomaterial	0.2-7.0 µM	86.32 nM	27
10	BOx/nano Au	nanorods	0.01 -500 µM	0.005 µM	22
11	RGO-PSS composite electrode	carbon electrode	0 - 450 µM	2.0 µM	55

12	BOx/GONP@Ppy/FTO	graphene oxide nanoparticle	0.01 – 500 mM	0.1 nM	56
13	MWCNT	nanotubes	0.5–500 µM	0.3 ± 0.022 nM	58

For investigating the reusability of the material towards bilirubin detection, the material was filtered off after the fluorescence titration experiment. After filtration, the material was washed with deionised water for several times and dried in oven. Interestingly, the probe showed excellent restoration of initial fluorescence property even after five cycles of repeated fluorescence detection experiments (Figure 5.20). In addition, the XRPD analysis disclosed that the framework structure of initial MOF material remained intact even after the five successive cycles of sensing events (Figure 5.21). Moreover, the influence of pH on the quenching of fluorescence emission of **4-NH_2@THB** by bilirubin was investigated. The sensing experiment was performed with solutions of different pH values (from pH = 2 to 12). Figure 5.22 revealed that the initial fluorescence emission intensity varies with changing the pH of the medium. Interestingly, large deviations in initial fluorescence emission intensity were observed at higher and lower pH. At very low pH medium (i.e. pH = 2), the incorporated ligand may exist in protonated form which leads to reduction of electronic charge transfer process in the system, resulting in poor emission intensity.[30] But, at pH range from 4 to 7, the material shows high fluorescent intensity due to the presence of lone pair of electrons on the hydroxyl group of THB molecule which is available for complete delocalization. It has already been reported that compounds having imine bonds show highest stability in the pH range 3 to 7.[71] On the other side, due to lower stability of the imine bond, gradual decrease in emission intensity of **4-NH_2@THB** was observed with increase in pH value of the medium.[72] Though the initial emission intensity of **4-NH_2@THB** varies with the pH of the medium, bilirubin could effectively quench the emission intensity of the probe at any pH value of the medium. All the above results suggest the reusability and high photo-stability of the MOF material, which make **4-NH_2@THB** a potential candidate for long term real field detection of bilirubin.

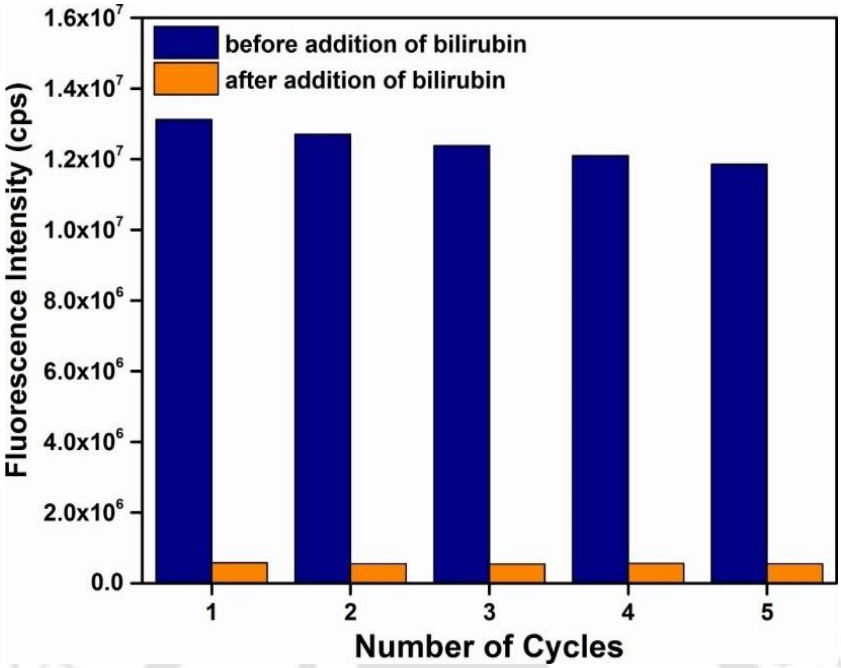

Figure 5.20 Recyclability of the quenching efficiency of the HEPES buffer suspension of **4-NH_2@THB** towards 1 mM bilirubin solution.

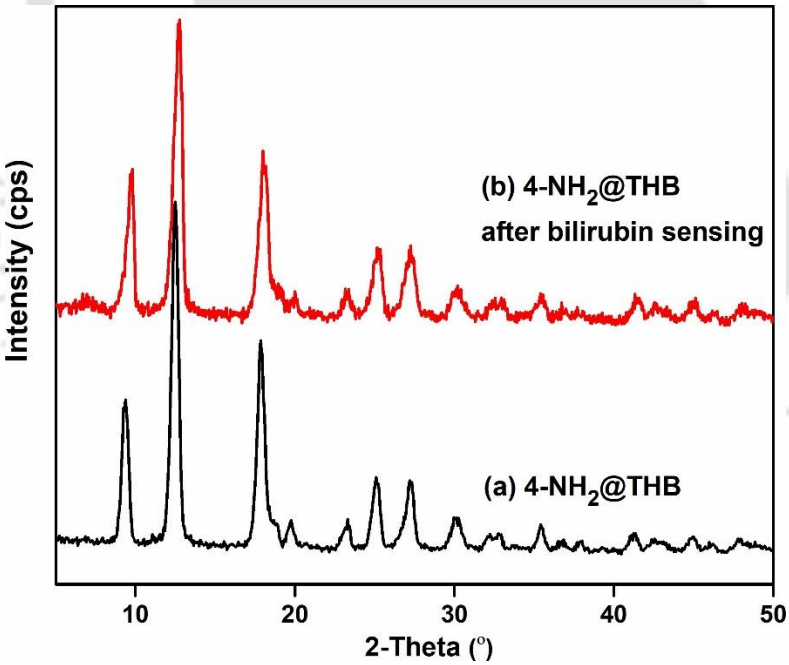

Figure 5.21 XRPD patterns of **4-NH_2@THB** before (a) and after sensing of bilirubin (b).

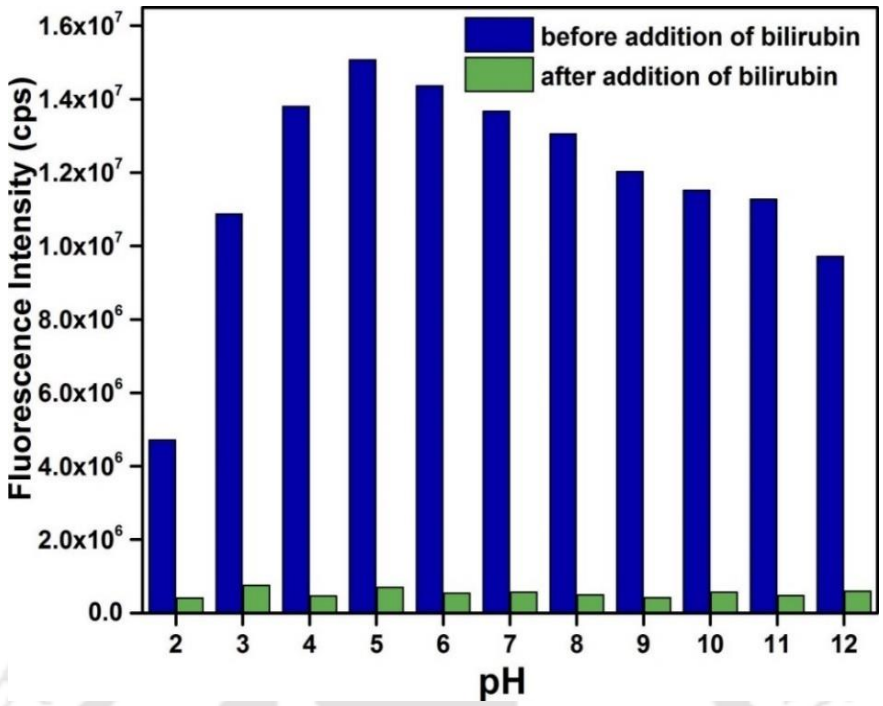

Figure 5.22 Effect of pH on fluorescence emission intensity of **4-NH_2@THB** before and after addition of 1 mM bilirubin solution (200 µL).

5.3.3 Sensing of bilirubin in portable paper strips

Recently, portable devices based on paper strips have drawn immense attention due to rapid and low cost detection. Here, paper strips obtained by dip coating method, which have been used for bilirubin detection. The obtained test strips were treated with various concentrations of bilirubin solution (15 µL volume in each test strip) by using a micropipette. It can be observed from Figure 5.23 that a dark spot appeared under UV lamp after the treatment of bilirubin solution. The darkness of the spot was low at lower concentrations of bilirubin solution. The dark spot appeared due to quenching of the strong blue fluorescence of the material coated paper strip. It is also observed that bilirubin solution up to a concentration of 10^{-12} M can be detected by this method. Hence, this technique is very much useful for the detection of bilirubin at low concentration.

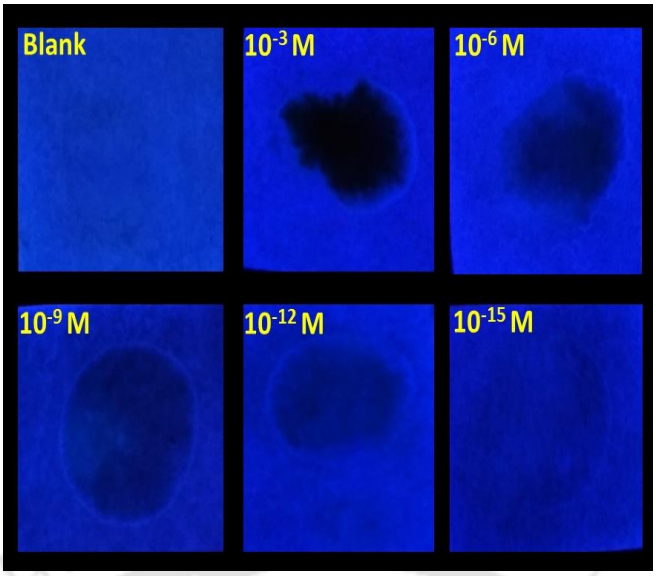

Figure 5.23 Digital images of **4-NH_2@THB** coated paper test strips (under UV lamp) after the introduction of 15 µL of bilirubin solution of various concentrations. A dark spot can be seen only in presence of bilirubin solution.

5.3.4 Detection of bilirubin in human biofluids (blood serum and urine)

As the probe retains its selectivity towards bilirubin even in presence of its congeners, we have performed the detection experiment for bilirubin in more complex media such as human blood serum and human urine. By employing the standard addition method, the detection performance of bilirubin in blood serum and urine was examined. The obtained results by this method for blood serum and urine samples are documented in Table 5.2 and Table 5.3, respectively. It is found that percentage recoveries of bilirubin fall in between 97.72-107.66% and relative standard deviation (RSD) values are in the range of 2.03-8.11%. Such low RSD values and good percentage recoveries signify that the present probe is an excellent material for the detection of bilirubin with high accuracy and precisions in human blood serum and as well as in urine samples.

Table 5.2 Detection of bilirubin in human blood serum samples in different concentration ranges.

Background (mol L^{-1})	Bilirubin Spiked (mol L^{-1})	Bilirubin Found[a] (mol L^{-1})	Recovery (%)	RSD (%) (n = 3)
1.24×10^{-6}	1×10^{-7}	0.97×10^{-7}	97.72	2.87
	1×10^{-9}	1.03×10^{-9}	103.83	2.03
	1×10^{-11}	1.07×10^{-11}	107.66	3.87

[a] excluding background

Table 5.3 Detection of bilirubin in human urine samples in different concentration ranges.

Background (mol L^{-1})	Bilirubin Spiked (mol L^{-1})	Bilirubin Found[a] (mol L^{-1})	Recovery (%)	RSD (%) (n = 3)
1.39×10^{-6}	1×10^{-7}	1.05×10^{-7}	105.77	8.11
	1×10^{-9}	0.99×10^{-9}	99.56	4.78
	1×10^{-11}	1.04×10^{-11}	104.38	4.14

[a] excluding background

5.3.5 Possible sensing mechanisms

Quenching of fluorescence emission intensity of **4-NH_2@THB** in presence of bilirubin can occur due to various types of interactions between fluorophore molecule and quencher molecule such as collision, energy transfer process, ground state complex formation, excited-state reaction or through inner filter effect (IFE). All of these processes belong to two types of fluorescence quenching mechanisms: one is dynamic quenching and another one is static quenching. Dynamic quenching primarily occurs via collision process or diffusion of quencher to the excited-state fluorophore. In static quenching, close association between quencher and fluorophore leads to decrease in emission intensity.[73]

Fluorescence lifetime measurement is a powerful technique to differentiate between dynamic and static quenching. In dynamic quenching process, the fluorescence lifetime of excited fluorophore decreases in presence of quencher molecule. In static quenching process, the lifetime of the fluorophore remains unchanged even in the presence of quencher.[74]

Time-resolved fluorescence lifetime decay profiles of the HEPES buffer suspension of **4-NH_2@THB** were measured in the absence and presence of bilirubin. The fluorescence lifetime decay profiles (Figure 5.24) and the fitting results are shown in Table 5.4. The data reveal that the presence of bilirubin (200 µL, 1 mM) could hardly bring any change in the lifetime of fluorophore. These results rule out the possibility of dynamic quenching in the present system. As we know, both the well-known photo-induced electron transfer (PET) processes and Förster resonance energy transfer (FRET) belong to the dynamic quenching mechanism. Hence, both of these processes are not acceptable in case of our system. Hence, static quenching is happening in this system.

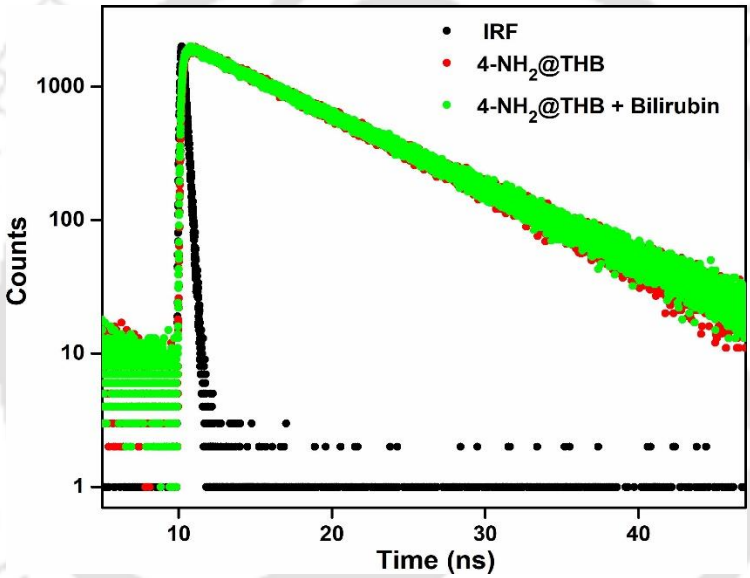

Figure 5.24 Lifetime decay profile of **4-NH_2@THB** in the absence and presence of bilirubin solution (λ_{ex} = 336 nm, monitored at 429 nm).

Table 5.4 Fluorescence lifetimes of **4-NH_2@THB** before and after the addition of bilirubin ((λ_{ex} = 336 nm, pulsed diode laser).

Volume of bilirubin (µL)	a_1	a_2	τ_1 (ns)	τ_2 (ns)	$\langle\tau\rangle^*$ (ns)	χ^2
0	0.985	0.014	7.852	0.019	7.734	1.012
200	0.990	0.009	7.675	0.028	7.598	1.013

Average lifetime $\langle\tau\rangle^* = a_1\tau_1 + a_2\tau_2$

The inner filter effect (IFE) is a very effective quenching phenomenon, which occurs due to the reabsorption of excitation and/or emission light by the quencher. A huge spectral overlap between the absorption band of quencher and/or emission band of the fluorophore is the prerequisite criteria for IFE to take place.[75-77] Moreover, the fluorescence lifetime remains unchanged during this process as no excited-state electron or energy transfer occurs in this quenching event.[78] The absorption spectrum of bilirubin shows sufficient overlapping region with both the excitation and emission spectrum of **4-NH_2@THB** (Figure 5.25), which points out that IFE is efficient in this sensing process. In addition, no change in lifetime of the fluorophore in presence of bilirubin undoubtedly suggests that the quenching process occurs due to IFE (Figure 5.24 and Table 5.4).

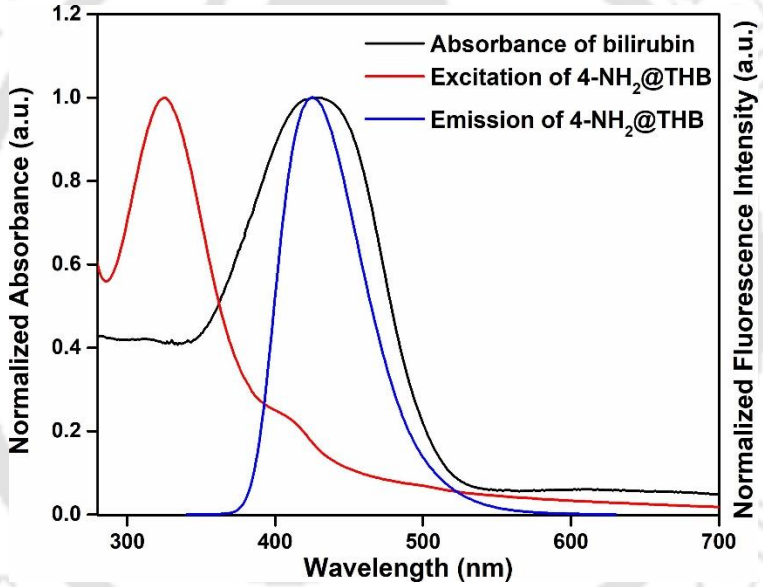

Figure 5.25 Normalized UV−vis spectrum of bilirubin overlapped with the normalized emission/excitation spectra of **4-NH_2@THB** in HEPES buffer.

Moreover, as the quenching is static in nature, some molecular interactions could be expected during quenching process of **4-NH_2@THB** in presence of bilirubin. According to the structural features of bilirubin and **4-NH_2@THB**, the following interactions could be expected: (i) coordination between carboxyl group of bilirubin moieties and the unsaturated metal site (Al) of MOF, (ii) hydrogen bonding interactions between –OH group rich **4-NH_2@THB** and -NH moiety rich bilirubin and (iii) π–π interaction in between the aromatic rings of bilirubin and **4-NH_2@THB**. Bilirubin can become immobilized on **4-NH_2@THB** due to the above

interactions, which decrease the distance between fluorophore and quencher and favours molecular interactions between them.

For the confirmation of molecular interactions between **4-NH_2@THB** and bilirubin, zeta potential of the material before and after addition of bilirubin was measured in HEPES buffer medium (pH = 7.4). Figure 5.26 suggest that a significant reduction of zeta potential of **4-NH_2@THB** was observed in presence of bilirubin (from -23.7 mV to -16.6 mV). This event confirms the presence of molecular interactions between **4-NH_2@THB** and bilirubin.[70, 79]

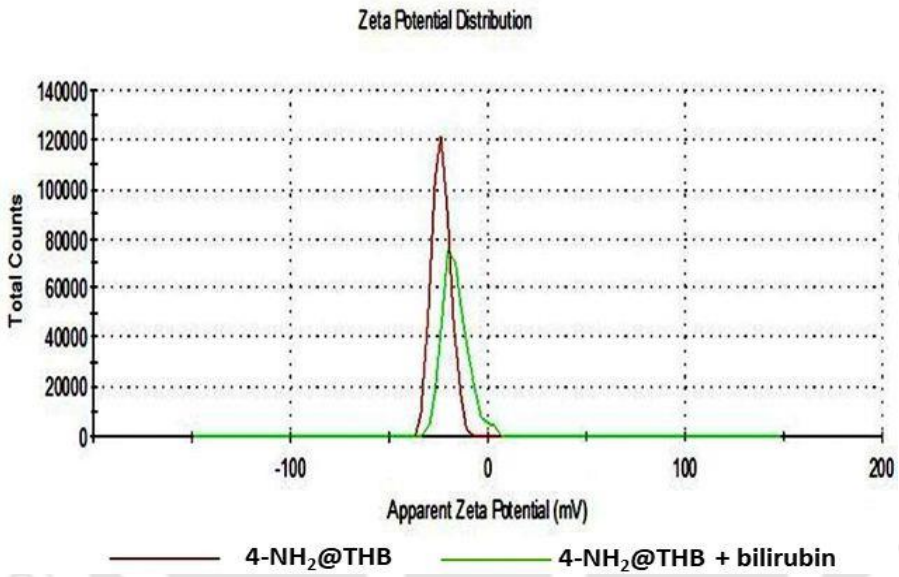

Figure 5.26 Zeta potential distribution of **4-NH_2@THB** in HEPES buffer medium (pH = 7.4) before and after addition of bilirubin.

Furthermore, the interactions between **4-NH_2@THB** and bilirubin have been confirmed by XPS measurement. The XPS spectra of Al 2p (Figure 5.27B) before and after treatment with bilirubin signify an enhancement in binding energy from 75.01 to 76.03 eV. This result clearly suggests that the carboxyl group of bilirubin undergoes co-ordination with the unsaturated metal (Al) sites of the MOF.[80] Moreover, in both N 1s and O 1s XPS spectra (Figure 5.27C-D), N 1s and O 1s signals of **4-NH_2@THB** (399.87 eV and 532.30 eV, respectively) are shifted towards higher binding energies (400.80 eV and 533.19 eV, respectively) for bilirubin treated **4-NH_2@THB**. This result attributes that imine bonded N atom and –OH functionality of **4-NH_2@THB** undergo hydrogen bonding interactions with the –NH group of bilirubin.[81]

In case of static quenching, binding constant (K_a) and number of binding sites (n) can be evaluated by employing the modified Stern-Volmer equation (double logarithm regression curve):[82]

$$\log[(I_0\text{-}I)/I] = \log K_a + n \log[Q]$$

where, I_0 and I are the fluorescence intensities of the suspension of **4-NH$_2$@THB** in absence and presence of bilirubin, respectively. The concentration of bilirubin is denoted by [Q]. From the slope and intercept of the curve (Figure 5.28), n and K_a can be determined which were summarized in Table 5.5. The binding constants (K_a) at different temperature (298, 308 and 318 K) fall in the range of $11.38 \times 10^5 - 0.13 \times 10^5$ L mol^{-1}. The binding constant values confirm the presence of molecular interactions between bilirubin and MOF material. It is notable that both K_a and n values gradually decrease at higher temperatures. At higher temperature, molecules become more disordered, vibrate faster, and increase in diffusion co-efficient occurs. Therefore, the molecular interactions are inhibited.[83] Hence, this study further reveals that quenching process is static in nature. It is worth to mention that as no fractional binding site can occur, the number of n is considered as 1 (as in Table 5.5, all values of n are approximately close to 1).

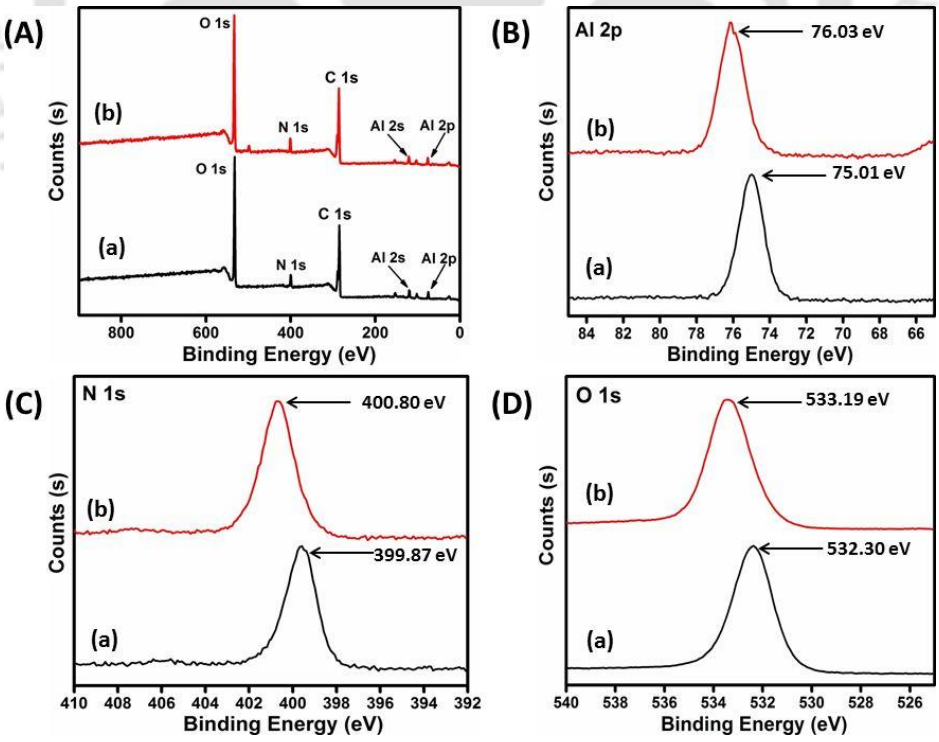

Figure 5.27 (A) XPS spectra of **4-NH$_2$@THB** (a) and bilirubin treated **4-NH$_2$@THB** (b), High resolution XPS spectra of (B) Al 2p (C) N 1s and (D) O 1s of **4-NH$_2$@THB** (a) and bilirubin treated **4-NH$_2$@THB** (b).

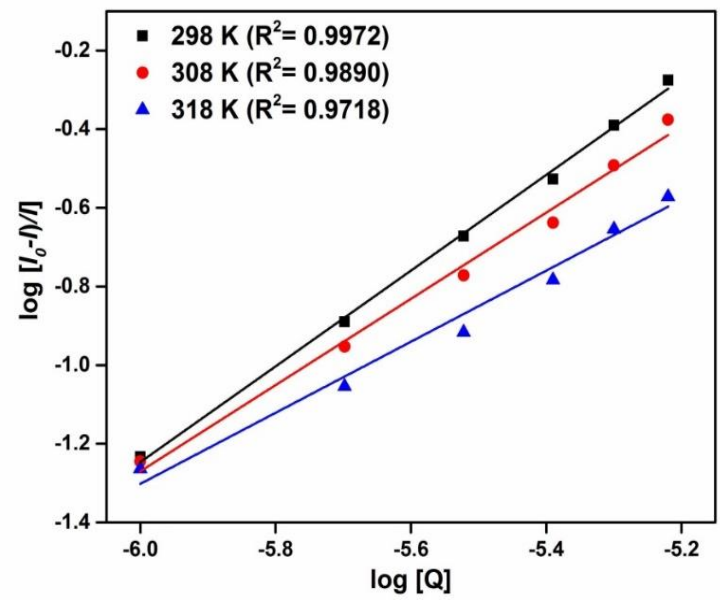

Figure 5.28 log[(I_0-I)/I] vs log[Q] plot at different temperatures.

For the characterization of binding forces (i.e. hydrogen bonding, hydrophobic force and electrostatic interaction), the values of several thermodynamic parameters such as changes in enthalpy (ΔH), entropy (ΔS) and Gibbs free energy (ΔG) play important roles.[84] $\Delta H>0$ and $\Delta S>0$ suggest hydrophobic interactions, $\Delta H <0$ and $\Delta S <0$ indicate hydrogen bond formation whereas, $\Delta H \approx 0$ and $\Delta S >0$ reflect electrostatic forces.[85] Changes in enthalpy (ΔH), entropy (ΔS) and Gibbs free energy (ΔG) were calculated based on the van't Hoff equation:

$$\log K_a = -\Delta H/RT + \Delta S/R$$

where K_a is the binding constant at the corresponding temperature (T) and R is the gas constant. ΔH and ΔS values were evaluated from the slope and intercept of the linear plot (Figure 5.29). At different temperatures, ΔG values were determined by employing the following equation:

$$\Delta G = \Delta H - T\Delta S$$

The negative values of ΔG (Table 5.5) suggest that the interaction process is spontaneous in nature. Moreover, the negative values of ΔH indicate the exothermic nature of binding which is in good agreement with the K_a values at different temperatures (Table 5.5). In addition, negative values of both ΔH and ΔS clearly suggest that hydrogen bond formation is predominantly responsible for the binding interactions between bilirubin and MOF.[86]

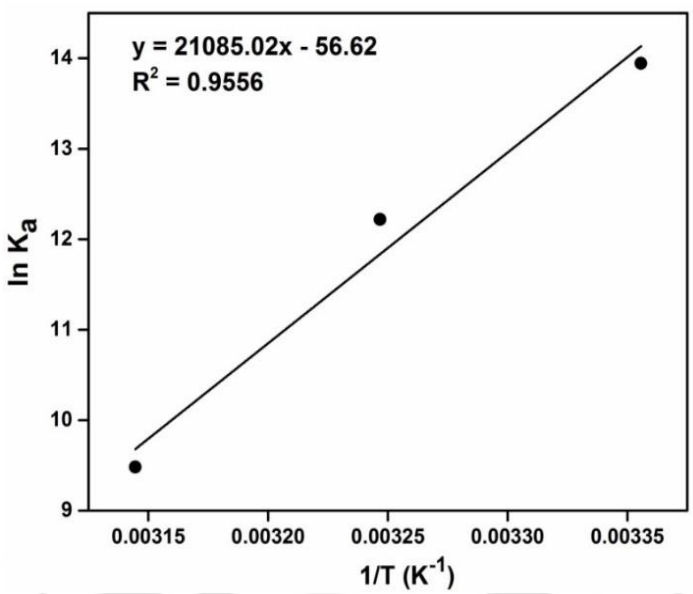

Figure 5.29 Van't Hoff plot for **4-NH_2@THB** and bilirubin interaction.

Table 5.5 Binding parameters and thermodynamic parameters for the binding process between **4-NH_2@THB** and bilirubin.

T (K)	$K_a \times 10^5$ (L mol^{-1})	*n*	ΔG (kJ mol^{-1})	ΔH (kJ mol^{-1})	ΔS (J $mol^{-1}K^{-1}$)
298	11.38	1.21	-15.20	-76.12	-204.41
308	2.03	1.09	-13.16		
318	0.13	0.90	-11.12		

5.4 Conclusions

A imine bond incorporated metal-organic framework (MOF) having MIL-53 framework topology was synthesized by the condensation reaction between MIL-53-NH_2 and 2,3,4-trihydroxy benzaldehyde. FT-IR spectroscopy, mass spectrometry and NMR spectroscopy clearly revealed the formation of an imine bond after the condensation reaction. Moreover, X-ray powder diffraction (XRPD) experiments revealed that the material retained its structural integrity even after the condensation reaction. The post-synthetically modified material was successfully employed for the selective and sensitive recognition of bilirubin (a key biomarker for jaundice) in HEPES buffer medium. The strong blue fluorescence of the HEPES buffer suspension of the probe was completely quenched by bilirubin solution due to static quenching process, which can be clearly visualized by naked eye.

Moreover, the detection limit (1.26 pM) of the probe towards bilirubin is quite lower than the normal concentration level of bilirubin in human blood plasma (25 μmol/L to 50 μmol/L). Furthermore, other bio-molecules and metal ions had no interference during the fluorescence quenching of the probe by bilirubin. The detection efficacy of bilirubin by the material was further examined in human blood serum and urine samples. Hence, this material can be applied as a clinical diagnostic tool for the identification of jaundice.

5.5 References

1. B. Rolinski, H. Küster, B. Ugele, R. Gruber and K. Horn, *Clin. Chem.*, 2001, **47**, 1845-1847.
2. Y.-F. Shen, M.-R. Tsai, S.-C. Chen, Y.-S. Leung, C.-T. Hsieh, Y.-S. Chen, F.-L. Huang, R. P. Obena, M. M. L. Zulueta, H.-Y. Huang, W.-J. Lee, K.-C. Tang, C.-T. Kung, M.-H. Chen, D.-B. Shieh, Y.-J. Chen, T.-M. Liu, P.-T. Chou and C.-K. Sun, *Anal. Chem.*, 2015, **87**, 7575-7582.
3. J. Fevery, *Liver Int.*, 2008, **28**, 592-605.
4. L. Vítek and H. A. Schwertner, *Adv. Clin. Chem.*, 2007, **43**, 1-57.
5. M. E. Vogel and S. D. Zucker, *Inflamm Cell Signal*, 2016, **3**, e1178.
6. S. Dore, M. Takahashi, C. D. Ferris, L. D. Hester, D. Guastella and S. H. Snyder, *Proc. Natl. Acad. Sci. USA*, 1999, **96**, 2445-2450.
7. P. J. Syapin, *Br J Pharmacol.*, 2008, **155**, 623-640.
8. K. E. Brown, D. D. Sin, H. Voelker, J. E. Connett, D. E. Niewoehner and K. M. Kunisak, *Respir Res.*, 2017, **18**, 179-186.
9. M. Szabó, Z. Veres, A. Bátai-Konczos, O. Kékesi, E. Kis, K. Szabó and K. Jemnitz, *Toxicol. In Vitro*, 2014, **28**, 1136-1143.
10. M. Franchini, G. Targher and G. Lippi, *Adv Clin Chem.*, 2010, **50**, 47-63.
11. M. A. Brito, A. I. Rosa, A. S. Falcão, A. Fernandes, R. F. M. Silva, D. A. Butterfield and D. Brites, *Neurobiology of Disease*, 2008, **29**, 30-40.
12. S. Silbernagl and A. Despopoulos, *Color Atlas of Physiology, 6th ed.*, Thieme: Stuttgart, 2009.
13. H. Wei, L. Xu, J. Ren and L. Jia, *Colloids Surf., A*, 2012, **405**, 38-44.
14. C. Carreira-Blanco, P. Singer, R. Diller and J. L. P. Lustres, *Phys. Chem. Chem. Phys.*, 2016, **18**, 7148-7155.

15. M. J. Maisels, *CMAJ*, 2015, **187**, 335-343.
16. B. T. Doumas, B. W. Perry, E. A. Sasse and J. V. J. Straumfjord, *Clin. Chem.*, 1973, **19**, 984-993.
17. G. J. Maghzal, M. C. Leck, E. Collinson, C. Li and R. J. Stocker, *J. Biol. Chem.*, 2009, **284**, 29251-29259.
18. K. H. Falchuk, J. M. Contin, T. S. Dziedzic, Z. Feng, T. C. French, G. J. Heffron and M. Montorzi, *Proc. Natl. Acad. Sci. U. S. A.*, 2002, **99**, 251-256.
19. J. Wang, D. B. Luo and P. A. M. Farias, *J. Electroanal. Chem. Interfacial Electrochem.*, 1985, **185**, 61-71.
20. L. P. Palilis, A. C. Calokerinos and N. Grekas, *Anal. Chim. Acta*, 1996, **333**, 267-275.
21. N. Nath and A. Chilkoti, *Anal. Chem.*, 2004, **76**, 5370-5378.
22. J. Narang, N. Chauhan, A. Mathur, V. Chaturvedi and C. S. Pundir, *Adv. Mater. Lett.*, 2015, **6**, 1012-1017.
23. M. A. Rahman, K. S. Lee, D. S. Park, M. S. Won and Y. B. Shim, *Biosens. Bioelectron.*, 2008, **23**, 857-864.
24. C. Wang, G. Wang and B. Fang, *Microchim. Acta*, 2009, **164**, 113-118.
25. R. N. Rand and A. d. Pasqua, *Clin. Chem.*, 1962, **8**, 570-578.
26. B. Batra, S. Lata, Sunny, J. S. Rana and C. S. Pundir, *Biosens. Bioelectron.*, 2013, **44**, 64-69.
27. M. Santhosh, S. R. Chinnadayyala, N. K. Singh and P. Goswami, *Bioelectrochemistry*, 2016, **111**, 7-14.
28. G.-J. Mao, T.-T. Wei, X. X. Wang, S. Huan, D.-Q. Lu, J. Zhang, X.-B. Zhang, W. Tan, G.-L. Shen and R.-Q. Yu, *Anal. Chem.*, 2013, **85**, 7875-7881.
29. H. Chen, Y. Xie, A. M. Kirillov, L. Liu, M. Yu, W. Liu and Y. A. Tang, *Chem. Commun.*, 2015, **51**, 5036-5039.
30. S. Ellairaja, K. Shenbagavalli, S. Ponmariappan and V. S. Vasantha, *Biosens. Bioelectron.*, 2017, **91**, 82-88.
31. T. Senthilkumar and S. K. Asha, *Macromolecules*, 2015, **48**, 3449-3461.
32. Y. Du, X. Li, X. Lv and Q. Jia, *ACS Appl. Mater. Interfaces*, 2017, **9**, 30925-30932.
33. N. Stock and S. Biswas, *Chem. Rev.*, 2012, **112**, 933-969.
34. W. P. Lustig, S. Mukherjee, N. D. Rudd, A. V. Desai, J. Li and S. K. Ghosh, *Chem.Soc.Rev.*, 2017, **46**, 3242-3285.
35. C. Wang, D. Liu and W. Lin, *J. Am. Chem. Soc.*, 2013, **135**, 13222-13234.

36. K. Vellingiri, A. Deep, K.-H. Kim, D. W. Boukhvalov, P. Kumar and Q. Yao, *Sens. Actuators, B*, 2017, **241**, 938-948.
37. A. Das, S. Banesh, V. Trivedi and S. Biswas, *Dalton Trans.*, 2018, **47**, 2690-2700.
38. M. SK and S. Biswas, *CrystEngComm.*, 2016, **18**, 3104-3113.
39. S. Nandi, H. Reinsch, S. Banesh, N. Stock, V. Trivedi and S. Biswas, *Dalton Trans.*, 2017, **46**, 12856-12864.
40. Y. S. Yang, K. Z. Wang and D. P. Yan, *ACS Appl. Mater. Interfaces*, 2016, **8**, 15489-15496.
41. L. E. Kreno, K. Leong, O. K. Farha, M. Allendorf, R. P. V. Duyne and J. T. Hupp, *Chem. Rev.*, 2012, **112**, 1105-1125.
42. Y. Cui, Y. Yue, G. Qian and B. Chen, *Chem. Rev.*, 2012, **112**, 1126-1162.
43. X. Zhang, J. Zhang, Q. Hu, Y. Cui, Y. Yang and G. Qian, *Appl. Surf. Sci.*, 2015, **355**, 814-819.
44. R. Dalapati and S. Biswas, *Sens. Actuators, B*, 2017, **239**, 759-767.
45. Z. Wang and S. M. Cohen, *Chem. Soc. Rev.*, 2009, **38**, 1315-1329.
46. S. M. Cohen, *Chem. Rev.*, 2012, **112**, 970-1000.
47. G. L. Fan and D. P. Yan, *Sci. Rep.*, 2015, **4**, 4933-4940.
48. J. N. Hao and B. Yan, *Chem. Commun.*, 2015, **51**, 14509-14512.
49. T. Ahnfeldt, D. Gunzelmann, T. Loiseau, D. Hirsemann, J. Senker, G. Fe´rey and N. Stock, *Inorg. Chem.*, 2009, **48**, 3057-3064.
50. S. Nandi, S. Banesh, V. Trivedi and S. Biswas, *Analyst*, 2018, **143**, 1482-1491.
51. T. Ahnfeldt, D. Gunzelmann, T. Loiseau, D. Hirsemann, J. Senker, G. Férey and N. Stock, *Inorg. Chem.*, 2009, **48**, 3057-3064.
52. X. Cheng, A. Zhang, K. Hou, M. Liu, Y. Wang, C. Song, G. Zhang and X. Guo, *Dalton Trans.*, 2013, **42**, 13698-13705.
53. D. L. Pavia, G. M. Lampman, G. S. Kriz and J. A. Vyvyan, *Introduction to spectroscopy*, Thomson Brooks/Cole Stamford, USA, 5th edn., 2015.
54. M. Kassymov, A. d. Mahieu, S. Chaemchuen, P. Demeyere, B. Mousavi, S. Zhuiykov, M. S. Yusubov and F. Verpoort, *Catal. Sci. Technol.*, 2018, **8**, 4129-4140.
55. T. Balamurugan and S. Berchmans, *RSC Adv.*, 2015, **5**, 50470-50477.
56. N. Chauhan, R. Rawal, V. Hooda and U. Jain, *RSC Adv.*, 2016, **6**, 63624-63633.
57. M. M. Rahman, M. M. Hussain and A. M. Asiri, *Prog. Nat. Sci.: Mater. Int.*, 2017, **27**, 566-573.

58. M. Thangamuthu, W. E. Gabriel, C. Santschi and O. J. F. Martin, *sensors*, 2018, **18**, E800.
59. L.-L. Liu, Y.-Z. Yu, X.-J. Zhao, Y.-R. Wang, F.-Y. Cheng, M.-K. Zhang, J.-J. Shu and L. Liu, *Dalton Trans.*, 2018, **47**, 7787-7794.
60. F. Zhang, H. Yao, Y. Zhao, X. Li, G. Zhang and Y. Yang, *Talanta*, 2017, **174**, 660-666.
61. C.-X. Yang, H.-B. Ren and X.-P. Yan, *Anal. Chem.*, 2013, **85**, 7441-7446.
62. L.-J. Zhou, W.-H. Deng, Y.-L. Wang, G. Xu, S.-G. Yin and Q.-Y. Liu, *Inorg. Chem.*, 2016, **55**, 6271-6277.
63. J. Wang, T. Xia, X. Zhang, Q. Zhang, Y. Cui, Y. Yang and G. Qian, *RSC Adv.*, 2017, **7**, 54892-54897.
64. A. Gopi, S. Lingamoorthy, S. Soman, K. Yoosaf, R. Haridas and S. Das, *J. Phys. Chem. C*, 2016, **120**, 26569-26578.
65. K. Campbell, A. Zappas, U. Bunz, Y. S. Thio and D. G. Bucknall, *J. Photochem. Photobiol., A*, 2012, **249**, 41-46.
66. H. He, Y. Song, F. Sun, Z. Bian, L. Gao and G. Zhu, *J. Mater. Chem. A*, 2015, **3**, 16598-16603.
67. S. Pramanik, Z. Hu, X. Zhang, C. Zheng, S. Kelly and J. Li, *Chem. Eur. J*, 2013, **19**, 15964 -15971.
68. K. S. k-Nagy and L. Biczók, *Photochem. Photobiol. Sci.*, 2004, **3**, 389-395.
69. T. Senthilkumar and S. K. Asha, *Macromolecules*, 2013, **46**, 2159-2171.
70. M. Santhosh, S. R. Chinnadayyala, A. Kakoti and P. Goswami, *Biosens. Bioelectron.*, 2014, **59**, 370-376.
71. Z. Zhang, C. He and X. Chen, *Mater. Chem. Front.*, 2018, **2**, 1765-1778.
72. Y. H. Lee, Y. Tang, P. Verwilst, W. Lin and J. S. Kim, *Chem. Commun.*, 2016, **52**, 11247-11250.
73. M. Maity, S. Dolui and N. C. Maiti, *Phys. Chem. Chem. Phys.*, 2015, **17**, 31216-31227.
74. Y. Li, K. Liu, W.-J. Li, A. Guo, F.-Y. Zhao, H. Liu and W.-J. Ruan, *J. Phys. Chem. C*, 2015, **119**, 28544-28550.
75. J. Sun, J. Zhao, L. Wang, H. Li, F. Yang and X. Yang, *ACS Sens.*, 2018, **3**, 183-190.
76. H. Lu, S. Quan and S. Xu, *J. Agric. Food Chem.*, 2017, **65**, 9807-9814.
77. H. Liu, M. Li, Y. Xia and X. Ren, *ACS Appl. Mater. Interfaces*, 2017, **9**, 120-126.

78. A. S. Tanwar, L. R. Adil, M. A. Afroz and P. K. Iyer, *ACS Sens.*, 2018, **3**, 1451-1461.
79. L. L. Liu, Y.-Z. Yu, X.-J. Zhao, Y.-R. Wang, F.-Y. Cheng, M.-K. Zhang, J.-J. Shu and L. Liu, *Dalton Trans.*, 2018, 7787-7794.
80. H. Yan, H. Ni, J. Jia, C. Shan, T. Zhang, Y. Gong, X. Li, J. Cao, W. Wu, W. Liu and Y. Tang, *Anal. Chem.*, 2019, **91**, 5225-5234.
81. H. Tai, X. Bao, Y. He, X. Du, G. Xie and Y. Jiang, *IEEE Sens. J.*, 2015, **15**, 6904-6911.
82. X. Xiong, J. He, H. Yang, P. Tang, B. Tang, Q. Sun and H. Li, *RSC Adv.*, 2017, **7**, 48942-48951.
83. T. A. Wani, A. H. Bakheit, S. Zargar, M. A. Hamidaddin and I. A. Darwish, *PLoS One*, 2017, **12**, e0176015.
84. Y. Ni, G. Liu and S. Kokot, *Talanta*, 2008, **76**, 513-521.
85. P. D. Ross and S. Subramanian, *Biochemistry*, 1981, **20**, 3096-3102.
86. M. Maity, S. Dolui and N. C. Maiti, *Phys. Chem. Chem. Phys.*, 2015, **17**, 31216-31227.

CONCLUSIONS & FUTURE PROSPECTS

Conclusions:

Metal–organic frameworks (MOFs) are actually open, crystalline coordination architectures with porous nature. Beside gas storage and separation, catalysis, proton conduction etc., MOFs recently have become a very hot topic in the area of chemical sensing. Diverse types of chemical functionalities have been carefully and rationally implanted into the framework of MOFs, which bring interesting properties to the material. MOFs with wide variety of fluorometric detection properties have been developed so far. For detection of environmental toxin and biomolecules, the detection study must be performed in aqueous medium to maintain the real environment. But, the preparation of aqua stable MOFs having great selectivity and sensitivity towards the targeted analyte is still a difficult job in the field of research. The work represented in this thesis emphasizes on the design, synthesis, characterization of aqua stable MOFs and thorough sensing study of environmental and biological threats. For this purpose, metal ions with higher oxidation states (i.e. Al(III), Zr(IV), etc.) and carboxylic acid ligands (i.e. terephthalic acid, isophthalic acid, etc.) were employed for the construction of the super aqua stable MOFs (i.e. CAU-10, MIL-53 and UiO-66). The frameworks were judiciously functionalized by particular functionality with the specially functionalized ligand or by post-synthetic modification. The specific functionalities act as recognition sites for the targeted analytes. Hence, basically site-specific detection of environmental toxin and biological compounds are demonstrated here.

In the initial attempt, synthesis, comprehensively characterization and fluorometric detection of H_2S by an Al(III)-based, azide-functionalized MOF material called CAU-10-N_3 are described. The activated material has been demonstrated to detect extracellular H_2S (in 10 mM HEPES having pH of 7.4) with rapidness, selectivity and high sensitivity. The compound is capable of sensing H_2S even in the presence of other interfering biological molecules and anions commonly found in biological systems. The limit of detection of the material (2.65 μM) for H_2S is lower than for the existing MOF-type fluorescent probes for H_2S. The MOF compound shows very short response time and considerably high fold-increase in

fluorescence emission intensity when treated with H_2S in HEPES buffer. Interestingly, the probe is capable of detecting H_2S inside the macrophage cells. H_2S-mediated reduction of azide groups into auxo-chromic amine group is the main reason behind the rapid emission enhancement of the material. The conversion of azide functionality to amine group is confirmed by several analytical techniques such as FT-IR spectroscopy, mass spectrometry and ^1H NMR spectroscopy. Furthermore, the excellent detection performance (in terms of short response time and extraordinary fold-increment in fluorescence intensity) in pure aqueous medium makes CAU-10-N_3 a possible candidate for the regulation of H_2S concentration in environmental (aqueous) samples.

After achieving great selectivity and sensitivity towards H_2S by the CAU-10-N_3 material, we have planned to design a material for colorimetric and fluorometric detection of H_2S in real water samples (i.e. in environmental water samples and human blood plasma). Hence, we have prepared a new dinitro-functionalized Zr(IV) MOF called UiO-66-$(NO_2)_2$ and detailed detection study of H_2S in different media was carried out. The material has excellent efficiency for selective detection of H_2S in the HEPES buffer medium with a detection limit of 14.14 µM. The fold increment (35-fold at saturation) in the fluorescence intensity of this material is remarkably higher than the formerly reported mononitro- and azide-functionalized Zr(IV) and Ce(IV) based UiO-66 MOFs. In addition, the compound is a promising platform for the naked-eye colorimetric recognition of H_2S under day light. In presence of other competing biomolecules, its selectivity towards H_2S remains unaltered. Apart from the sensing of extracellular H_2S, the presence of H_2S in living cells can be detected by this biocompatible, nontoxic MOF using live-cell imaging experiment. Hence, the presented material is a suitable probe for the selective and sensitive recognition of H_2S in biological medium. In addition, we have demonstrated the aptness of the probe for detection of H_2S concentration in human blood plasma and also analyze sulfide concentration in environmental water samples. Furthermore, the possible detection mechanism was thoroughly investigated by mass spectrometry and ^1H NMR spectroscopy.

In our next work, we moved for the detection of formaldehyde in liquid and gaseous phase. Formaldehyde is a potent preservative and it is widely applied in different industries. For its carcinogenic effect, real time monitoring of formaldehyde is a challenging job. Keeping focus on selective detection of formaldehyde, a hydrazine functionalized Al-MIL-53 MOF material was prepared. The activated compound can be utilized as a fluorescence turn-on probe for the selective detection of formaldehyde (in

aqueous, HEPES buffer and vapor phase), even in the presence of potentially intrusive species. The fluorescence turn-on phenomenon can be explained by the inhibition of PET event (from hydrazine group to phenyl ring) owing to hydrazone formation. The anticipated mechanism was confirmed by mass analyses as well as by the specially designed inhibition experiments. The Al-MIL-53-N_2H_3 probe exhibited short response time (1 min) for formaldehyde in 10 mM HEPES buffer. It was also highly sensitive for formaldehyde having a detection limit of 8.37 μM (0.25 ppm) in HEPES buffer. In addition to the solution phase, the probe was capable of detecting formaldehyde in the vapor phase. Moreover, intracellular formaldehyde in breast cancer cells could be efficiently sensed by the material. As corroborated by the XRPD experiments, the crystallinity of the compound remained intact after the fluorescence sensing experiments. Therefore, the newly synthesized material is a potential probe for the real-time detection of formaldehyde in aqueous, vapor and simulated physiological media as well as inside the cancer cells.

Our last work mainly deals with the detection of bilirubin under biological conditions by an imine bond incorporated MIL-53 metal-organic framework (MOF). The MOF was synthesized by the condensation reaction between MIL-53-NH_2 and 2,3,4-trihydroxy benzaldehyde. FT-IR spectroscopy, mass spectrometry and NMR spectroscopy clearly revealed the formation of an imine bond after the condensation reaction. Moreover, X-ray powder diffraction (XRPD) experiments revealed that the material retained its structural integrity even after the condensation reaction. The post-synthetically modified material was successfully employed for the selective and sensitive recognition of bilirubin (a key biomarker for jaundice) in HEPES buffer medium. The strong blue fluorescence of the HEPES buffer suspension of the probe was completely quenched by bilirubin solution due to static quenching process, which can be clearly visualized by naked eye. Moreover, the detection limit (1.26 pM) of the probe towards bilirubin is quite lower than the normal concentration level of bilirubin in human blood plasma (25 μmol/L to 50 μmol/L). Furthermore, other bio-molecules and common biologically relevant metal ions had no interference during the fluorescence quenching of the probe by bilirubin. The detailed mechanistic investigation was also performed to find out the actual mechanism behind the quenching of emission intensity of the material in presence of bilirubin. The detection efficacy of bilirubin by the material was further examined in human blood serum and urine samples. Hence, this material can be applied as a clinical diagnostic tool for the identification of jaundice.

The thesis work mainly focuses on the design and synthesis of aqua stable MOFs and their potential applications in fluorescence-based detection of environmental and biological threats under physiological conditions. The fluorogenic sensing of environmental and biological toxic species by MOFs is still in the stage of infancy. There is a huge challenge and opportunity for the development of new MOF probes and evaluation of their sensing performances in terms of LOD, fold increment, response time, etc. Hence, it is believed that our study will trigger the research interests in the field of MOF-related sensors for fluorescence based chemical sensing.

Future prospects:

In future, we are planning to prepare stable MOFs with various functional groups, which can be applied in sensing and catalysis fields. There are several relatively unexplored functional groups like acetoxy, phthalimide, maleimide, boronic, allyloxy, etc. These functional groups can be incorporated in the linkers and the functionalized ligands can be employed for the synthesis of new MOFs by the reaction with several metal ions like Ga(III), Sc(III), Ti(IV), Cr(III), Cu(II), Zn(II), Cd(II), etc. The newly synthesized MOFs can be utilized for the detection purpose of several toxic compounds. For examples, ligands with acetoxy groups are prone to attack by hydrazine and perborate, maleimide functional MOFs can be utilized for thiol sensing etc. Furthermore, Ti-MOFs are reported for good photocatalytic applications. Hence, great possibilities are there for the application of proposed functionalized MOFs in the field of sensing and catalysis.

Copyright Clearance Center RightsLink®

Home | Help | Live Chat | SOUTICK NANDI

ACS Publications
Most Trusted. Most Cited. Most Read.

New Functionalized Flexible Al-MIL-53-X (X = -Cl, -Br, -CH3, -NO2, -(OH)2) Solids: Syntheses, Characterization, Sorption, and Breathing Behavior

Author: Shyam Biswas, Tim Ahnfeldt, Norbert Stock
Publication: Inorganic Chemistry
Publisher: American Chemical Society
Date: Oct 1, 2011

PERMISSION/LICENSE IS GRANTED FOR YOUR ORDER AT NO CHARGE

This type of permission/license, instead of the standard Terms & Conditions, is sent to you because no fee is being charged for your order. Please note the following:

- Permission is granted for your request in both print and electronic formats, and translations.
- If figures and/or tables were requested, they may be adapted or used in part.
- Please print this page for your records and send a copy of it to your publisher/graduate school.
- Appropriate credit for the requested material should be given as follows: "Reprinted (adapted) with permission from (COMPLETE REFERENCE CITATION). Copyright (YEAR) American Chemical Society." Insert appropriate information in place of the capitalized words.
- One-time permission is granted only for the use specified in your request. No additional uses are granted (such as derivative works or other editions). For any other uses, please submit a new request.

If credit is given to another source for the material you requested, permission must be obtained from that source.

BACK CLOSE WINDOW

Structures, Sorption Characteristics, and Nonlinear Optical Properties of a New Series of Highly Stable Aluminum MOFs

Author: Helge Reinsch, Monique A. van der Veen, Barbara Gil, et al
Publication: Chemistry of Materials
Publisher: American Chemical Society
Date: Jan 1, 2013

PERMISSION/LICENSE IS GRANTED FOR YOUR ORDER AT NO CHARGE

This type of permission/license, instead of the standard Terms & Conditions, is sent to you because no fee is being charged for your order. Please note the following:

- Permission is granted for your request in both print and electronic formats, and translations.
- If figures and/or tables were requested, they may be adapted or used in part.
- Please print this page for your records and send a copy of it to your publisher/graduate school.
- Appropriate credit for the requested material should be given as follows: "Reprinted (adapted) with permission from (COMPLETE REFERENCE CITATION). Copyright (YEAR) American Chemical Society." Insert appropriate information in place of the capitalized words.
- One-time permission is granted only for the use specified in your request. No additional uses are granted (such as derivative works or other editions). For any other uses, please submit a new request.

If credit is given to another source for the material you requested, permission must be obtained from that source.

BACK CLOSE WINDOW

Pyrazolate-Based Porphyrinic Metal–Organic Framework with Extraordinary Base-Resistance

Author: Kecheng Wang, Xiu-Liang Lv, Dawei Feng, et al
Publication: Journal of the American Chemical Society
Publisher: American Chemical Society
Date: Jan 1, 2016

Luminescent Functional Metal–Organic Frameworks

Author: Yuanjing Cui, Yanfeng Yue, Guodong Qian, et al
Publication: Chemical Reviews
Publisher: American Chemical Society
Date: Feb 1, 2012

PERMISSION/LICENSE IS GRANTED FOR YOUR ORDER AT NO CHARGE

This type of permission/license, instead of the standard Terms & Conditions, is sent to you because no fee is being charged for your order. Please note the following:

- Permission is granted for your request in both print and electronic formats, and translations.
- If figures and/or tables were requested, they may be adapted or used in part.
- Please print this page for your records and send a copy of it to your publisher/graduate school.
- Appropriate credit for the requested material should be given as follows: "Reprinted (adapted) with permission from (COMPLETE REFERENCE CITATION). Copyright (YEAR) American Chemical Society." Insert appropriate information in place of the capitalized words.
- One-time permission is granted only for the use specified in your request. No additional uses are granted (such as derivative works or other editions). For any other uses, please submit a new request.

If credit is given to another source for the material you requested, permission must be obtained from that source.

BACK CLOSE WINDOW

Highly Sensitive and Selective Sensing of Free Bilirubin Using Metal–Organic Frameworks-Based Energy Transfer Process

Author: Yaran Du, Xiqian Li, Xueju Lv, et al
Publication: Applied Materials
Publisher: American Chemical Society
Date: Sep 1, 2017

PERMISSION/LICENSE IS GRANTED FOR YOUR ORDER AT NO CHARGE

This type of permission/license, instead of the standard Terms & Conditions, is sent to you because no fee is being charged for your order. Please note the following:

- Permission is granted for your request in both print and electronic formats, and translations.
- If figures and/or tables were requested, they may be adapted or used in part.
- Please print this page for your records and send a copy of it to your publisher/graduate school.
- Appropriate credit for the requested material should be given as follows: "Reprinted (adapted) with permission from (COMPLETE REFERENCE CITATION). Copyright (YEAR) American Chemical Society." Insert appropriate information in place of the capitalized words.
- One-time permission is granted only for the use specified in your request. No additional uses are granted (such as derivative works or other editions). For any other uses, please submit a new request.

If credit is given to another source for the material you requested, permission must be obtained from that source.

BACK CLOSE WINDOW

Copyright Clearance Center RightsLink®

Home | Help | Live Chat | SOUTICK NANDI

Coordination polymers constructed from transition metal ions and organic N-containing heterocyclic ligands: Crystal structures and microporous properties

Author: Shin-ichiro Noro,Susumu Kitagawa,Tomoyuki Akutagawa,Takayoshi Nakamura
Publication: Progress in Polymer Science
Publisher: Elsevier
Date: March 2009

Order Completed

Thank you for your order.

This Agreement between Research Scholar -- SOUTICK NANDI ("You") and Elsevier ("Elsevier") consists of your license details and the terms and conditions provided by Elsevier and Copyright Clearance Center.

Your confirmation email will contain your order number for future reference.

License Number	4832030614008
License date	May 18, 2020

Printable Details

Licensed Content

Licensed Content Publisher	Elsevier
Licensed Content Publication	Progress in Polymer Science
Licensed Content Title	Coordination polymers constructed from transition metal ions and organic N-containing heterocyclic ligands: Crystal structures and microporous properties
Licensed Content Author	Shin-ichiro Noro,Susumu Kitagawa,Tomoyuki Akutagawa,Takayoshi Nakamura
Licensed Content Date	Mar 1, 2009
Licensed Content Volume	34
Licensed Content Issue	3
Licensed Content Pages	40
Journal Type	S&T

Order Details

Type of Use	reuse in a thesis/dissertation
Portion	figures/tables/illustrations
Number of figures/tables/illustrations	1
Format	both print and electronic
Are you the author of this Elsevier article?	No
Will you be translating?	No

About Your Work

Title	Fluorescence Based Detection of Environmental and Biological Threats by Functionalized Aqua-Stable Metal-Organic Frameworks
Institution name	IIT Guwahati
Expected presentation date	Oct 2020

Additional Data

Portions	Fig. 3

Requestor Location

Requestor Location	Research Scholar CHL-203, Department of Chemistry IIT Guwahati Assam Guwahati, 781039 India Attn: Research Scholar

Price

Total	0.00 USD

Tax Details

Publisher Tax ID	GB 494 6272 12

Total: 0.00 USD

CLOSE WINDOW ORDER MORE

Copyright Clearance Center RightsLink®

Home | Help | Live Chat | SOUTICK NANDI

The sensitive detection of formaldehyde in aqueous media using zirconium-based metal organic frameworks

Author: Kowsalya Vellingiri,Akash Deep,Ki-Hyun Kim,Danil W. Boukhvalov,Pawan Kumar,Qu Yao
Publication: Sensors and Actuators B: Chemical
Publisher: Elsevier
Date: 31 March 2017

Order Completed

Thank you for your order.

This Agreement between Research Scholar -- SOUTICK NANDI ("You") and Elsevier ("Elsevier") consists of your license details and the terms and conditions provided by Elsevier and Copyright Clearance Center.

Your confirmation email will contain your order number for future reference.

License Number	4832030206187
License date	May 18, 2020

Printable Details

Licensed Content

Licensed Content Publisher	Elsevier
Licensed Content Publication	Sensors and Actuators B: Chemical
Licensed Content Title	The sensitive detection of formaldehyde in aqueous media using zirconium-based metal organic frameworks
Licensed Content Author	Kowsalya Vellingiri,Akash Deep,Ki-Hyun Kim,Danil W. Boukhvalov,Pawan Kumar,Qu Yao
Licensed Content Date	Mar 31, 2017
Licensed Content Volume	241
Licensed Content Issue	n/a
Licensed Content Pages	11
Journal Type	S&T

Order Details

Type of Use	reuse in a thesis/dissertation
Portion	figures/tables/illustrations
Number of figures/tables/illustrations	1
Format	both print and electronic
Are you the author of this Elsevier article?	No
Will you be translating?	No

About Your Work

Title	Fluorescence Based Detection of Environmental and Biological Threats by Functionalized Aqua-Stable Metal-Organic Frameworks
Institution name	IIT Guwahati
Expected presentation date	Oct 2020

Additional Data

Portions	Fig. 3

Requestor Location

Requestor Location	Research Scholar CHL-203, Department of Chemistry IIT Guwahati Assam Guwahati, 781039 India Attn: Research Scholar

Price

Total	0.00 USD

Tax Details

Publisher Tax ID	GB 494 6272 12

Total: 0.00 USD

CLOSE WINDOW ORDER MORE

Copyright Clearance Center RightsLink® Home Help Live Chat SOUTICK NANDI

Luminescent sensors based on metal-organic frameworks

Author: Yingmu Zhang,Shuai Yuan,Gregory Day,Xuan Wang,Xinyu Yang,Hong-Cai Zhou
Publication: Coordination Chemistry Reviews
Publisher: Elsevier
Date: 1 January 2018

Order Completed

Thank you for your order.

This Agreement between Research Scholar -- SOUTICK NANDI ("You") and Elsevier ("Elsevier") consists of your license details and the terms and conditions provided by Elsevier and Copyright Clearance Center.

Your confirmation email will contain your order number for future reference.

License Number	4832031432378
License date	May 18, 2020

Printable Details

Licensed Content

Licensed Content Publisher	Elsevier
Licensed Content Publication	Coordination Chemistry Reviews
Licensed Content Title	Luminescent sensors based on metal-organic frameworks
Licensed Content Author	Yingmu Zhang,Shuai Yuan,Gregory Day,Xuan Wang,Xinyu Yang,Hong-Cai Zhou
Licensed Content Date	Jan 1, 2018
Licensed Content Volume	354
Licensed Content Issue	n/a
Licensed Content Pages	18
Journal Type	S&T

Order Details

Type of Use	reuse in a thesis/dissertation
Portion	figures/tables/illustrations
Number of figures/tables/illustrations	1
Format	both print and electronic
Are you the author of this Elsevier article?	No
Will you be translating?	No

About Your Work

Title	Fluorescence Based Detection of Environmental and Biological Threats by Functionalized Aqua-Stable Metal-Organic Frameworks
Institution name	IIT Guwahati
Expected presentation date	Oct 2020

Additional Data

Portions	Scheme 1

Requestor Location

Requestor Location	Research Scholar CHL-203, Department of Chemistry IIT Guwahati Assam Guwahati, 781039 India Attn: Research Scholar

Price

Total	0.00 USD

Tax Details

Publisher Tax ID	GB 494 6272 12

Total: 0.00 USD

CLOSE WINDOW ORDER MORE

Copyright Clearance Center RightsLink®

Home | Help | Live Chat | SOUTICK NANDI

SPRINGER NATURE

Reticular synthesis and the design of new materials

Author: Omar M. Yaghi et al
Publication: Nature
Publisher: Springer Nature
Date: Jun 12, 2003

Order Completed

Thank you for your order.

This Agreement between Research Scholar -- SOUTICK NANDI ("You") and Springer Nature ("Springer Nature") consists of your license details and the terms and conditions provided by Springer Nature and Copyright Clearance Center.

Your confirmation email will contain your order number for future reference.

License Number	4832031151981
License date	May 18, 2020

Printable Details

Licensed Content

Licensed Content Publisher	Springer Nature
Licensed Content Publication	Nature
Licensed Content Title	Reticular synthesis and the design of new materials
Licensed Content Author	Omar M. Yaghi et al
Licensed Content Date	Jun 12, 2003

Order Details

Type of Use	Thesis/Dissertation
Requestor type	academic/university or research institute
Format	print and electronic
Portion	figures/tables/illustrations
Number of figures/tables/illustrations	1
High-res required	no
Will you be translating?	no
Circulation/distribution	1 - 29
Author of this Springer Nature content	no

About Your Work

Title	Fluorescence Based Detection of Environmental and Biological Threats by Functionalized Aqua-Stable Metal-Organic Frameworks
Institution name	IIT Guwahati
Expected presentation date	Oct 2020

Additional Data

Portions	Figure 2

Requestor Location

Requestor Location	Research Scholar CHL-203, Department of Chemistry IIT Guwahati Assam Guwahati, 781039 India Attn: Research Scholar

Tax Details

Price

Total	0.00 USD

Total: 0.00 USD

CLOSE WINDOW ORDER MORE

Copyright Clearance Center Marketplace™

Royal Society of Chemistry - License Terms and Conditions

This is a License Agreement between Soutick Nandi ("You") and Royal Society of Chemistry ("Publisher") provided by Copyright Clearance Center ("CCC"). The license consists of your order details, the terms and conditions provided by Royal Society of Chemistry, and the CCC terms and conditions.

All payments must be made in full to CCC.

Order Date	21-May-2020	Type of Use	Republish in a thesis/dissertation
Order license ID	1036418-1	Publisher	Royal Society of Chemistry
ISSN	2050-7496	Portion	Image/photo/illustration

LICENSED CONTENT

Publication Title	Journal of materials chemistry. A, Materials for energy and sustainability	Country	United Kingdom of Great Britain and Northern Ireland
Author/Editor	Royal Society of Chemistry (Great Britain)	Rightsholder	Royal Society of Chemistry
		Publication Type	e-Journal
Date	01/01/2013	URL	http://pubs.rsc.org/en/journals/journalissues/ta
Language	English		

REQUEST DETAILS

Portion Type	Image/photo/illustration	Distribution	Worldwide
Number of images / photos / illustrations	1	Translation	Original language of publication
Format (select all that apply)	Print, Electronic	Copies for the disabled?	No
		Minor editing privileges?	No
Who will republish the content?	Academic institution	Incidental promotional use?	No
Duration of Use	Life of current edition	Currency	USD
Lifetime Unit Quantity	Up to 499		
Rights Requested	Main product		

NEW WORK DETAILS

Title	Fluorescence Based Detection of Environmental and Biological Threats by Functionalized Aqua-Stable Metal-Organic Frameworks	Institution name	IIT Guwahati
		Expected presentation date	2020-10-21
Instructor name	Dr. Shyam P. Biswas		

ADDITIONAL DETAILS

Order reference number	N/A	The requesting person / organization to appear on the license	Soutick Nandi

REUSE CONTENT DETAILS

Title, description or numeric reference of the portion(s)	Fig. 1	**Title of the article/chapter the portion is from**	Nickel-substituted zeolitic imidazolate frameworks for time-resolved alcohol sensing and photocatalysis under visible light
Editor of portion(s)	N/A	**Author of portion(s)**	Royal Society of Chemistry (Great Britain)
Volume of serial or monograph	N/A	**Issue, if republishing an article from a serial**	N/A
Page or page range of portion	5725	**Publication date of portion**	2013-01-01

CCC Republication Terms and Conditions

1. Description of Service; Defined Terms. This Republication License enables the User to obtain licenses for republication of one or more copyrighted works as described in detail on the relevant Order Confirmation (the "Work(s)"). Copyright Clearance Center, Inc. ("CCC") grants licenses through the Service on behalf of the rightsholder identified on the Order Confirmation (the "Rightsholder"). "Republication", as used herein, generally means the inclusion of a Work, in whole or in part, in a new work or works, also as described on the Order Confirmation. "User", as used herein, means the person or entity making such republication.

2. The terms set forth in the relevant Order Confirmation, and any terms set by the Rightsholder with respect to a particular Work, govern the terms of use of Works in connection with the Service. By using the Service, the person transacting for a republication license on behalf of the User represents and warrants that he/she/it (a) has been duly authorized by the User to accept, and hereby does accept, all such terms and conditions on behalf of User, and (b) shall inform User of all such terms and conditions. In the event such person is a "freelancer" or other third party independent of User and CCC, such party shall be deemed jointly a "User" for purposes of these terms and conditions. In any event, User shall be deemed to have accepted and agreed to all such terms and conditions if User republishes the Work in any fashion.

3. Scope of License; Limitations and Obligations.

   3.1. All Works and all rights therein, including copyright rights, remain the sole and exclusive property of the Rightsholder. The license created by the exchange of an Order Confirmation (and/or any invoice) and payment by User of the full amount set forth on that document includes only those rights expressly set forth in the Order Confirmation and in these terms and conditions, and conveys no other rights in the Work(s) to User. All rights not expressly granted are hereby reserved.

   3.2. General Payment Terms: You may pay by credit card or through an account with us payable at the end of the month. If you and we agree that you may establish a standing account with CCC, then the following terms apply: Remit Payment to: Copyright Clearance Center, 29118 Network Place, Chicago, IL 60673-1291. Payments Due: Invoices are payable upon their delivery to you (or upon our notice to you that they are available to you for downloading). After 30 days, outstanding amounts will be subject to a service charge of 1-1/2% per month or, if less, the maximum rate allowed by applicable law. Unless otherwise specifically set forth in the Order Confirmation or in a separate written agreement signed by CCC, invoices are due and payable on "net 30" terms. While User may exercise the rights licensed immediately upon issuance of the Order Confirmation, the license is automatically revoked and is null and void, as if it had never been issued, if complete payment for the license is not received on a timely basis either from User directly or through a payment agent, such as a credit card company.

   3.3. Unless otherwise provided in the Order Confirmation, any grant of rights to User (i) is "one-time" (including the editions and product family specified in the license), (ii) is non-exclusive and non-transferable and (iii) is subject to any and all limitations and restrictions (such as, but not limited to, limitations on duration of use or circulation) included in the Order Confirmation or invoice and/or in these terms and conditions. Upon completion of the licensed use, User shall either secure a new permission for further use of the Work(s) or immediately cease any new use of the Work(s) and shall render inaccessible (such as by deleting or by removing or severing links or other locators) any further copies of the Work (except for copies printed on paper in accordance with this license and still in User's stock at the end of such period).

   3.4. In the event that the material for which a republication license is sought includes third party materials

(such as photographs, illustrations, graphs, inserts and similar materials) which are identified in such material as having been used by permission, User is responsible for identifying, and seeking separate licenses (under this Service or otherwise) for, any of such third party materials; without a separate license, such third party materials may not be used.

3.5. Use of proper copyright notice for a Work is required as a condition of any license granted under the Service. Unless otherwise provided in the Order Confirmation, a proper copyright notice will read substantially as follows: "Republished with permission of [Rightsholder's name], from [Work's title, author, volume, edition number and year of copyright]; permission conveyed through Copyright Clearance Center, Inc. " Such notice must be provided in a reasonably legible font size and must be placed either immediately adjacent to the Work as used (for example, as part of a by-line or footnote but not as a separate electronic link) or in the place where substantially all other credits or notices for the new work containing the republished Work are located. Failure to include the required notice results in loss to the Rightsholder and CCC, and the User shall be liable to pay liquidated damages for each such failure equal to twice the use fee specified in the Order Confirmation, in addition to the use fee itself and any other fees and charges specified.

3.6. User may only make alterations to the Work if and as expressly set forth in the Order Confirmation. No Work may be used in any way that is defamatory, violates the rights of third parties (including such third parties' rights of copyright, privacy, publicity, or other tangible or intangible property), or is otherwise illegal, sexually explicit or obscene. In addition, User may not conjoin a Work with any other material that may result in damage to the reputation of the Rightsholder. User agrees to inform CCC if it becomes aware of any infringement of any rights in a Work and to cooperate with any reasonable request of CCC or the Rightsholder in connection therewith.

4. Indemnity. User hereby indemnifies and agrees to defend the Rightsholder and CCC, and their respective employees and directors, against all claims, liability, damages, costs and expenses, including legal fees and expenses, arising out of any use of a Work beyond the scope of the rights granted herein, or any use of a Work which has been altered in any unauthorized way by User, including claims of defamation or infringement of rights of copyright, publicity, privacy or other tangible or intangible property.

5. Limitation of Liability. UNDER NO CIRCUMSTANCES WILL CCC OR THE RIGHTSHOLDER BE LIABLE FOR ANY DIRECT, INDIRECT, CONSEQUENTIAL OR INCIDENTAL DAMAGES (INCLUDING WITHOUT LIMITATION DAMAGES FOR LOSS OF BUSINESS PROFITS OR INFORMATION, OR FOR BUSINESS INTERRUPTION) ARISING OUT OF THE USE OR INABILITY TO USE A WORK, EVEN IF ONE OF THEM HAS BEEN ADVISED OF THE POSSIBILITY OF SUCH DAMAGES. In any event, the total liability of the Rightsholder and CCC (including their respective employees and directors) shall not exceed the total amount actually paid by User for this license. User assumes full liability for the actions and omissions of its principals, employees, agents, affiliates, successors and assigns.

6. Limited Warranties. THE WORK(S) AND RIGHT(S) ARE PROVIDED "AS IS". CCC HAS THE RIGHT TO GRANT TO USER THE RIGHTS GRANTED IN THE ORDER CONFIRMATION DOCUMENT. CCC AND THE RIGHTSHOLDER DISCLAIM ALL OTHER WARRANTIES RELATING TO THE WORK(S) AND RIGHT(S), EITHER EXPRESS OR IMPLIED, INCLUDING WITHOUT LIMITATION IMPLIED WARRANTIES OF MERCHANTABILITY OR FITNESS FOR A PARTICULAR PURPOSE. ADDITIONAL RIGHTS MAY BE REQUIRED TO USE ILLUSTRATIONS, GRAPHS, PHOTOGRAPHS, ABSTRACTS, INSERTS OR OTHER PORTIONS OF THE WORK (AS OPPOSED TO THE ENTIRE WORK) IN A MANNER CONTEMPLATED BY USER; USER UNDERSTANDS AND AGREES THAT NEITHER CCC NOR THE RIGHTSHOLDER MAY HAVE SUCH ADDITIONAL RIGHTS TO GRANT.

7. Effect of Breach. Any failure by User to pay any amount when due, or any use by User of a Work beyond the scope of the license set forth in the Order Confirmation and/or these terms and conditions, shall be a material breach of the license created by the Order Confirmation and these terms and conditions. Any breach not cured within 30 days of written notice thereof shall result in immediate termination of such license without further notice. Any unauthorized (but licensable) use of a Work that is terminated immediately upon notice thereof may be liquidated by payment of the Rightsholder's ordinary license price therefor; any unauthorized (and unlicensable) use that is not terminated immediately for any reason (including, for example, because materials containing the Work cannot reasonably be recalled) will be subject to all remedies available at law or in equity, but in no event to a payment of less than three times the Rightsholder's ordinary license price for the most closely analogous licensable use plus Rightsholder's and/or CCC's costs and expenses incurred in collecting such payment.

8. Miscellaneous.

8.1. User acknowledges that CCC may, from time to time, make changes or additions to the Service or to these

terms and conditions, and CCC reserves the right to send notice to the User by electronic mail or otherwise for the purposes of notifying User of such changes or additions; provided that any such changes or additions shall not apply to permissions already secured and paid for.

8.2. Use of User-related information collected through the Service is governed by CCC's privacy policy, available online here:https://marketplace.copyright.com/rs-ui-web/mp/privacy-policy

8.3. The licensing transaction described in the Order Confirmation is personal to User. Therefore, User may not assign or transfer to any other person (whether a natural person or an organization of any kind) the license created by the Order Confirmation and these terms and conditions or any rights granted hereunder; provided, however, that User may assign such license in its entirety on written notice to CCC in the event of a transfer of all or substantially all of User's rights in the new material which includes the Work(s) licensed under this Service.

8.4. No amendment or waiver of any terms is binding unless set forth in writing and signed by the parties. The Rightsholder and CCC hereby object to any terms contained in any writing prepared by the User or its principals, employees, agents or affiliates and purporting to govern or otherwise relate to the licensing transaction described in the Order Confirmation, which terms are in any way inconsistent with any terms set forth in the Order Confirmation and/or in these terms and conditions or CCC's standard operating procedures, whether such writing is prepared prior to, simultaneously with or subsequent to the Order Confirmation, and whether such writing appears on a copy of the Order Confirmation or in a separate instrument.

8.5. The licensing transaction described in the Order Confirmation document shall be governed by and construed under the law of the State of New York, USA, without regard to the principles thereof of conflicts of law. Any case, controversy, suit, action, or proceeding arising out of, in connection with, or related to such licensing transaction shall be brought, at CCC's sole discretion, in any federal or state court located in the County of New York, State of New York, USA, or in any federal or state court whose geographical jurisdiction covers the location of the Rightsholder set forth in the Order Confirmation. The parties expressly submit to the personal jurisdiction and venue of each such federal or state court.If you have any comments or questions about the Service or Copyright Clearance Center, please contact us at 978-750-8400 or send an e-mail to support@copyright.com.

v 1.1

Copyright Clearance Center Marketplace™

Royal Society of Chemistry - License Terms and Conditions

This is a License Agreement between Soutick Nandi ("You") and Royal Society of Chemistry ("Publisher") provided by Copyright Clearance Center ("CCC"). The license consists of your order details, the terms and conditions provided by Royal Society of Chemistry, and the CCC terms and conditions.

All payments must be made in full to CCC.

Order Date	21-May-2020	**Type of Use**	Republish in a thesis/dissertation
Order license ID	1036417-2		
ISSN	1460-4744	**Publisher**	ROYAL SOCIETY OF CHEMISTRY
		Portion	Image/photo/illustration

LICENSED CONTENT

Publication Title	Chemical Society reviews	**Country**	United Kingdom of Great Britain and Northern Ireland
Author/Editor	Royal Society of Chemistry (Great Britain)	**Rightsholder**	Royal Society of Chemistry
Date	01/01/1972	**Publication Type**	e-Journal
Language	English	**URL**	http://www.rsc.org/csr

REQUEST DETAILS

Portion Type	Image/photo/illustration	**Distribution**	Worldwide
Number of images / photos / illustrations	1	**Translation**	Original language of publication
Format (select all that apply)	Print, Electronic	**Copies for the disabled?**	No
		Minor editing privileges?	No
Who will republish the content?	Academic institution	**Incidental promotional use?**	No
Duration of Use	Life of current edition	**Currency**	USD
Lifetime Unit Quantity	Up to 499		
Rights Requested	Main product		

NEW WORK DETAILS

Title	Fluorescence Based Detection of Environmental and Biological Threats by Functionalized Aqua-Stable Metal-Organic Frameworks	**Institution name**	IIT Guwahati
		Expected presentation date	2020-10-21
Instructor name	Dr. Shyam P. Biswas		

ADDITIONAL DETAILS

Order reference number	N/A	**The requesting person / organization to appear on the license**	Soutick Nandi

REUSE CONTENT DETAILS

Title, description or numeric reference of the portion(s)	Fig. 3	Title of the article/chapter the portion is from	Postsynthetic modification of metal–organic frameworks—a progress report
Editor of portion(s)	N/A	Author of portion(s)	Royal Society of Chemistry (Great Britain)
Volume of serial or monograph	N/A	Issue, if republishing an article from a serial	N/A
Page or page range of portion	501	Publication date of portion	2010-11-23

CCC Republication Terms and Conditions

1. Description of Service; Defined Terms. This Republication License enables the User to obtain licenses for republication of one or more copyrighted works as described in detail on the relevant Order Confirmation (the "Work(s)"). Copyright Clearance Center, Inc. ("CCC") grants licenses through the Service on behalf of the rightsholder identified on the Order Confirmation (the "Rightsholder"). "Republication", as used herein, generally means the inclusion of a Work, in whole or in part, in a new work or works, also as described on the Order Confirmation. "User", as used herein, means the person or entity making such republication.

2. The terms set forth in the relevant Order Confirmation, and any terms set by the Rightsholder with respect to a particular Work, govern the terms of use of Works in connection with the Service. By using the Service, the person transacting for a republication license on behalf of the User represents and warrants that he/she/it (a) has been duly authorized by the User to accept, and hereby does accept, all such terms and conditions on behalf of User, and (b) shall inform User of all such terms and conditions. In the event such person is a "freelancer" or other third party independent of User and CCC, such party shall be deemed jointly a "User" for purposes of these terms and conditions. In any event, User shall be deemed to have accepted and agreed to all such terms and conditions if User republishes the Work in any fashion.

3. Scope of License; Limitations and Obligations.

   3.1. All Works and all rights therein, including copyright rights, remain the sole and exclusive property of the Rightsholder. The license created by the exchange of an Order Confirmation (and/or any invoice) and payment by User of the full amount set forth on that document includes only those rights expressly set forth in the Order Confirmation and in these terms and conditions, and conveys no other rights in the Work(s) to User. All rights not expressly granted are hereby reserved.

   3.2. General Payment Terms: You may pay by credit card or through an account with us payable at the end of the month. If you and we agree that you may establish a standing account with CCC, then the following terms apply: Remit Payment to: Copyright Clearance Center, 29118 Network Place, Chicago, IL 60673-1291. Payments Due: Invoices are payable upon their delivery to you (or upon our notice to you that they are available to you for downloading). After 30 days, outstanding amounts will be subject to a service charge of 1-1/2% per month or, if less, the maximum rate allowed by applicable law. Unless otherwise specifically set forth in the Order Confirmation or in a separate written agreement signed by CCC, invoices are due and payable on "net 30" terms. While User may exercise the rights licensed immediately upon issuance of the Order Confirmation, the license is automatically revoked and is null and void, as if it had never been issued, if complete payment for the license is not received on a timely basis either from User directly or through a payment agent, such as a credit card company.

   3.3. Unless otherwise provided in the Order Confirmation, any grant of rights to User (i) is "one-time" (including the editions and product family specified in the license), (ii) is non-exclusive and non-transferable and (iii) is subject to any and all limitations and restrictions (such as, but not limited to, limitations on duration of use or circulation) included in the Order Confirmation or invoice and/or in these terms and conditions. Upon completion of the licensed use, User shall either secure a new permission for further use of the Work(s) or immediately cease any new use of the Work(s) and shall render inaccessible (such as by deleting or by removing or severing links or other locators) any further copies of the Work (except for copies printed on paper in accordance with this license and still in User's stock at the end of such period).

   3.4. In the event that the material for which a republication license is sought includes third party materials (such as photographs, illustrations, graphs, inserts and similar materials) which are identified in such material as having been used by permission, User is responsible for identifying, and seeking separate

licenses (under this Service or otherwise) for, any of such third party materials; without a separate license, such third party materials may not be used.

3.5. Use of proper copyright notice for a Work is required as a condition of any license granted under the Service. Unless otherwise provided in the Order Confirmation, a proper copyright notice will read substantially as follows: "Republished with permission of [Rightsholder's name], from [Work's title, author, volume, edition number and year of copyright]; permission conveyed through Copyright Clearance Center, Inc. " Such notice must be provided in a reasonably legible font size and must be placed either immediately adjacent to the Work as used (for example, as part of a by-line or footnote but not as a separate electronic link) or in the place where substantially all other credits or notices for the new work containing the republished Work are located. Failure to include the required notice results in loss to the Rightsholder and CCC, and the User shall be liable to pay liquidated damages for each such failure equal to twice the use fee specified in the Order Confirmation, in addition to the use fee itself and any other fees and charges specified.

3.6. User may only make alterations to the Work if and as expressly set forth in the Order Confirmation. No Work may be used in any way that is defamatory, violates the rights of third parties (including such third parties' rights of copyright, privacy, publicity, or other tangible or intangible property), or is otherwise illegal, sexually explicit or obscene. In addition, User may not conjoin a Work with any other material that may result in damage to the reputation of the Rightsholder. User agrees to inform CCC if it becomes aware of any infringement of any rights in a Work and to cooperate with any reasonable request of CCC or the Rightsholder in connection therewith.

4. Indemnity. User hereby indemnifies and agrees to defend the Rightsholder and CCC, and their respective employees and directors, against all claims, liability, damages, costs and expenses, including legal fees and expenses, arising out of any use of a Work beyond the scope of the rights granted herein, or any use of a Work which has been altered in any unauthorized way by User, including claims of defamation or infringement of rights of copyright, publicity, privacy or other tangible or intangible property.

5. Limitation of Liability. UNDER NO CIRCUMSTANCES WILL CCC OR THE RIGHTSHOLDER BE LIABLE FOR ANY DIRECT, INDIRECT, CONSEQUENTIAL OR INCIDENTAL DAMAGES (INCLUDING WITHOUT LIMITATION DAMAGES FOR LOSS OF BUSINESS PROFITS OR INFORMATION, OR FOR BUSINESS INTERRUPTION) ARISING OUT OF THE USE OR INABILITY TO USE A WORK, EVEN IF ONE OF THEM HAS BEEN ADVISED OF THE POSSIBILITY OF SUCH DAMAGES. In any event, the total liability of the Rightsholder and CCC (including their respective employees and directors) shall not exceed the total amount actually paid by User for this license. User assumes full liability for the actions and omissions of its principals, employees, agents, affiliates, successors and assigns.

6. Limited Warranties. THE WORK(S) AND RIGHT(S) ARE PROVIDED "AS IS". CCC HAS THE RIGHT TO GRANT TO USER THE RIGHTS GRANTED IN THE ORDER CONFIRMATION DOCUMENT. CCC AND THE RIGHTSHOLDER DISCLAIM ALL OTHER WARRANTIES RELATING TO THE WORK(S) AND RIGHT(S), EITHER EXPRESS OR IMPLIED, INCLUDING WITHOUT LIMITATION IMPLIED WARRANTIES OF MERCHANTABILITY OR FITNESS FOR A PARTICULAR PURPOSE. ADDITIONAL RIGHTS MAY BE REQUIRED TO USE ILLUSTRATIONS, GRAPHS, PHOTOGRAPHS, ABSTRACTS, INSERTS OR OTHER PORTIONS OF THE WORK (AS OPPOSED TO THE ENTIRE WORK) IN A MANNER CONTEMPLATED BY USER; USER UNDERSTANDS AND AGREES THAT NEITHER CCC NOR THE RIGHTSHOLDER MAY HAVE SUCH ADDITIONAL RIGHTS TO GRANT.

7. Effect of Breach. Any failure by User to pay any amount when due, or any use by User of a Work beyond the scope of the license set forth in the Order Confirmation and/or these terms and conditions, shall be a material breach of the license created by the Order Confirmation and these terms and conditions. Any breach not cured within 30 days of written notice thereof shall result in immediate termination of such license without further notice. Any unauthorized (but licensable) use of a Work that is terminated immediately upon notice thereof may be liquidated by payment of the Rightsholder's ordinary license price therefor; any unauthorized (and unlicensable) use that is not terminated immediately for any reason (including, for example, because materials containing the Work cannot reasonably be recalled) will be subject to all remedies available at law or in equity, but in no event to a payment of less than three times the Rightsholder's ordinary license price for the most closely analogous licensable use plus Rightsholder's and/or CCC's costs and expenses incurred in collecting such payment.

8. Miscellaneous.

8.1. User acknowledges that CCC may, from time to time, make changes or additions to the Service or to these terms and conditions, and CCC reserves the right to send notice to the User by electronic mail or

otherwise for the purposes of notifying User of such changes or additions; provided that any such changes or additions shall not apply to permissions already secured and paid for.

8.2. Use of User-related information collected through the Service is governed by CCC's privacy policy, available online here:https://marketplace.copyright.com/rs-ui-web/mp/privacy-policy

8.3. The licensing transaction described in the Order Confirmation is personal to User. Therefore, User may not assign or transfer to any other person (whether a natural person or an organization of any kind) the license created by the Order Confirmation and these terms and conditions or any rights granted hereunder; provided, however, that User may assign such license in its entirety on written notice to CCC in the event of a transfer of all or substantially all of User's rights in the new material which includes the Work(s) licensed under this Service.

8.4. No amendment or waiver of any terms is binding unless set forth in writing and signed by the parties. The Rightsholder and CCC hereby object to any terms contained in any writing prepared by the User or its principals, employees, agents or affiliates and purporting to govern or otherwise relate to the licensing transaction described in the Order Confirmation, which terms are in any way inconsistent with any terms set forth in the Order Confirmation and/or in these terms and conditions or CCC's standard operating procedures, whether such writing is prepared prior to, simultaneously with or subsequent to the Order Confirmation, and whether such writing appears on a copy of the Order Confirmation or in a separate instrument.

8.5. The licensing transaction described in the Order Confirmation document shall be governed by and construed under the law of the State of New York, USA, without regard to the principles thereof of conflicts of law. Any case, controversy, suit, action, or proceeding arising out of, in connection with, or related to such licensing transaction shall be brought, at CCC's sole discretion, in any federal or state court located in the County of New York, State of New York, USA, or in any federal or state court whose geographical jurisdiction covers the location of the Rightsholder set forth in the Order Confirmation. The parties expressly submit to the personal jurisdiction and venue of each such federal or state court.If you have any comments or questions about the Service or Copyright Clearance Center, please contact us at 978-750-8400 or send an e-mail to support@copyright.com.

v 1.1

Copyright Clearance Center Marketplace™

Royal Society of Chemistry - License Terms and Conditions

This is a License Agreement between Soutick Nandi ("You") and Royal Society of Chemistry ("Publisher") provided by Copyright Clearance Center ("CCC"). The license consists of your order details, the terms and conditions provided by Royal Society of Chemistry, and the CCC terms and conditions.

All payments must be made in full to CCC.

Order Date	21-May-2020	Type of Use	Republish in a thesis/dissertation
Order license ID	1036423-1		
ISSN	2050-7496	Publisher	Royal Society of Chemistry
		Portion	Image/photo/illustration

LICENSED CONTENT

Publication Title	Journal of materials chemistry. A, Materials for energy and sustainability	Country	United Kingdom of Great Britain and Northern Ireland
Author/Editor	Royal Society of Chemistry (Great Britain)	Rightsholder	Royal Society of Chemistry
		Publication Type	e-Journal
Date	01/01/2013	URL	http://pubs.rsc.org/en/journals/journalissues/ta
Language	English		

REQUEST DETAILS

Portion Type	Image/photo/illustration	Distribution	Worldwide
Number of images / photos / illustrations	1	Translation	Original language of publication
Format (select all that apply)	Print, Electronic	Copies for the disabled?	No
		Minor editing privileges?	No
Who will republish the content?	Academic institution	Incidental promotional use?	No
Duration of Use	Life of current edition	Currency	USD
Lifetime Unit Quantity	Up to 499		
Rights Requested	Main product		

NEW WORK DETAILS

Title	Fluorescence Based Detection of Environmental and Biological Threats by Functionalized Aqua-Stable Metal-Organic Frameworks	Institution name	IIT Guwahati
		Expected presentation date	2020-10-21
Instructor name	Dr. Shyam P. Biswas		

ADDITIONAL DETAILS

Order reference number	N/A	The requesting person / organization to appear on the license	Soutick Nandi

REUSE CONTENT DETAILS

Title, description or numeric reference of the portion(s)	Fig. 3	Title of the article/chapter the portion is from	Fine-tuning metal–organic framework performances by spatially-differentiated postsynthetic modification
Editor of portion(s)	N/A	Author of portion(s)	Royal Society of Chemistry (Great Britain)
Volume of serial or monograph	N/A	Issue, if republishing an article from a serial	N/A
Page or page range of portion	4	Publication date of portion	2017-12-19

CCC Republication Terms and Conditions

1. Description of Service; Defined Terms. This Republication License enables the User to obtain licenses for republication of one or more copyrighted works as described in detail on the relevant Order Confirmation (the "Work(s)"). Copyright Clearance Center, Inc. ("CCC") grants licenses through the Service on behalf of the rightsholder identified on the Order Confirmation (the "Rightsholder"). "Republication", as used herein, generally means the inclusion of a Work, in whole or in part, in a new work or works, also as described on the Order Confirmation. "User", as used herein, means the person or entity making such republication.

2. The terms set forth in the relevant Order Confirmation, and any terms set by the Rightsholder with respect to a particular Work, govern the terms of use of Works in connection with the Service. By using the Service, the person transacting for a republication license on behalf of the User represents and warrants that he/she/it (a) has been duly authorized by the User to accept, and hereby does accept, all such terms and conditions on behalf of User, and (b) shall inform User of all such terms and conditions. In the event such person is a "freelancer" or other third party independent of User and CCC, such party shall be deemed jointly a "User" for purposes of these terms and conditions. In any event, User shall be deemed to have accepted and agreed to all such terms and conditions if User republishes the Work in any fashion.

3. Scope of License; Limitations and Obligations.

   3.1. All Works and all rights therein, including copyright rights, remain the sole and exclusive property of the Rightsholder. The license created by the exchange of an Order Confirmation (and/or any invoice) and payment by User of the full amount set forth on that document includes only those rights expressly set forth in the Order Confirmation and in these terms and conditions, and conveys no other rights in the Work(s) to User. All rights not expressly granted are hereby reserved.

   3.2. General Payment Terms: You may pay by credit card or through an account with us payable at the end of the month. If you and we agree that you may establish a standing account with CCC, then the following terms apply: Remit Payment to: Copyright Clearance Center, 29118 Network Place, Chicago, IL 60673-1291. Payments Due: Invoices are payable upon their delivery to you (or upon our notice to you that they are available to you for downloading). After 30 days, outstanding amounts will be subject to a service charge of 1-1/2% per month or, if less, the maximum rate allowed by applicable law. Unless otherwise specifically set forth in the Order Confirmation or in a separate written agreement signed by CCC, invoices are due and payable on "net 30" terms. While User may exercise the rights licensed immediately upon issuance of the Order Confirmation, the license is automatically revoked and is null and void, as if it had never been issued, if complete payment for the license is not received on a timely basis either from User directly or through a payment agent, such as a credit card company.

   3.3. Unless otherwise provided in the Order Confirmation, any grant of rights to User (i) is "one-time" (including the editions and product family specified in the license), (ii) is non-exclusive and non-transferable and (iii) is subject to any and all limitations and restrictions (such as, but not limited to, limitations on duration of use or circulation) included in the Order Confirmation or invoice and/or in these terms and conditions. Upon completion of the licensed use, User shall either secure a new permission for further use of the Work(s) or immediately cease any new use of the Work(s) and shall render inaccessible (such as by deleting or by removing or severing links or other locators) any further copies of the Work (except for copies printed on paper in accordance with this license and still in User's stock at the end of such period).

   3.4. In the event that the material for which a republication license is sought includes third party materials (such as photographs, illustrations, graphs, inserts and similar materials) which are identified in such material as having been used by permission, User is responsible for identifying, and seeking separate

licenses (under this Service or otherwise) for, any of such third party materials; without a separate license, such third party materials may not be used.

3.5. Use of proper copyright notice for a Work is required as a condition of any license granted under the Service. Unless otherwise provided in the Order Confirmation, a proper copyright notice will read substantially as follows: "Republished with permission of [Rightsholder's name], from [Work's title, author, volume, edition number and year of copyright]; permission conveyed through Copyright Clearance Center, Inc. " Such notice must be provided in a reasonably legible font size and must be placed either immediately adjacent to the Work as used (for example, as part of a by-line or footnote but not as a separate electronic link) or in the place where substantially all other credits or notices for the new work containing the republished Work are located. Failure to include the required notice results in loss to the Rightsholder and CCC, and the User shall be liable to pay liquidated damages for each such failure equal to twice the use fee specified in the Order Confirmation, in addition to the use fee itself and any other fees and charges specified.

3.6. User may only make alterations to the Work if and as expressly set forth in the Order Confirmation. No Work may be used in any way that is defamatory, violates the rights of third parties (including such third parties' rights of copyright, privacy, publicity, or other tangible or intangible property), or is otherwise illegal, sexually explicit or obscene. In addition, User may not conjoin a Work with any other material that may result in damage to the reputation of the Rightsholder. User agrees to inform CCC if it becomes aware of any infringement of any rights in a Work and to cooperate with any reasonable request of CCC or the Rightsholder in connection therewith.

4. Indemnity. User hereby indemnifies and agrees to defend the Rightsholder and CCC, and their respective employees and directors, against all claims, liability, damages, costs and expenses, including legal fees and expenses, arising out of any use of a Work beyond the scope of the rights granted herein, or any use of a Work which has been altered in any unauthorized way by User, including claims of defamation or infringement of rights of copyright, publicity, privacy or other tangible or intangible property.

5. Limitation of Liability. UNDER NO CIRCUMSTANCES WILL CCC OR THE RIGHTSHOLDER BE LIABLE FOR ANY DIRECT, INDIRECT, CONSEQUENTIAL OR INCIDENTAL DAMAGES (INCLUDING WITHOUT LIMITATION DAMAGES FOR LOSS OF BUSINESS PROFITS OR INFORMATION, OR FOR BUSINESS INTERRUPTION) ARISING OUT OF THE USE OR INABILITY TO USE A WORK, EVEN IF ONE OF THEM HAS BEEN ADVISED OF THE POSSIBILITY OF SUCH DAMAGES. In any event, the total liability of the Rightsholder and CCC (including their respective employees and directors) shall not exceed the total amount actually paid by User for this license. User assumes full liability for the actions and omissions of its principals, employees, agents, affiliates, successors and assigns.

6. Limited Warranties. THE WORK(S) AND RIGHT(S) ARE PROVIDED "AS IS". CCC HAS THE RIGHT TO GRANT TO USER THE RIGHTS GRANTED IN THE ORDER CONFIRMATION DOCUMENT. CCC AND THE RIGHTSHOLDER DISCLAIM ALL OTHER WARRANTIES RELATING TO THE WORK(S) AND RIGHT(S), EITHER EXPRESS OR IMPLIED, INCLUDING WITHOUT LIMITATION IMPLIED WARRANTIES OF MERCHANTABILITY OR FITNESS FOR A PARTICULAR PURPOSE. ADDITIONAL RIGHTS MAY BE REQUIRED TO USE ILLUSTRATIONS, GRAPHS, PHOTOGRAPHS, ABSTRACTS, INSERTS OR OTHER PORTIONS OF THE WORK (AS OPPOSED TO THE ENTIRE WORK) IN A MANNER CONTEMPLATED BY USER; USER UNDERSTANDS AND AGREES THAT NEITHER CCC NOR THE RIGHTSHOLDER MAY HAVE SUCH ADDITIONAL RIGHTS TO GRANT.

7. Effect of Breach. Any failure by User to pay any amount when due, or any use by User of a Work beyond the scope of the license set forth in the Order Confirmation and/or these terms and conditions, shall be a material breach of the license created by the Order Confirmation and these terms and conditions. Any breach not cured within 30 days of written notice thereof shall result in immediate termination of such license without further notice. Any unauthorized (but licensable) use of a Work that is terminated immediately upon notice thereof may be liquidated by payment of the Rightsholder's ordinary license price therefor; any unauthorized (and unlicensable) use that is not terminated immediately for any reason (including, for example, because materials containing the Work cannot reasonably be recalled) will be subject to all remedies available at law or in equity, but in no event to a payment of less than three times the Rightsholder's ordinary license price for the most closely analogous licensable use plus Rightsholder's and/or CCC's costs and expenses incurred in collecting such payment.

8. Miscellaneous.

8.1. User acknowledges that CCC may, from time to time, make changes or additions to the Service or to these terms and conditions, and CCC reserves the right to send notice to the User by electronic mail or

otherwise for the purposes of notifying User of such changes or additions; provided that any such changes or additions shall not apply to permissions already secured and paid for.

8.2. Use of User-related information collected through the Service is governed by CCC's privacy policy, available online here:https://marketplace.copyright.com/rs-ui-web/mp/privacy-policy

8.3. The licensing transaction described in the Order Confirmation is personal to User. Therefore, User may not assign or transfer to any other person (whether a natural person or an organization of any kind) the license created by the Order Confirmation and these terms and conditions or any rights granted hereunder; provided, however, that User may assign such license in its entirety on written notice to CCC in the event of a transfer of all or substantially all of User's rights in the new material which includes the Work(s) licensed under this Service.

8.4. No amendment or waiver of any terms is binding unless set forth in writing and signed by the parties. The Rightsholder and CCC hereby object to any terms contained in any writing prepared by the User or its principals, employees, agents or affiliates and purporting to govern or otherwise relate to the licensing transaction described in the Order Confirmation, which terms are in any way inconsistent with any terms set forth in the Order Confirmation and/or in these terms and conditions or CCC's standard operating procedures, whether such writing is prepared prior to, simultaneously with or subsequent to the Order Confirmation, and whether such writing appears on a copy of the Order Confirmation or in a separate instrument.

8.5. The licensing transaction described in the Order Confirmation document shall be governed by and construed under the law of the State of New York, USA, without regard to the principles thereof of conflicts of law. Any case, controversy, suit, action, or proceeding arising out of, in connection with, or related to such licensing transaction shall be brought, at CCC's sole discretion, in any federal or state court located in the County of New York, State of New York, USA, or in any federal or state court whose geographical jurisdiction covers the location of the Rightsholder set forth in the Order Confirmation. The parties expressly submit to the personal jurisdiction and venue of each such federal or state court.If you have any comments or questions about the Service or Copyright Clearance Center, please contact us at 978-750-8400 or send an e-mail to support@copyright.com.

v 1.1

Publications and conferences attended

List of publications:

1. Rapid and highly sensitive detection of extracellular and intracellular H_2S by an azide-functionalized Al(III)-based metal-organic framework.
   S. Nandi, H. Reinsch, S. Banesh, N. Stock, V. Trivedi and S. Biswas, *Dalton Trans*., 2017, **46**, 12856-12864.

2. A dinitro-functionalized metal-organic framework featuring visual and fluorogenic sensing of H_2S in living cells, human blood plasma and environmental samples.
   S. Nandi, S. Banesh, V. Trivedi and S. Biswas, *Analyst*, 2018, **143**, 1482-1491.

3. Fluorogenic naked-eye sensing and live-cell imaging of cyanide by hydrazine-functionalized CAU-10 metal-organic framework.
   R. Dalapati, **S. Nandi**, H. Reinsch, B. K. Bhunia, B. B. Mandal, N. Stock and S. Biswas, *CrystEngComm*, 2018, **20**, 4194-4201.

4. Selective sensing of peroxynitrite by Hf-based UiO-66-$B(OH)_2$ metal-organic framework: Applicability to cell imaging.
   M. SK, **S. Nandi**, R. K. Singh, V. Trivedi and S. Biswas, *Inorg. Chem*., 2018, **57**, 10128-10136.

5. Metal-organic framework showing selective and sensitive detection of exogenous and endogenous formaldehyde.
   S. Nandi, E. Sharma, V. Trivedi and S. Biswas, *Inorg. Chem*., 2018, **57**, 15149-15157.

6. A recyclable post-synthetically modified Al(III) based metal-organic framework for fast and selective fluorogenic recognition of bilirubin in human biofluids.
   S. Nandi and S. Biswas, *Dalton Trans*., 2019, **48**, 9266-9275.

7. A phthalimide functionalized UiO-66 metal-organic framework for the fluorogenic detection of hydrazine in live-cells.
   M. SK, M. R. Uz Zama Khan, A. Das, **S. Nandi**, V. Trivedi and S. Biswas, *Dalton Trans.*, 2019, **48**, 12615- 12621.

8. An ultra-robust luminescent CAU-10 MOF acting as a fluorescent turn-off sensor for $Cr_2O_7^{2-}$ in aqueous medium.
   S. Nandi, A. Mondal, H. Reinsch and S. Biswas, *Inorg. Chim. Acta*, 2019, **497**, 119078. (Invited article in special issue: "MOFs for Energy and Environmental Applications")

.

9. Fluorescence modulation of an Aggregation-Induced Emission active ligand via rigidification in a coordination polymer and its application in singlet oxygen sensing.
   R. Dalapati, **S. Nandi**, K. Van Hecke and S. Biswas, *Cryst. Growth Des*., 2019, **19**, 6388-6397. (Invited article in virtual special issue: "Structure Property Relationship in Crystalline Solids")

10. A vinyl functionalized mixed linker CAU-10 metal-organic framework acting as a fluorescent sensor for the selective detection of H_2S and palladium(II).
    S. Nandi, H. Reinsch and S. Biswas, *Microporus Mesoporous Mater*., 2020, **293**, 109790.

11. A diamino functionalized metal-organic framework for fluorometric recognition of free chlorine in environmental water samples.
    S. Nandi and S. Biswas, *Microporous Mesoporous Mater*., 2020, **299**, 110116,

List of conferences attended:

1. Chemconvene-17, 25th July, 2017, Department of Chemistry, IIT Guwahati, Assam, India.

2. 29thAnnual General Meeting of Materials Research Society of India and National Symposium on Advances in Functional and Exotic Materials, 14th-16th February, 2018, Bharathidasan University, Tiruchirappalli-620024, India.

3. Frontiers in Chemical Sciences (FICS-2018), 6th-8th December, 2018, Department of Chemistry, IIT Guwahati, Assam, India.

4. 25th ISCB International Conference (ISCBC-2019) Trends in Chemical and Biological Sciences: Impact on Health and Environment, 12th-14th January, 2019, Lucknow, India.

5. Research Conclave '19, Department of Chemistry, 14th-17th March, 2019, IIT Guwahati, Assam, India.

6. Modern Trends in Inorganic Chemistry-XVIII**,** 11th-14th December, 2019, Department of Chemistry, IIT Guwahati, Assam, India.

THE END